NOTE TO USERS

Synthesis of Heterocyclic Macrocycles and Folding Oligomers

Liyan Xing

A Thesis

In

The Department

of

Chemistry and Biochemistry

Presented in Partial Fulfillment of the Requirements
for the Degree of Master of Science (Chemistry) at
Concordia University
Montreal, Quebec, Canada

January 2005

Your file Votre référence
ISBN: 0-494-04347-4
Our file Notre référence
ISBN: 0-494-04347-4

Abstract

Synthesis of Heterocyclic Macrocycles and Folding Oligomers

Liyan Xing

Naphthyridine-based macrocycles with urea and formamidine linkages and pyridazine-based macrocyclic ureas with alternating 3,6-pyridazine/2,6-toluene subunits were synthesized in one-step reactions with acceptable to good yields. The non-covalent intramolecular interactions inherent in the designed subunits, particularly, intramolecular hydrogen bonding, play the key role in guiding the cyclization process. Various spectroscopic techniques (NMR, MS, IR, X-ray crystallography, STM) were used to characterize these macrocycles. This self-templated synthesis of macrocycles points to the possibility of preparing folding oligomeric strands with these heterocyclic systems. A crescent trimer and a helical pentamer were obtained with a urea linked 3,6-pyridazine/2,6-toluene system. The trimer exists as a mixture of two helical segments of opposite chirality, and toluene methyl groups and urea carbonyl groups adopt an *anti* conformation in the crystal structure. The pentamer forms one helical turn with overlapping termini in solution: the π-π stacking of the terminal toluene rings was confirmed by ^{1}H NMR studies. To our knowledge, this is the first reported synthetic helical architecture that utilizes both hydrogen bonding and steric interactions to drive and stabilize the folded conformation. Attempts were also made to prepare longer strands with a convergent protection/deprotection methodology.

Acknowlegement

I would like to express my gratitude to my supervisor, Dr. Louis A. Cuccia for his continual inspiration, encouragement and support leading to a fulfilling graduate study experience. I am also grateful to Dr. Sébastien Robidoux and Dr. Heidi Muchall for serving on my research committee. Sincere thanks are also extended to Dr. Ann English for giving me access to the MS facilities and offering much generous help; Dr. Bruce Lennox for allowing me to present my research at his group meetings and providing priceless advice; Dr. Anne Petitjean, Dr. Todd Sutherland, and Evelyn Martins for proofreading my thesis. Furthermore, I would like to thank the people that have assisted me throughout my research at Concordia: Dr. Sébastien Robidoux and Dr. Paul Xia for NMR, Dr. Scott Bohle, Dr. Lijuan Zhang, and Dr. Francine Bèlanger-Gariépy for X-ray crystallography, Dr. Alain Tessier, Dr. Nadim Saade, Heng Jiang, and David Yeung for MS, Dr. Ulrich Ziener and Dr. Louis Cuccia for the STM measurements, Dr. Ivan Huc for useful advice, and Franco Nudo for assistance with the IR. Particularly, I would like to express my gratitude to the former and current members in the Cuccia lab for their scientific contributions and friendship: Nathalie, Jyothi, Lawrence, Ying, Neenah, Neil, Aurelie, Josephine, Jesse, Angela, James, Johnston, Marta, Monica, Aylin, Fiorezo, and Rolf. I also acknowledge the assistance from my fellow graduates, the administration and staff in this department. The assistance provided by Carole Coutts, Donna Gordon and Lisa Montesano is much appreciated.

I am extremely grateful to my doctor Jill Harrison for her professional guidance and great friendship. Most importantly, I thank all my family for their unconditional love and support.

Dedicated to my family

Table of contents

List of Figures

List of schemes

List of Tables

List of abbreviations

AFM: atomic force microscopy

am: amino

Boc_2O: di-*tert*-butyl dicarbonate

CD: circular dichroism

CDI: 1,1'-carbonyl-diimidazole

COSY: correlated spectroscopy

DIT: dithranol

DHB: 2,5-dihydroxybenzoic acid

DMSO: dimethylsulfoxide

ESI: electro spray ionization

eq.: equivalence

FAB: fast atomic bombardment

FTIR: Fourier transform infrared spectroscopy

GPC: gel permeation chromatography

HPLC: high performance liquid chromatography

HOPG: highly oriented pyrolitic graphite

hr: hour

IAA: *trans*-indoleacrylic acid

im: imino

MALDI-TOF: matrix assisted laser desorption ionization-time-of-flight

min.: minutes

m.p.: melting point

MS: mass spectrometry

NMR: nuclear magnetic resonance

NOESY: nuclear overhauser effect spectroscopy

Np: naphthyridine

ORTEP: Oak Ridge thermal ellipsoid plot

PDI: 1,3-phenyl-diisocyanate

ppm: parts per million

R_f: retention factor

r.t.: room temperature

STM: scanning tunneling microscopy

TEM: transmission electron microscopy

THF: tetrahydrofuran

TDI: tolylene-2,6-diisocyanate

TEOF: triethylorthoformate

TLC: thin layer chromatography

UV: ultraviolet spectroscopy

Chapter 1

Introduction

1.1 Macrocycles

Cyclic molecules are widespread in nature and they contribute to some of the amazing functions of life[1]. Inspired by natural macromolecules that exhibit complexing properties, cyclic antibiotics, cyclodextrins, *etc.*, chemists are very interested in synthesizing cyclic compounds with properly distributed binding sites and cavities large enough to complex organic or inorganic guest molecules.[1] Cyclic molecules with more than a 12-membered backbone are conventionally regarded as large rings or macrocycles.[2]

Macrocyclic molecules are commonly obtained by reactions of multifunctional monomers. The competition between macrocyclization and polymerization is the key concern when chemists choose the appropriate methods to obtain designed structures. Among the numerous ring closure procedures, high dilution techniques and templated ring closure are among the most well developed and frequently utilized techniques.[1]

The high dilution technique is based on kinetic factors that balance the competitive reactions between polymerization and macrocyclization.[3] The intramolecular ring closure reaction is first order, its rate being proportional to concentration, while intermolecular condensation reactions are second order, and therefore the rate is proportional to the product [reagent A]*[reagent B] of the concentrations, so dilute conditions should favor intramolecular reactions. In highly dilute solutions, the molecules are much more separated from each other than in

concentrated solutions, so the probability of intramolecular reactions is increased. The concentration is typically in the range of 10^{-4}-10^{-3}M when this technique is applied.[3]

The high dilution technique is usually carried out in liquid-liquid medium involving addition of dissolved reagents into a large amount of solvent under vigorous stirring over a substantially long time period to make the stationary concentration of the intermediate very low.[1, 3] The relatively long reaction time and large amounts of solvents are disadvantages associated with the dilution technique. Chemists have endeavored to make up 'disguised dilutions' while keeping the local concentration of the reacting species low to tackle this problem.[1, 3] For example, the dilution effect can be achieved by making use of a multiple-phase system, in which a component is less soluble and it goes into the reacting solution successively as the reaction proceeds, thus maintaining the stationary concentration low.[4] Numerous cyclic compounds have been obtained with this technique since Ruggli initiated the dilution concept in 1912.[5] As one of the earliest developed cyclization methods, it is still widely used independently or combined with other techniques.[4, 6-11]

According to Busch, "A chemical template organizes an assembly of atoms, with respect to one or more geometric loci, in order to achieve a particular linking of atoms".[12] This concept is a natural development of continual progress made in coordination chemistry, organic and supramolecular chemistry. The templating effects could be realized with metal-ligand binding, electrostatic interactions and hydrogen bonding.[13]

Metal ions have been applied extensively to obtain crown ethers and related compounds. In 1967, Pedersen reported the synthesis of the crown ether dibenzo-18-crown-6 (Figure1.1) and the templating effect asserted by sodium ions.[14]

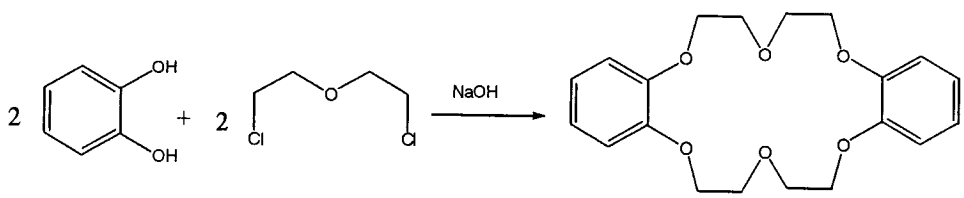

Figure 1.1. Synthesis of dibenzo-18-crown-6 by Pedersen.

In the presence of sodium hydroxide, a macrocyclization yield of *ca.* 45% was obtained in contrast with a yield of 0.4% when sodium ions were not added. The sodium ion, "by dipole-ion interactions, 'wraps' the molecular pieces around itself to form a three-quarter circle and dispose them for the final ring closure".[15] Crown ethers display exceptional binding abilities towards alkali metal ions. By incorporating heteroatoms other than oxygen, many other types of crown ethers have been obtained with this principle to further exploit their binding properties. Besides crown ethers, metal ions have been employed to template the formation of many complicated cyclic and bicyclic structures, such as cage complexes, catenanes and knots.[1]

With the rapid development of supramolecular chemistry, non-covalent interactions are receiving more attention in templating the synthesis of novel macrocyclic motifs. By taking advantage of aromatic stacking between electron-rich and electron-poor aromatic systems, Stoddart and coworkers reported the synthesis of the tetracationic

cyclophane shown in Figure 1.2.[16] The stacking between the aromatic π-electron-rich ring of the diol and the electron-poor bipyridinium units preorganize the substrate to form intermediate conformations that favor cyclization.

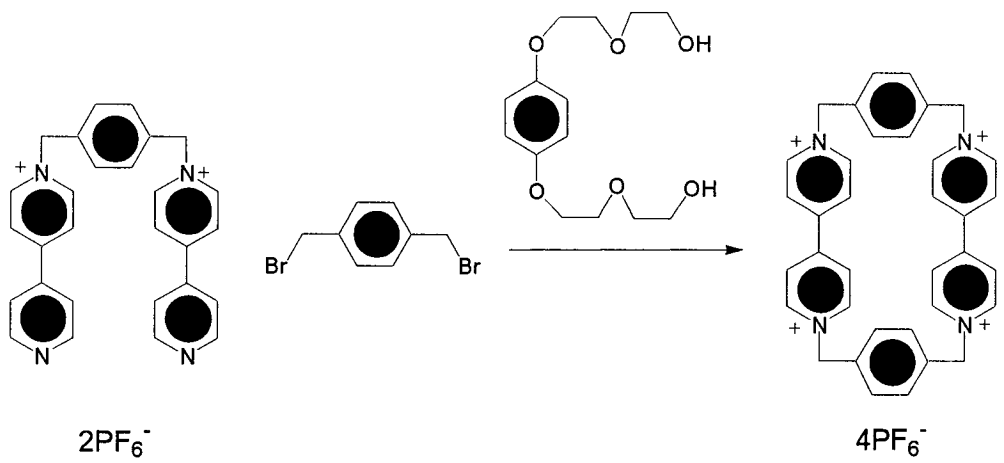

Figure 1.2. An example of π-π stacking templated synthesis of a tetracationic cyclophane by Stoddart *et al.*

Hydrogen bonding interactions are the preferred method for nature to design and construct some of the most important biomolecules like proteins and DNA.[17, 18] The replication of DNA molecules best exemplifies the templating role played by hydrogen bonding interactions between the base pairs. The extraordinary behavior of proteins can be correlated to the folding and unfolding mechanisms in which hydrogen bonding plays an indispensable role and has attracted tremendous attention from both biologists and chemists.[19-25] In our supramolecular chemistry lab, we are interested in studying the non-covalent interactions in both biological and synthetic molecules. The goal of this work was to synthesize macrocycles and foldamers for later use in biophysical investigations. Hydrogen bonding has high strength and directionality,[26-28] which makes

it an ideal templating candidate. Compared to other templates, one obvious advantage is that the final products obtained are 'clean' (*i.e.* without the inclusion of added templates, which is often a problem with externally templated processes when the template is unwanted in the final product but is difficult to remove or must remain to stabilize certain conformations).[13] Hydrogen bonding interactions can be used in macrocycle syntheses to enforce and stabilize folding conformations and facilitate ring closure processes. Examples given below will show the simplified conditions required, the good yields obtained and the structural versatility attained. The foundation that all these attractive features build on is the art of 'design' that combines the chemist's knowledge in this field as well as aesthetic taste.

Hunter and coworkers developed a series of macrocycles and catenanes to evaluate the role played by both intermolecular and intramolecular hydrogen bonding for macrocyclization. To make macrocycle **VI** shown in Figure 1.3,[29] isophthaloyl dichloride, **II**, and pyridine-2,6-dicarbonyl chloride, **III**, were used as carbonyl generating reagents. Route **a** and **b,** differing only in the sequence of the reaction of diamine **I** with diacid chloride **II** and **III**, resulted in strikingly different yields (15% for route **a** and 88% for route **b**). They rationalized this phenomenon on the basis of the conformational preferences of the individual diamide subunits. The pyridyl nitrogen lone pair could form hydrogen bonds with both adjacent amide hydrogens and thus holds the acid chloride and the amine in proximity facilitating the ring closure. For the isophthaloyl intermediate **IV**, the absence of hydrogen bonding separates the acid chloride and amine functionalities too far apart to react. Clearly, in this case, hydrogen bonding plays the role

of a template to bring the functional groups in the oligomeric intermediate near each other to assist the ring closure process.

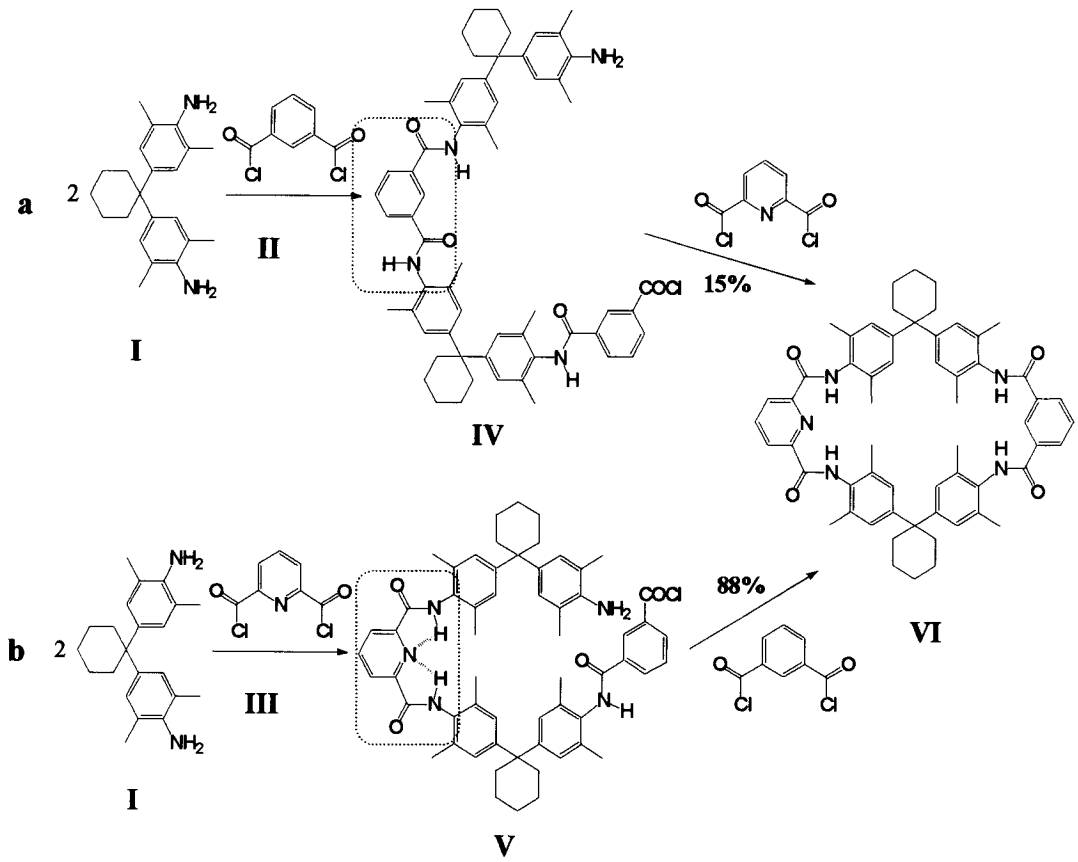

Figure 1.3. Comparison of two routes for the synthesis of a macroamide **VI** by Hunter *et al.* In both cases, the yields are for the second step only. Conformational preferences of the diamide subunits adopted by the intermediates **IV** and **V** are highlighted while dashed lines represent hydrogen bonds.

By taking advantage of hydrogen bonding, macrocycles can also be prepared from one-step reactions[30, 31] with the benefits of simplified procedures, ease of intermediate purification, and lower cost. Huc *et al.* have recently reported the isolation of aromatic oligoamide macrocycles in the polycondensation reaction to synthesize foldamers (Figure 1.4).[30]

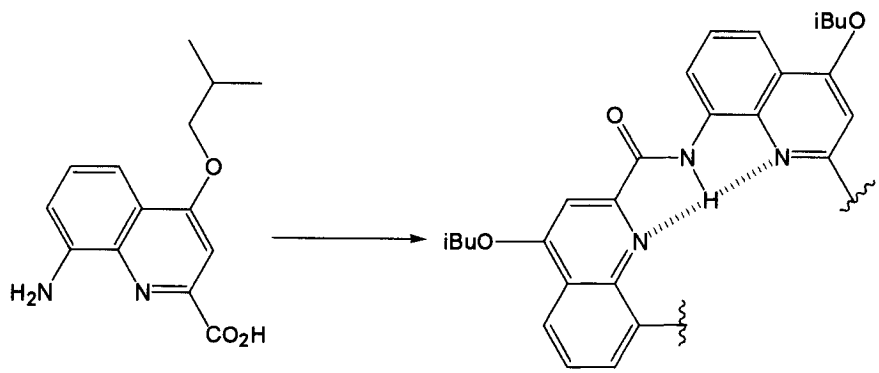

Figure 1.4. Polycondensation reaction to prepare oligoamides by Huc *et al.* A trimeric (20 %) and a tetrameric (20 %) macrocycle along with linear oligomers were obtained in the self-condensation reaction of 8-amino-2-quinolinecarboxylic acid with a high initial concentration of monomer (0.36 M). Hydrogen bonds are represented by dashed lines.

The three-center intramolecular hydrogen bonds between adjacent aromatic nitrogen lone pairs and amide hydrogens enforce the curved conformation to allow the cyclization to proceed readily. While the trimer was largely planar, the tetramer was saddle-shaped, self-assembled into discrete circular dodecamers and showed the potential as a molecular clip to bind aromatic acid guests in solution.[30] Coincidently, when carrying out a polymerization reaction with diacid chloride, Gong *et al.* found hexameric macrocycles as *overwhelmingly* major products in the polycondensation reaction between aromatic diacid chlorides and diamines (Figure 1.5).[31]

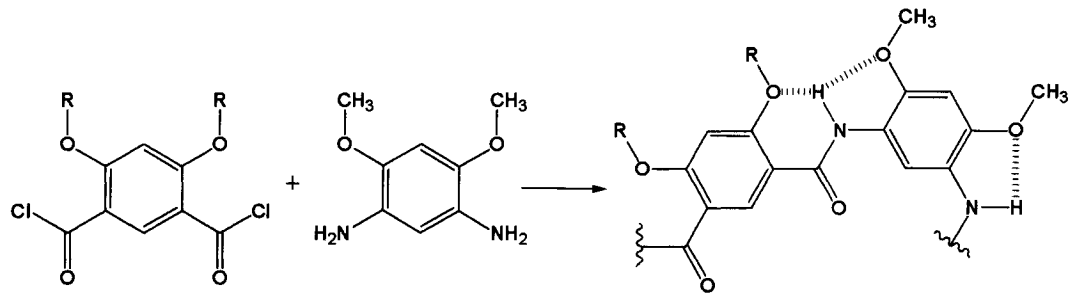

Figure 1.5. One-step synthesis of hexameric macrocycles by Gong *et al.* The hydrogen bonding pattern is illustrated with dashed lines.

In the above examples, apart from using hydrogen bonding interactions, aromatic motifs are incorporated into the ring backbone for two major reasons: (a) the aromatic systems can be in full or partial conjugation with the linker group, *i.e.* the amide in the aforementioned examples, to obtain relatively coplanar and thus well-defined conformations; (b) the induction of rigid aromatic groups can level off the entropic difference between formation of macrocycles and oligomers: for flexible backbones, the entropy favors the formation of longer strands instead of oligomers.[1]

In designing our macrocycles, these factors were carefully considered. We focus on two series of macrocycles in our lab, the classification of which is based on the aromatic motifs that make up the backbone. One series is composed of two macrocycles with 2,7-diamino-1,8-naphthyridine as the building block with urea or formamidine linkages (Figure 1.6).

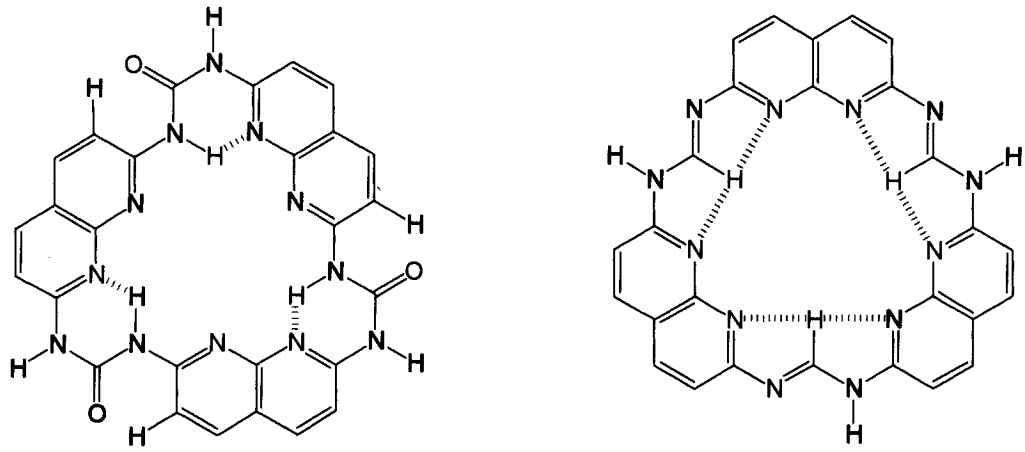

6 7

Figure 1.6. Chemical structures of naphthyridine-based macrocycles **6** and **7** with urea and formamidine linkages. Hydrogen bonds are represented by dashed lines.

In both cases, the hydrogen-bonding pattern lining the interior is assumed to be the major force for the formation of a cyclic conformation. For urea macrocycle **6**, hydrogen bonds should be formed between naphthyridine nitrogen atoms and urea protons, while in formamidine macrocycle **7**, formal protons should hydrogen bond to naphthyridine lone pairs. The second series of macrocycles consists of three subdivisions with (*i*) 3,6-pyridazine, (*ii*) 4,6-pyrimidine and (*iii*) 2,3-pyrazine as building blocks and 2,6-toluene/1,3-benzene as spacers alternatively connected with urea groups (Figure 1.7).

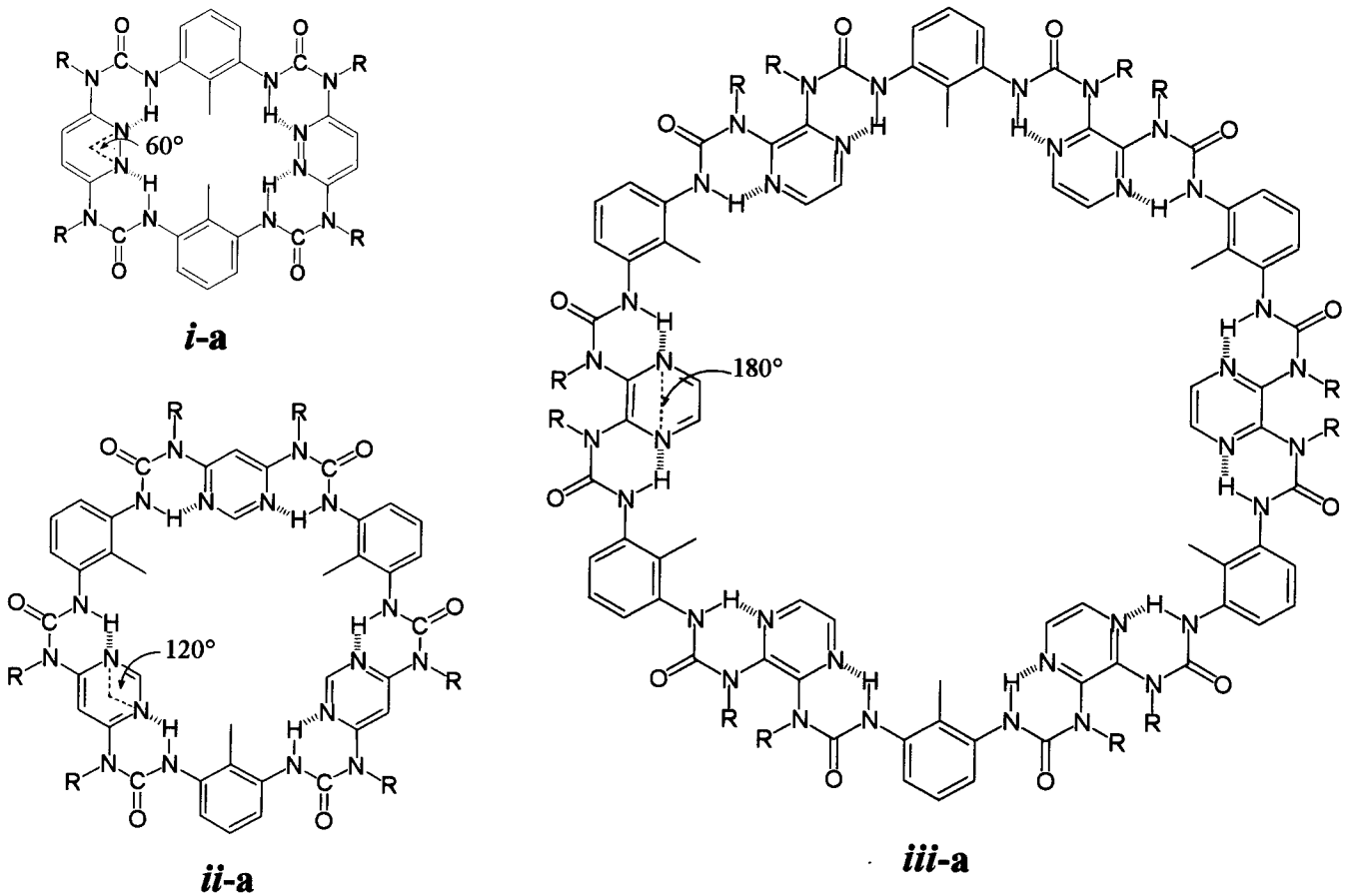

i-a

ii-a

iii-a

Figure 1.7. Chemical structures with (*i*-a) pyridazine, (*ii*-a) pyrimidine and (*iii*-a) pyrazine as building blocks and 2,6-toluene as spacers that are alternatively connected with urea linkages. Hydrogen bonds are represented by dashed lines.

Non-covalent hydrogen bonding and steric interactions that are responsible for the folded conformation are illustrated in Figure 1.8 with oligourea 3,6-pyridazine/2,6-toluene as an example.

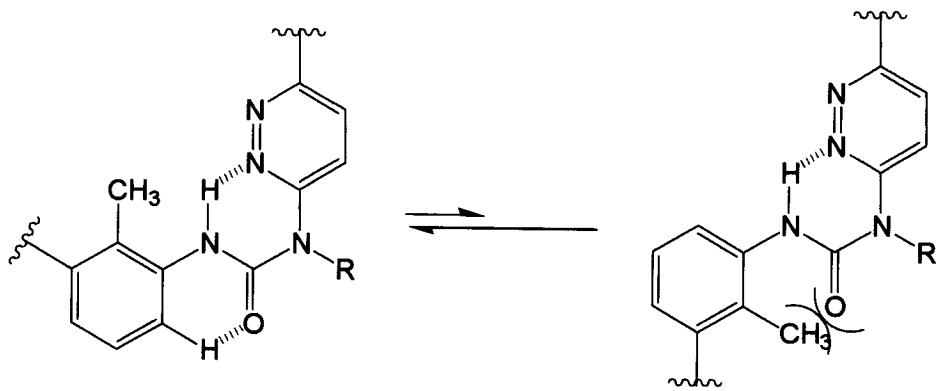

Figure 1.8. Non-covalent interactions for the folded conformation versus linear conformation of oligourea 3,6-pyridazine/2,6-toluene.

The size of the inner cavities of these three types of macrocycles increases as the angle NxN increases from 60° to 120° to 180°, where N is each nitrogen atom from the heterocycle and x is the center of the heterocycle. The hydrogen bonding between the urea protons and nitrogen atoms of the heterocycles and the steric repulsion between toluene methyl groups and carbonyl groups are believed to be the major driving forces to induce and stabilize the curved conformation. The macrocycles and helical oligomers can be formed by reacting 3,6-diaminopyridazine, 4,6-diaminopyrimidine, or 2,3-diaminopyrazine with tolylene-2,6-diisocyanate in a one-step reaction. Phenyl, xylyl and pyridyl analogues of tolylene-2,6-diisocyanate might also be used as spacers to test the

versatility and tunability [23, 24] of our design. The diamines can be synthesized by nucleophilic substitution starting from the corresponding dichloride, while tolylene-2,6-diisocyanate is commercially available.

The introduction of hydrophobic side chains should increase the solubility in organic solvents thus facilitating characterization and may play an important role in supramolecular interactions of the macrocycles as well as the corresponding foldamers[21] discussed in the next section. To meet the requirements for different analysis techniques, derivatives with varying side chains were synthesized. For example, with long aliphatic chains, macrocycles may display self-assembly properties in solution and could be examined with electron microscopy and scanning tunneling microscopy, while isobutyl derivatives show better crystallinity for X-ray diffraction experiments.

1.2 Foldamers

Foldamers are polymers or oligomers with a strong tendency to form compact conformations in solution.[21] This concept is inspired by the structures found in nature with polypeptides[32, 33] and polynucleotides[34] as the most studied representatives. The compact conformations adopted by biopolymers are crucial for sophisticated chemical reactions in biological processes such as catalysis, tight and specific binding and directed flow of electrons.[35]

The folding mechanism of biopolymers is intriguing because entropic effects normally favor internal disorder.[19] The folding process of biopolymers is not fully understood, but the entropy loss is believed to be counterbalanced by weak and cooperative non-covalent intra- and/or inter-molecular interactions which include ion complexation, hydrogen bonding, steric effects and hydrophobic interactions, which are the main components for chemists to design simplified synthetic systems as models to investigate complicated biological processes.[20, 24, 36-38]

Lehn *et al.* developed a series of helicity codons to enforce the helical wrapping of polyheterocyclic strands with alternating pyridine-pyrimidine,[39] pyridine-pyridazine [40] and naphthyrine-pyrimidine[41] moieties (Figure 1.9).

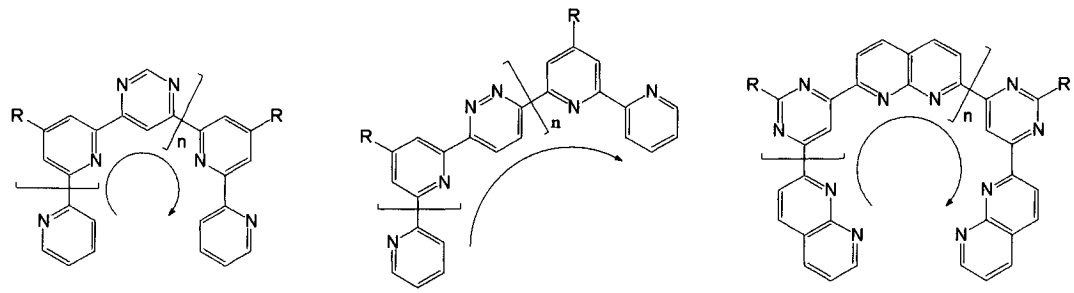

Figure 1.9. Helical structures with alternating (a) pyridine-pyrimidine, (b) pyridine-pyridazine and (c) pyrimidine-naphthyridine.

This type of design was based on the preferential *transoid* conformation of 2,2'-bipyridine that is believed to be attributed to the favorable interactions between the lone pair of electrons on the nitrogen atoms and *ortho* hydrogen atoms on the neigbouring aromatic ring, the favorable *anti*-parallel nitrogen dipoles in the *transoid* conformer, steric repulsion between neighboring C-H groups and electronic repulsion in the *cisoid* conformation (Figure 1.10). [40]

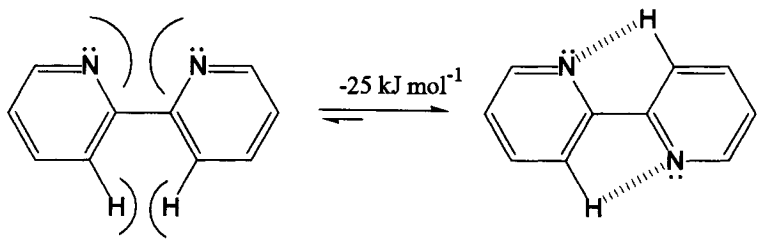

Figure 1.10. *Cisoid-transoid* conformers of 2,2'-bipyridine with an energy gap of 25 kJ mol^{-1}.[42] The dashed lines in the *transoid* conformer represent weak hydrogen bonding interactions.

The same non-covalent interactions were preserved in extended longer strands and thus steer the helical growth. Aromatic π-π stacking over one helical turn further

stablizes the folded conformation.[40, 41, 43] By replacing 4,6-substituted pyrimidine (Figure 1.9 (a)) with 2,6-substituted pyridazine, the helix obtained was widened (Figure 1.9 (b)). In Figure 1.9 (c) the naphthyridine heterocycle was used as an extended pyridine ring to obtain a more spacious inner cavity. Additionally, naphthyridine units displayed good binding properties to a variety of cations (alkali ions, hydronium and guanidinium ions) to promote hierarchical formation of supramolecular assemblies from this type of foldamer.[41]

Moore *et al.* focus their studies on solvophobically driven foldamers with *m*-phenylene ethynylene (*m*PE) as the backbone and polar side chains with the general structure shown in Figure 1.11(a).[35, 44, 45] In polar solvents, this type of oligomer adopts folded conformations due to the solubilizing effect of polar side chains and unfavorable interactions of the hydrocarbon backbone with polar solvents, as well as the local constraints caused by the covalent structure of the backbone and intramolecular aromatic stacking interactions.[35]

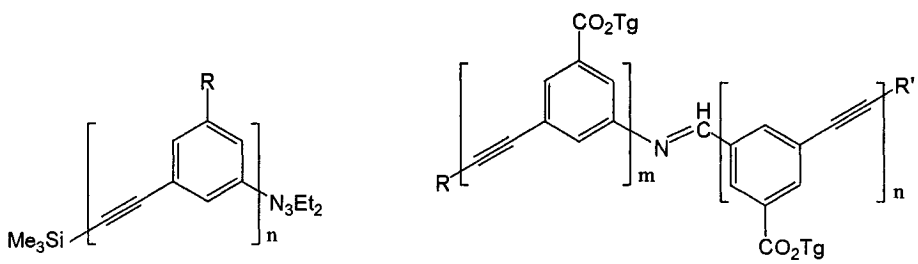

Figure 1.11. Chemical structures of *m*-phenylene/ethynylene foldamers by Moore *et al.*

The folding conformations create tubular hydrophobic cavities that display certain binding properties to non-polar guests.[44, 46] The stability gained from folding was taken advantage of to synthesize longer *m*PE strands from short chain segments by reversible imine metathesis. The geometry of the imine bond was shown to match with the acetylene groups in the *m*PE helices (Figure 1.11 (b)).[47] *m*PE oligomers could be unfolded and folded by adjusting the surrounding solvents, which emulates the denaturing and folding processes in proteins.[45]

Hydrogen bonding interactions are the most widely used tools for chemists to design foldamers. Aromatic amides comprise a major category of abiotic foldamers. Lehn *et al.* performed studies on the folding behavior of oligopyridine-dicarboxamide strands (Figure 1.12).[48]

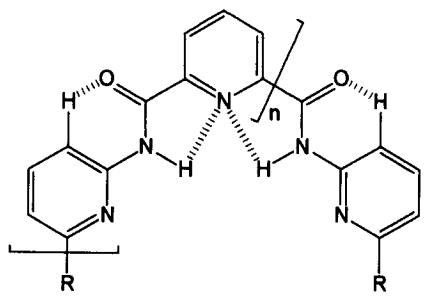

Figure 1.12. Structures of pyridine-dicarboxamide oligomers. The intramolecular hydrogen bonding interactions in one repeating unit is shown by dashed lines.

In Figure 1.12, the hydrogen bonds between (a) the amide protons and adjacent pyridine nitrogen lone pairs through a 5-membered ring, and (b) the carbonyl oxygens and the *ortho* aromatic C-H groups, were the major non-covalent interactions to enforce the curved conformation. The helical structures were confirmed to dimerize into double

helices both in solution and the solid state by NMR and X-ray single crystal diffraction experiments.[49, 50]

Huc *et al.* reported manipulating the conformations of this type of amide-based foldamer by changing the hydrogen bonding pattern through stepwise protonation[51] (Figure 1.13). The oligomers they chose have two different pyridine rings with one possessing a *para*-substituted decyloxyl ($OC_{10}H_{21}$) group. In the original state, the nitrogen atoms of this substituted pyridine form intramolecular hydrogen bonds with the adjacent amide protons, which is believed to result in a lower basicity of the pyridine nitrogen in comparison to the other pyridine rings making successive and selective protonation possible.[51]

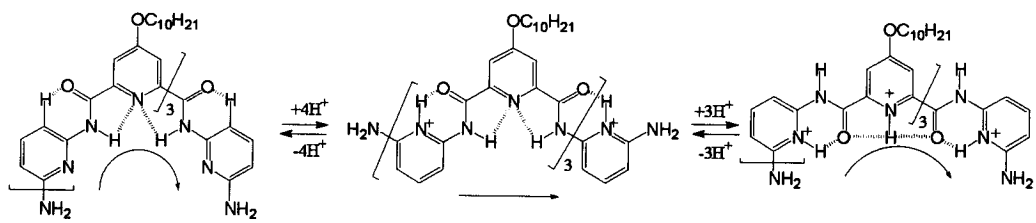

Figure 1.13. Illustration of the protonation induced folding-refolding processes *via* a linear intermediate.

The protonation alters the donor-acceptor map and causes the rotation of relevant covalent bonds. A linear conformation is achieved when the nitrogen atoms of the unsubstituted pyridine rings are protonated with TFA (CF_3CO_2H, p*K*a = 0) or MsOH (CH_3SO_3H, p*K*a = -2); further protonation on the decyloxyl substituted pyridine nitrogens

with stronger acid TfOH (CF_3SO_3H, p*Ka* = -16) refolded the strand with different intramolecular hydrogen bonding patterns from the original state.

Gong *et al.* developed helical foldamers based on a strategy of backbone-rigidification (Figure 1.14).[52, 53] In this system, the free rotation of an acetylene group[54] was constrained and the phenylacetylene/phenyl motif was fixed to be relatively coplanar with the aromatic moiety by intramolecular hydrogen bonding interactions, so the intrinsically flexible *m*PE oligomers or polymers are expected to adopt well-defined conformations. Helical conformations are enforced by the intramolecular hydrogen bonding network along the outer rim combined with the *meta*-substituted covalent connections of the phenyl rings.

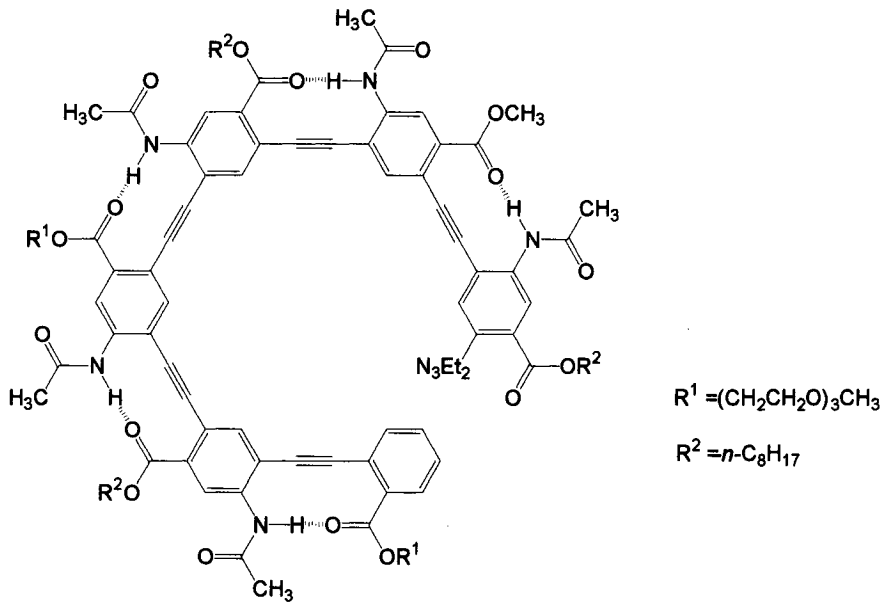

Figure 1.14. Helical *m*PE oligomers with backbone-rigidified strategy by intramolecular hydrogen bonding interactions.

In our lab, we are interested in the synthesis of oligoureas that are expected to form folded (*i.e.* crescent or helical) conformations with intramolecular hydrogen

bonding interactions as the major driving force. Poly- or oligoureas with well-defined conformations are less studied compared to aromatic amides. In 2001, Zimmerman *et al.* proposed a naphthyridyl urea strand that would be expected to equilibrate between intermolecularly hydrogen-bonded sheet-like structures and intramolecularly hydrogen-bonded helices (Figure 1.15).[55]

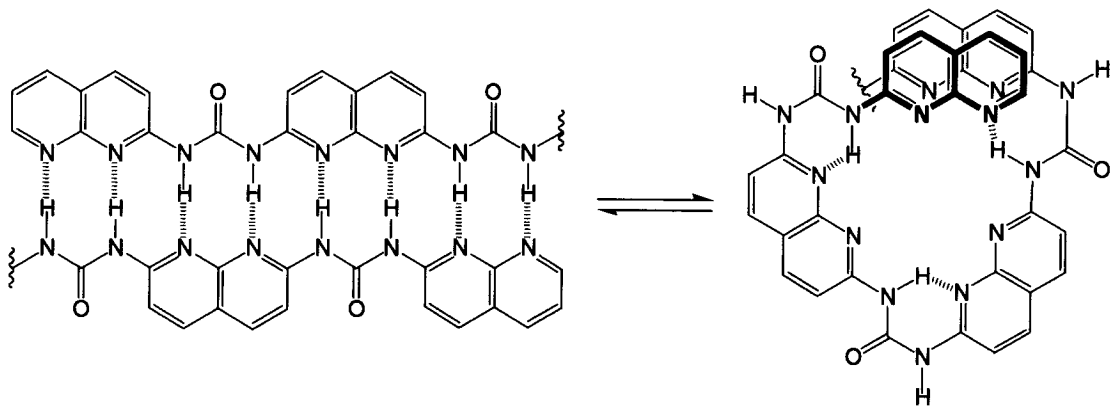

Figure 1.15. Transition between intermolecularly hydrogen-bonded sheet-like structure (left) and intramolecularly hydrogen-bonded helices (right) by Zimmerman *et al.*

Meijer *et al.* recently reported the synthesis of a chiral poly-ureidophthalimide in a single condensation step from which a broad spectrum of oligomers were isolated ranging from a dimer up to *ca.* 30 repeating units (Figure 1.16).[56]

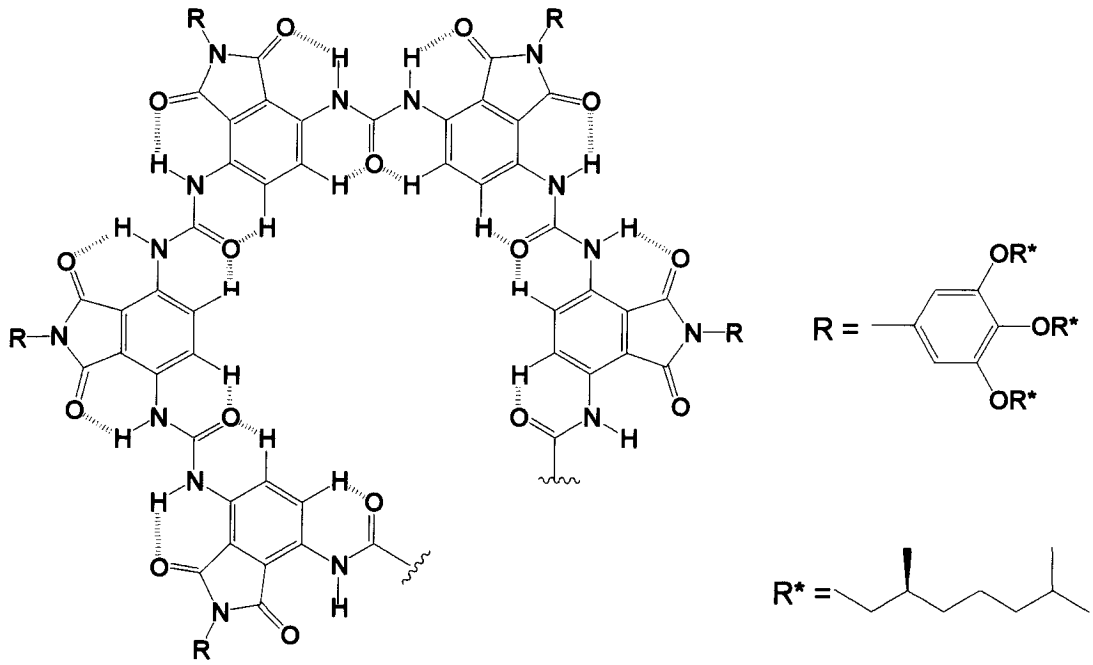

Figure 1.16. Chemical structures of poly-ureidophthalimide by Meijer *et al.*

By incorporating chiral side chains, the folding behavior of the oligomers with different lengths could be easily monitored with CD spectroscopy. In THF, longer strands that were expected to form one or more helical turns showed an obvious Cotton effect, while no Cotton effect was observed for the shorter oligomers. They reasoned that the longer oligomers formed well-defined helical architectures and the chirality could transfer from the peripheral side chains to helically arranged phthalimide chromophores. The oligomers also displayed solvent and temperature dependent folding-unfolding behaviors. The Cotton effect was not observed in chloroform that was assumed to compete as a proton donor to disrupt the intended bonding interactions. In addition, helical order was almost lost at higher temperatures which is evidence that the structures are participating in hydrogen bonding and π-π stacking interactions.[56] Gong *et al* are also working on

folding oligoureas that make use of a similar hydrogen bonding interaction between urea N-H protons and carbonyl oxygen or ether oxygen lone pairs on the outer rim of the helices[57]. Being chemically robust and resistant to most natural enzymes, these oligoureas are proposed to be used as ion carriers and ion channels[57].

Conventional analytical techniques in organic and polymer chemistry are useful in foldamer characterization.[36] Mass spectrometry, GPC, and vapor-pressure osmometry can be used to obtain molecular weight. X-ray single crystal diffraction experiments provide the most direct structural information in the solid state. Folding patterns are usually temperature and concentration sensitive and display corresponding changes in chemical shifts in the NMR spectra, especially proton NMR. Likewise, 2D NMR experiments are used to probe the spatial correlations of some signature groups. UV, IR, fluorescence and CD spectroscopies are important analysis tools for biomolecules and they are also widely used for the characterization of synthetic foldamers. Furthermore, the topology and assembly patterns could be examined with different microscopic techniques, such as TEM, STM and AFM.

In our lab, we designed three types of oligoureas with alternating 3,6-pyridazine/2,6-toluene, 4,6-pyrimidine/2,6-toluene and 2,3-pyrazine/2,6-toluene repeat units (Figure 1.17) that are based on the same design principle as that described in Section 1.1. The folding should be induced and stabilized by hydrogen bonding interactions between nitrogen lone pairs of three types of six-membered aromatic heterocycles and urea protons in conjunction with the unfavorable steric repulsion between carbonyl groups.[58]

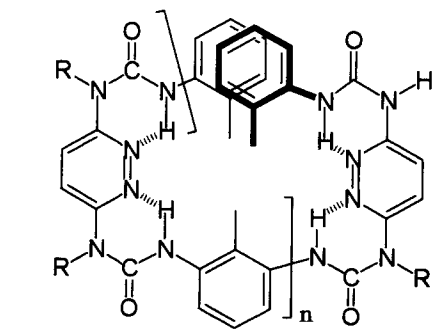

i-b

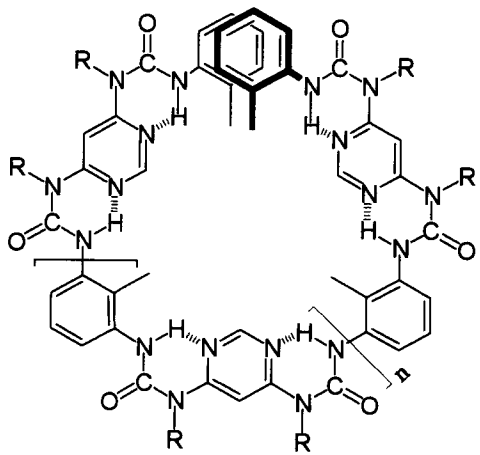

ii-b

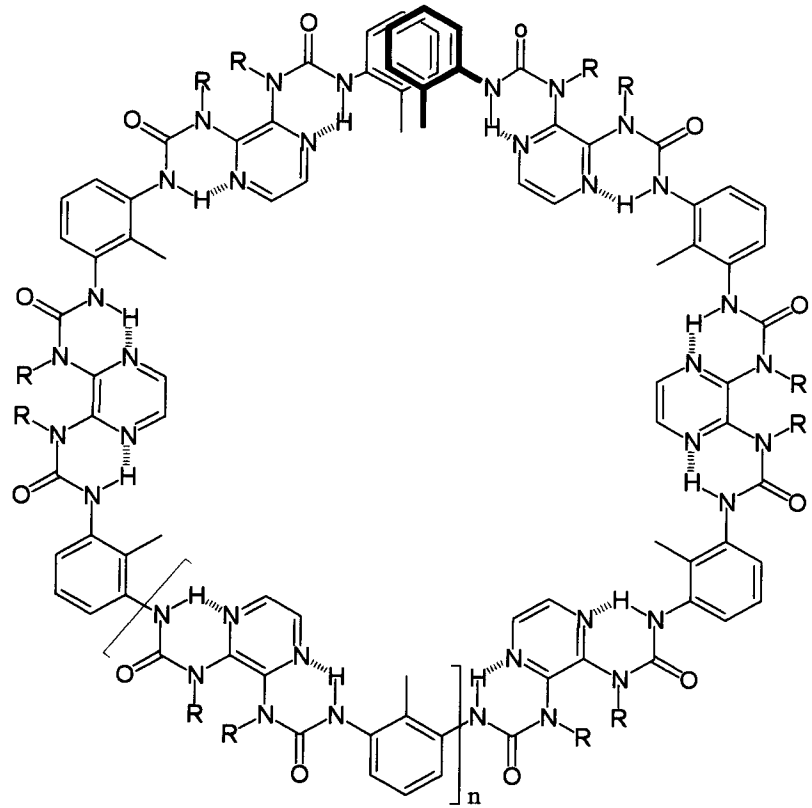

iii-b

Figure 1.17. Chemical structures of oligoureas: (*i*-b) 3,6-pyridazine/2,6-toluene, (*ii*-b) 4,6-pyrimidine/2,6-toluene and (*iii*-b) 2,3-pyrazine/2,6-toluene.

1.3 Macrocycles versus foldamers

Macrocycles were synthesized to confirm the folding propensity of this type of motif and to provide the necessary groundwork for foldamer synthesis and characterization.[30, 31, 59] The macrocycles themselves are interesting target compounds to validate the effectiveness of self-templated, one-step macrocyclization methods and to study their unique physical and supramolecular properties. Since the macrocycles and foldamers are structurally correlated and obtained from the same starting materials, they will be discussed together in one chapter, with the simpler macrocycles being described first due to their symmetrical structures.

1.4 Organization of this thesis

This thesis is composed of four chapters. Chapter 1 is a general introduction. Chapter 2 describes the synthesis and characterization of 2,7-diamino-1,8-naphthyridine based macrocycles. Chapter 3 combines the description of the 3,6-diaminopyridazine-based macrocycles and foldamers. The synthesis and characterization of a series of macrocycles with different N-substituted side chains, a crescent trimer and helical pentamer will be discussed. Chapter 4 is the experimental section.

Chapter 2

Naphthyridine-based macrocycles

2.1 Naphthyridyl urea macrocycle

2.1.1 Introduction

The interest in urea molecules often focuses on self-complementary bi-directional intermolecular hydrogen bonds.[60-63] Cyclic urea compounds have displayed potential for the formation of nanotubes through urea-type intermolecular hydrogen bonding.[64-68] Well-defined structures are possible by making use of intramolecular hydrogen bonding as exemplified in cyclic amide molecules.[29-31, 50] Böhme *et al.* reported the synthesis of a macrocyclic urea compound **VII** based on a 2,6-diaminopyridyl unit (Scheme 2.1).[69]

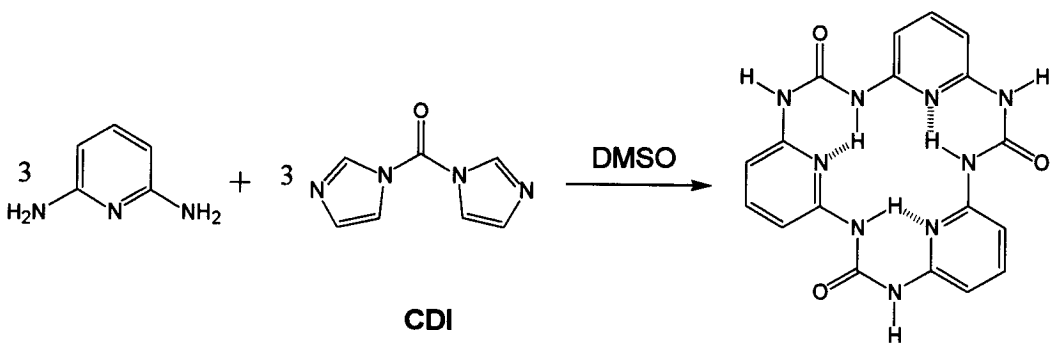

Scheme 2.1. Synthesis of macrocycle **VII** by Böhme *et al.*

The trimeric macrocycle **VII** was the major product from the reaction of 2,6-diaminopyridine with 1,1'-carbonyl diimidazole (CDI) and the formation of intramolecular hydrogen bonds between the urea protons and the non-adjacent pyridine

nitrogen lone pairs was observed using ^{1}H NMR. A minor macrocyclic tetramer was also observed with mass spectrometry and ^{1}H NMR when the reaction was carried out at higher temperature. A control experiment was executed by replacing 2,6-diaminopyridine with 1,3-diaminobenzene that produced a series of oligomers. The absence of hydrogen bonds in the latter case was proposed to be the major reason for this difference.

We report here the synthesis and characterization of macrocycle **6** (cyclo-tris (2,7-(1,8-naphthyridyl)-urea)) with 2,7-diamino-1,8-naphthyridine **5** and CDI as reagents. Naphthyridine-based compounds, with both hydrogen bond donors and acceptors, are ideal model compounds in studying recognition and binding phenomena.[55, 70, 71] In our case, the naphthyridine can be treated as an elongated and enriched (two nitrogen lone pairs) pyridine in relation to Böhme's work. The resulting macrocycle is expected to possess a larger cavity and more binding sites and may find applications both academically and industrially.

2.1.2 Preparation of 2,7-diamino-1,8-naphthyridine

2,7-diamino-1,8-naphthyridine **5** was synthesized with modified literature procedures[55, 72, 73] as shown in Scheme 2.2.

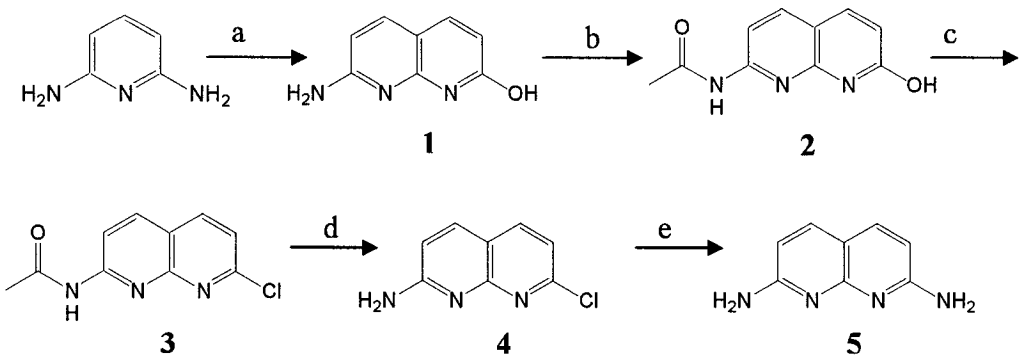

Scheme 2.2. Synthesis of 2,7-diamino-1,8-naphthyridine: a) malic acid, H_2SO_4, 110 °C; b) acetic anhydride, reflux; c) $POCl_3$, 90-95 °C; d) H_2SO_4 (20%), 100 °C; e) ammonium hydroxide, 180 °C.

2,6-diaminopyridine was treated with malic acid in concentrated sulfuric acid to form 2-amino-7-hydroxy-1,8-naphthyriyidine **1**. To facilitate substitution of the hydroxide moiety by a chloro group in **1**, the amino group was acetylated with acetic anhydride to afford 2-acetamido-7-hydroxy-1,8-naphthyridine **2**, whose hydroxide group was subsequently substituted by a chloro group using $POCl_3$ that acted as both reagent and solvent. In the literature, 2,7-diamino-1,8-naphthyridine **5** was synthesized from 2-acetamido-7-chloro-1,8-naphthyridine **3** directly in a steel bomb with ethanolic ammonia (saturated) to cleave the acetamide group and displace the chloride atom concomitantly.[55] We followed this procedure using a sealed tube instead of a steel bomb and found that 2-amino-7-hydroxy-1,8-naphthryidine **4** was the major product. From our observations, the deprotection of the chloroacetamide group in **3** occurred readily as compared to the displacement of the chloro group with the amine functionality in ethanolic ammonia. We deprotected **3**, followed by treatment with aqueous ammonium hydroxide to yield predominantly **5** as the final product with 2-amino-7-hydroxide-1,8-

naphthyridine, **1**, and unreacted 2-amino-7-chloro-1,8-naphthyridine, **4**, as side products. **4** and most other impurities were extracted into the organic phase using continuous chloroform/water extraction.

Unfortunately, impurity **1** remained in the aqueous phase with the desired diamine **5**. Relatively pure diamine **5** could be obtained by repeated recrystallization from dilute ammonium hydroxide with a poor yield of approximately 20%. Preparative column chromatography proved to be a more effective purification method. The R_f values on silica (chloroform/methanol, 8/2) for diamine **5** and hydroxide **1** were *ca.* 0.2 and 0.7, respectively. However the solubility of both **1** and **5** was very low in the solvent combination used for running TLC. Before looking for a solution to this purification problem, we tried to determine where impurity **1** originated. From steps **a** to **d** (Scheme 2.2), no purification procedure was involved and impurity **1** in the final product could be due to unreacted **1** from step **b** or from the aminolysis product in step **c** when residual $POCl_3$ was neutralized with ice water. **1** could also be formed in step **e**. The NH_2^- ion was the major nucleophile to substitute the chlorine atom. However, hydroxide ion in the ammonium hydroxide solution, which is less nucleophilic, may also react with **4** to form **1**. If impurity **1** only originates from steps **b** and **c**, it would be removed very easily by purifying the acetamidochloride **3** with chromatography. Unfortunately, the hydroxide impurity **1** was still found in the final product mixture when purified **3** was subjected to steps **d** and **e**. After different purification procedures such as recrystallization, liquid/solid extraction, sublimation, and column chromatography[73] were attempted and compared, column chromatography (dry loading) proved to be a relatively efficient method to obtain pure diamine **5** as starting material for the synthesis of macrocycle **6** (cyclo-tris (2,7-(1,8-

naphthyridyl)-urea)) and macrocycle **7** (cyclo-tris (2,7-(1,8-naphthyridyl) formamidine)).

2.1.3 Synthesis of naphthyridyl urea macrocycle (6)

Macrocycle **6** was synthesized by the condensation reaction between 2,7-diamino-1,8- naphthyridine **5** and 1,1'-carbonyldiimidazole (CDI) as shown in Scheme 2.3.

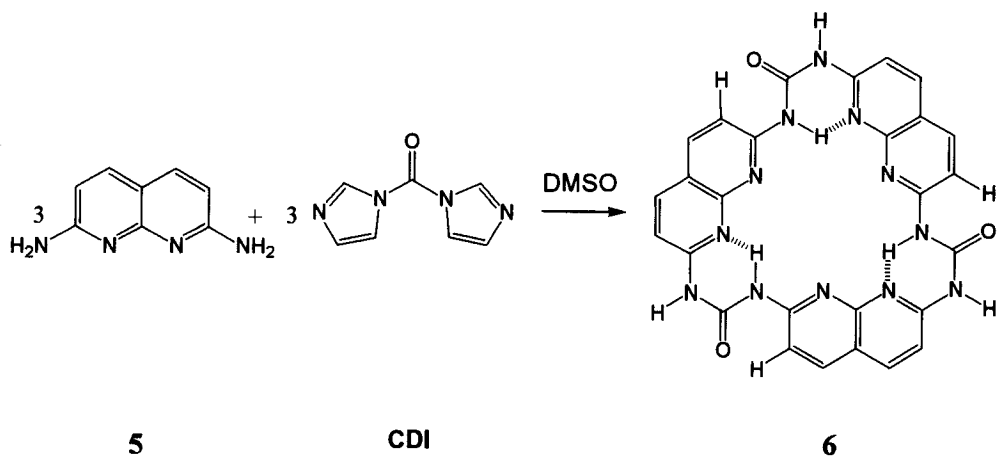

5 **CDI** **6**

Scheme 2.3. Condensation reaction of diamine **5** and CDI.

This general procedure was adapted from a literature procedure.[69] Diamine **5** was suspended in DMSO at 120 °C. The mixture became clear immediately after CDI was added and a new precipitate appeared gradually. After 24 hours, the precipitate was filtered and washed with methanol and dried at 60 °C for 24 hours under vacuum.[74] The final product was a yellow powder, slightly soluble in DMSO (< 0.5mg/mL) and insoluble in most other common organic solvents; therefore characterization was carried out in DMSO when solvent was required.

2.1.4 Results and discussion

2.1.4.1 NMR analysis

^{1}H NMR experiments in DMSO indicate the presence of almost exclusively one major product. The ^{1}H NMR spectrum (Figure 2.1) shows 6 major sets of signals: 2 singlets at 10.68 and 12.22 ppm and 4 doublets at 7.26, 8.37, 8.39 and 8.61 ppm. The relatively simple NMR spectrum suggests a symmetric molecular conformation in solution. By referring to a similar structure prepared from 2,6-diaminopyridine,[69] a macrocycle of C_3-type symmetry as shown in Figure 2.1(a) is proposed. The ^{1}H NMR spectrum can be reasonably explained based on this structure. The urea proton N-H6 that forms a 6-membered ring hydrogen bonding network with the neighboring naphthyridine nitrogen gives the most downfield shifted signal at 12.22 ppm. N-H5 points outward and gives an upfield shifted signal compared to N-H6 at 10.68 ppm.

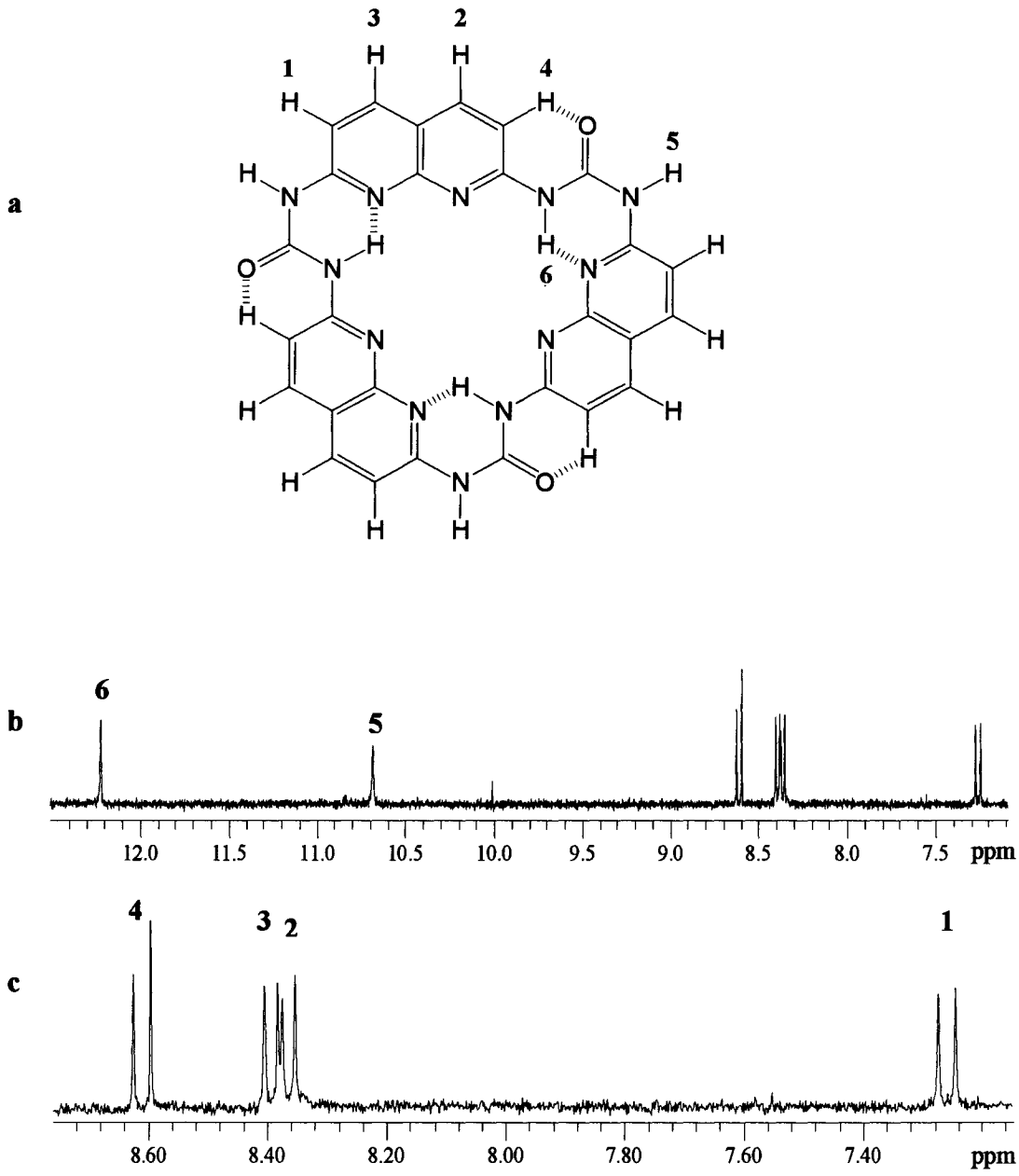

Figure 2.1. ^{1}H NMR spectrum of macrocycle **6** and the peak assigment: (a) Structure of macrocycle **6** with hydrogen bonds represented by dashed lines; (b) ^{1}H NMR spectrum of trimeric macrocycle **6** in DMSO-d_6 at 24.2 °C and (c) expansion of the aromatic region of the NMR spectrum.

Hydrogen/deuterium exchange experiments were carried out to confirm the identity of both urea protons (Figure 2.2). The signal assigned to N-H5 disappeared in 5 minutes after D_2O was added to the NMR tube, while the N-H6 signal was still observed. 30 minutes later, both signals disappeared. This suggests that the N-H6 hydrogen is locked in the conformation shown in Figure 2.1(a) by intramolecular hydrogen bonding, so exchange with deuterium is not as facile as with the N-H5 hydrogen.

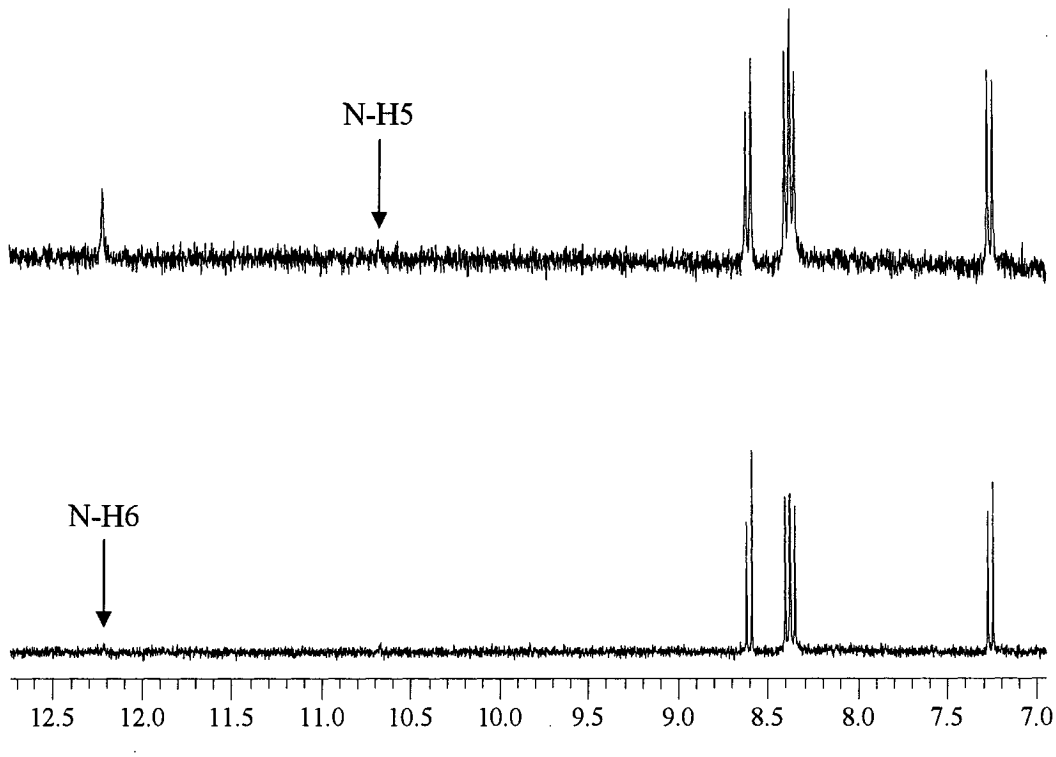

Figure 2.2. ^{1}H NMR spectra of macrocycle **6** after D_2O (5 μL) was added at room temperature (*ca.* 25 °C): (a) 5 minutes and (b) 30 minutes after addition. The arrows indicate the original positions of the urea protons.

Other evidence for the difference between the two urea N-H protons was observed with variable temperature NMR experiments (Figure 2.3).

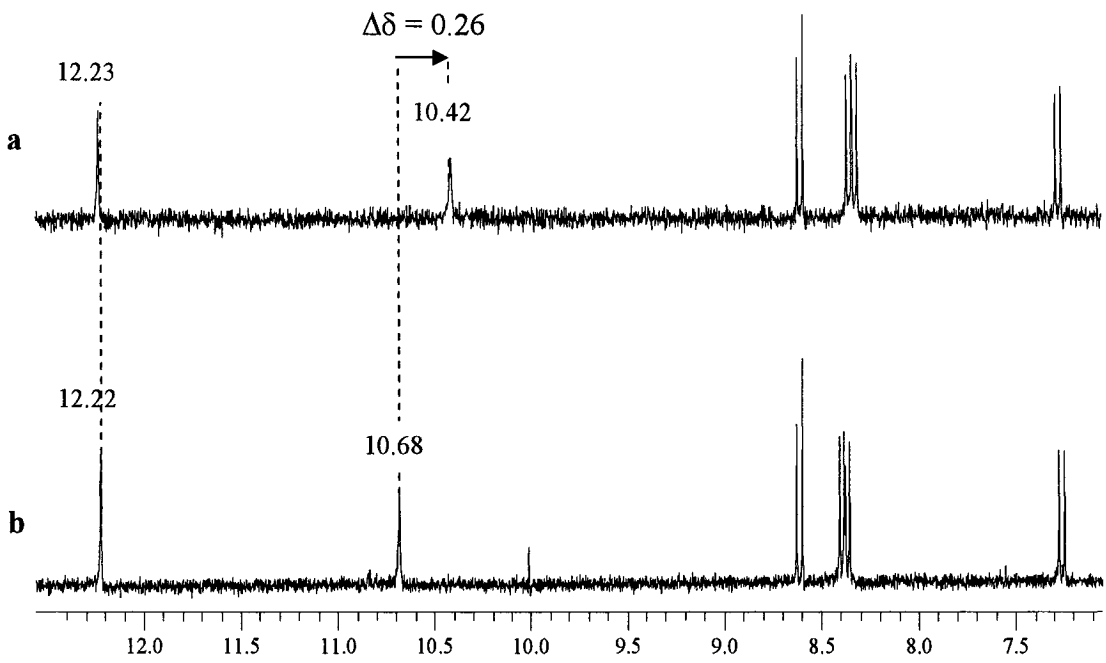

Figure 2.3. ^{1}H NMR spectra of macrocycle **6** at (a) 80 °C and (b) 24 °C; with DMSO-d_6 as solvent.

All N-H5 protons point outwards and are incapable of forming intramolecular hydrogen bonds. However it is possible for these protons to form intermolecular hydrogen bonds with the carbonyl oxygens of other macrocycles (Figure 2.4) even though ^{1}H NMR studies were carried out in DMSO-d_6 that normally disrupts intermolecular hydrogen bonds.[75] The chemical shift (10.68 ppm at ambient temperature) of N-H5 falls in the expected region for intermolecular hydrogen bonded urea protons.[70, 71, 76-78]

Intermolecular hydrogen bonding and π-π aromatic stacking are major reasons for the aggregation of this macrocycle in solution and its resulting low solubility. Compared to intramolecular hydrogen bonds, intermolecular hydrogen bonds are more easily

influenced by environmental changes such as concentration, solvent and temperature. The low solubility poses serious difficulties in carrying out concentration-dependent studies. Herein, only the results of variable temperature ^{1}H NMR experiments are discussed.

In Figure 2.3, the chemical shift of the N-H6 proton changed only slightly ($\Delta\delta$ = 0.01 ppm) when the temperature increased from 24 °C to 80 °C; while the signal of the N-H5 proton broadened and shifted upfield significantly ($\Delta\delta$ = 0.26 ppm). This result again shows that the intramolecular hydrogen bond network inside the cavity is rather strong and not affected by temperature variations.

Another type of hydrogen bonding present in macrocycle **6** is the Ar-CH···O around the periphery of the macrocycle (Figure 2.4).

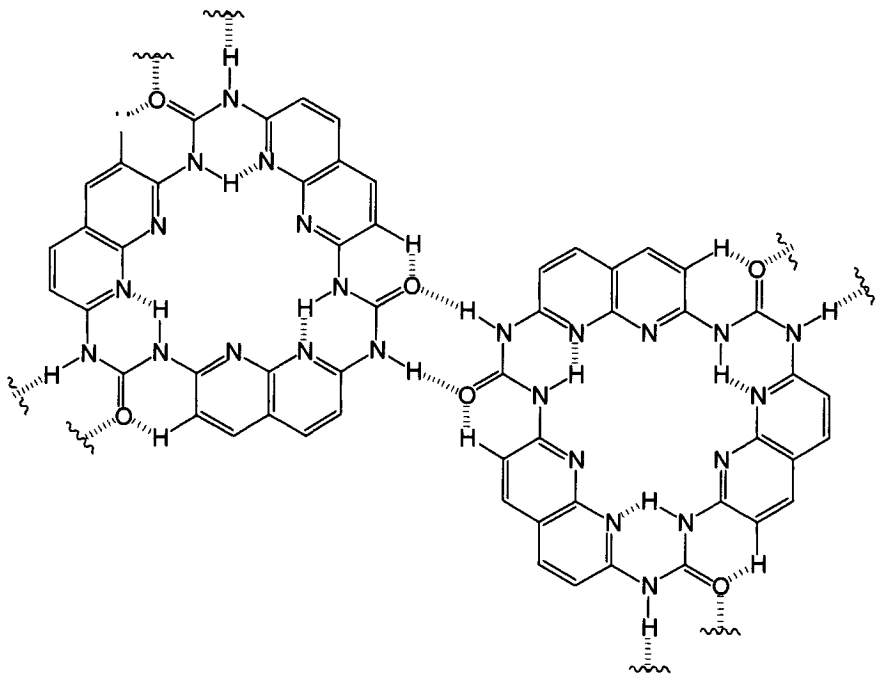

Figure 2.4. Aggregation in the plane of the naphthyridine ring enforced and stabilized by intermolecular hydrogen bonds.

The CH···O interaction is a weaker H-bond compared to the traditional XH···Y bond where both X and Y are electronegative atoms.[61, 62] However, it is regularly treated as an important factor to understand non-covalent interactions.[61, 79-84] In our case, the significance of this type of hydrogen bonding is reflected in the difference in chemical shifts ($\Delta\delta = 1.35$ ppm) between C-H1 and C-H4 that otherwise have the same connectivity (Figure 2.1 (a) & (c)). The electron withdrawing ability of the aromatic carbon to which H4 is connected is enhanced by being *ortho* to the urea functional group and *meta* to the naphthyridine nitrogen atom, and this, in turn, increases the acidity of H4 to make it a reasonable hydrogen bond donor.[85]

2.1.4.2 MS analysis

MS further confirmed the identity of macrocycle **6**. In Figure 2.5, the primary signal at m/z = 558.69 corresponds to the mass of the protonated macrocycle **6** ($C_{27}H_{18}N_{12}O_3$; exact mass = 558.16).

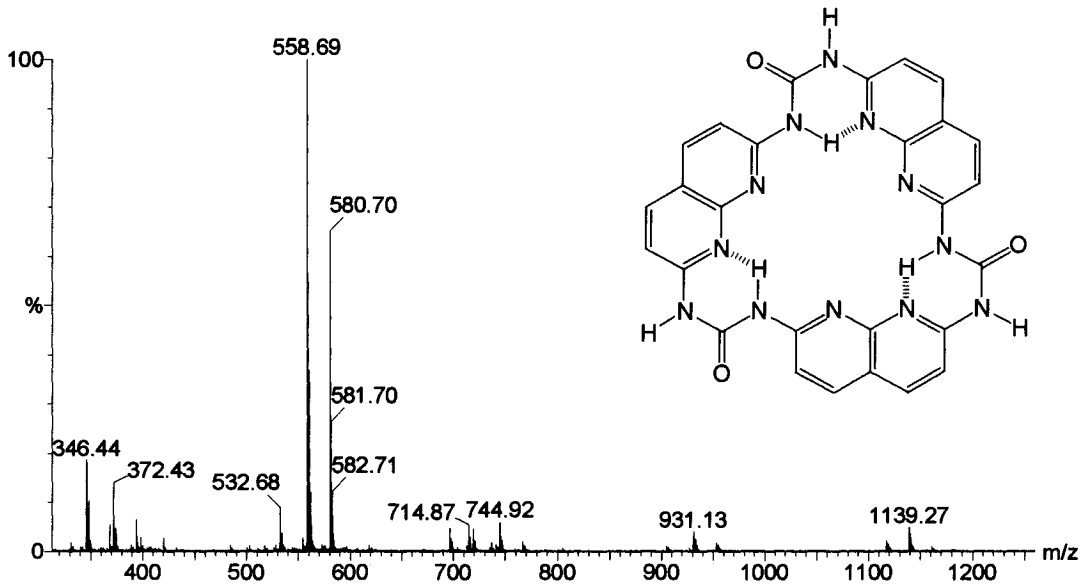

Figure 2.5. MALDI-TOF-MS of macrocycle **6** with DHB (2,5-hydroxylbenzoic acid) as matrix.

The signals at 580.69 that were *ca.* 22 mass units higher than the main signals are sodium ion adducts. The metal ion can come from the glassware used for the reaction and/or the workup. The expansion of these signal groups is shown in Figure 2.6.

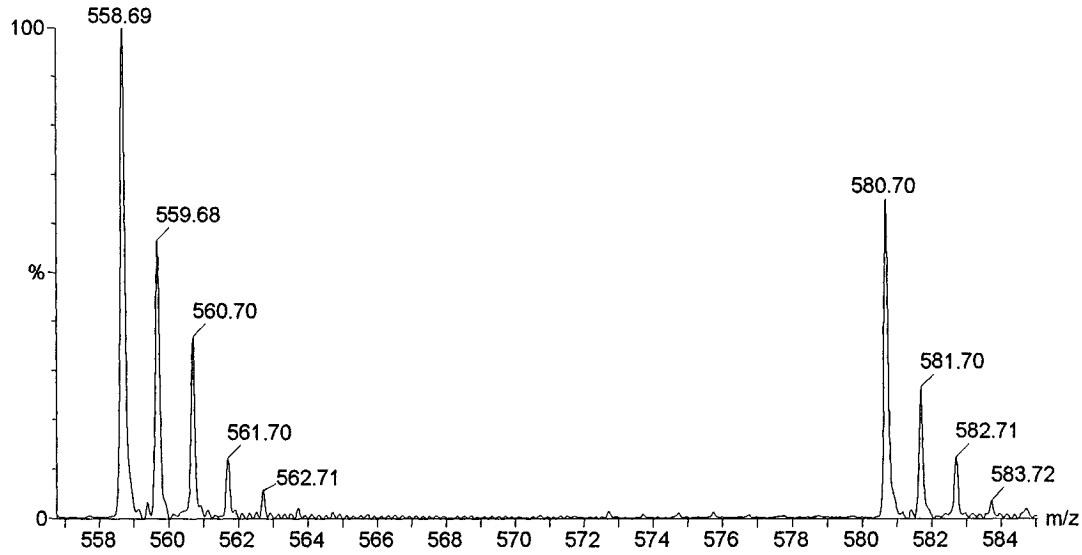

Figure 2.6. Isotopic distribution of $[M+H]^+$ and $[M+Na]^+$ of macrocycle **6**.

There are also other signals that appear at much higher mass. When the areas above m/z 1160, which are about twice the mass of the cyclic trimer are expanded, it shows two major signal groups (Figure 2.7). The first signal group starting from m/z 1117.25 corresponds to the mass of the protonated dimer $[2M+H]^+$ and the second signal group starting from m/z 1139.27 originates from the sodium adduct of the dimer $[2M+Na]^+$. The nature of the dimer observed in the mass spectra is unknown and may reflect the self-aggregation of the molecules in the solid state or may be formed during the ionization process.

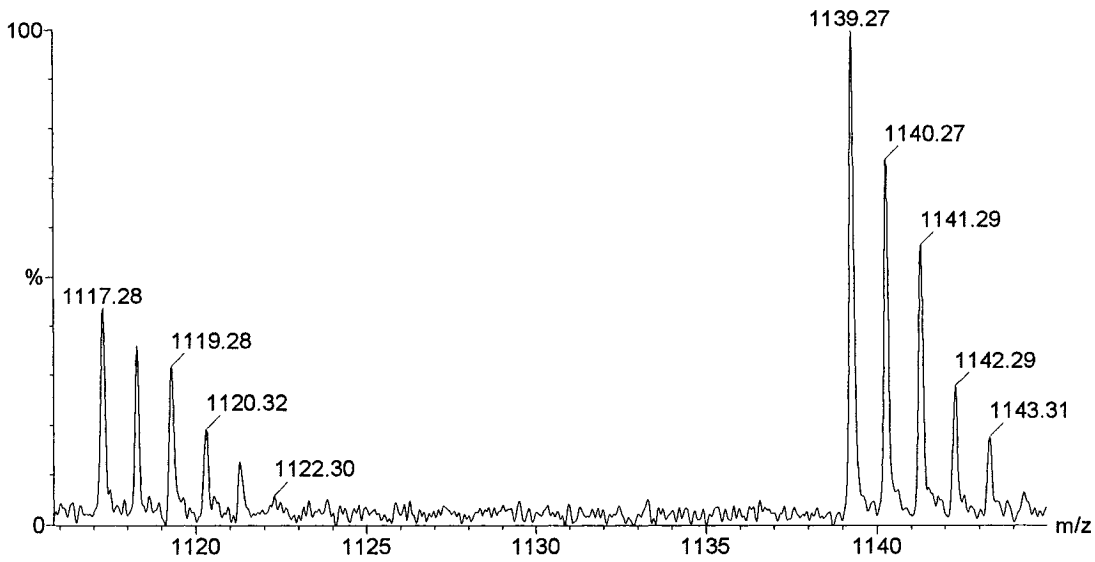

Figure 2.7. Isotopic distribution of $[2M+H]^+$ and $[2M+Na]^+$ of macrocycle **6**.

Besides macrocycle **6**, some other minor products could also be observed in the mass spectrum (Figure 2.5) and, surprisingly, they correspond to other macrocycles. No signs of linear oligomers or polymers were detected. The signal group at m/z 372.43 corresponds to protonated macrocyclic dimer with the formula $C_{18}H_{12}N_8O_2$ and exact mass 372.10. The sodium associate appeared at 394.50. The signals at 744.92 ($[M+H]^+$) and 766.94 ($[M+Na]^+$) are consistent with a cyclic tetramer ($C_{36}H_{24}N_{16}O_4$, exact mass = 744.22), while the signals at 931.13 ($[M+H]^+$) and 953.12 ($[M+Na]^+$) correspond to a cyclic pentamer ($C_{45}H_{30}N_{20}O_5$, exact mass = 930.27). Poor solubility and low yield are the major problems encountered to isolate these macrocycles from each other and to perform further investigations. However, this does not indicate that they are less important or cannot be synthesized as independent compounds in the future. Compared with macrocycle **6** that has the ideal geometry to be flat, the urea groups of other macrocyclic compounds require conformational changes to compensate for steric strain.

Jiang *et al.* reported the serendipitous discovery of a strained tetrameric oligoamide macrocycle that could be used as molecular clips.[30] Under the current experimental conditions, these macrocycles (dimer, tetramer and pentamer) are extremely minor products that were only detected by mass spectrometry. In comparable systems,[30, 69] by raising the reaction temperature, higher yields of kinetically less favored products can result.

2.1.4.3 The self-templating process

For disubstituted ureas, the conjugation between the carbonyl group and amino nitrogen results in partial double bond character of the urea linkage, so that free rotation about the urea C–N bond is restricted. Conformational studies were carried out on 3-dipyridyl thioureas by Sudha *et al.*[86] and pyrid-2-yl ureas by Chien *et al.*[76] Their results, based on experiments and calculations, revealed that when 2-aminopyridine was converted to a urea or thiourea group, the E-Z[87] conformation is adopted in both solution and the solid state due to intramolecular hydrogen bonds.

In our case, the naphthyridine group of 2,7-diamino-1,8-naphthyridine can be considered as two fused pyridine rings, and the folding/cyclization process is directed by the preferred E-Z conformation encoded in the individual subunits (Figure 2.8). In this conformation, the urea protons and the non-adjacent naphthyridine nitrogen lone pairs, as well as the carbonyl oxygen and adjacent naphthyridine proton (Ar-CH···O) are well aligned to form intramolecular hydrogen bonds. Moreover, the unfavorable dipole repulsion between the naphthyridine nitrogens and carbonyl oxygen, and steric repulsion between the urea proton and the adjacent *ortho* naphthyridine proton are avoided.

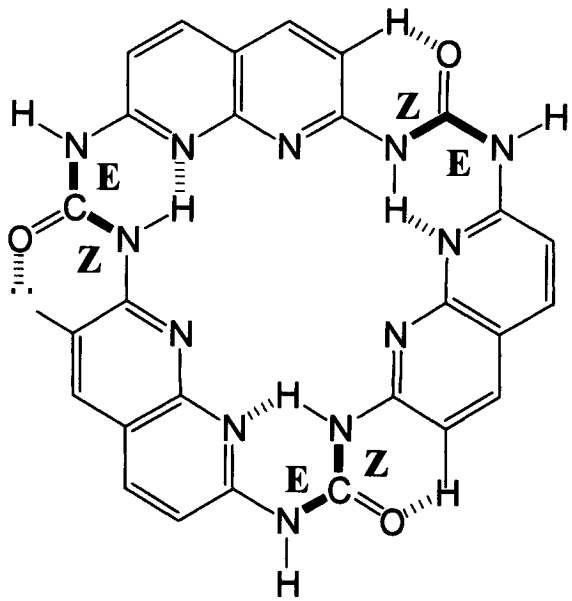

Figure 2.8. Illustration of the preferred consecutive E-Z/E-Z/E-Z conformations of trimeric macrocycle **6**. Urea C-N bonds are highlighted; hydrogen bonds are represented with dashed lines.

The folding process in the formation of macrocycle **6** can be interpreted on the basis of conformational preferences of the individual urea subunits[29] shown in Figure 2.9. The curved conformation adopted by the intermediate dimer composed of two naphthyridine rings sets the tone for the sequential reaction to favor cyclization over linear polymerization (Scheme 2.4).

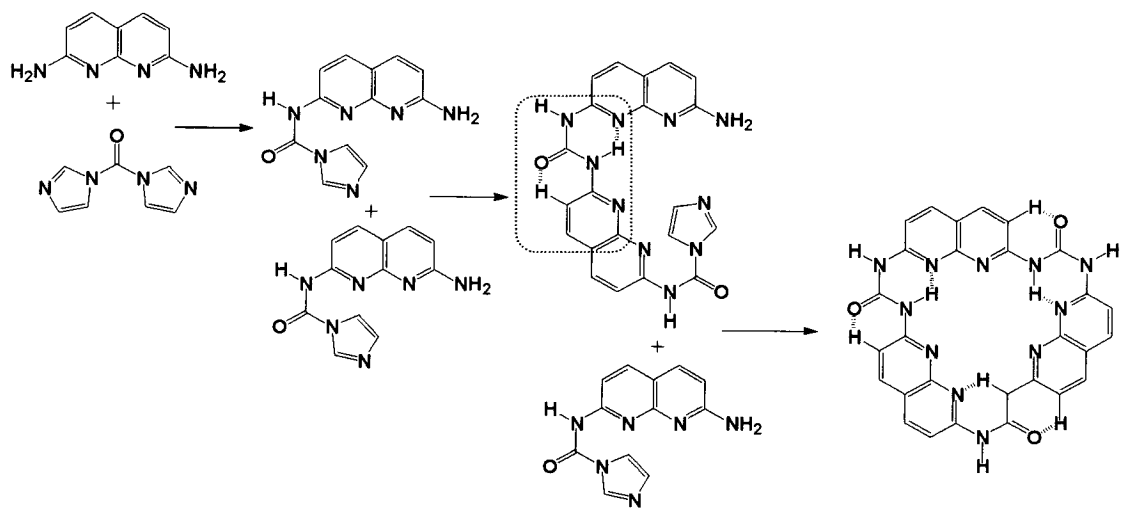

Scheme 2.4. A proposed pathway for the formation of macrocycle **6**.

2.1.5 Conclusions and future work

In the bifunctional condensation reaction between 2,7-diamino-1,8-naphthyridine and 1,1'-carbonyl diimidazole, trimeric macrocycle **6** was synthesized as the predominant product and was characterized by MALDI-TOF-MS and ^{1}H NMR. The cyclisation was self-directed by six-membered intramolecular hydrogen bonding between urea protons and napthyridine nitrogen lone pairs inside the ring, and between the *ortho* naphthyridine protons and the carbonyl oxygens around the periphery. In this reaction, hydrogen bonding plays the role of a template that holds the reaction intermediates in a conformation that favors macrocyclisation.[29, 88]

With a relatively spacious cavity and several donor and acceptor sites, this trimeric macrocycle is expected to find applications in both fundamental and applied research.

2.2 Naphthyridyl formamidine macrocycle

2.2.1 Introduction

Amidine-containing compounds are the nitrogen analogs of carboxylic acids and esters and they are the subject of studies in medicinal chemistry, organometallic chemistry, polymer chemistry, etc.[89] The lone pair of the amino nitrogen forms a conjugated system with the imino π-system to make the N=C-N moiety coplanar where both carbon nitrogen bonds have partial double bond character.[89, 90] For formamidine, the formal hydrogen is electron-deficient due to the electron withdrawing effect from the nitrogen atoms, which make it a possible hydrogen bond donor.[91-94]

Compared to some more frequently used functional groups, such as amides,[29-31, 95-103] ureas,[64, 66-68, 104, 105] and ethynylenes[88, 106-109] in designing structures with well-defined conformations, the formamidine motif receives much less attention than it deserves. In 1995, Böhme and coworkers reported the synthesis of a cyclic pyridyl formamidine trimer (Scheme 2.5).[110-112]

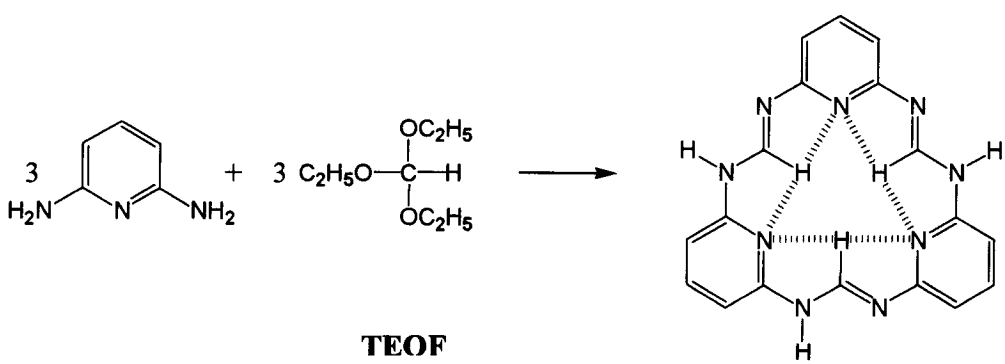

Scheme 2.5. The synthesis of macrocyclic formamidine compound **VIII** by Böhme *et al.*

The trimeric macrocycle **VIII** was the major product from the reaction of 2,6-diaminopyridine with triethylorthoformate (TEOF) and the favorable hydrogen bonding interaction between the formal protons and the pyridine nitrogen lone pairs was observed using ^{1}H NMR.[110] The conformation shown in Scheme 2.5 in the solid state was verified with X-ray powder diffraction in conjunction with theoretical calculations.[112] A control experiment was executed by replacing pyridyl-2,6-diamines with 1,3-phenyl diamines that produced a series of oligomers. The lack of hydrogen bonding interactions in the latter case was proposed to be the major reason to account for this difference. Theoretical and experimental investigations show that the formal hydrogen atoms point inside the ring due to the favorable interactions between the pyridyl lone pairs and the formal hydrogen atoms.[110, 112, 113]

In this section of the thesis, the synthesis and characterization of macrocycle **7** with naphthyridine building blocks and formamidine linkages is described, which further exemplifies the self-templating macrocyclization process featuring non-covalent interactions. Dipole moment minimization, steric repulsion and especially intramolecular hydrogen bonding formed between the formal hydrogen and the naphthyridyl nitrogen lone pairs drive macrocyclization. The naphthyridine ring can be thought of as an extended pyridine ring possessing two nitrogen electron lone pairs. The resulting formamidine-linked macrocycle can be more coplanar and has a more spacious inner cavity than the pyridyl analogue. This larger cavity has the advantage to act as potential binding sites for guest molecules in supramolecular studies and for possible industrial applications.[114-118]

A well-established method for synthesizing formamidines is the reaction of a primary amine with triethylorthoformate (TEOF)[90, 110, 113, 119-121] that is commercially available. 2,7-diamino-1,8-naphthyridine **5** was synthesized in our lab and behaves as an ideal hydrogen bond acceptor (aromatic nitrogen lone pairs) and donor (amino hydrogens) in the trimeric urea macrocycle **6** discussed above. Diamine **5** underwent [3+3] condensation with TEOF in DMSO to obtain the formamidine-linked naphthyridyl macrocycle. ^{1}H NMR, ^{13}C NMR, MALDI-TOF-MS, IR and single crystal X-ray diffraction were used to characterize the final product.

2.2.2 Synthesis of naphthyridyl formamidine macrocycle (7)

Macrocycle **7** was prepared by the [3+3] condensation reaction between 2,7-diamino-1,8-naphthyridine and triethyl orthoformate (TEOF) in anhydrous DMSO as illustrated in Scheme 2.6.

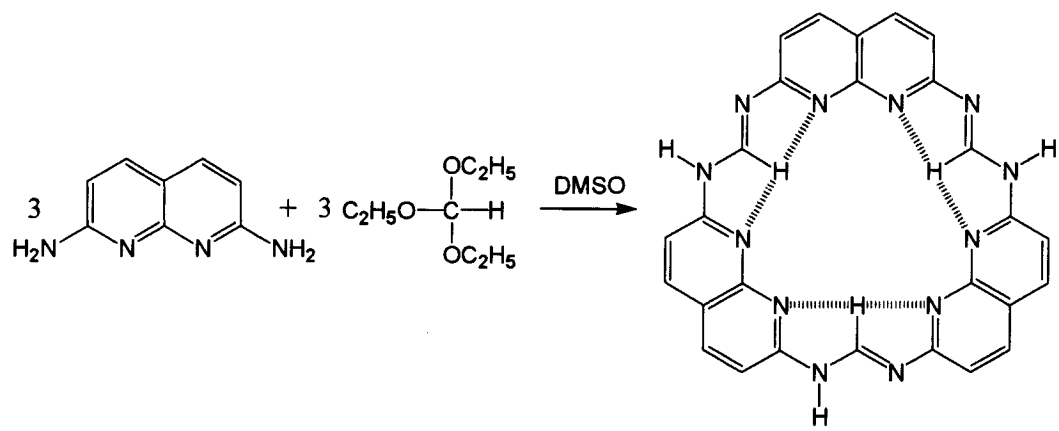

5 **TEOF** **7**

Scheme 2.6. Synthesis of macrocycle **7**.

Diamine **5** formed a yellow suspension in DMSO at 120 °C to which TEOF was added. The suspension became clear at once to form a bright yellow solution that turned to dark orange quickly. After 24 hours, the product was precipitated from the mixture with methanol. The solid was washed with cold methanol and dried under vacuum.

2.2.3 Results and discussion

2.2.3.1 MS analysis

The product was examined with MALDI-TOF-MS with *trans*-3-indoleacrylic acid (IAA) as matrix. The spectrum obtained showed a very simple signal pattern with only one major signal group and several minor groups (Figure 2.9). The primary peak at m/z 510.93 corresponds to the mass of a protonated cyclic trimer ($C_{27}H_{18}N_{12}$, 510.18), followed by the metal ion associates with sodium ($[M + Na]^+$) and potassium ($[M + K]^+$) at 532.94 and 548.93, respectively. The expansion of the spectrum is shown in Figure 2.10.

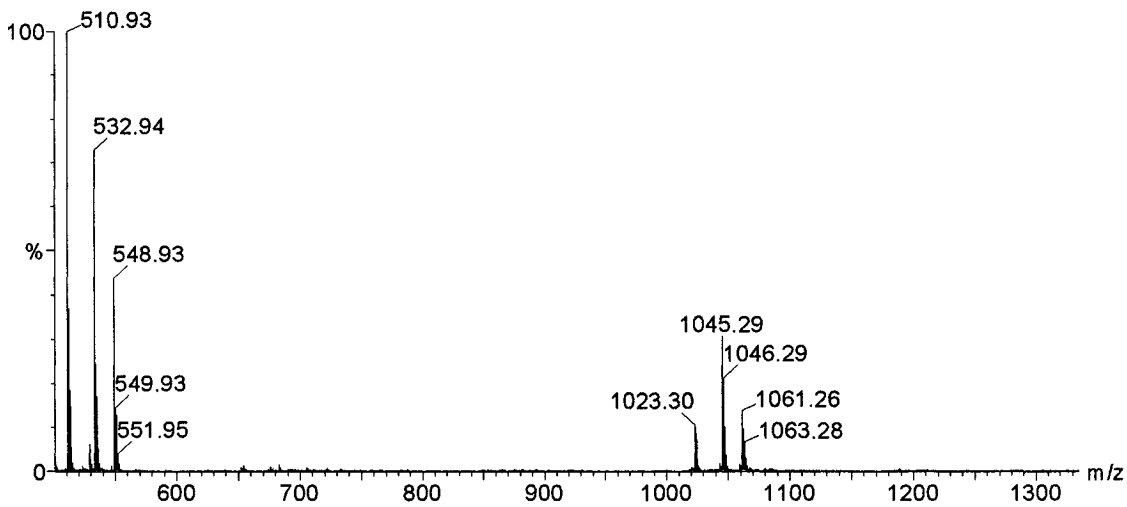

Figure 2.9. MALDI-TOF-MS macrocycle 7 with IAA as matrix.

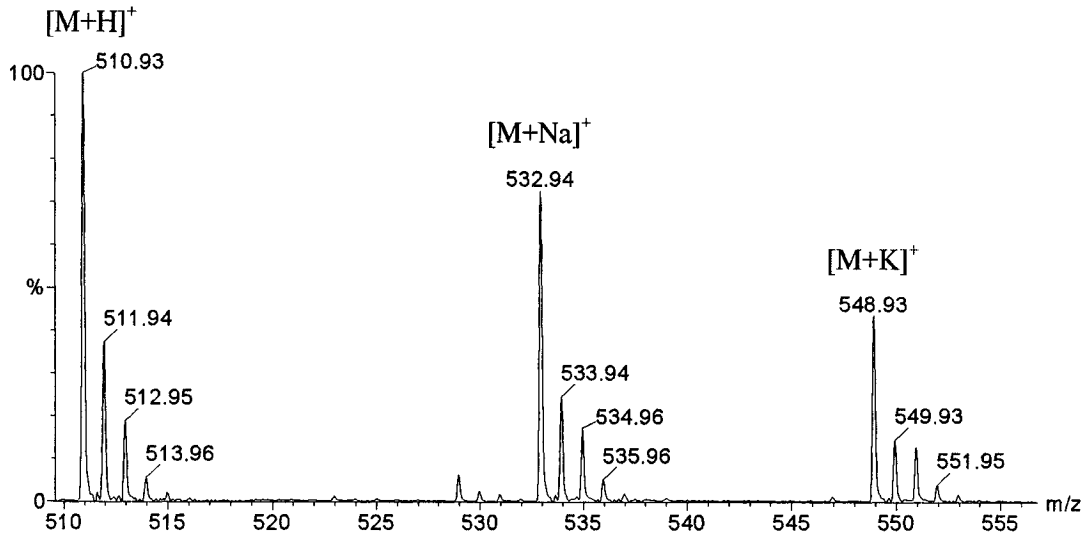

Figure 2.10. Isotope distribution pattern of proton, sodium and potassium ion adducts of macrocyle 7.

The minor signal groups starting with peak m/z 1023.30 is consistent with the dimer of 7 with the corresponding metal ion associates with sodium and potassium appearing at m/z 1045.29 and 1061.26, respectively (Figure 2.11).

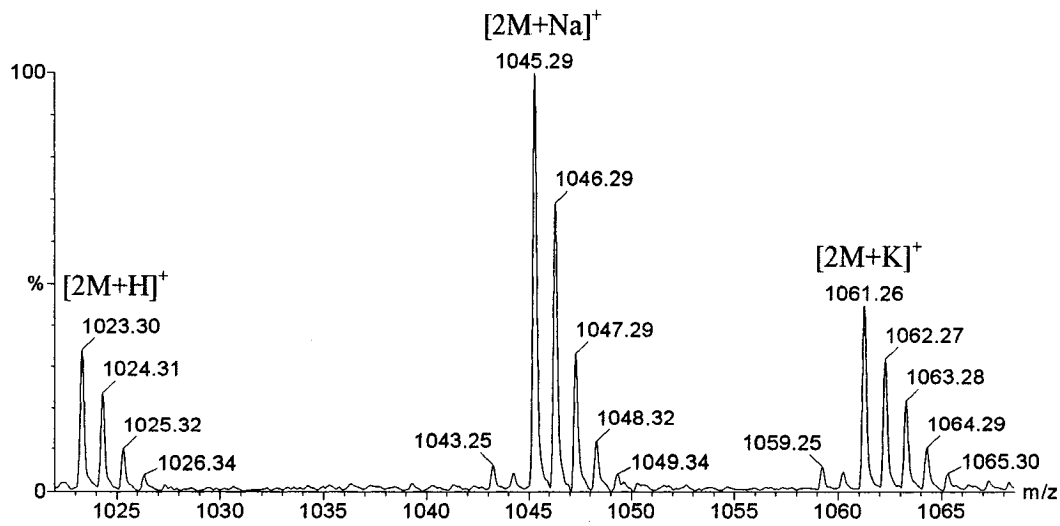

Figure 2.11. Isotope distribution pattern of proton, sodium and potassium ion adducts of dimerized 7.

2.2.3.2 Crystal structure

The solid-state structure of macrocycle 7 (Figure 2.12) was obtained by X-ray diffraction analysis of a single crystals that was grown from a DMSO / Methanol solvent mixture as yellow needles.

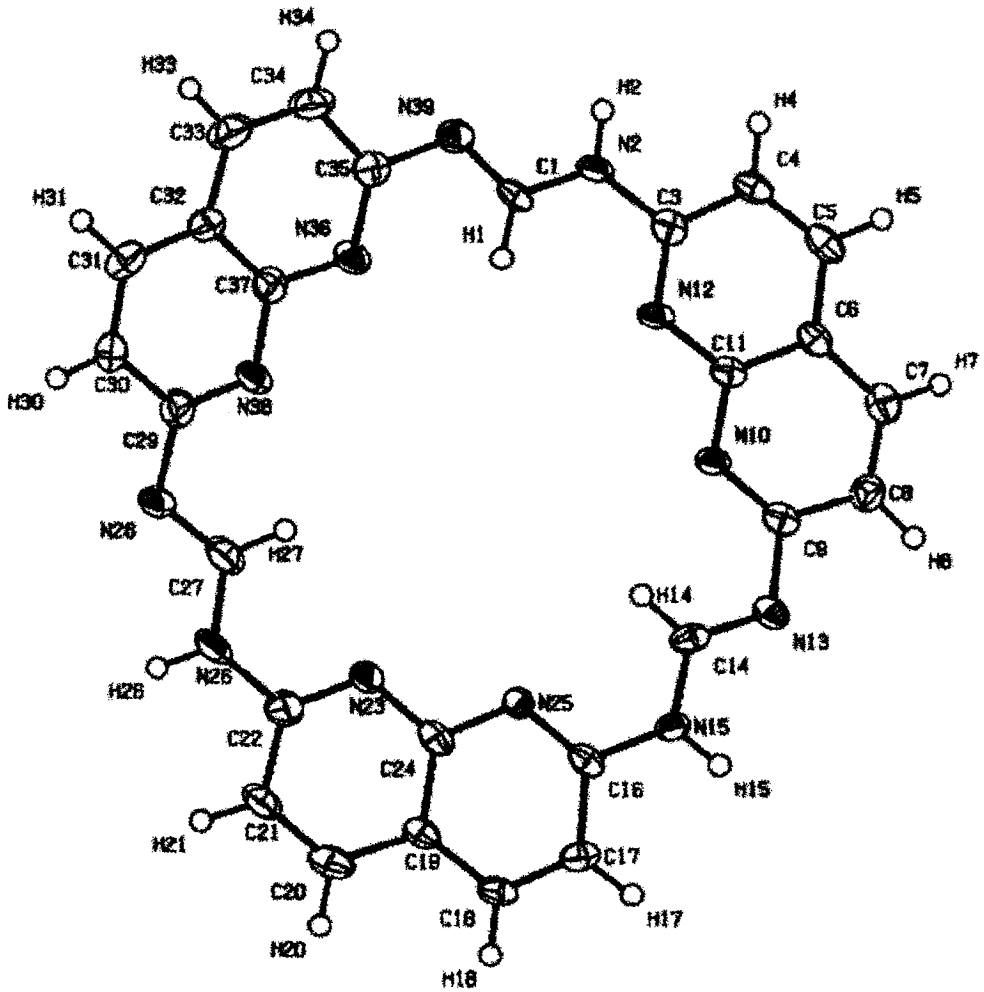

Figure 2.12. ORTEP view of formamidine macrocycle 7. The solvent molecules are omitted for clarity.

The 24-membered macrocycle is composed of three *ortho* bis-substituted naphthyridine rings linked by formamidine functional groups and adopts an essentially planar conformation (Figure 2.13).

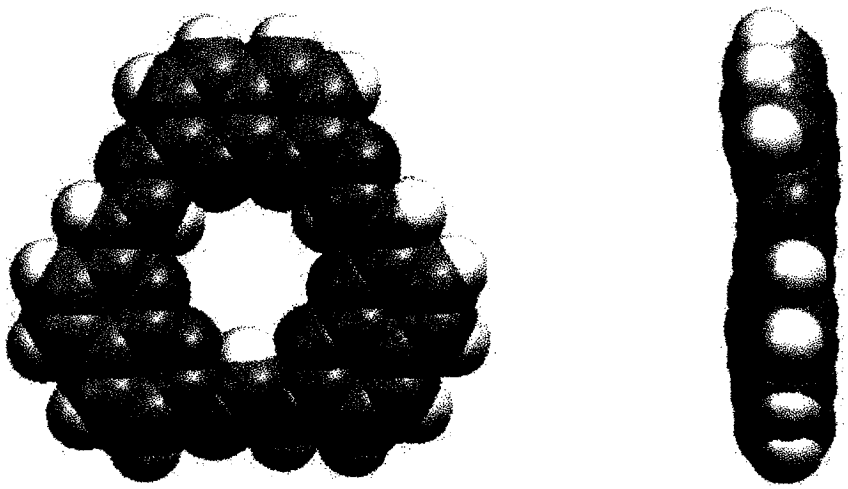

a b

Figure 2.13. (a) Top and (b) side view of space-filling representations of macrocycle 7.

All the formal hydrogens point inward, forming 3-centered intramolecular hydrogen bonds (S5[75]) with the adjacent naphthyridine nitrogen lone pairs (Figure 2.14). The intramolecular hydrogen bond networks are believed to be the major forces that induce and stabilize the coplanar conformation.

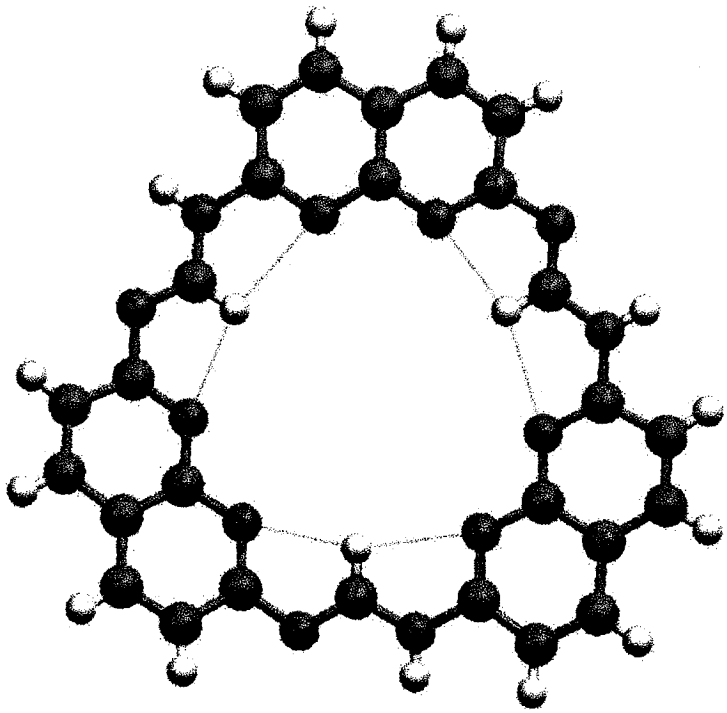

Figure 2.14. Three-centered intramolecular hydrogen bonding network (represented by blue dot line) inside the cavity of crystal **7**.

The formamidine amino protons are involved in intermolecular hydrogen bonding with oxygen of the included methanol and DMSO solvent molecules (Figure 2.15).

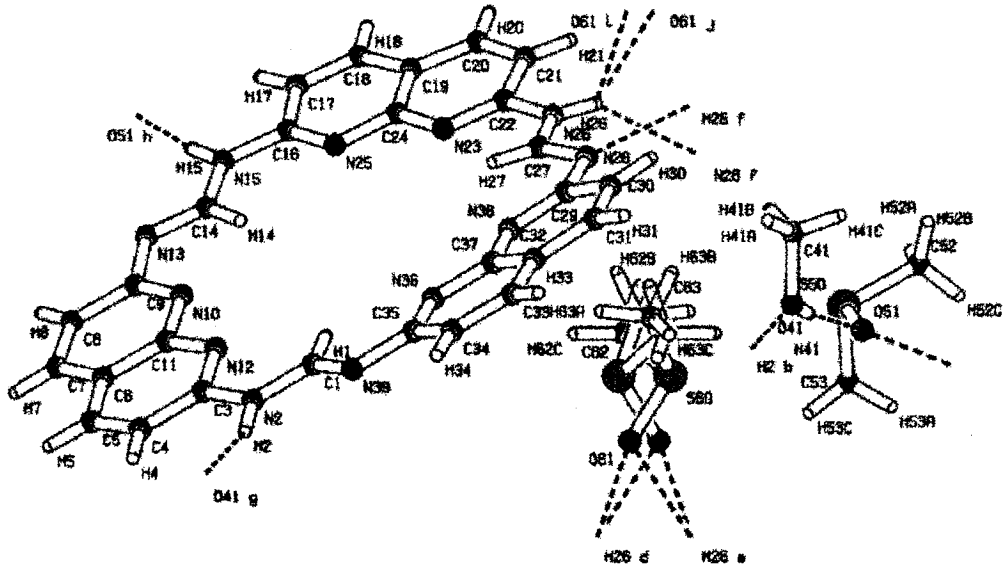

Figure 2.15. Intermolecular hydrogen bonds formed between formamidine amino N-H and oxygen lone pairs of methanol and DMSO molecules.

Some selective hydrogen bonding geometry data (bond length Å and angle °) are given below (Table 2.1) and complete crystallographic data are in Appendix A.

Table 2.1. Hydrogen-bonding bond length (Å) and bond angle (°).

D—H···A	D—H	H···A	D···A	D—H···A
N2—H2···O41i	0.88	1.99	2.832	160.5°
N15—H15···O51ii	0.88	1.96	2.832	170.3°
N26—H26···O61iii	0.88	2.28	2.773	115.1°
N26—H26···O61iv	0.88	2.34	3.017	133.4°
O41—H41···O51	0.84	1.86	2.692	168.5°
N10—H14···N25	2.277	2.502	4.702	159.4°
N23—H27···N38	2.501	2.309	4.709	156.4°
N36—H1···N12	2.307	2.502	4.740	160.6°

In the crystal structure, one of the formamidine groups appears reversed in comparison to the other two formamidine groups (Figure 2.16a). In this conformation, two imino double bonds could conjugate with one aromatic ring (a); while in the symmetric conformation, no such extended conjugation is possible (Figure 2.16b).

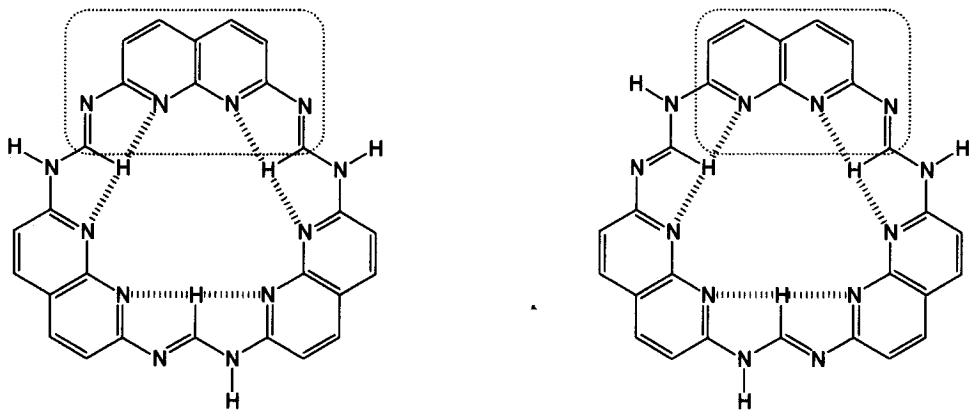

a **b**

Figure 2.16. Different conjugation patterns in (a) asymmetric and (b) symmetric isomers of macrocycle **7**. The dotted squares highlight the largest conjugation that could be formed in both isomers.

In the crystal structure, macrocycle **7** packed into interdigitated vertical columnar arrays through aromatic π-π stacking (Figure 2.17). Interestingly, the naphthyridine moiety highlighted in Figure 2.16(a) was the overlapped part of two adjacent interdigitated stacks.

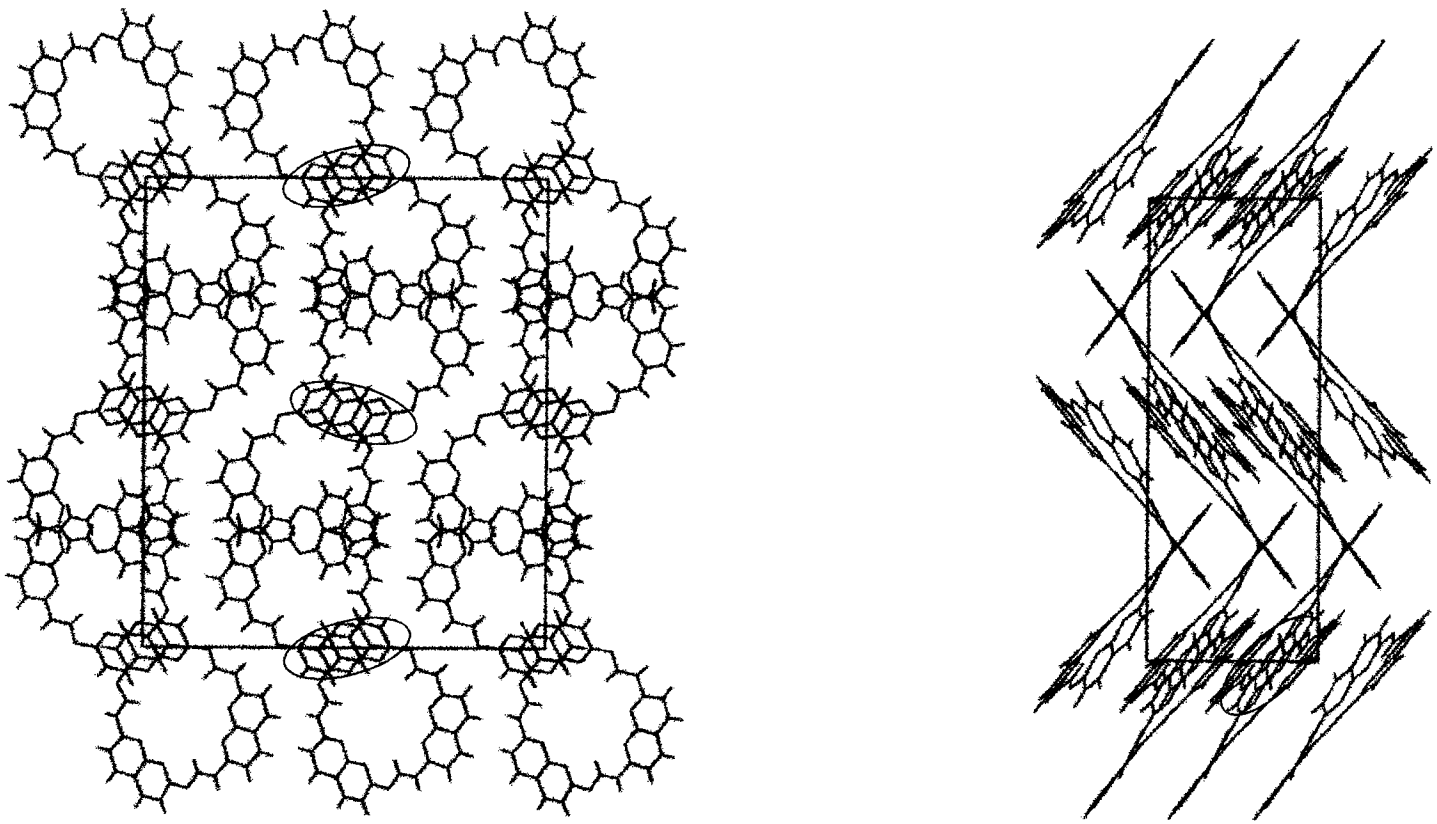

a b

Figure 2.17. (a) Top view & (b) side view of the packing pattern in crystal **7**. The interdigitated napthyridine rings are highlighted red.

2.2.3.3 NMR analysis

The ^{1}H NMR spectrum obtained for macrocycle 7 in DMSO-d_6 shows only four sets of signals (Figure 2.18) that were assigned based on the crystal structure. The sharp singlet at 10.42 ppm was assigned to the formal hydrogen that is in agreement with the analogous cyclo-tris (2,6-pyridylformamidine) reported by Böhme *et al*[110, 111]. This formal hydrogen signal is shifted significantly downfield compared to other aromatic formamidine compounds that normally appear between 7.83-8.26 ppm.[110] The three-centered hydrogen bonding to the naphthyridine nitrogen lone pairs and the electron withdrawing effect from the naphthyridine rings are the main deshielding factors.

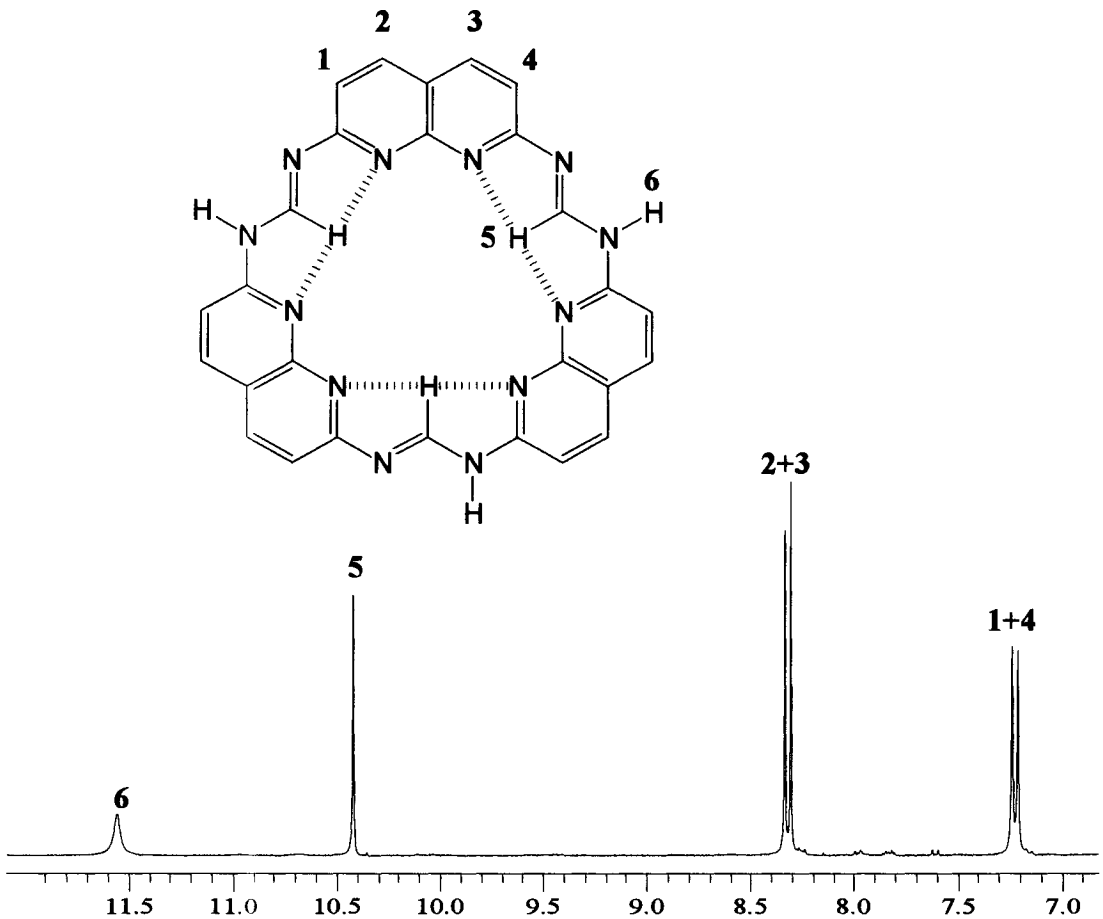

Figure 2.18. ^{1}H NMR spectrum of macrocycle 7 in DMSO-d_6.

The most downfield singlet at 11.27 ppm was assigned to the amino hydrogen with the aid of deuterium exchange experiments (Figure 2.19).

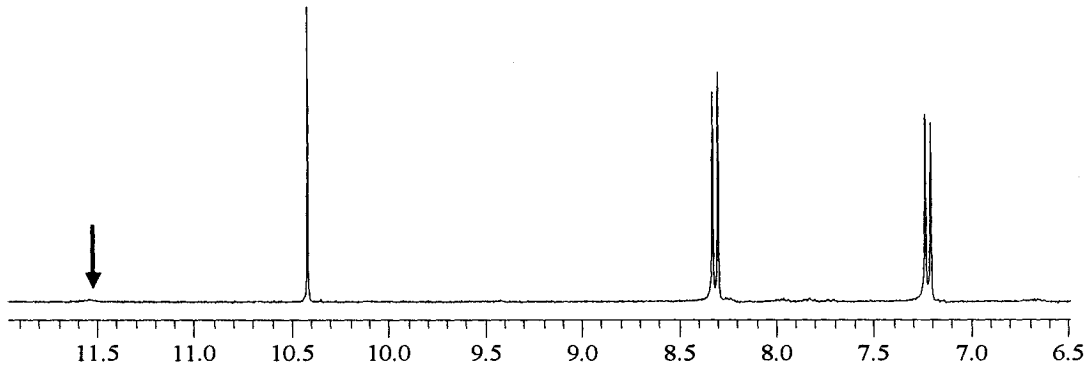

Figure 2.19. D/H exchange ^{1}H NMR experiment in DMSO-d_6. The spectrum was obtained 3 days after one drop of methanol-d_4 was added to the NMR tube. The arrow points to the residual signal after deuterium exchange.

The deshielding is probably caused by the electron withdrawing effect from naphthyridine and the imino groups and intermolecular hydrogen bonding as shown in the crystal structure. The broadened shape of the amino hydrogen indicates rapid intermolecular proton exchange by forming cyclic dimers that may be catalyzed by protic solvent[90, 111, 122] (Figure 2.20). Relatively strong water signals with magnitudes similar to that of the DMSO residue (0.2 %) were observed in the spectra.

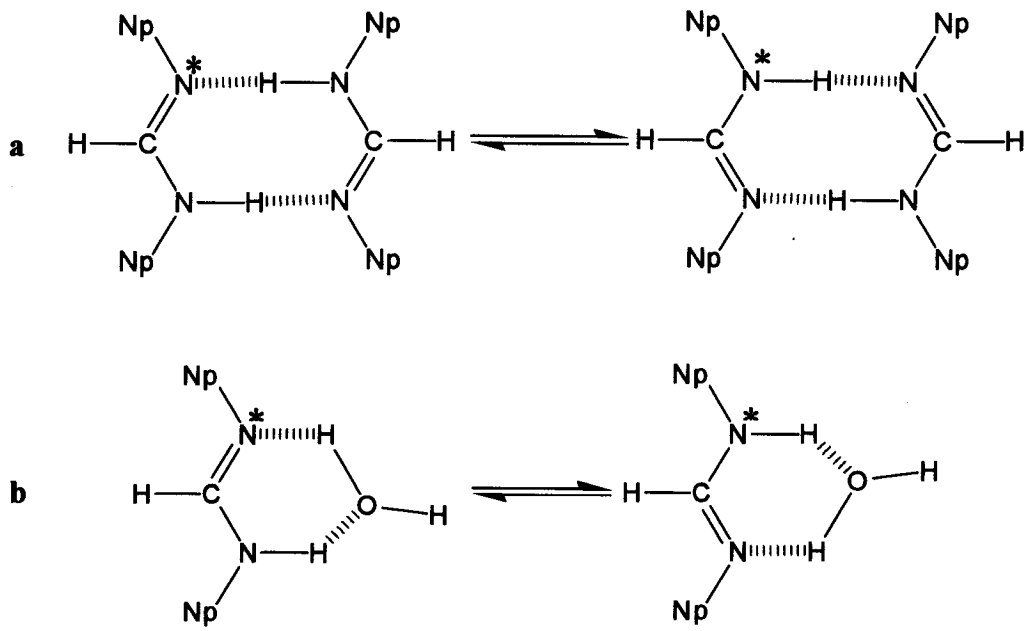

Figure 2.20. Proton exchange (a) in a cyclic dimer; (b) catalyzed by a water molecule. Np represents a naphthyridine ring.

The temperature dependent behavior in the variable temperature NMR experiments (Figure 2.21) provides more evidence that the amino hydrogen is involved in intermolecular interactions. Contrary to the formal hydrogen that was shifted downfield slightly (0.03 ppm), the amino hydrogen was shifted upfield significantly (0.34 ppm) as temperature increased from 24 °C to 90 °C.

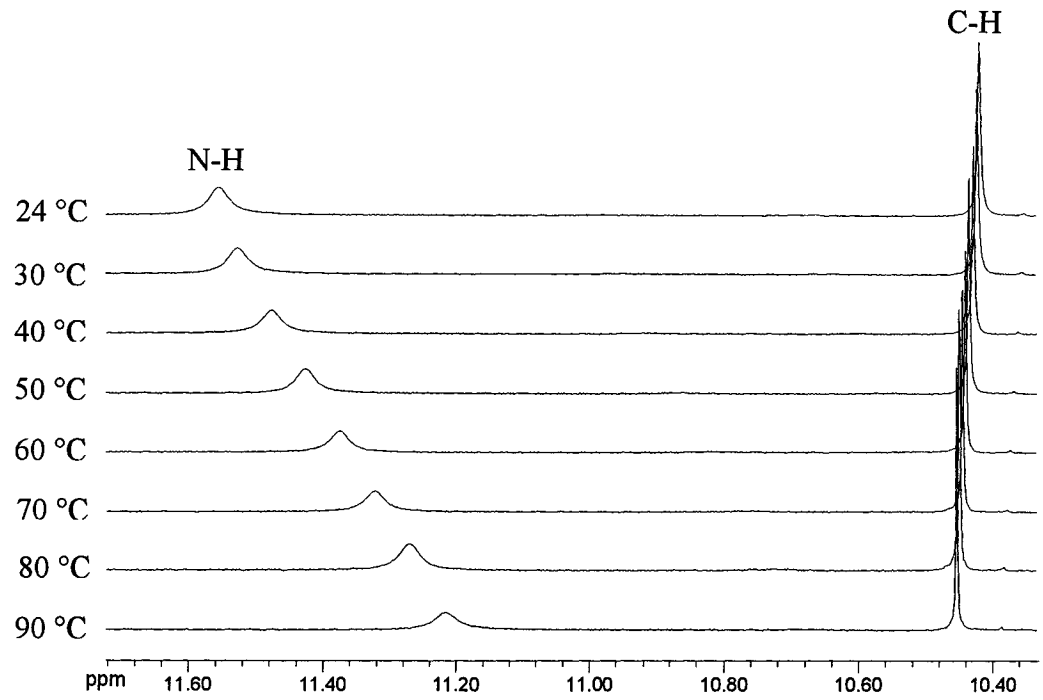

Figure 2.21. Variable temperature ^{1}H NMR spectra in DMSO-d_6.

The 'proton jump'[122] between two formamidine nitrogens illustrated in Figure 2.20 is also responsible for the apparent symmetry displayed in the simple NMR spectrum in which only two aromatic peaks are observed. Komber and coworkers investigated the proton exchange at the formamidine group on cyclo-tris(4-R-2,6-pyridylformamidine)s (R = H, CH_3) in solution with low-temperature NMR experiments.[111] Their results showed that fast intermolecular proton exchange results in interconversion of two types of tautomers: symmetric (S) and asymmetric (A) resulting in averaged NMR signals at room temperature. The doublet at higher field (7.22 ppm) could be assigned to the naphthyridine hydrogen *ortho* to the formamidine group and the lower field doublet can be assigned to the *meta* hydrogens.

2.2.3.4 Conformational analysis

The formation of a macrocycle instead of polymers in the bifunctional condensation between 2,7-diamino-1,8-naphthyridine and triethylorthoformate indicates that certain curved conformation(s) should predominate in the intermediate(s) and facilitate macrocyclization.

According to theoretical and experimental studies on N'-pyridylformamidines (Pyridyl-N_{im}=CH-N_{am}-),[92-94, 113] conformation (a) in Figure 2.22 is expected to be favored over conformation (b).

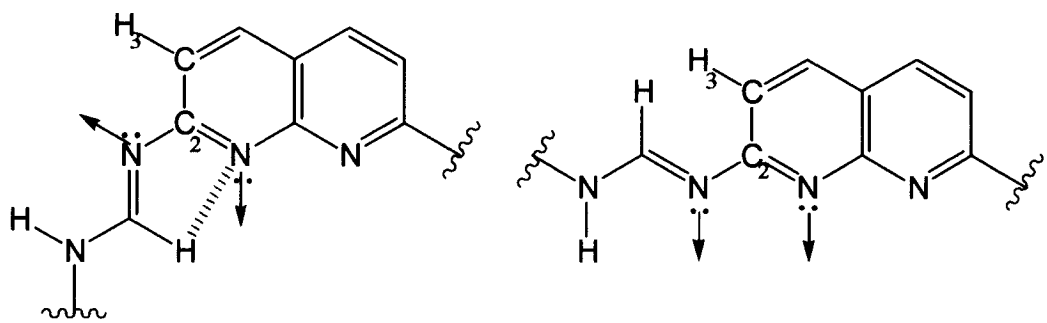

Figure 2.22. Conformations in one naphthyridyl-formamidine unit: (a) is adopted by macrocycle 7; (b) leads to linear polymers. Hydrogen bonds are represented by dashed lines and dipole moments by arrows.

The conjugation of the formamidine double bond with the naphthyridine ring affords partial double bond character to C2-N_{im}, thus restricting the free rotation about this bond. In conformation (a), electronic repulsion between the imino nitrogen lone pair and the naphthyridine lone pair(s) is minimized and the unfavorable steric interaction

between H3 and the formal H shown in conformation (b) is avoided. Furthermore, hydrogen bonds are formed between the formal hydrogen and the adjacent naphthyridine nitrogen lone pair to further stabilize the curved conformation.[91-94, 113] Apparently, the dimer (two naphthyridine rings linked by one formamidine functional group) is the most important intermediate that favors the cyclization process over polymerization. With all the naphthyridine nitrogen atoms and formamidine hydrogens involved, the hydrogen bond network inside the macrocycle strictly locks the formal motif coplanar with the aromatic rings. In the pyridyl macrocycle **VIII** reported by Böhme and coworkers (Scheme 2.5), with one pyridyl nitrogen lone pair bonded to two formal hydrogen atoms, the strength of the hydrogen bond network is expected to be weakened. In their work, based on the combination of X-ray powder diffraction and theoretical calculations, one formamidine group was found to be out of plane, which is probably caused by the lower electron contributing ability when one nitrogen lone pair has to be shared to form two hydrogen bonds.[110, 112]

2.2.4 Conclusions and future work

A 24-membered macrocycle **7** was synthesized in a one-step condensation reaction between 2,7-diamino-1,8-naphtyridine and triethylorthoformate and characterized with various spectroscopic techniques. All three formal hydrogens point inside the macrocyle to form intramolecular hydrogen bonds with the naphthyridyl nitrogen lone pairs. The three-centered hydrogen bonds (N_{np}-H_f-N_{np})[123] lock the formamidine group coplanar with the naphthyridine rings. The folding information is encoded in the subunits and guides the cyclization process. While macrocycle **7** is asymmetric in the crystal structure, it displayed averaged NMR signals in solution at room temperature that can be explained by proton transfer between the amino and imino nitrogens. In the crystal structure, macrocycle **7** packs into a supramolecular columnar structure by offset face-to-face aromatic π-stacking.[124]

With a relatively spacious cavity, essentially flat conformation, abundant electron donor and acceptor groups, and a propensity to self-assemble by π-π stacking interactions, macrocycle **7** might find applications in organometallic and catalytic chemistry, biochemistry, supramolecular chemistry and materials science.[64, 67, 68, 111, 116] One problem with this macrocycle is its poor solubility, though it is more soluble than macrocycle **6** due to less intensive intermolecular interactions, it will still pose serious difficulties when potential applications are concerned. Derivatization of the formamidine amino group and/or the naphthyridine ring with solubilizing alkyl chains is underway. Investigations of the physical properties and practical applications of macrocycle **7** and its derivatives will be the focus of future studies in our group.

Chapter 3

Pyridazine-based macrocycles and folding oligomers

3.1 Introduction

In our lab, we have designed three types of macrocycles and oligoureas with alternating 3,6-pyridazine/2,6-toluene, 4,6-pyrimidine/2,6-toluene and 2,3-pyrazine/2,6-toluene repeating units to investigate the folding phenomena driven by noncovalent interactions (*i.e.* hydrogen bonding and steric interactions (Chapter 1)). Significant progress has been made in these systems where the goal set for the 3,6-pyridazine/2,6-toluene system is realized and presented in this part of the thesis.

The 3,6-pyridazine/2,6-toluene macrocycles and foldamers are obtained with largely the same synthetic methodology by reacting 3,6-diaminopyridazines with tolylene-2,6-diisocyanate (TDI) to form urea linkages (*N.B.* *o*-tolylene-isocyanate (OTI) was used to cap the oligomer strands). The structures are illustrated in Figure 3.1, where the hydrogen bonding interactions between urea protons and pyridazine nitrogen lone pairs are expected to be the major driving force for curvature formation in conjunction with the *para*/*meta* substitution pattern of the aromatic moieties in the backbone.

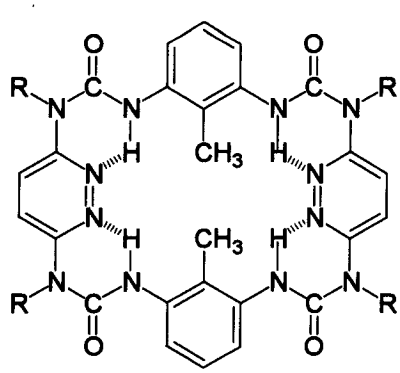

20 R = Ph-$C_{10}H_{21}$,
21 R = *n*-$C_{12}H_{25}$,
22 R = *i*-C_4H_9

a

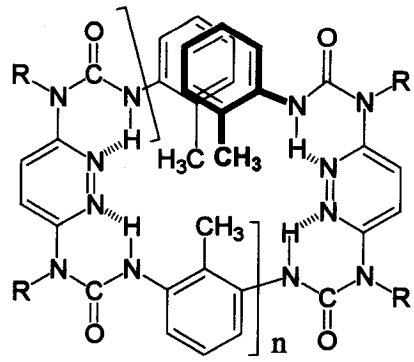

24 n = 0 R = *i*-C_4H_9
26 n = 1 R = *i*-C_4H_9

b

Figure 3.1. Chemical structures of 3,6-pyridazine/2,6-toluene: (a) macrocycles and (b) foldamers.

The macrocycles, composed of two alternating *p*-pyridazine/*m*-toluene repeat units, were prepared to test the folding propensity of this design and to provide the necessary groundwork for foldamer synthesis and characterization.[30, 31, 59] The macrocycles themselves are interesting target compounds to validate the effectiveness of self-templated macrocyclization methods and to study their unique physical and supramolecular properties. Macrocycles **20**, **21**, and **22** (Figure 3.1(a)) were synthesized by reaction of diamine **11**, **13**, or **15** with TDI in chloroform in a one-step condensation reaction, respectively. In order to test the effect of steric interactions between toluene methyl groups and urea carbonyl groups, a 3,6-pyridazine/1,3-benzene macrocycle **23** (Figure 3.2) was prepared as a control molecule by reaction of diamine **15** and 1,3-phenyl diisocyanate (PDI). The design principle was confirmed by the full characterization of the 3,6-pyridazine / 2,6-toluene macrocycles with NMR analysis in solution and X-ray

crystallography. A trimer **24** (n = 0) and a pentamer **26** (n = 1) were made to test the folding properties of urea-linked foldamers (Figure 3.1(b)).

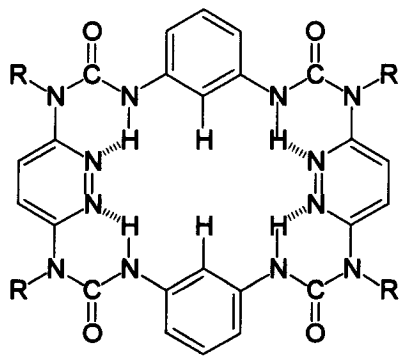

Figure 3.2. Chemical structure of 3,6-pyridazine/1,3-benzene macrocycle **23**.

A systematic protocol was used to synthesize a variety of diamines with different aromatic and aliphatic side chains that were also applicable to prepare 4,6-diaminopyrimidine and 2,3-diaminopyrazine. The isocyanate reagents (TDI, PDI and OTI) are commercially available. The preparation of 3,6-diaminopyridazines will be described first followed by the synthesis and characterization of macrocycles and foldamers.

3.2 Preparation of 3,6-diaminopyridazines

3.2.1 Introduction

Kumagai has carried out extensive research on the reactions between 3,6-dichloropyridazine and different amines[125]. Both mono- and bis-substituted pyridazine derivatives were isolated from the product mixture using aromatic amines but only mono-substituted pyridazine derivatives were obtained with aliphatic amines under similar reaction conditions. On the other hand, Vorbruggen and coworkers report the conversion of 3,6-dihydroxylpyridazine into 3,6-diaminopyridazines through a one-step silylation-amination procedure[126].

Solid phase synthesis is another interesting route to make diaminopyridazines. Parrot *et al.* reported the use of resin-bound thiophenol linkers to obtain a wide range of disubstituted pyridazines following Scheme 3.1[127].

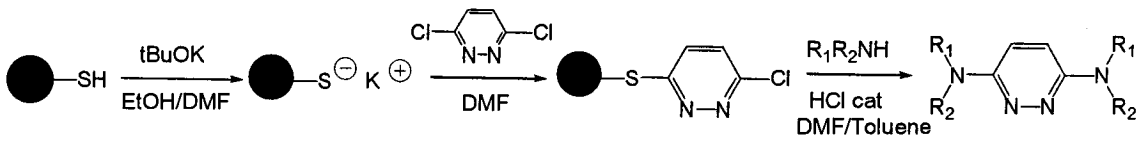

Scheme 3.1. Solid phase synthesis of 3,6-diaminopyridazines.

This method is especially useful for aliphatic amines. However, we preferred a simpler method that could yield multi-gram quantities of starting materials.

We prepared a series of 3,6-diaminopyridazines to allow us to choose the ideal reactant that possesses all the desired qualities: reactivity, solubility and crystallinity. The substituents influence the reactivity of the diamine with the diisocyanate. Aromatic substituents contribute to the delocalization of the electrons of the amine nitrogen and decrease the nucleophilicity. Solubility and crystallinity are often a contradictory pair. For example, the long alkyl chains used in these diamines can aid the solubility to facilitate analysis by NMR, MS, UV, CD, *etc.* which are usually carried out in solution, but may hamper the growth of suitably sized crystals for X-ray diffraction experiments. To increase the crystallinity of our products we preferred to use isobutyl side-chains.

3.2.2 Results and discussion

Six 3,6-diaminopyridazines were obtained *via* the reaction between 3,6-dichloro-pyridazine and different types of primary amines and/or their hydrochloride salts. These diamines have the general structure shown in Figure 3.3, where R and R' can be either the same or different substituents.

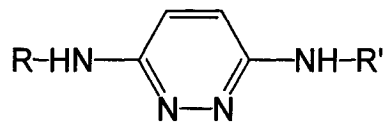

Figure 3.3. The general structure for *N, N'*-substituted 3,6-diaminopyridazines.

Some mono-substituted pyridazines were also synthesized as intermediates of the diamines, which have the general structures shown in Figure 3.4.

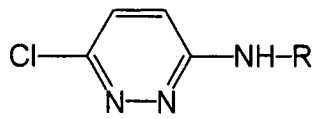

Figure 3.4. The general structure of N-substituted 3-amino-6-chloropyridazines.

The mono-substituted pyridazines were obtained for all the amines. For the reaction with aromatic amines, milder reaction conditions were required to avoid formation of the bis-substituted products. Bis-substituted pyridazines with aromatic and ethanolic subtituents were synthesized in a one-step reaction. For dialkylamines, the two chloro groups were substituted sequentially. The mono-substituted product was synthesized first and then the amine hydrochloride salt was used to replace the second chloro group. The synthesis of 3-amino-6-chloropyridazines **8**, **10**, **12** and **14** and 3,6-diaminopyridzines **9**, **11**, **13**, **15**, **16** and **17** is outlined in Scheme 3.2.

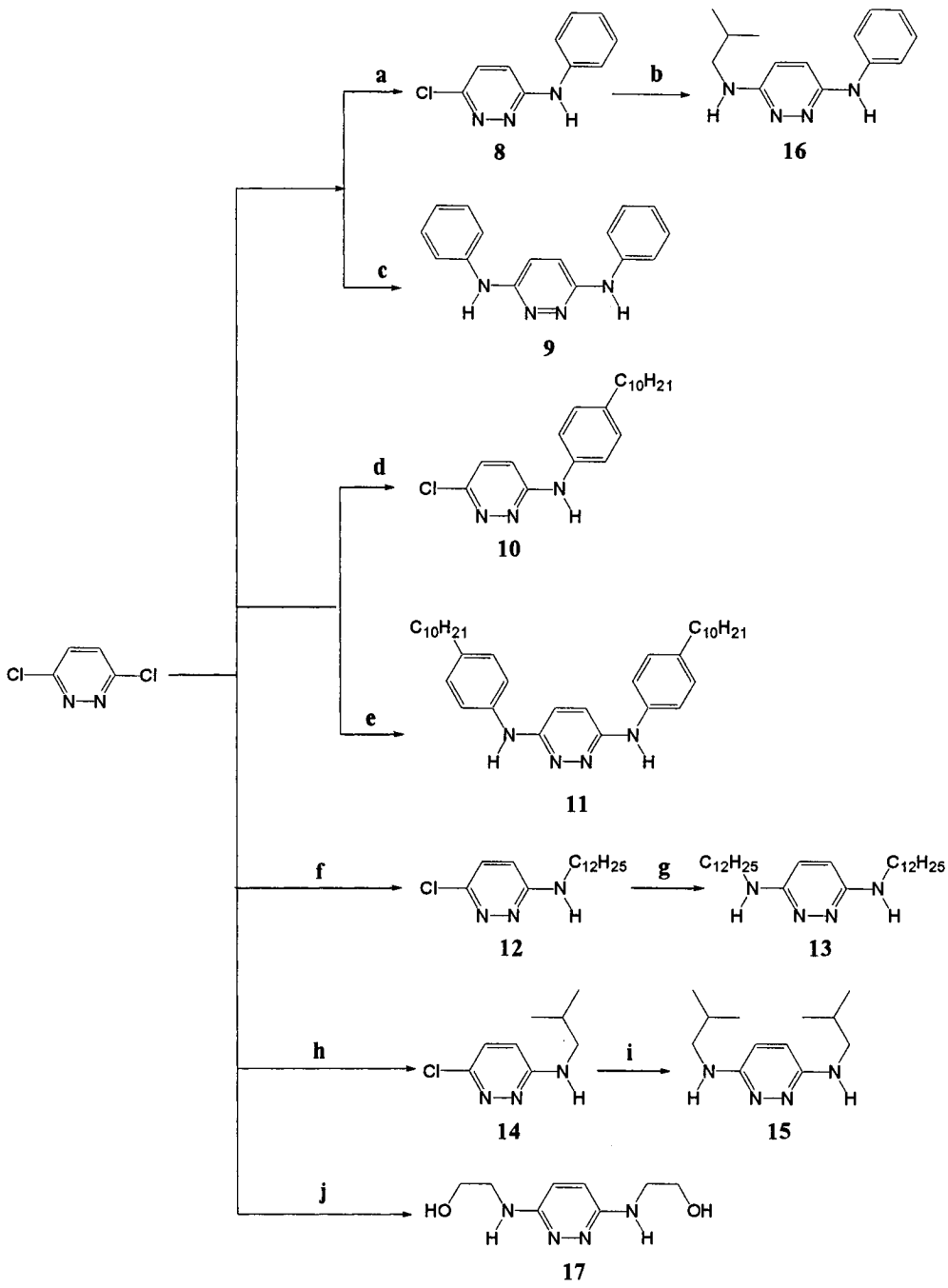

Scheme 3.2. Synthesis of 3,6-diaminopyridazines; (**a**) aniline (1 eq.), ethanol, 60 °C, 3.5 hrs; (**b**) isobutylamine hydrochloride **19** (2.4 eq.), 170 °C, nitrogen, 3 hrs; (**c**) aniline (3 eq.), 120 °C, 20 min; (**d**) 4-decylaniline (1 eq.), 70-80 °C, 1 hr; (**e**) 4-decylaniline (2.3 eq), 120 °C, 15 min; (**f**) 1-dodecylamine (3 eq.), 90-100 °C, 0.5 hr; (**g**) dodecylamine hydrochloride **18** (2 eq.), 170 °C, nitrogen, 3 hrs; (**h**) isobutylamine (5 eq.), ethanol, reflux, 3 hrs; (**i**) **19** (2.8 eq.), 140 °C, nitrogen, 3 hrs;(**j**) ethanolamine (7.3 eq.), 150-160 °C, 6 hrs.

To explain the different reactivities of the chloro at the 6-position towards aromatic and aliphatic amines, Kumagai suggested a two-step mechanism as shown in Scheme 3.3.[125]

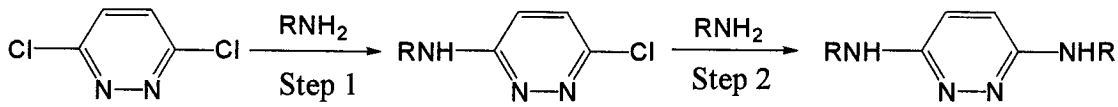

Scheme 3.3. 2-step reaction for the synthesis of *N,N'*-substituted 3,6-diamino-pyridazines.

The chloro group at the 3-postion is easily substituted due to the electron withdrawing effect from the second chloro group at the 6-position. After monosubstitution, the amine at the 3-position would decrease the reactivity of the chloro group at position 6 *via* an electron-donating effect. Aromatic amines could delocalize the amine electrons and thus diminish the electron-donating effect. To confirm his supposition, Kumagai[125] purposely prepared mono-substituted 3-anilino-6-chloro-pyridazine as a starting material to react with a variety of aromatic and aliphatic amines to obtain bis-substituted products. The reaction conditions were usually harsher than those for the preparation of diarylamines. There is some inconsistency in this rationalization. Aliphatic amines are stronger bases than aromatic amines (for aliphatic amine pKa ~10; for aromatic amine pKa ~5)[128] and better nucleophiles, so when the chloro group at the 3-position is substituted by an aromatic amine, the second chloro group at 6 position is expected to be just as easily substituted by an aliphatic amine as an aromatic amine. However, we were unable to obtain this type of mixed diamine with the

aforementioned procedure. Nevertheless, the fundamental idea of a 2-step pathway and the change of electron density at the 3-position and thus the 6-position after mono-substitution is reasonable and can also explain the ease of disubstiututions with aminoethanol, 3-aminopropanol and amino-2-propanol.[129] In these cases, electron withdrawing through induction and/or five- and six-membered hydrogen bonding conformations (Figure 3.5) are proposed to reduce the electron density of the amine nitrogen.[129]

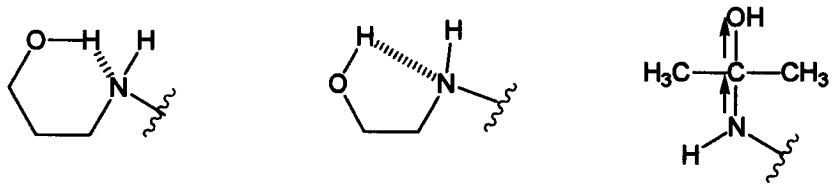

Figure 3.5. Schematic representation of the hydrogen bonding and the induction effects in different alcoholic amines.

The dialkylamines in this thesis were synthesized with a procedure adapted from the work of Moghioros *et al.*[130] In their syntheses, a halogen group (Br or Cl) at the 3-position *para* to a phenyl group was substituted by a primary or secondary amine by adding one equivalent of the corresponding hydrochloride salt to initialize the nucleophilic substitution reaction that was difficult to carry out otherwise. The mechanism is illustrated in Figure 3.6.

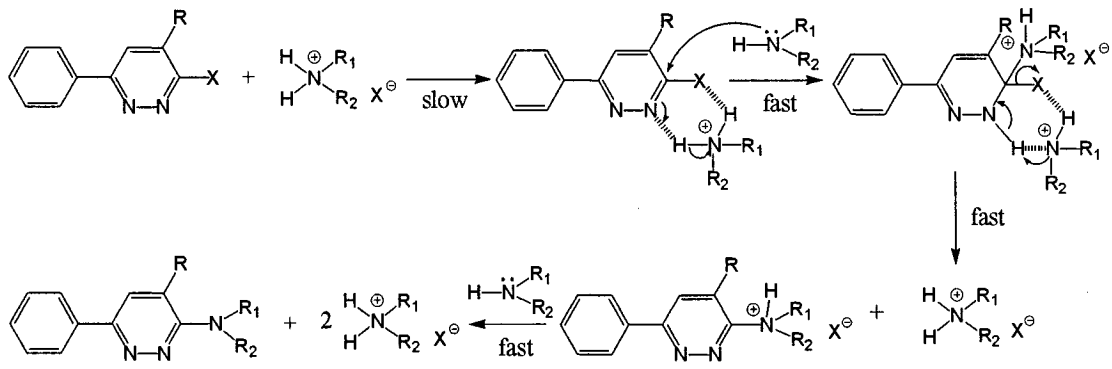

Figure 3.6. Mechanism of nucleophilic substitution with amine salts by Moghioros *et al.*

This mechanism does not explain why the chloro group at the 6-position is more difficult to substitute by an aliphatic amine. According to Moghioros' mechanism, when the first chloro group is substituted, 1 eq. of HCl is produced, which could act as a catalyst for the sequential substitution of an amine at position 6.

One important factor that should be considered is the protonation of pyridazine nitrogen(s) by hydrochloric acid either added externally or produced *in situ*. One equivalent of HCl is produced after substitution of the chloro group at position 3 (Figure 3.7), which can combine with either the starting primary amine or the product secondary

amine depending on their relative pKa values. If the starting primary amine is protonated, there will be no benefit in compensating the electron contributing effect of the amine *para* to the Cl. On the other hand, if the mono-substituted amine is protonated, it will lower the electron density at position 6 to facilitate the second substitution as illustrated in Figure 3.7.

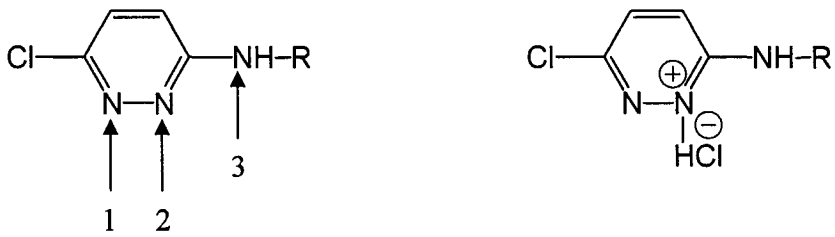

a **b**

Figure 3.7. (a) The possible protonation sites in mono-substituted pyridazine; (b) the product after protonation at site 2.

It was reported that N-2 was protonated with one equivalent of H^+[131]. Aliphatic amines are stronger bases than aromatic amines as well as mono-substituted amino-pyridazines, so they are more likely to be protonated (Figure 3.7(b)). In the case of aromatic amines, the mono-substituted product is the stronger base and will be protonated at N-2 to make the substitution of the second chloro group easier. When the hydrochloride salt of the amine is used as the nucleophile, Moghioros' mechanism is followed and the HCl produced *in situ* protonates the N-2 of the mono-substituted product without competition from the external amines. Experimentally, for both mono- and bis-substitution by aromatic amines, workup was required to neutralize the products; while aliphatic mono- and bis-substituted products were obtained as neutral products.

3.2.3 Conclusions

A series of 3,6-diamino pyridazines with different substituents were synthesized successfully with 3,6-dichloropyridazine as starting material. Aromatic and ethanolic derivatives were easily obtained in a one-step nucleophilic substitution reaction with the corresponding diamines. Aliphatic N-substituted diamines were synthesized in two consecutive reactions.

There is room for improvement in the synthesis of dialkylaminopyridazines with isolated yields reported herein of *ca.* 50%. An important portion of the loss comes from the incomplete reaction between the mono-substituted products and the amine salts. Improvements may be possible if one were to protonate the mono-substituted products before the reaction with the ammonium salts.

Due to time limitations, diamine **17** was not used in the subsequent preparation of macrocycles and foldamers. This diamine has some interesting features since the hydroxyl groups could be functionalized to prepare interesting structures. For example, the hydroxyl groups could be protected during macrocyclization, and after deprotection, the products, unlike those with hydrophobic side chains, might be more soluble in polar solvents. The hydroxyl group could be also used as a starting point to prepare dendrimers with a macrocyclic core. Also, the hydroxy group could be first transformed to halogen derivatives which can subsequently be used to prepare macrocycle networks.

3.3 Tetrameric pyridazine macrocycles

3.3.1 Synthesis

The 26-membered macrocycles were synthesized by a one step reaction of N-substituted *p*-diamino pyridazines and TDI or PDI with anhydrous chloroform as solvent at 50 °C under nitrogen for 24 hours (Scheme 3.4). The reactants and resulting products are summarized in Table 3.1.

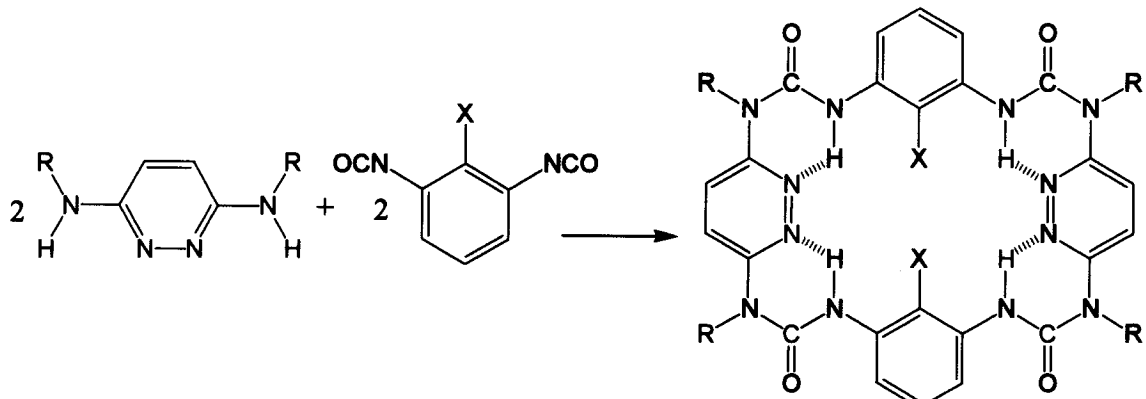

20 R = Ph-$C_{10}H_{21}$, X = CH_3

21 R = n-$C_{12}H_{25}$, X = CH_3

22 R = *i*-C_4H_9 X = CH_3

23 R = *i*-C_4H_9 X = H

Scheme 3.4. The syntheses of tetrameric 3,6-pyridazine/2,6-toluene macrocycles: chloroform, 60°C, 24 hrs.

The isocyanate group is very reactive towards moisture or alcohol, so anhydrous and controlled reaction conditions are required for this reaction. To achieve this, the diamines were vacuum-dried at 50 °C for two days, and the reaction flasks were flame-dried before use. The average yield of macrocycle starting with TDI or PDI was *ca.* 70 % or 40 %, respectively. The difference could be accounted for by the fact that with TDI, steric interactions favor macrocycle formation (Figure 1.8).

Table 3.1. List of the reactants and the resulting macrocycles **20-23.**

R	diamine	X	diisocyanate	macrocycle
Ph-$C_{10}H_{21}$	**9**	CH_3	TDI	**20**
n-$C_{12}H_{25}$	**11**	CH_3	TDI	**21**
i-C_4H_9	**13**	CH_3	TDI	**22**
i-C_4H_9	**15**	H	PDI	**23**

All the macrocycles were characterized with NMR (^1H, ^{13}C, NOESY), MS and IR. Crystal structures were also obtained for macrocycles **22** and **23**, and will be discussed in greater detail in Section 3.3.2.2. The self-assembly of macrocycle **21** on highly oriented pyrolytic graphite (HOPG) observed using scanning tunneling microscopy (STM) will also be described (Section 3.3.2.3).

3.3.2 Results and discussion

3.3.2.1 NMR and MS analyses

The ^{1}H NMR for all macrocycles shows a singlet at *ca.* 12 ppm that is characteristic of an intramolecular hydrogen bonded urea proton and the simple signal pattern suggests a relatively symmetric structure in solution. One example is given in Figure 3.8 that shows the ^{1}H NMR spectrum and the signal assignment of macrocycle **22**. The most downfield shifted signal **1** is assigned to the urea hydrogen. This downfield shifted signal is indicative of the formation of hydrogen bonds that is also observed in the naphthyridine urea macrocycle described in Section 2.1.4.1. The singlet, signal **3,** in the aromatic region belongs to the two equivalent pyridazine hydrogens; the other signals are assigned to the toluene hydrogens. According to the splitting pattern, the triplet is assigned to hydrogen **4** and the doublet to proton **2**. The relatively large difference in chemical shift could be rationalized by the formation of Ar-H···O hydrogen bonds between proton **2** and the carbonyl oxygen (Section 2.1.4.1). There are four types of protons in the aliphatic region: three are assigned to isobutyl hydrogens (doublet **5** (CH_2), multiplet **7** (CH) and doublet **8** (CH_3)), and the remaining singlet at *ca.* 2.5 ppm is from toluene methyl hydrogens. The relative position of the urea hydrogens and toluene methyl hydrogens was confirmed by a NOESY experiment. In the NOESY spectrum (Figure 3.9) the cross peak due to urea proton **1** and toluene methyl protons **6** indicates the proximity of these two types of hydrogens that is only possible in the curved conformation. For macrocycle **23**, there is a cross peak of the urea protons and the 2-position phenyl protons in the NOESY spectrum (Figure 3.10), which agrees with a curved conformation. The correlations of the other protons are similar to macrocycle **22**.

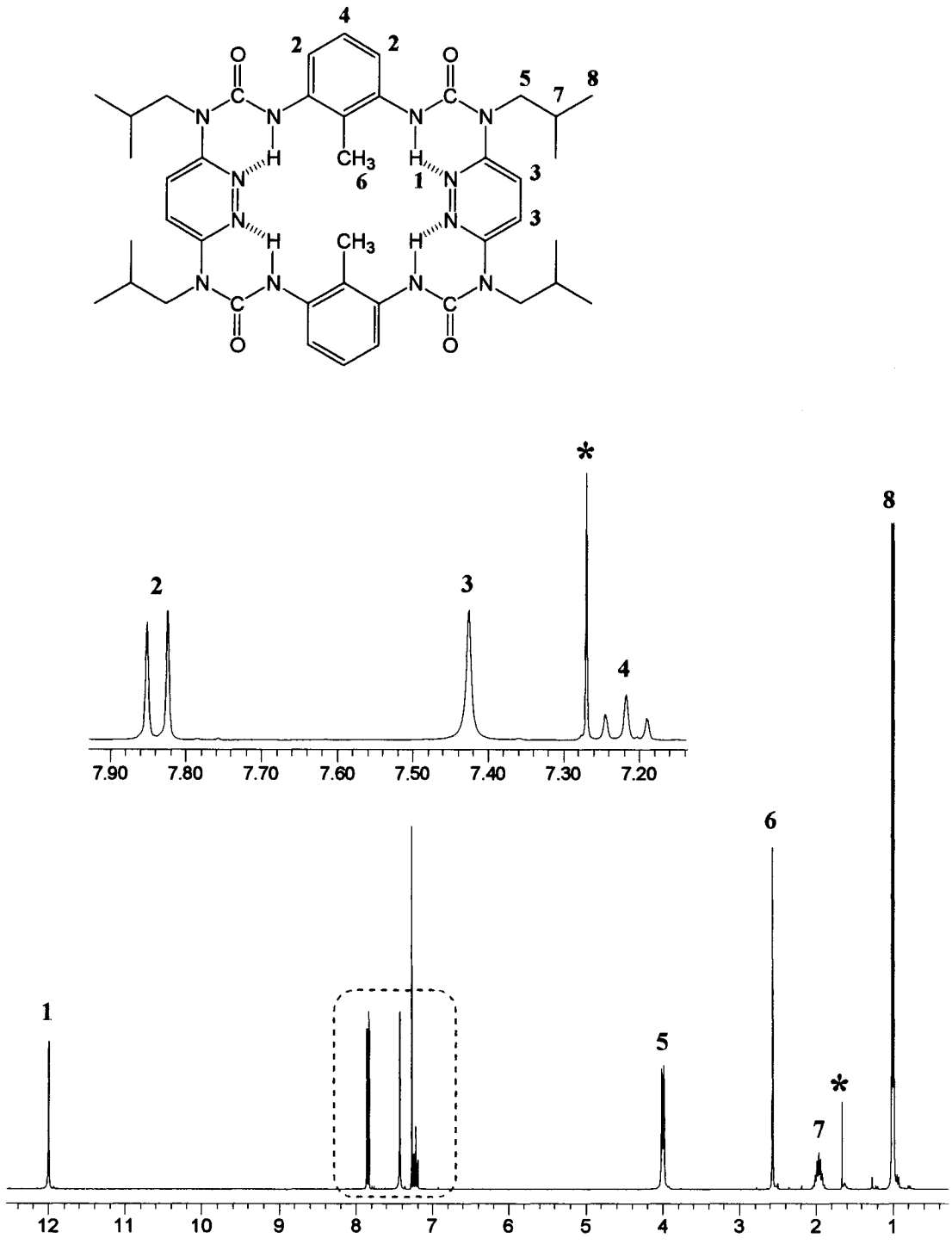

Figure 3.8. ^{1}H NMR spectrum of macrocycle **22** in $CDCl_3$ with the aromatic region expanded. The signals labeled with asterisks are due to residual chloroform and water.

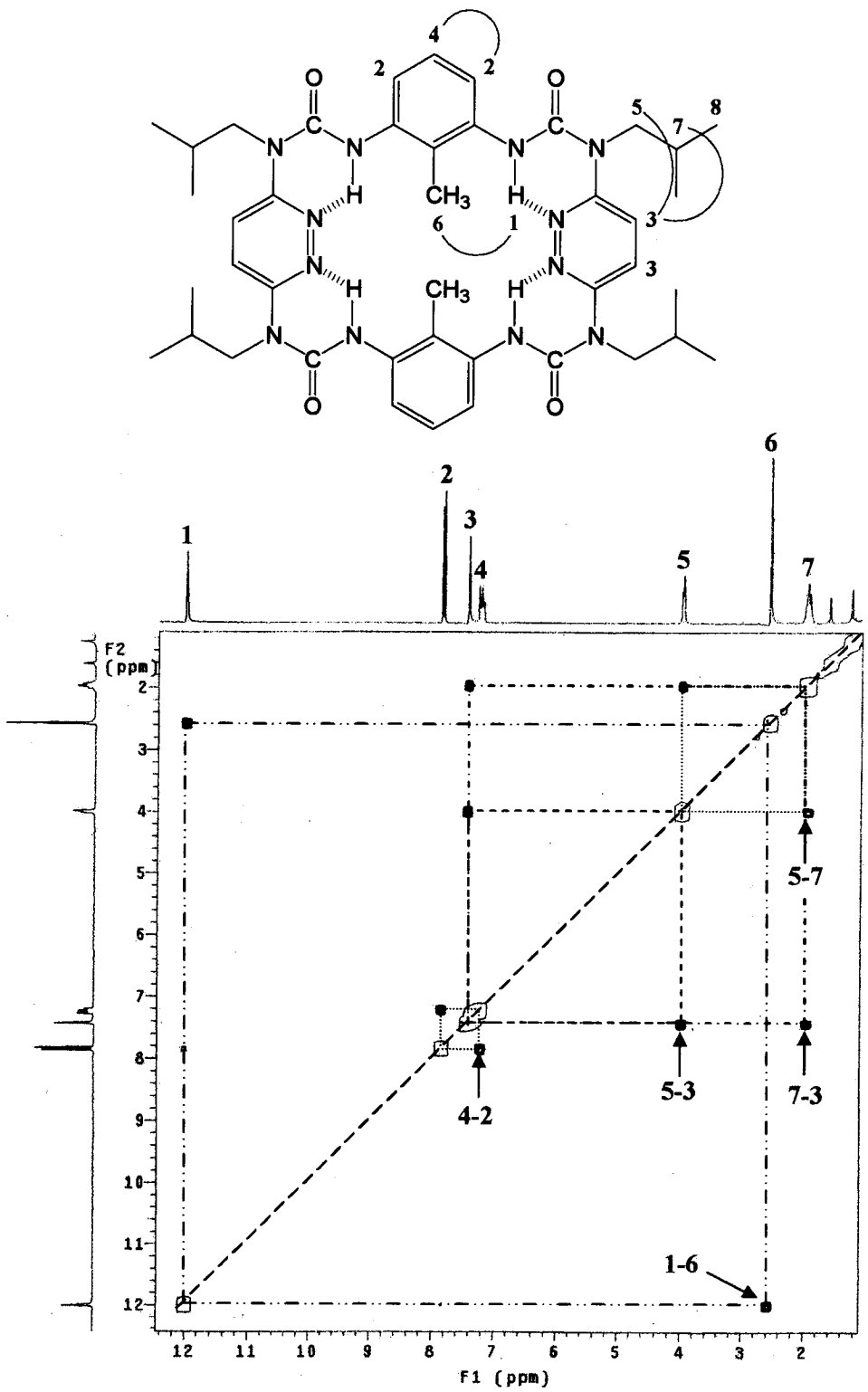

Figure 3.9. NOESY spectra of macrocycle **22** in $CDCl_3$ (r.t., mixing time : 0.3s).

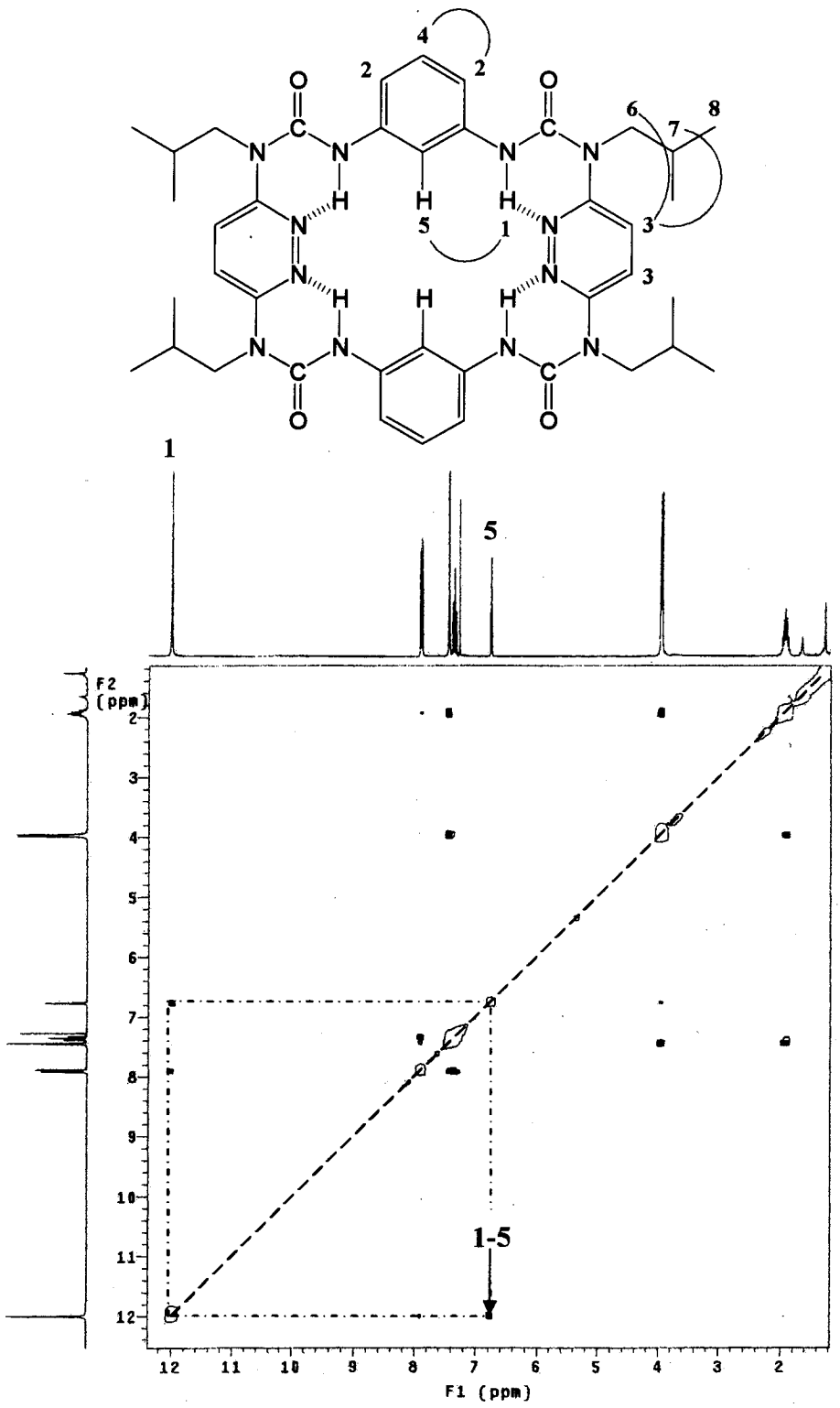

Figure 3.10. NOESY spectrum of macrocycle **23** in $CDCl_3$ (r.t., mixing time: 0.3 s).[132]

The identity of macrocycle **22** was further verified by mass spectrometry. The signal at m/z 793.3 in the MALDI-TOF mass spectrum corresponds to the protonated macrocycle **22** $[M + H]^+$ ($C_{42}H_{56}N_{12}O_4$, exact mass = 792.45), while the signal at m/z 815.1, *ca.* 22 units higher in mass corresponds to the sodium adduct $[M + Na]^+$. The MS data is summarized in Table 3.2.

Table 3.2. MS data for macrocycles **20 - 23**

Macrocycle	Formula	Exact mass	m/z ($[M+H]^+$)	m/z ($[M+Na]^+$)
20	$C_{90}H_{120}N_{12}O_4$	1432.96	1433.3	1456.6
21	$C_{74}H_{120}N_{12}O_4$	1240.96	-----	1263.6
22	$C_{42}H_{56}N_{12}O_4$	792.45	793.3	815.1
23	$C_{40}H_{52}N_{12}O_4$	764.42	765.3	787.3

3.3.2.2 Crystal structures

Single crystals suitable for X-ray diffraction were obtained for macrocycles **22** and **23** by slow diffusion of methanol into chloroform solutions of the samples. The crystal characteristics and crystallographic parameters are provided in Appendix B.

In crystal structures of both **22** (Figure 3.11 - 3.16) and **23** (Figure 3.17 & 3.18), the backbones are composed of four alternating pyridazine and non-heterocyclic aromatic rings (toluene for **22** and benzene for **23**). Urea N-H hydrogens are directed inwards, forming four intramolecular hydrogen bonds with pyridazine nitrogens, and the carbonyl groups pointing outwards.

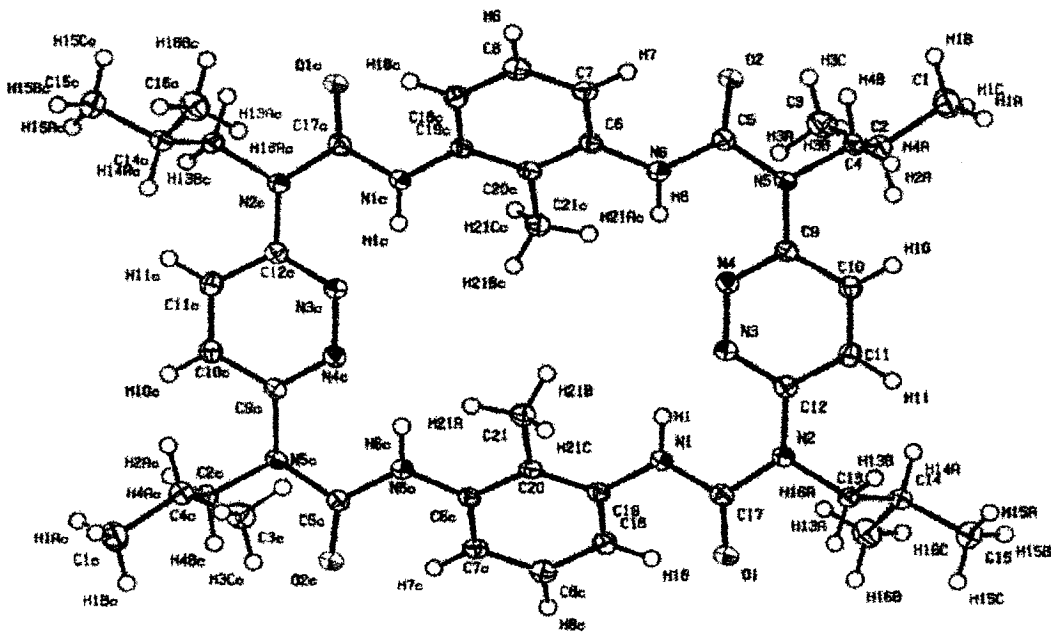

N4····H6 = 1.888 Å, N6-H6····N4 = 139.42°
N3····H1 = 1.866 Å, N1-H1····N3 = 140.16°

Figure 3.11. ORTEP view of macrocycle **22**.

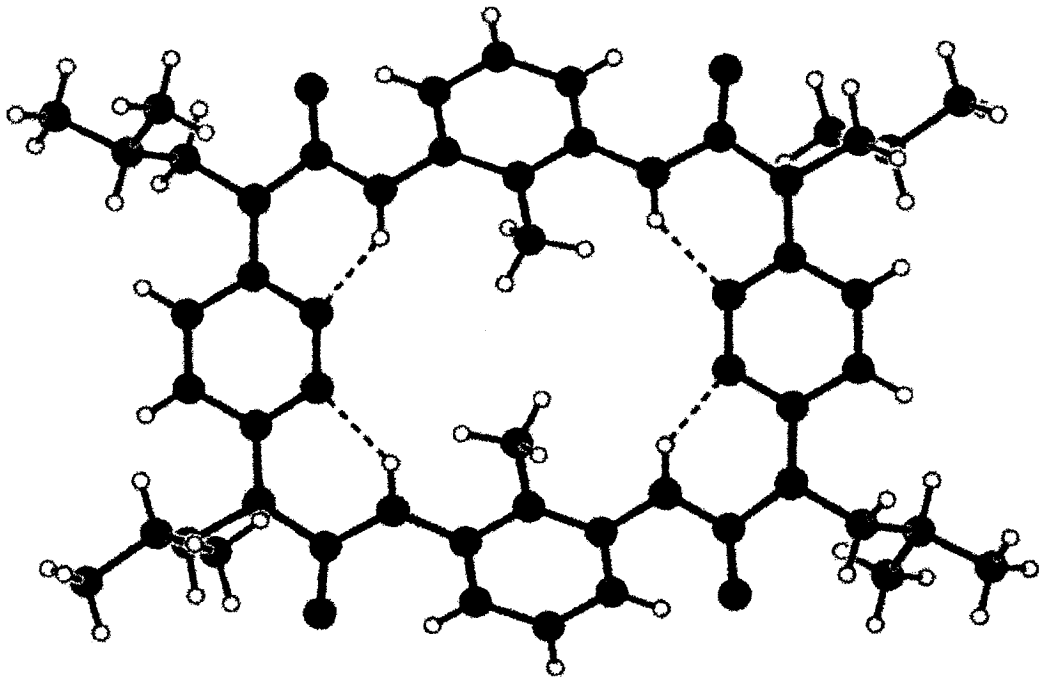

Figure 3.12. Ball-and-stick view of macrocycle **22** with hydrogen bonds represented by dashed lines.

In the crystal structure of **22**, the two pyridazine rings are relatively coplanar, while the toluene rings tilt out of plane in different directions: two isobutyl side chains associated with one pyridazyl group point upward while those associated with the second pyridazyl group point downward (Figure 3.13).

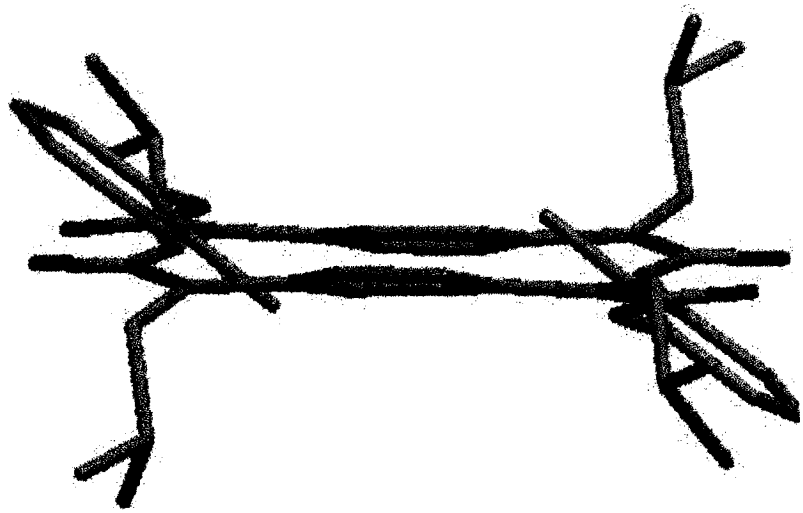

Figure 3.13. The conformation adopted by macrocycle **22**. Hydrogens are omitted for clarity. The two pyridazine rings are largely coplanar and the two toluene rings are tilted out of the pyridazine plane in opposite directions. Isobutyl groups of the side chains are situated on both sides of the macrocycle ring plane.

Macrocycle **22** packs into intertwined hexamers (Figure 3.14) viewed along the c axis by three-centered intermolecular hydrogen bonds (R^1_6 (7))[60] between the carbonyl oxygen of one molecule and the pyridazine hydrogen and the methylene hydrogen of another molecule (Figure 3.15). Along the symmetry axis (C_2) of the macrocycle, a columnar pattern is formed by face-to-face aromatic π-π stacking (Figure 3.16).

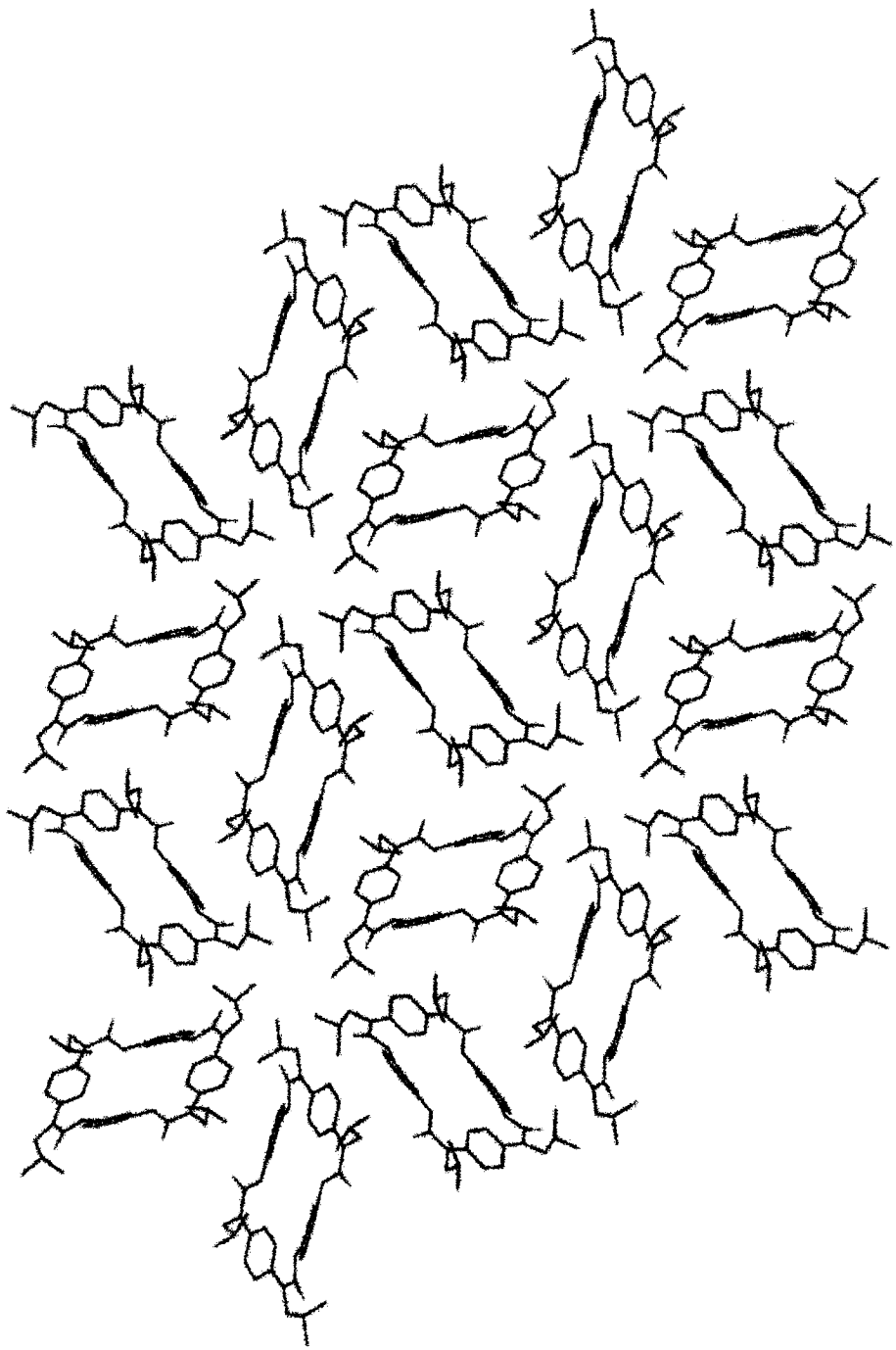

Figure 3.14. Intertwined hexameric network of macrocycle **22**.

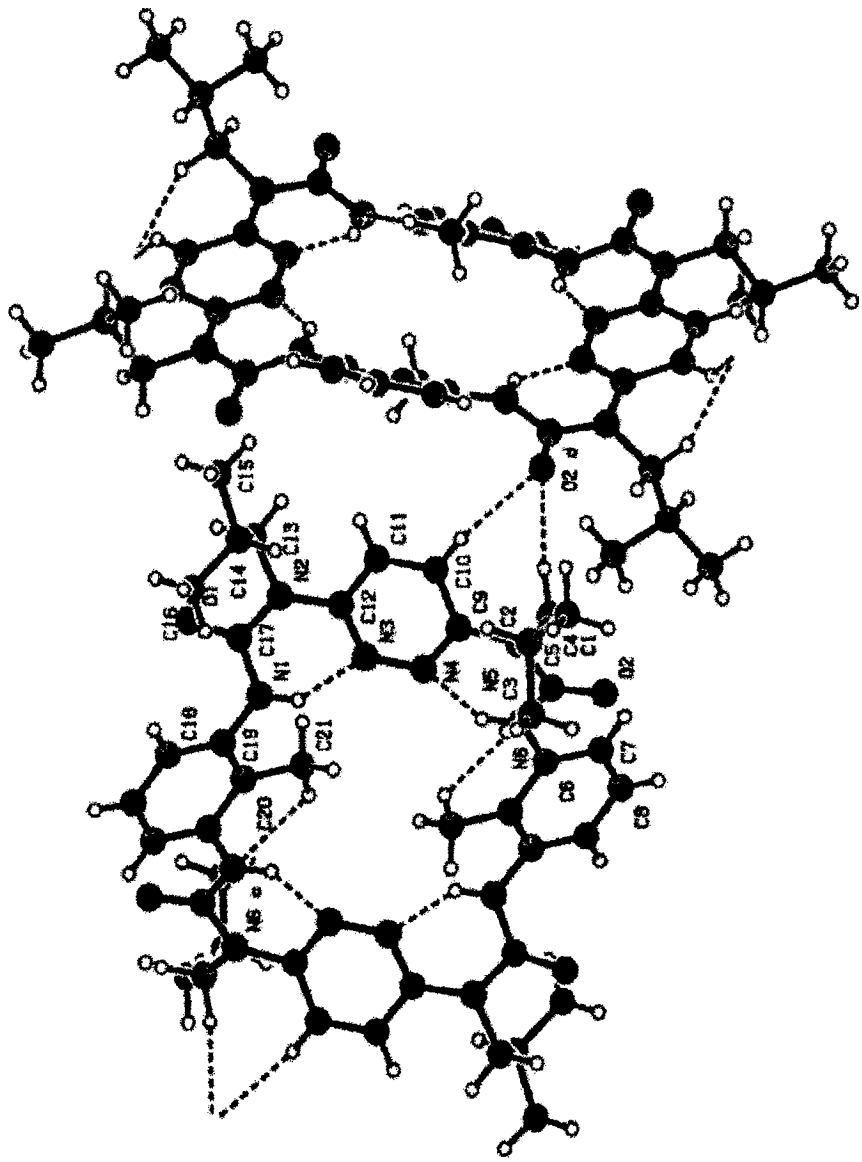

O10·····H10 = 2.483 Å, C10-H10·····O10 = 136.93 °
O2 ·····H4 = 2.431 Å, C4-H4·····O10 = 150.83 °

Figure 3.15. Intra/intermolecular hydrogen bonded dimer of macrocycle **22**.

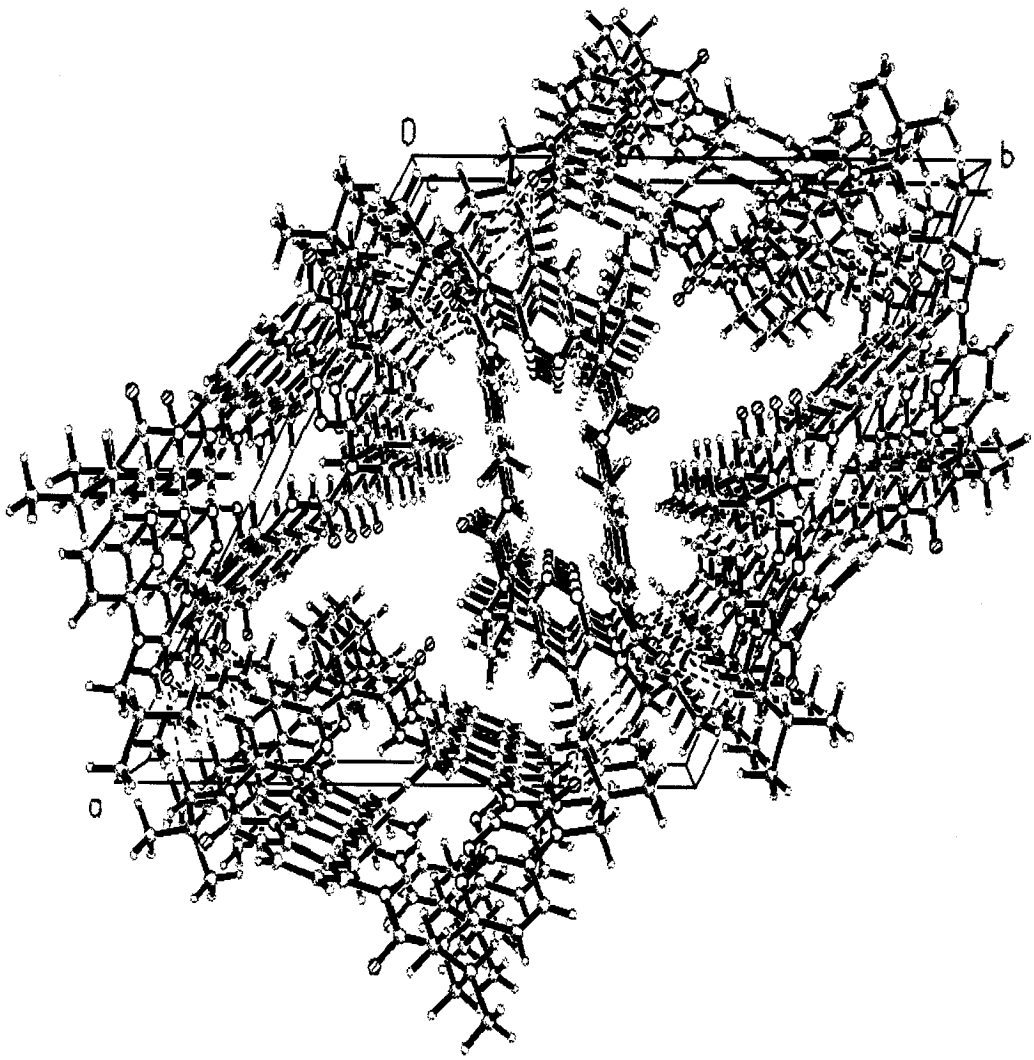

Figure 3.16. Top view of stacked macrocycle **22**.

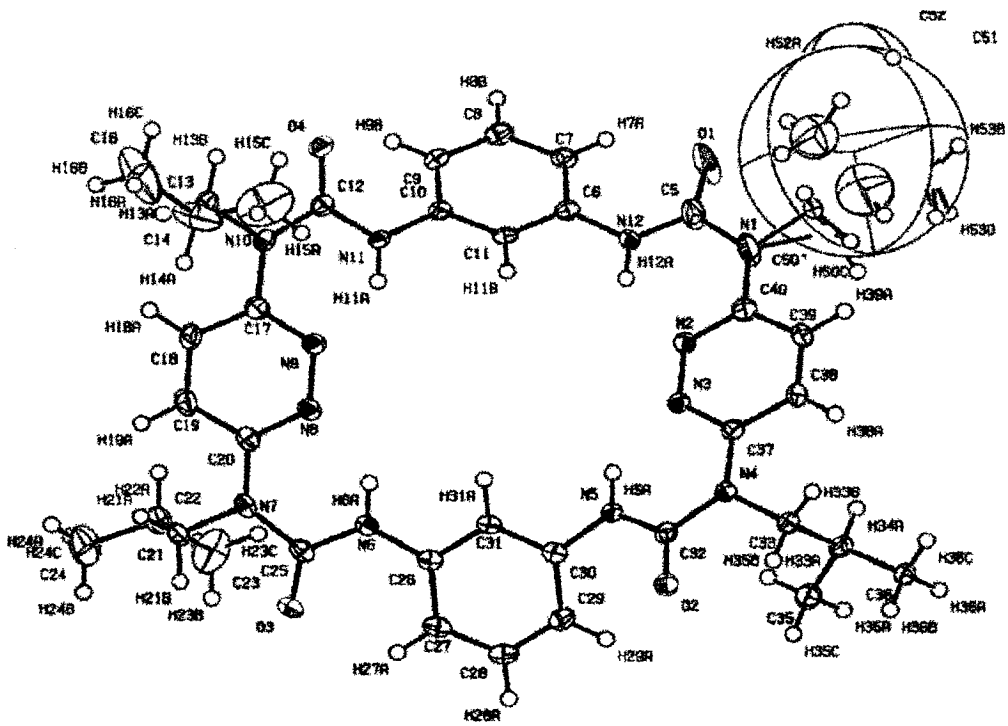

H5A...N3 = 1.925 Å, N5-H5A...N3 = 135.48 °
H12A...N2 = 1.903 Å, N12-H12A...N2 = 139.14 °

Figure 3.17. ORTEP view of macrocycle **23**.

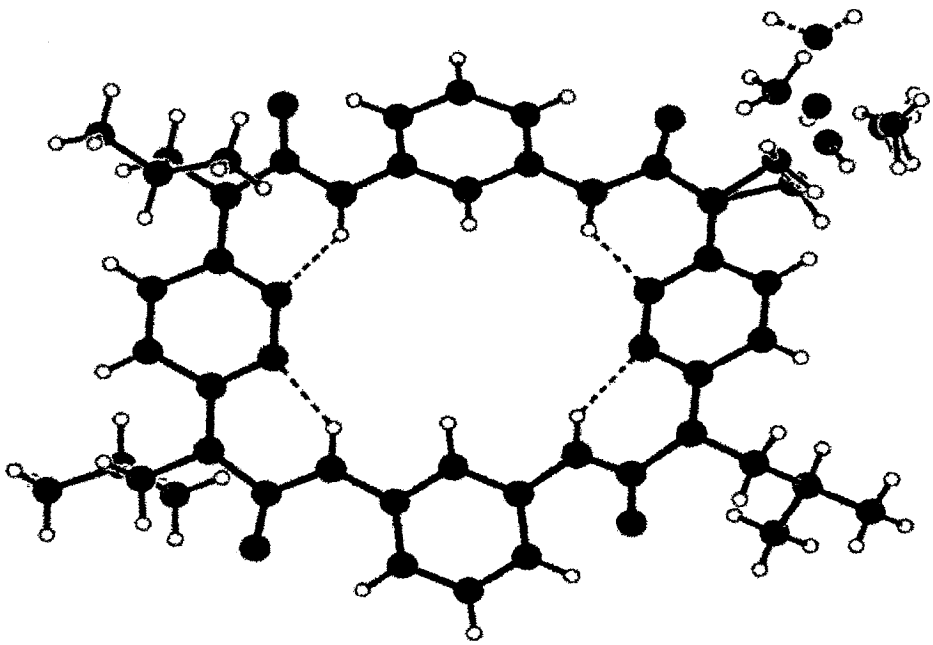

Figure 3.18. Ball-and-stick view of macrocycle **23** with hydrogen bonds represented by dashed lines.

In the crystal structure of **23** (Figure 3.19) all four aromatic rings are twisted out of the macrocycle plane to a greater extent than in **22**, which is quite unexpected. In the crystal structure, one of the isobutyl groups is disordered. Macrocycle **23** was designed after macrocycles of type **22** were synthesized, to obtain flatter structures due to decreased steric repulsion between two hydrogens (**23**) versus two methyl groups (**22**). In the crystal structure of **22** (Figure 3.15), the methyl hydrogen forms hydrogen bonds with the urea (NH) nitrogen (N6c···H21A=2.318Å, N6c···H21A-C21 = 110.01°) that, to some extent, counterbalances the steric repulsion between the bulky methyl groups. This may assist in forming the coplanar conformation, along with the hydrogen bonding between urea hydrogens and pyridazine nitrogen lone pairs. While in the structure of **23**, there is no such hydrogen bonding interaction (H31A···N5 = 2.555Å, C31-H31A···N5 = 70.22°).

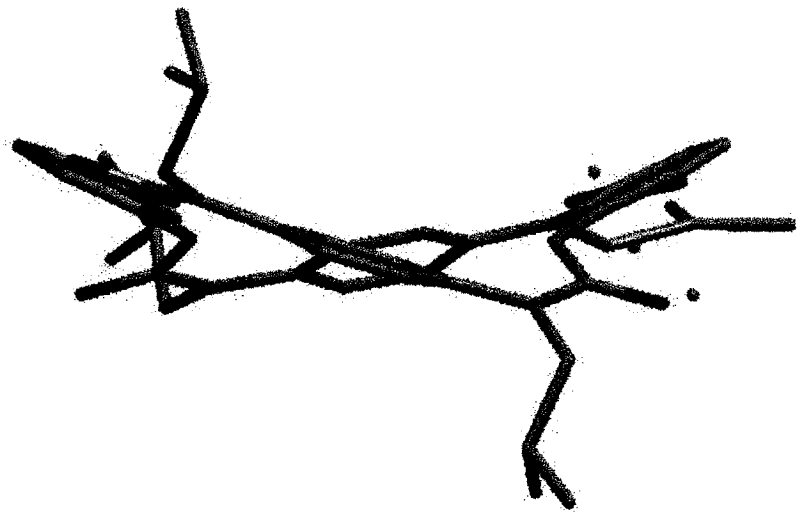

Figure 3.19. The conformation adopted by macrocycle **23**. Hydrogens are omitted for clarity. All the aromatic rings are twisted out of plane.

However, the goal of obtaining a relatively spacious cavity by replacing the bulky methyl groups with hydrogen atoms was realized in macrocycle **23** (Fig 3.20).

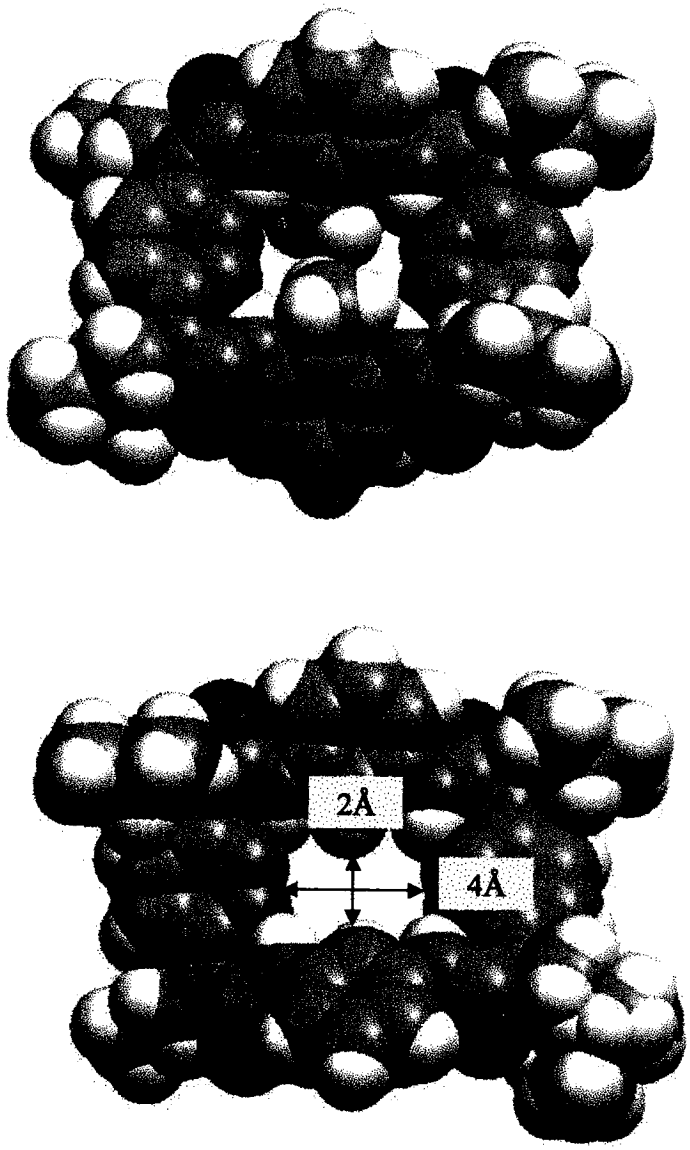

Figure 3.20. Spacefilling representations of macrocycles **22** (top) and **23** (bottom).

3.3.2.3 Self-assembly studies by STM [133]

Scanning tunneling microscopy (STM) allows one to image atomic structures on conducting surfaces. The technique relies on a tunneling current between a scanning fine tip and a sample surface.[134] There is great interest in the 2D self-assembly of organic molecules on surfaces due to their potential applications in nanotechnology.[135] There are many examples of 'adsorption induced self-organization' of organic molecules on surfaces observed using scanning tunneling microscopy.[136] This prompted our STM investigation of physisorbed layers of macrocycle **21** at the graphite-solvent interface. Figures 3.21 and 3.22 show the STM images of two dimensional monolayers of macrocycle **21** physisorbed at the liquid HOPG (highly oriented pyrolytic graphite) interface. 1,2,4-trichlorobenzene was used as solvent due to its low vapor pressure thus facilitating experiments in a liquid drop.

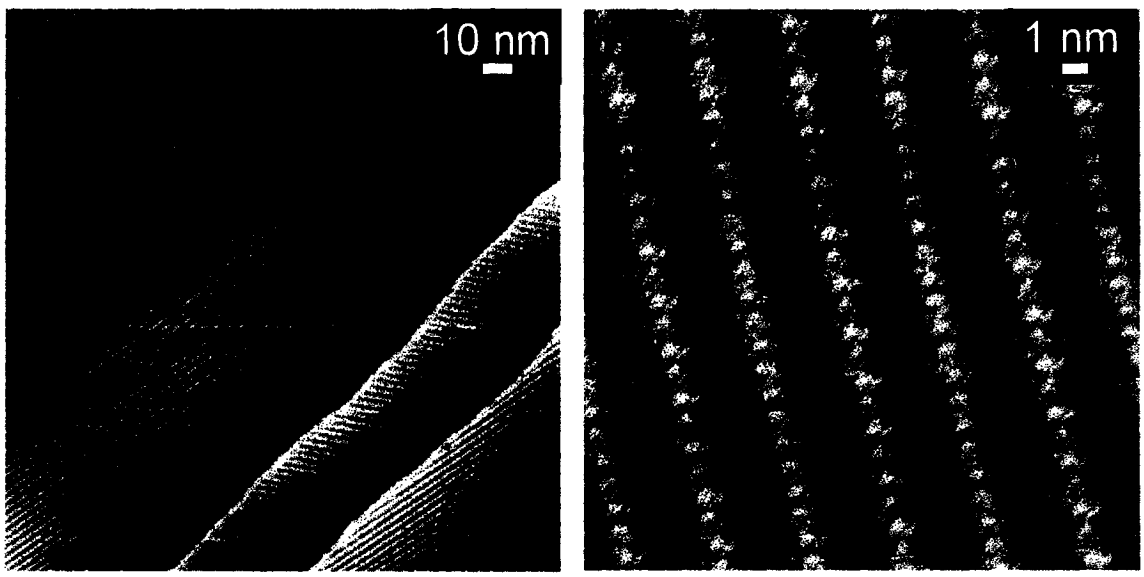

Figure 3.21. STM images of macrocycle **21** on HOPG in 1,2,4-trichlorobenzene in constant current mode using a Pt/Ir tip: a) 26.9 pA, -564 mV; b) 95.5 pA, -1.00V.

Macrocycle **21** forms extended stripe domains at the HOPG/solution interface where changes in direction on the same layer and different layers of graphite are observed (Figure 3.21 (a)). Figure 3.21 (b) shows a typical high resolution image of macrocycle **21** on graphite where the macrocyclic cores are arranged in parallel stripes (lighter regions) and there is evidence for interdigitated alkyl chains in the two adjacent stripes (darker regions). Figure 3.22 (a) shows the highest resolution image that was obtained and, based on the periodicities of the features, the space-filling model of the macrocyclic core was superimposed on the image (Figure 3.22 (b)). The peripheral groups are not included since well-resolved images of the alkyl chains were not obtained.

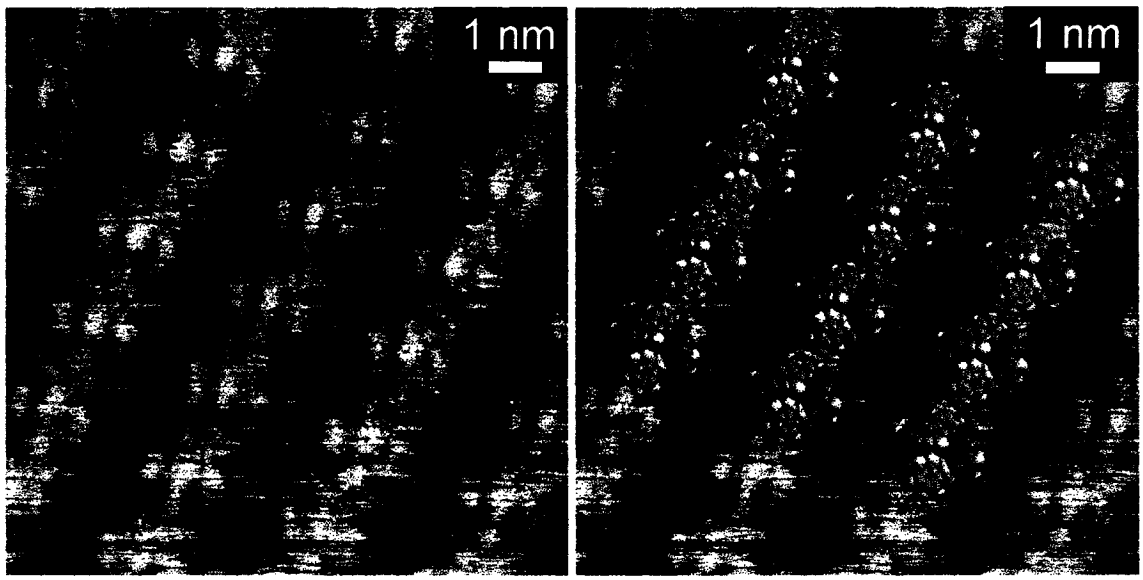

Figure 3.22. STM images of macrocycle **21** on HOPG in 1,2,4-trichlorobenzene in constant current mode using a Pt/Ir tip; 16.7 pA, -668 mV.

3.3.2.4 Self-aggregation in solution

Macrocycle **22** packs into 3D columnar arrays by face-to-face aromatic π-π stacking (Section 3.3.2.2). Macrocycle **21** self-assembles into 2D crystalline arrays on highly oriented pyrolytic graphite from concentrated solutions as revealed in STM images. In this section, concentration dependent ^{1}H NMR experiments are used to study the aggregation behavior in solution. Tables 3.3-3.6 list the ^{1}H NMR data (chemical shift *vs.* concentration) of macrocycle **20 -23**.

Table 3.3. ^{1}H NMR data (chemical shift vs. concentration) of macrocycle **20***

Concentration (mM)	Pyridazine-H4, 5	Tolylene-H3	Urea-H
0.4	6.490	7.937	12.160
1	6.487	7.936	12.155
2	6.484	7.936	12.151
4	6.476	7.935	12.140
10	6.459	7.932	12.116
20	6.433	7.929	12.078

Table 3.4. ^{1}H NMR data (chemical shift vs. concentration) of macrocycle **21***

Concentration (mM)	Pyridazine-H4, 5	Tolylene-H3	Urea-H
0.625	7.438	7.882	12.011
1.25	7.438	7.882	12.012
2.5	7.416	7.875	11.978
5	7.381	7.868	11.926
10	7.332	7.852	11.851
20	7.281	7.833	11.773

Table 3.5. ^{1}H NMR data (chemical shift vs. concentration) of macrocycle **22***

Concentration (mM)	Pyridazine-H4, 5	Tolylene-H3	Urea-H
0.5	7.395	7.775	11.977
1	7.393	7.775	11.975
2.5	7.390	7.774	11.970
5	7.381	7.770	11.958
10	7.367	7.766	11.940
20	7.345	7.758	11.911

Table 3.6. ^{1}H NMR data of (chemical shift vs. concentration) macrocycle **23***

Concentration (mM)	Benzene-H2	Pyridazine -H4, 5	Benzene -H4, 6	Urea-H
2	6.765	7.449	7.909	11.994
4	6.765	7.448	7.908	11.993
8	6.765	7.448	7.907	11.993
16	6.763	7.446	7.904	11.994
24	6.762	7.445	7.902	11.996
40	6.760	7.443	7.899	11.996

*The proton positions in the above tables are numbered according to the corresponding monomer.

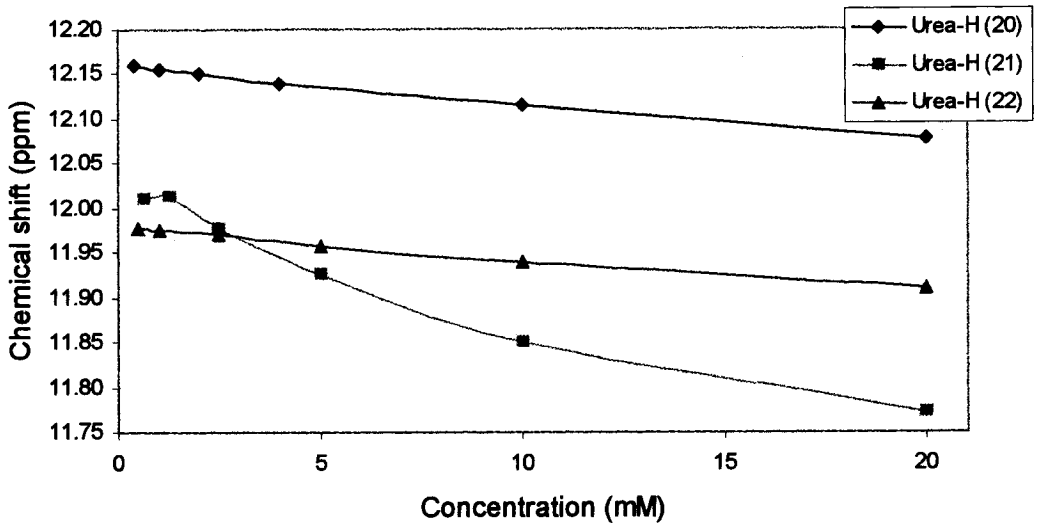
Urea-H (20)
Urea-H (21)
Urea-H (22)
Chemical shift (ppm)
12.20
12.15
12.10
12.05
12.00
11.95
11.90
11.85
11.80
11.75
0
5
10
15
20
Concentration (mM)

a

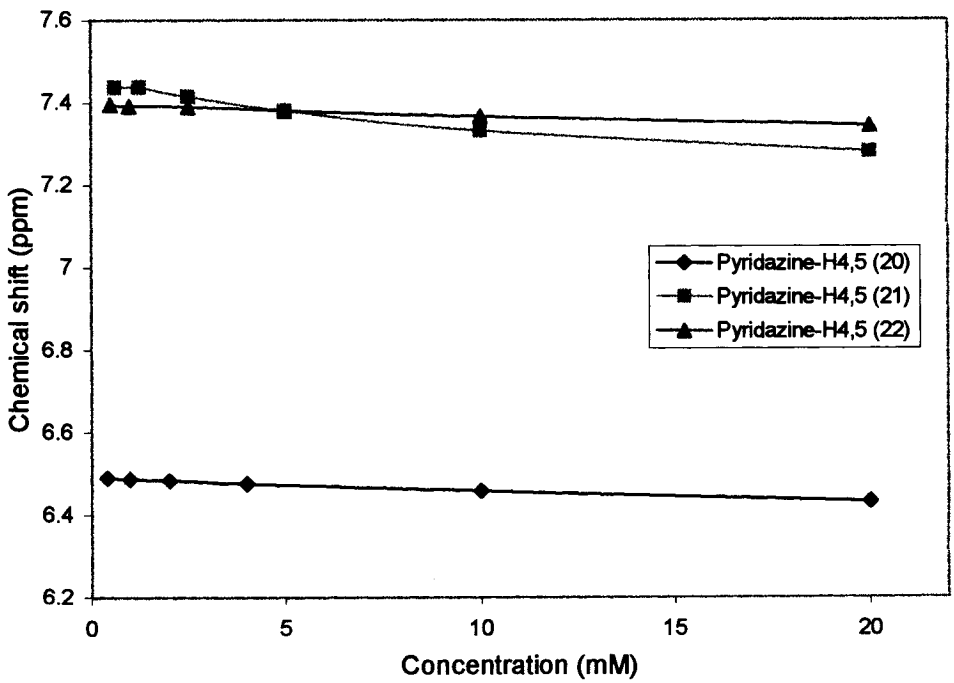
Pyridazine-H4,5 (20)
Pyridazine-H4,5 (21)
Pyridazine-H4,5 (22)
Chemical shift (ppm)
7.6
7.4
7.2
7
6.8
6.6
6.4
6.2
0
5
10
15
20
Concentration (mM)

b

(Continued)

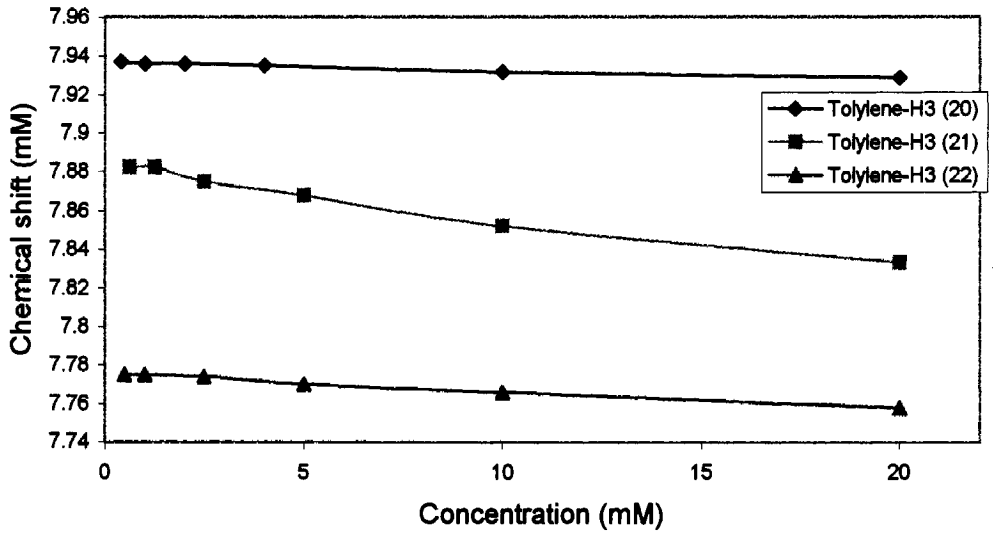

c

Figure 3.23. Concentration dependent ^{1}H NMR studies of (a) urea NH protons; (b) pyridazine protons (c) toluene protons (H3) of macrocycles **20**, **21** and **22**.

Macrocycles **20**, **21** and **22,** constructed with the toluene group, all show concentration dependent signals in the ^{1}H NMR, *i.e.* as concentration increased, the chemical shifts of the backbone protons decreased (Figure 3.23), suggesting self-aggregation in solution.[40, 41, 137, 138] Macrocycle **21,** with long aliphatic side chains ($-C_{12}H_{25}$) shows the most drastic concentration dependent ^{1}H NMR signals. Contrary to what was expected, concentration dependent ^{1}H NMR behavior was not observed for macrocycle **23** (Table 3.6). The aggregation is likely caused by π-π stacking of the aromatic backbone and side chain interactions. The difference may be caused by (a) the planarity of the backbone structure and (b) the side chain properties.[137] Macrocycle **23** possesses a less coplanar backbone conformation in the solid state compared to **22**, which

might deter the proper orientation for stacking interactions. While macrocycle **20**, **21** and **22** have the same backbone structures, the side chain interactions lead to the variant concentration dependent behavior. The aryl group in **20** and the branching isobutyl group in **22** may cause unfavorable steric interactions to hinder stacking. It is interesting to note that macrocycle **21** which displays the most obvious self-aggregation behavior in solution, was the only macrocycles whose self-assembly was detected by STM.

3.3.3 Conclusions

A series of tetrameric macrocycles (26-membered rings) were synthesized in one-step [2+2] condensation reactions between 3,6-diaminopyridazines and 2,6-tolylene-diisocyanate or 1,3-phenyl-diisocyanate. Intramolecular hydrogen bonding between the urea hydrogens and pyridazine nitrogen lone pairs was the major driving force for the preferential formation of curved conformations that lead to macrocyclic products instead of linear polymers.

Crystal structures were obtained for macrocycles **22** and **23** with isobutyl side chains. In both structures, urea hydrogens align inside the cavity of the macrocycle and form hydrogen bonds with the pyridazine lone pairs, while the carbonyl groups orient outwards forming intermolecular hydrogen bonds. Columnar packing patterns through face-to-face aromatic π-π stacking were observed for both crystals. Macrocycle **22** adopts a more coplanar conformation than macrocycle **23** possibly due to intramolecular hydrogen bonding between the toluene methyl hydrogens and the urea nitrogens. Nevertheless, the aim to obtain a more spacious cavity by replacing the relatively bulky methyl groups with hydrogen atoms was realized in macrocycle **23**. Macrocycle **21** self-assemble into 2D crystalline arrays on HOPG from concentrated solutions as revealed in STM images. Self-aggregation in solution of macrocycles **20**, **21** and **22** with toluene as the backbone component was reflected in concentration dependent ^{1}H NMR experiments with **21** showing the clearest dependence. Coincidently, macrocycle **21** was the only macrocycle whose self-assembly was detected by STM. Macrocycle **23** did not show concentration dependent behavior probably due to a less planar ring conformation also observed in the crystal structure.

The strong propensity to curve suggests the possibility of obtaining helical structures with this system. In the next section (Section 3.4), the synthesis of a cresent-shaped trimer **24** and a helical pentamer **26** from 3,6-diaminopyridazine **15**, 2,6-tolylene-diisocyanate and *o*-tolylene isocyanate will be described.

3.4 Foldamers

3.4.1 Introduction

The strong propensity to form macrocycles, enforced by intramolecular hydrogen bonds, described in Section 3.3, suggests the possibility to design foldamers with this same system.[50] In fact, the initial goal of this project was to synthesize helical foldamers. Isobutyl side chains afford macrocycles **22** and **23** with good solubility and crystallinity for characterization, so we decided to include this motif in designing our foldamers. Diamine **15** and TDI were used as the major reagents in preparing trimer **24** and pentamer **26** (Figure 3.24).

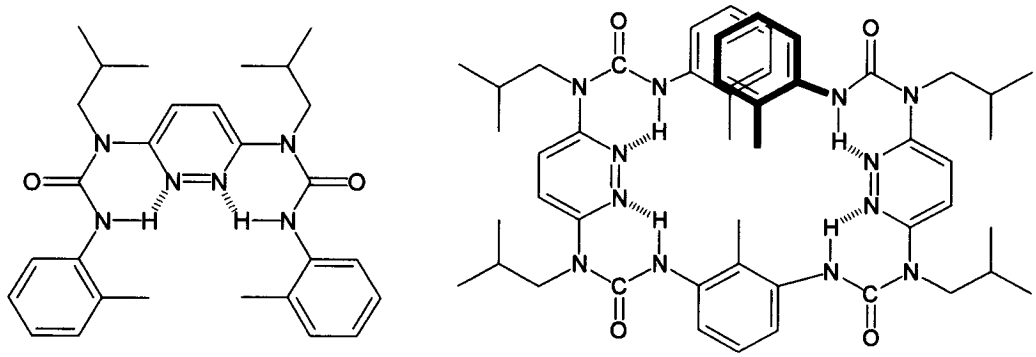

24 **26**

Figure 3.24. Chemical structures of trimer **24** and pentamer **26**.

Trimer **24** was prepared to test whether the *anti* conformation of the carbonyl groups and the toluene methyl groups observed in the macrocycles could exist in open chain systems and be a model compound for analyzing pentamer **26**.

Pentamer **26** is made of five alternating urea-linked 3,6-pyridazine/2,6-toluene aromatic rings and is expected to form one helical turn with overlapping toluene termini. The purpose of making pentamer **26** was twofold: (a) to test whether the folding pattern could be repeated in the formation of longer oligomeric strands; and (b) if the helix is formed, to study its conformation which will be useful for studying the conformation of longer strands.

3.4.2 Synthesis

Trimer **24** was synthesized in a one-step reaction of diamine **15** and *o*-tolylene isocyanate (OTI) (Scheme 3.5). Diamine **15** could be completely converted into **24** by using excess OTI. The unreacted OTI was hydrolyzed with methanol when the reaction was shown to be complete by TLC.

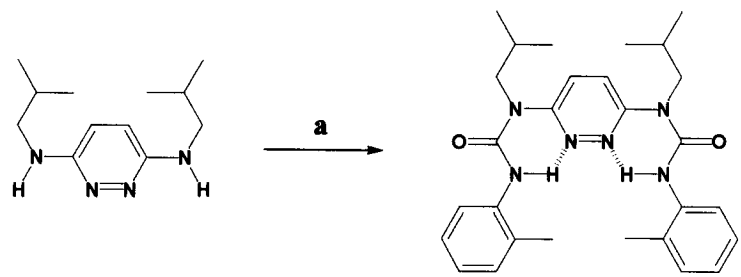

15 **24**

Scheme 3.5. The synthesis of trimer **24**: (a) OTI (2.5 eq.), anhydrous chloroform, 60°C, nitrogen, 3 hrs.

Pentamer **26** was prepared in a two-step reaction (Scheme 3.6): diamine **15** was reacted with OTI to form mono-capped dimer **25**, which, after purification, was reacted with TDI.

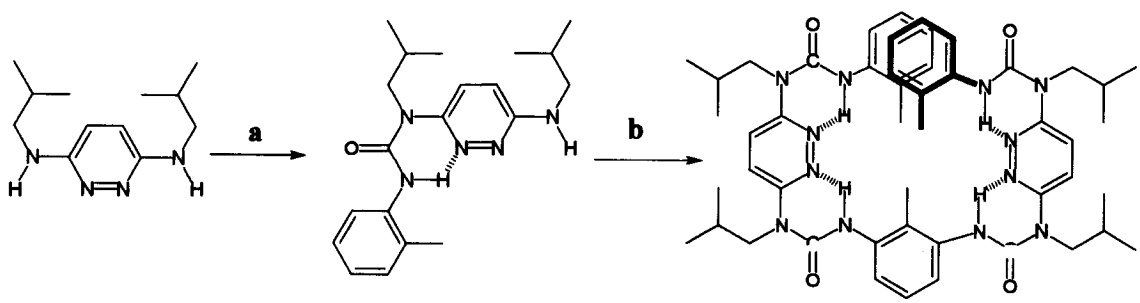

15 **25** **26**

Scheme 3.6. The synthesis of pentamer **26**: (a) OTI (1.2 eq.), anhydrous chloroform, 60 °C, nitrogen, 3 hrs; (b) TDI (0.5 eq.), anhydrous chloroform, 60 °C, nitrogen, 24 hrs.

3.4.3 Results and discussion

3.4.3.1 Trimer (24)

Trimer **24** was obtained as a white wax after purification by column chromatography. In the ^{1}H NMR spectrum (Figure 3.25), there is a singlet at 11.45 ppm that is characteristic of an intramolecular hydrogen bonded urea N-H proton. The integration ratio of 2:2 relative to the pyridazine hydrogens indicates the urea N-H protons are equivalent. Both urea protons form hydrogen bonds with the pyridazine nitrogen lone pairs and enforce the formation of a crescent structure. The complete assignment of the signals was determined with COSY NMR data (Figure 3.26).

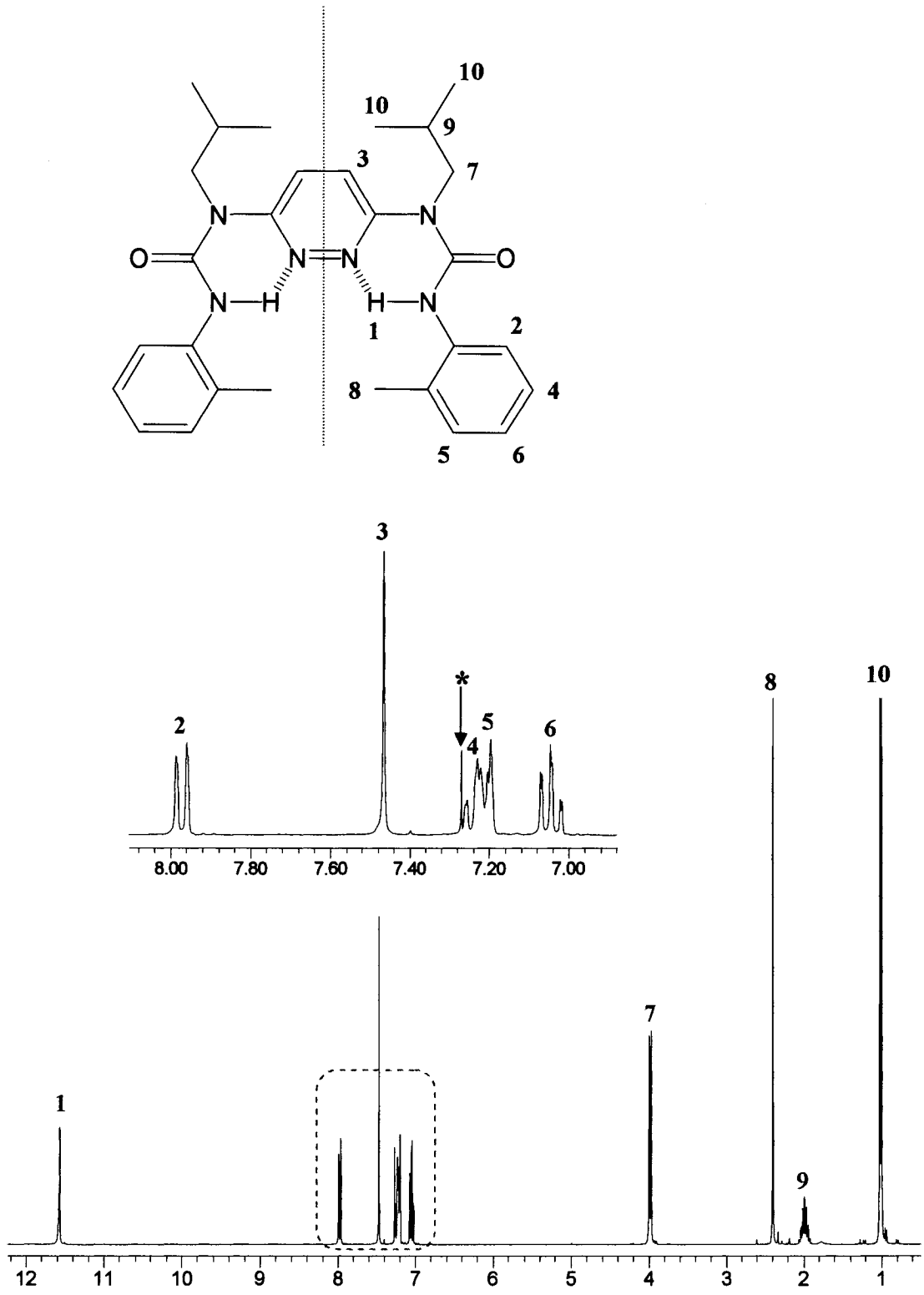

Figure 3.25. ^{1}H NMR spectrum of trimer **24** in $CDCl_3$. The aromatic region is highlighted and expanded. The solvent signal is marked with an asterisk. The structure has C_2 symmetry.

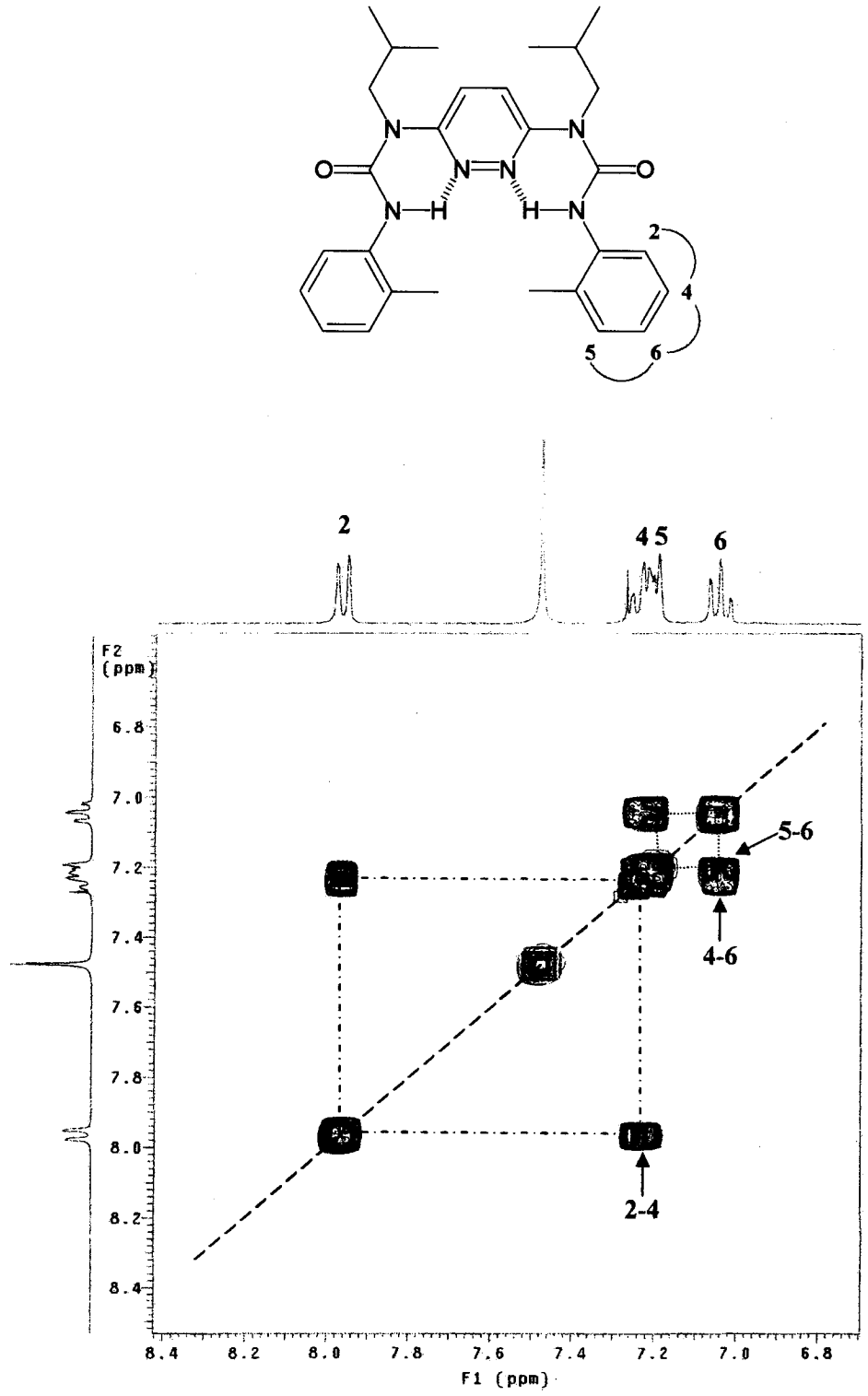

Figure 3.26. Aromatic region of the COSY spectrum for trimer **24** in $CDCl_3$.

The urea N-H and toluene methyl protons show a cross peak in the NOESY spectrum (Figure 3.27) that indicates the proximity of these two types of protons. This confirms the shown folded conformation. Further characterization of this molecule was obtained by mass spectrometry. The m/z peak at 489.2 is consistent with protonated trimer **24** ($C_{28}H_{36}N_6O_2$, exact mass = 488.29) and the sodium adduct ($[M+Na]^+$) appeared at m/z 511.1.

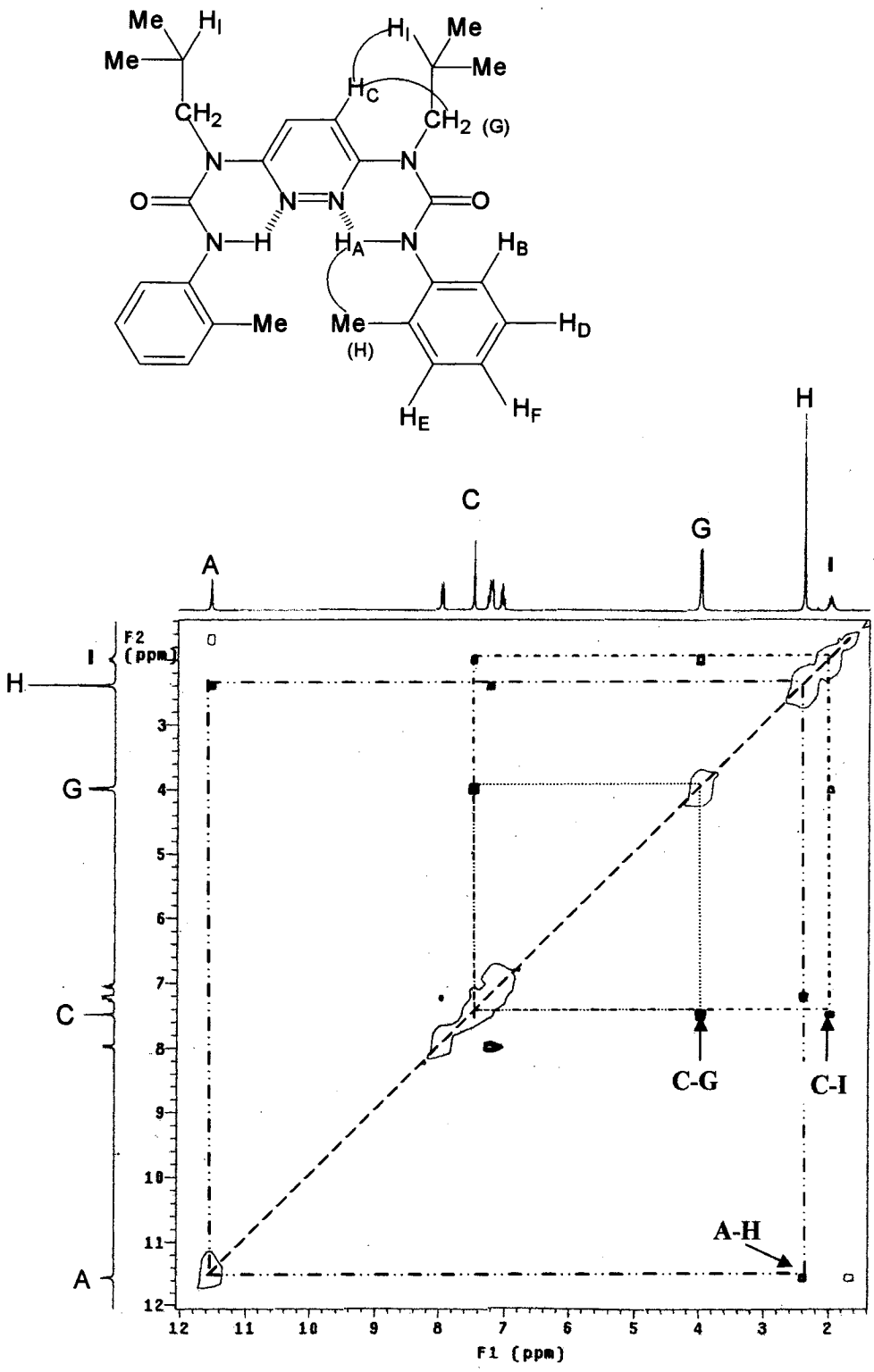

Figure 3.27. NOESY spectrum of trimer **24** in $CDCl_3$ (r.t., mixing time: 0.3s).

Crystals suitable for X-ray single crystal diffraction were grown by slow evaporation from ethanol (crystallographic data is available in Appendix D) Trimer **24** (Figures 3.28 - 3.31) crystallized as a mixture of two helical segments with opposite chirality. Hydrogen bonding interactions were observed between the urea protons and pyridazine nitrogens, and the carbonyl groups and toluene methyl groups were *anti* to each other as expected due to steric repulsions.

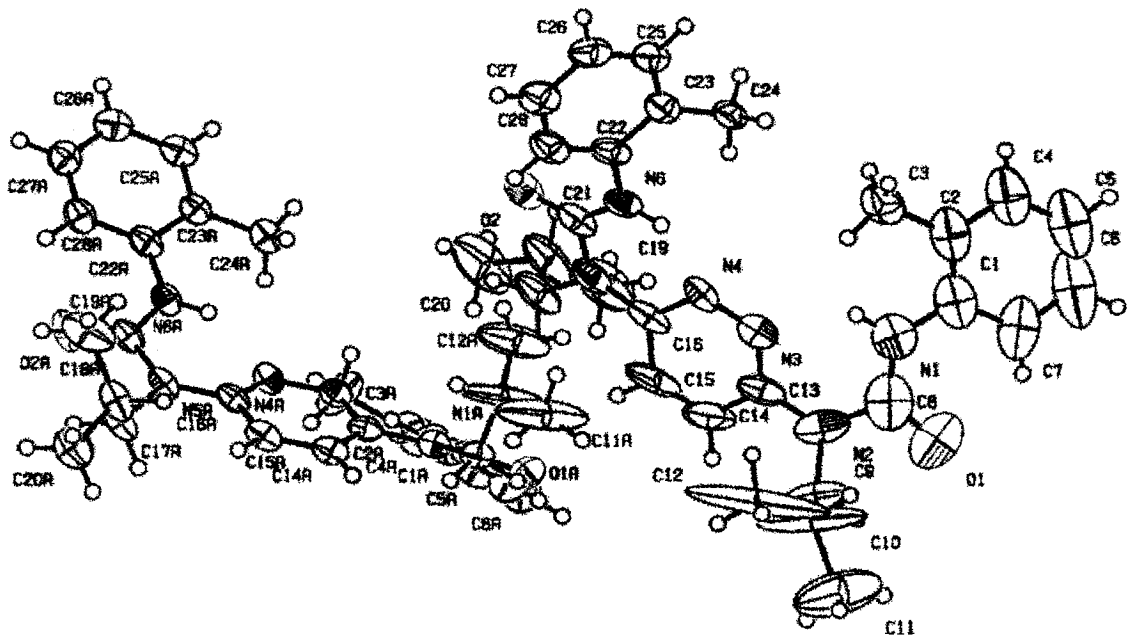

N6AA...N4A = 1.923 Å, N6AA-H6AA...N3A = 138.18 °

H1AA...N3A = 1.914 Å, N1AA-H1AA...N3A = 138.75 °

Figure 3.28. ORTEP view of trimer **24**.

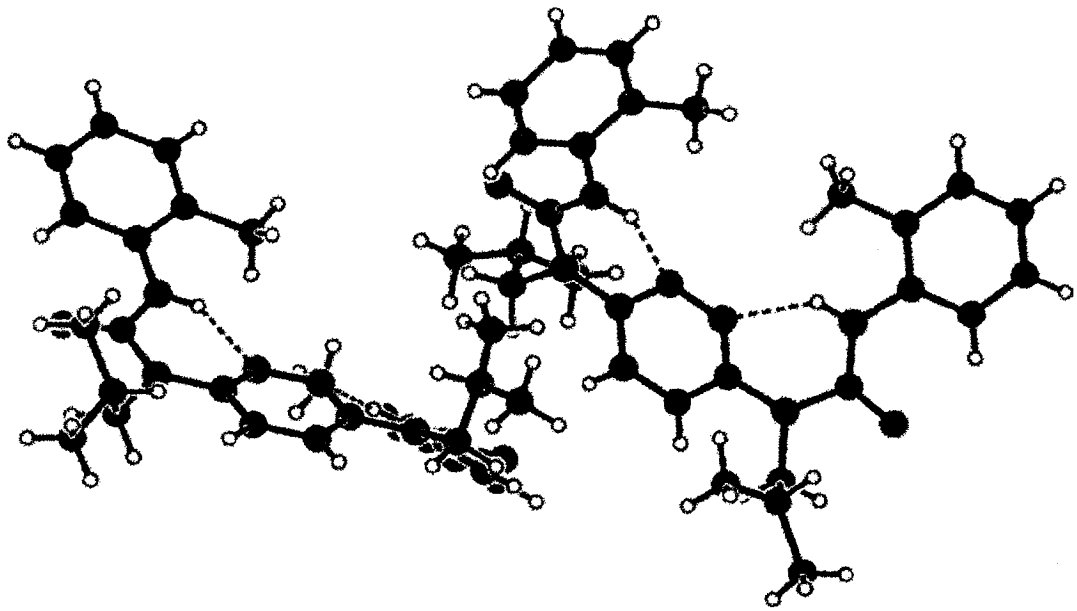

Figure 3.29. Intramolecular hydrogen bonding interactions in trimer **24**.

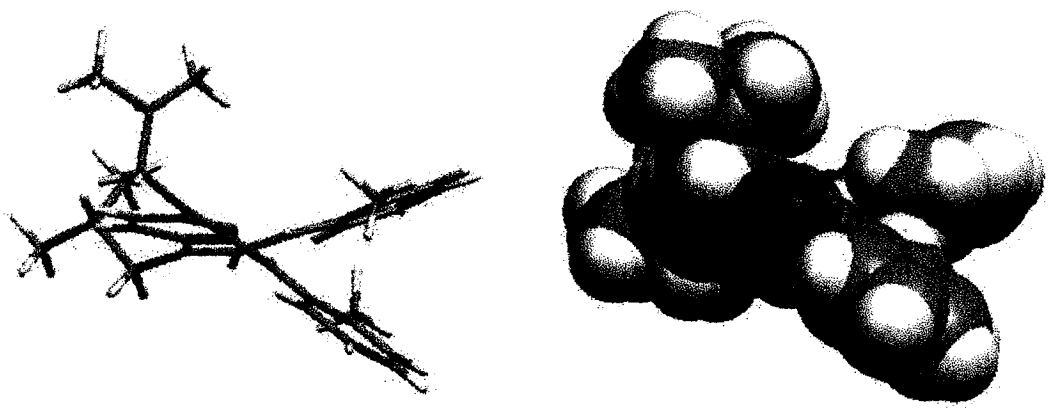

Figure 3.30. (Left) capped stick and (right) space-filling representations of one helical conformation of trimer **24**.

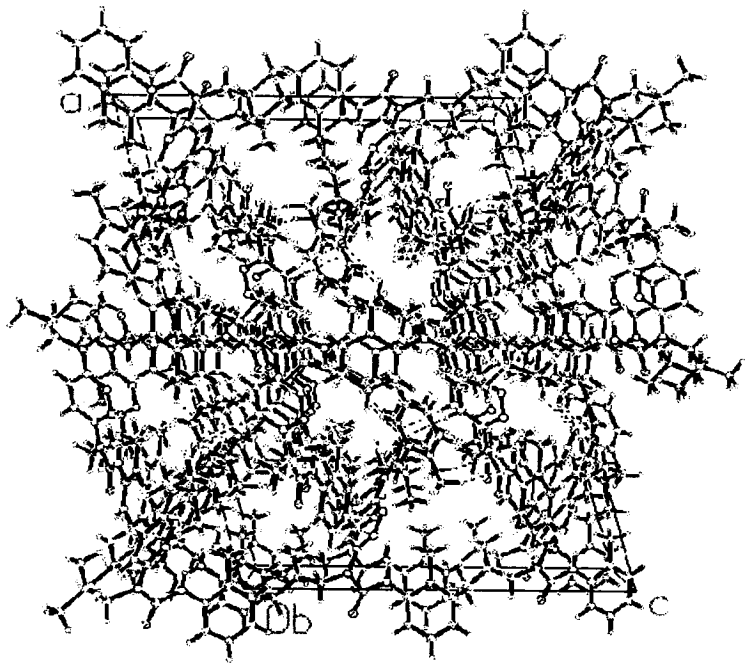

Figure 3.31. Top view of packing pattern in trimer **24**.

3.4.3.2 Pentamer (26)

Pentamer **26** was the major product from the reaction of mono-capped dimer **25** and TDI. In the mass spectrum (Figure 3.32), there are three groups of signals: the signals starting at m/z 885.5 correspond to the proton adduct of pentamer **26** ($C_{49}H_{64}N_{12}O_4$, exact mass = 884.52), and the isotopic groups at m/z 907.4 and 923.4 are consistent with the sodium and potassium ion adducts.

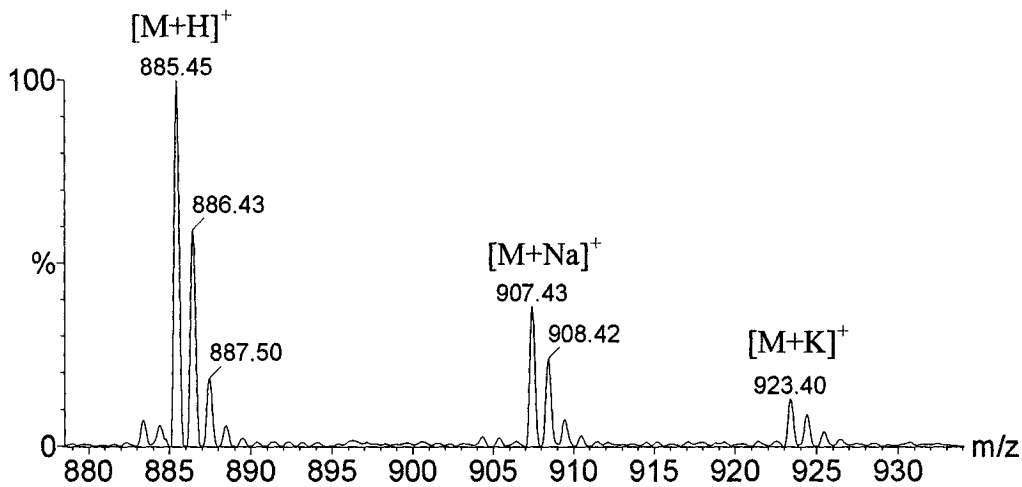

Figure 3.32. MALDI-TOF-MS spectrum of pentamer **26** mixture with DIT (dithranol) as matrix.

The urea N-H protons and toluene methyl protons in the ^{1}H NMR spectrum are the fingerprint signals of folding for this structure (Figure 3.33).

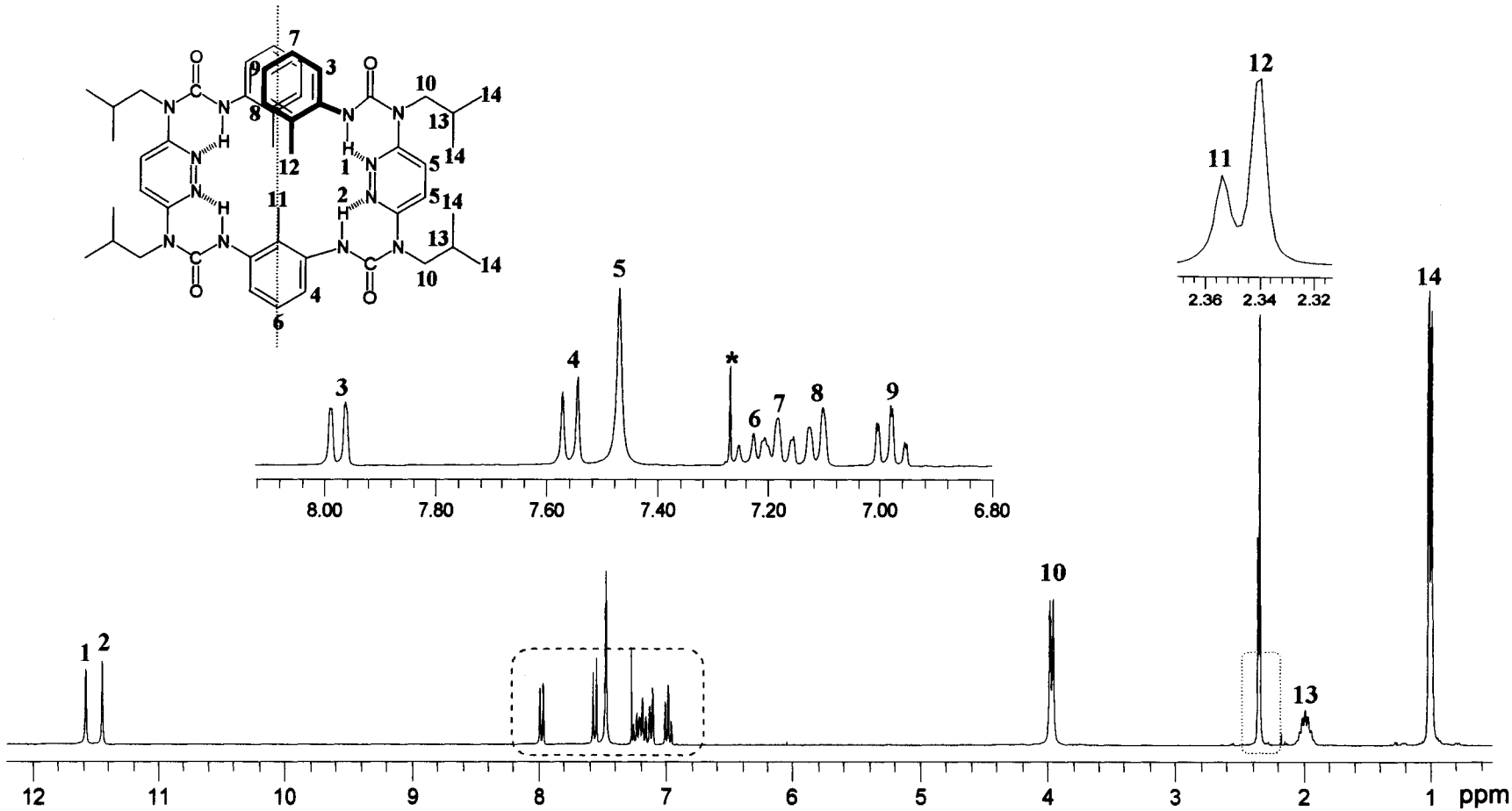

Figure 3.33. ^{1}H NMR spectrum of pentamer **26** in $CDCl_3$. The asterisk represents solvent residue.

There are two types of hydrogen bonded urea protons with a 1:1 integration ratio that appear at 11.56 and 11.43 ppm, respectively. Also, there are two types of methyl protons from the interior and terminal toluene groups that show an integration ratio of 1:2 and they appear as partially overlapping peaks at 2.34 and 2.35 ppm. The two pyridazine protons in the aromatic region overlap and merge into one relatively broad singlet with a 1:1 integration ratio compared to the urea protons. The assignment of the signals was determined with COSY NMR data (Figure 3.34).

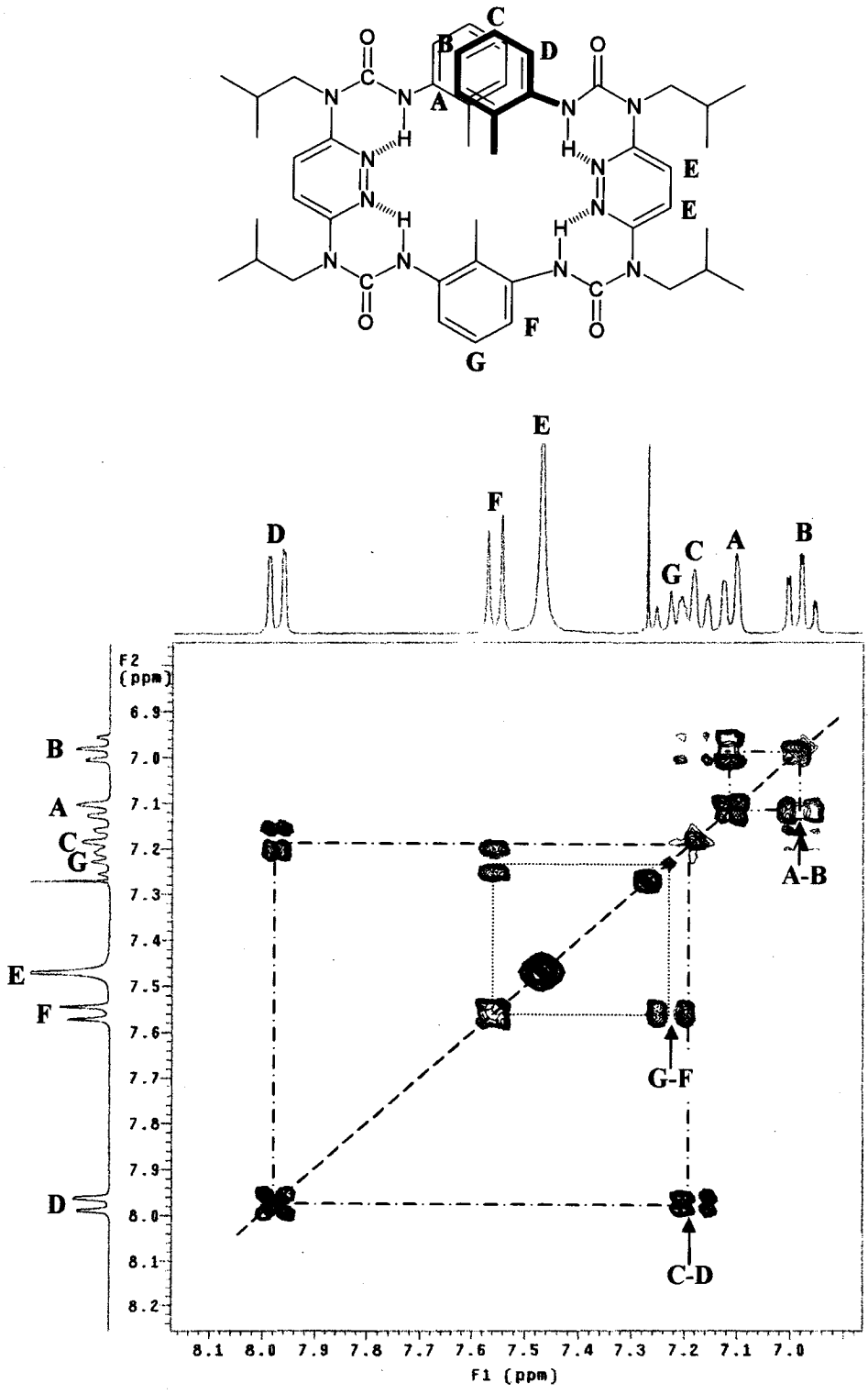

Figure 3.34. Aromatic region of COSY spectrum of pentamer **26** in $CDCl_3$.

The terminal toluene protons are structurally similar to those of trimer **24**; however, except for **H1**, the other three protons show appreciably lowered chemical shifts (Figure 3.35). The shielding effect is proposed to be due to intramolecular stacking when the terminal toluene groups overlap: **H3** and **H4** are affected more and thus show larger upfield shifting, while **H1**, being further away from the overlapped area, is less shielded. This type of shielding is diagnostic of helix formation in isomeric pyridine-pyrimidine,[39, 43, 139] pyridine-pyridazine[40] and pyrimidine-naphthyridine[41] molecular strands and is also characteristic for the aromatic termini of helicenes and heterohelicenes[140, 141].

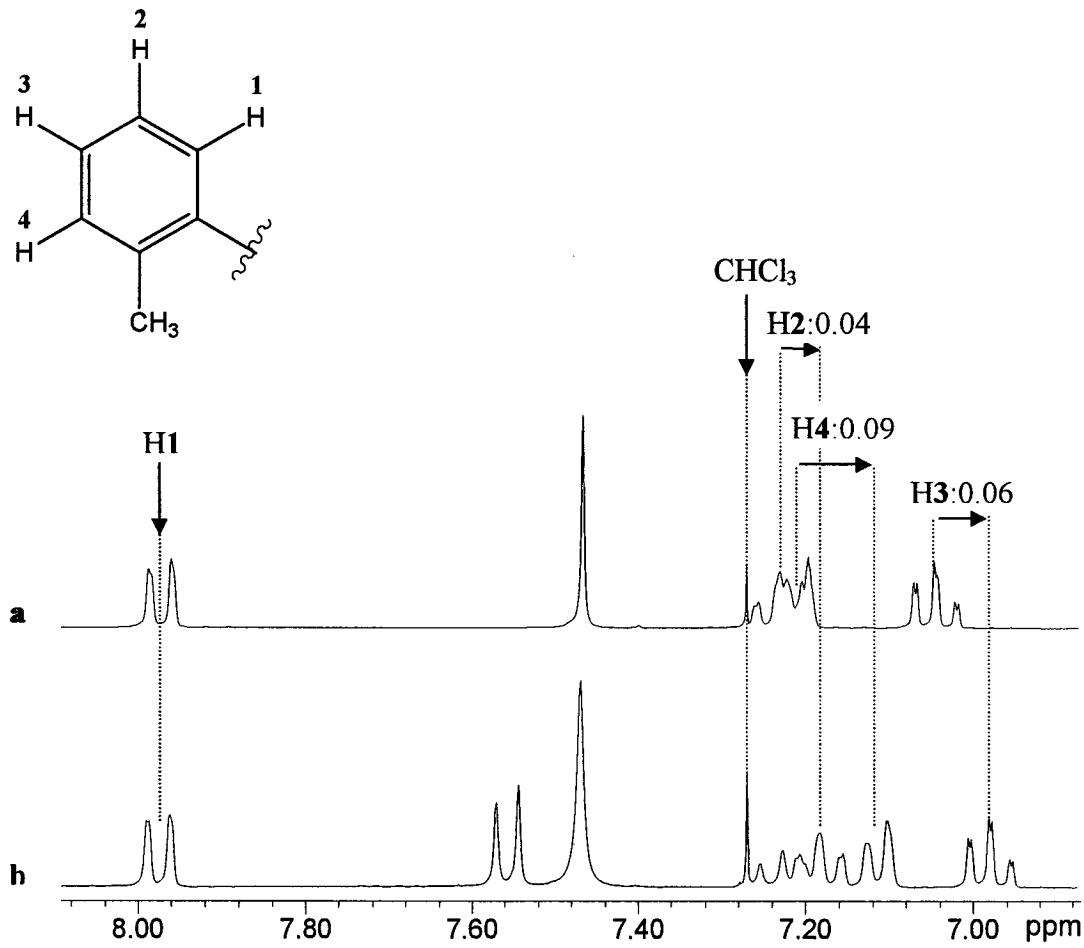

Figure 3.35. Comparison of the chemical shifts for the terminal toluene protons in (a) trimer **24** and (b) pentamer **26** in $CDCl_3$.

Another key difference between trimer **24** and pentamer **26** was observed in the NOESY spectrum (Figure 3.36). For pentamer **26**, there are two cross peaks corresponding to the two urea protons (N-H) and the two methyl groups, but only one for trimer **24**. By zooming in these two cross peaks, the two types of correlation could be distinguished from each other (Figure 3.37). The *anti* conformation of the methyl groups and carbonyl groups was thus verified.

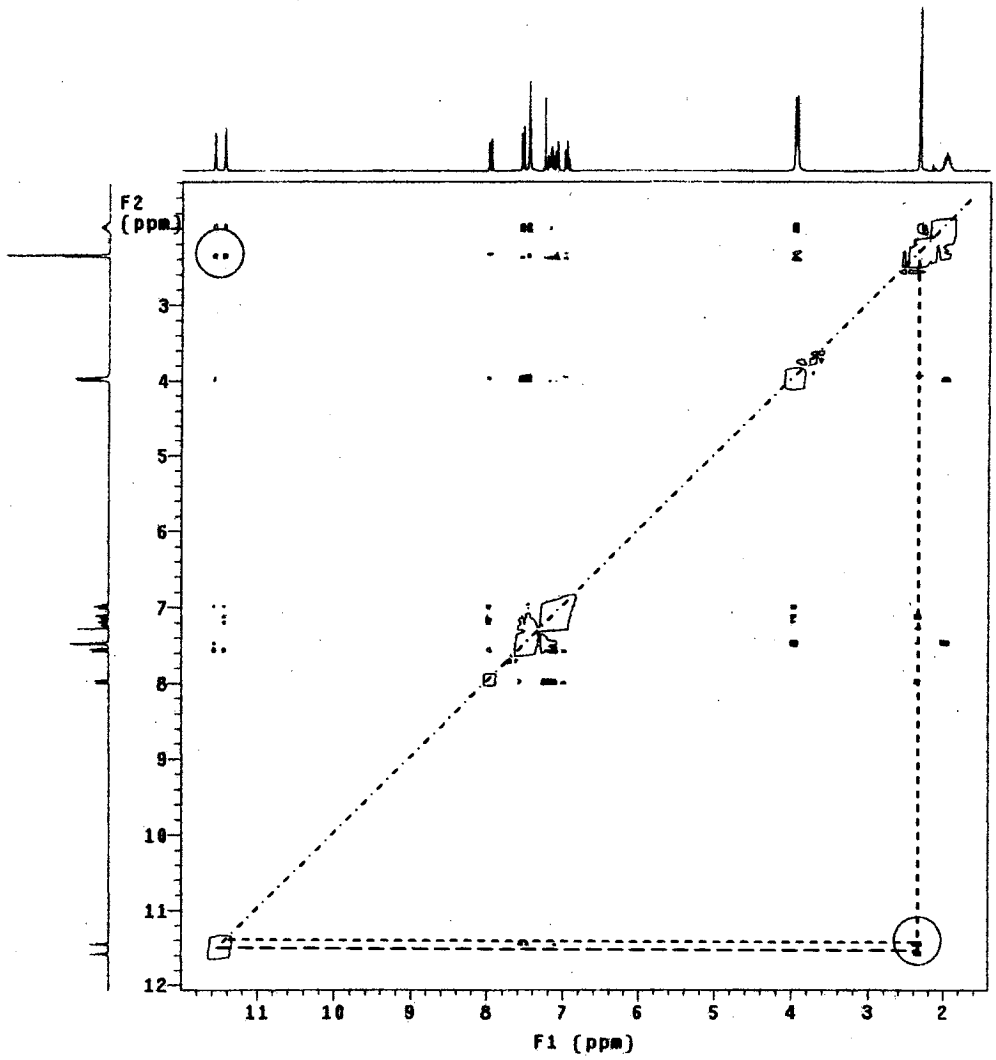

Figure 3.36. NOESY spectrum for pentamer **26** in $CDCl_3$ (r.t., mixing time: 0.3s).

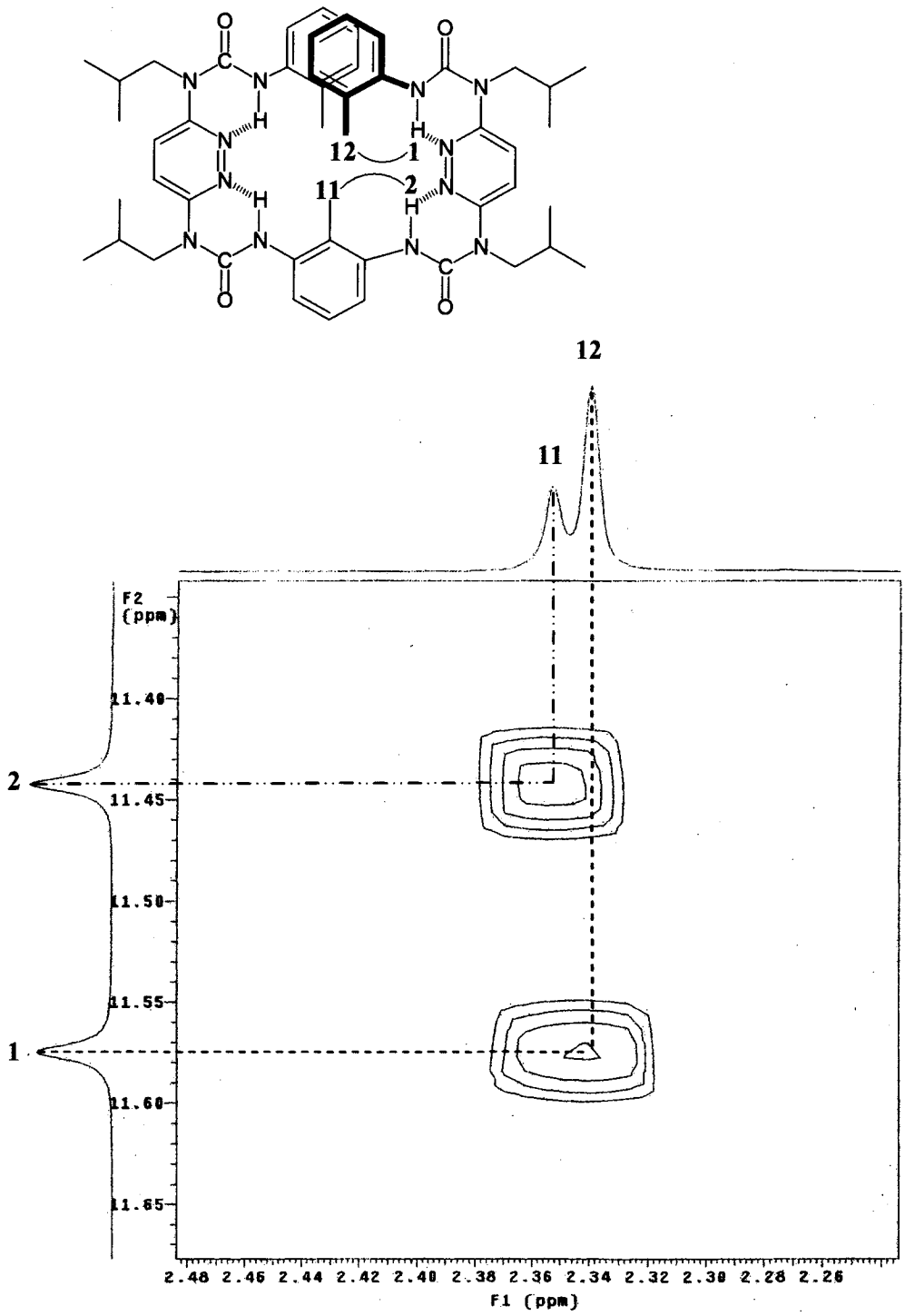

Figure 3.37. Expansion of the NOESY spectrum for pentamer **26** in $CDCl_3$ (r.t., mixing time: 0.3s).

3.4.4 Conclusions and future work

A crescent trimer **24** and helical pentamer **26** based on alternating urea linked pyridazine and toluene aromatic rings were synthesized. Similarly as shown for the macrocycles, the folded structures were mainly enforced by hydrogen bonding between urea protons and pyridazine nitrogen lone pairs and the unfavorable steric interactions of toluene methyl groups and carbonyl groups.

The crescent conformation for trimer **24** was confirmed by the two equivalently hydrogen bonded urea protons revealed in the ^{1}H NMR spectrum. The proximity of the terminal toluene methyl protons and adjacent urea proton was verified by a NOESY experiment. Two helical conformers with different chirality (P and M) were observed in the unit cell of the crystal structure. We are currently preparing oliogmers of this type with chiral side chains to obtain homochiral helices.

For pentamer **26,** two types of urea protons with a 1:1 integration ratio and two types of toluene methyl protons with a 1:2 integration ratio of the interior and terminal toluene groups in the ^{1}H NMR spectrum are consistent with the proposed pentameric helical strand. The upfield shifting of the terminal toluene signals is indicative of intramolecular stacking, which indicates the folding pattern persists as the termini overlap and points to the possibility of preparing longer helical strands with this design. Unfortunately, we have not yet obtained a crystal structure of pentamer **26**.

The aim to obtain foldamers by making use of intramolecular hydrogen bonding and steric interactions was realized by the successful preparation of trimer **24** and pentamer **26**, which also opens the way to make longer helical strands. We are currently attempting a protection/deprotection methodology to prepare a nonamer in a convergent

approach (Scheme 3.7). Diamine **15** was partially protected with $(Boc)_2O$ to form **27** which was then reacted with TDI to prepare the bis-protected trimer **28** with a yield of 75%. We are currently investigating appropriate deprotection methods of **28** to obtain trimeric diamine **29** that will react with TDI to form bis-protected heptamer **30**. The same deprotecting procedure will be applied to obtain heptameric diamine **31** that will be subsequently 'bis-capped' to make the target nonamer **32**.

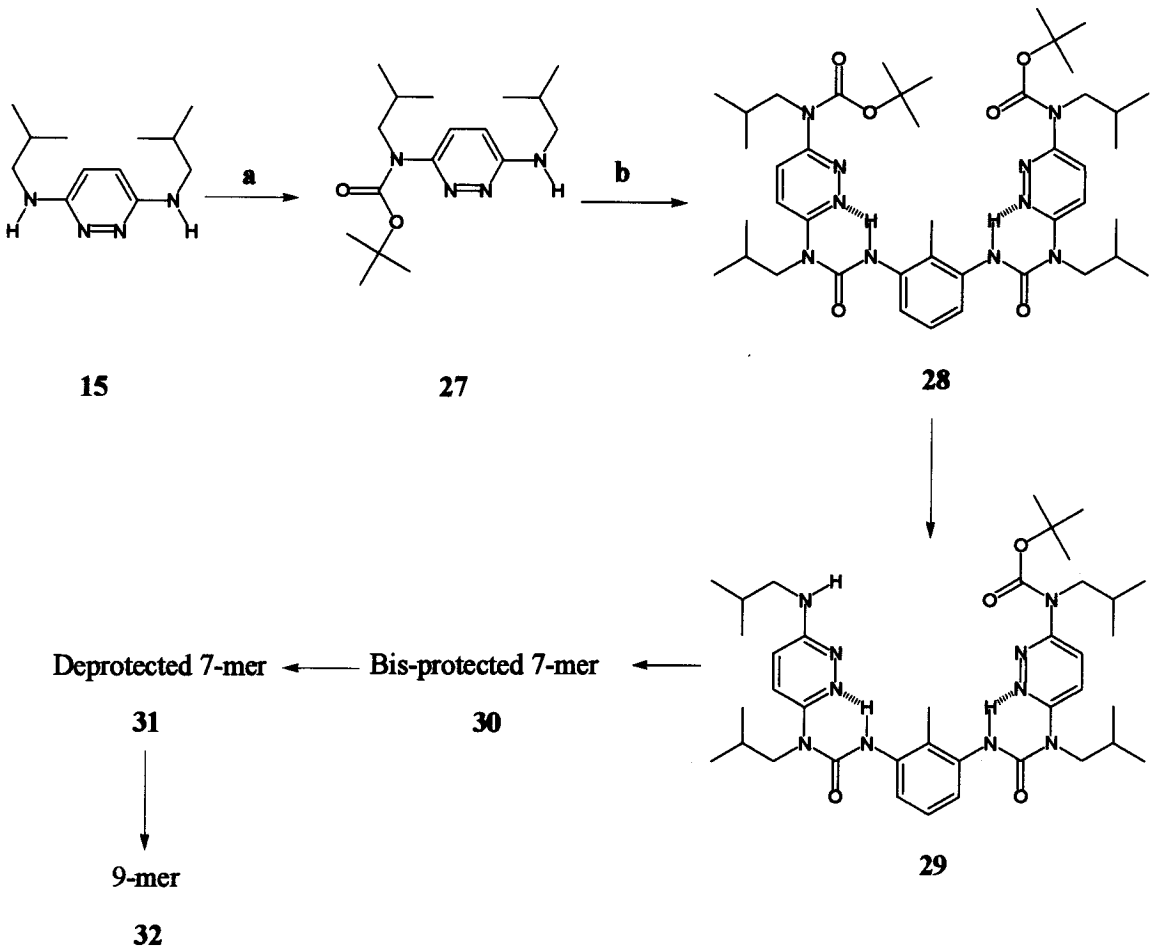

Scheme 3.7. The synthesis of nonamer **32** *via* a protection-deprotection approach: (a) $(Boc)_2O$, (1.1 eq.), TEA (2 eq.) anhydrous methylene chloride, r.t., 3 hrs; (b) TDI (0.5 eq.), anhydrous chloroform, 60 °C, nitrogen, 24 hrs.

Chapter 4

Experimental

4.1 General methods

All the chemicals were obtained from Aldrich and were used without further purification unless specified otherwise. All the solvents used were HPLC grade. Dimethyl sulfoxide (DMSO), tetrahydrofuran (THF) and chloroform used in reactions were obtained anhydrous in SureSeal bottles and used under nitrogen flow. Choroform-d ($CDCl_3$, 99.8%) and DMSO-d_6 (99.8%) were purchased from Cambridge Isotopes. 1,3-phenyl diisocyanate (PDI), 2,6–tolylene diisocyanate (TDI) and *o*-tolylene isocyanate (OTI) were stored at 4 °C and were warmed to room temperature before use.

Melting points (m.p.) were recorded with a capillary melting point apparatus (Thomas Hoover) and are uncorrected. The recorded R_f values were determined by a standard thin-layer chromatography (TLC) procedure: 0.25 mm silica gel plates (Aldrich, Z122785-25EA) eluting with the specified solvents. FTIR spectra were recorded with a Magna-IR Spectrometer 550 (Nicolet) in KBr pellets. 300 MHz ^1H NMR spectra and 75 MHz ^{13}C NMR spectra were recorded on a Varian 300 spectrometer. 500 MHz ^1H NMR were recorded on a Varian 500 spectrometer. The spectra were recorded at room temperature unless specified otherwise. The residual proton signals of the deuterated solvents were used as internal standards (DMSO-d_6: $\delta(^1H)$ = 2.50 ppm, $\delta(^{13}C)$ = 39.51 ppm; $CDCl_3$: $\delta(^1H)$ = 7.27 ppm, $\delta(^{13}C)$ = 77.23 ppm). The following notation is used for the ^1H NMR splitting patterns: singlet (s), doublet (d), triplet (t), quartet (q), doublet-doublet (d-d), triplet-doublet (t-d), mutiplet (m) and broad signal (br). ^1H coupling

constants are given in Hz and the values are for three-bond coupling protons unless specified otherwise. MALDI-TOF mass spectra were obtained using a Micromass BAA037 (Micromass, UK) time-of-flight mass spectrometer. A nitrogen laser (337 nm wavelength) was used to desorb the sample ions. The matrices used were dihydroxybenzoic acid (DHB), dithranol (DIT), or *trans*-indoacrylic acid (IAA) and the spectra were recorded in the positive reflectron mode. FAB mass spectra (8 KV, Xe) were recorded on a KRATOS MS25RFA with *m*NBA (*meta*-nitrobenzyl alcohol) as matrix. ESI spectra were recorded on a FINNIGAN LCQ DUO mass spectrometer using ESI probe by infusion (10μL/min) with integrated syringe pump. X-ray diffraction data for **7** was collected on a Bruker AXS Smart 2K/Platform diffractometer with a graphite monochromated CuKα radiation (1.54178 Å), ω scans at 100(2) K. For **22**, **23** and **24**, the data was collected on a Bruker D8 X-ray diffractometer with a graphite monochromatized MoKα radiation (0.71073Å), θ scans at 100(2) K.

Compounds **1**, **2** and **3** were synthesized following literature procedures and the products were used in next step without purification. The ^{1}H NMR spectra were in agreement with the literature data[55, 72, 73].

4.2 Experimental procedures

2-amino-7-hydroxyl-1,8-naphthyridine (1)

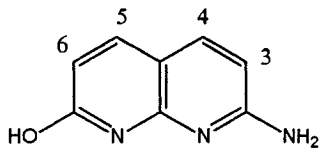

Concentrated sulfuric acid (20 mL) was slowly added to a solid mixture of 2,6-diaminopyridine (5.63 g, 51.6 mmol) and malic acid (8.19 g, 61.1 mmol). The solution was then heated at 110 °C for 3 hours. After cooling to room temperature, the dark red solution was poured on ice and made basic (pH~8) with concentrated ammonium hydroxide. A bright yellow precipitate appeared and the mixture was washed with water and centrifuged 4 to 5 times. The product was lyophilized giving a quantitative yield of a yellow powder. ^{1}H NMR (300 MHz, DMSO-d_6): δ = 7.61 (d, J = 9.0 Hz, 2H, H-4, 5), 6.67 (s, 2H, NH_2), 6.31 (d, J = 9.0 Hz, 1H, H-6), 6.08 (d, J = 9.0 Hz, 1H, H-3).

2-acetamido-7-hydroxy-1,8-naphthyridine (2)

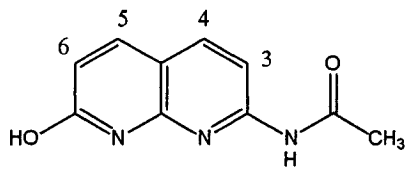

2-amino-7-hydroxyl-1,8-naphthyridine **1** (2.70 g, 16.8 mmol) and acetic anhydride (27 mL, 286mmol) were reacted at 145 °C for 3 hours. After the mixture was cooled to room temperature, the solution was filtered and washed with diethyl ether to yield dark yellow crystals (3.20 g, 94%). ^{1}H NMR (300 MHz, DMSO-d_6): δ = 11.88 (s, 1H, naphthyridinone NH), 10.56 (s, 1H, NH), 8.04 (d, J = 8.7 Hz, 1H, H-4), 7.95 (d, J = 8.4 Hz, 1H, H-3), 7.84 (d, J = 8.7 Hz, 1H, H-5), 6.42 (d, J = 8.4Hz, 1H, H-6), 2.14 (s, 3H, CH_3).

2-acetamido-7-chloro-1,8-naphthyridine (3)

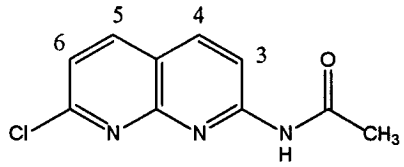

$POCl_3$ (55 mL, 590mmol) was slowly added to 2-acetamido-7-hydroxy-1,8-naphthyridine **2** (3.10 g, 15 mmol) and the mixture was reacted at 90 °C for 1.5 hours. The solution became black once the reaction was completed. Most of the remaining $POCl_3$ was removed by vacuum distillation. Ice was slowly added to the black sticky product to hydrolyze the remaining POCl3 (caution! – delayed exothermic reaction). The solution was kept on ice and cold water was subsequently added and the solution was then made basic (pH~8) with concentrated ammonium hydroxide to give a dark brown precipitate. The solid was collected by vacuum filtration and vacuum dried. The dried product was extracted by Soxhlet extraction in chloroform overnight and the solvent was evaporated under vacuum to yield a yellow powder (2.40 g, 70%). ^1H NMR (300 MHz, DMSO-d_6): δ = 11.16 (s, 1H, NH), 8.44 (m, 3H, H3, 4, 5), 7.56 (d, J = 8.4 Hz, 1H, H-6), 2.18 (s, 3H, CH_3).

2-amino-7-chloro-1,8-naphthyridine (4)

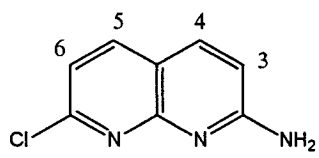

2-acetamido-7-chloro-1,8-naphthyridine **3** (2.0 g, 9 mmol) was dissolved in 15% sulfuric acid (10 mL, ca. 27 mmol) and refluxed for 1 hour. After cooling to room temperature, 30% ammonium hydroxide was added slowly to adjust the pH to 8. A light yellow product precipitated out. The mixture was filtered and washed with water and then vacuum dried to yield 1.23 g of product (76%). R_f = 0.5 (methylene chloride/methanol, 9/1); m.p. = 134-135 °C; ^{1}H NMR (300 MHz, DMSO-d_6): δ = 8.18 (d, J = 8.1 Hz, 1H, H-5), 8.07(d, J = 8.7 Hz, 1H, H-4), 7.52 (s, 2H, NH_2), 7.30(d, J = 8.1 Hz, 1H, H-6), 6.90 (d, J = 8.7Hz, 1H, H-3), ^{13}C NMR (75 MHz, DMSO-d_6): δ = 160.13, 154.03, 151.36, 139.90, 138.57, 118.25, 115.53, 113.98 ; MS (MALDI-TOF): m/z 179.5 $[M+H]^+$ (100%).

2,7-diamino-1,8-naphthyridine (5)

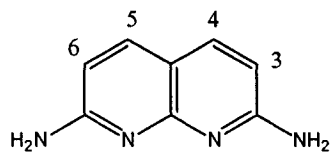

2-amino-7-chloro-1,8-naphthyridine **4** (1.0 g, 5.5 mmol) was dissolved in saturated ammonium hydroxide (150 mL) in a thick-walled sealed tube* and heated at 150 °C for 24 hours. After cooling to room temperature, water was removed under vacuum and the resulting product was dried under vacuum. The dried product was purified by column chromatography (the crude product was dissolved in methanol and some silica gel was added. The solvent was removed from the sample-silica mixture under vacuum and then loaded on the top of a pre-packed column of silica gel) to yield a light yellow powder (0.56 g, 63 %). R_f= 0.80 (chloroform/methanol, 8/3); ^{1}H NMR (500

MHz, DMSO-d_6): δ = 7.77 (d, J = 8.5 Hz, 2H, H-4,5), 7.09 (s, 4H, NH_2), δ 6.50 (d, J = 8.5 Hz, 2H, H-3,6); ^{13}C NMR (75 MHz, DMSO-d_6): δ = 159.50, 152.61, 138.62, 108.64, 107.07; MS (MALDI-TOF): m/z 160.5 $[M+H]^+$ (100%). *To avoid the potentially hazardous sealed tube reaction, another method for the preparation of this product that involves the reaction of 2-amino-7-chloro-1, 8-naphthyridine **4** with 4-methoxybenylamine in pyridine at 120 °C has recently been suggested by Zimmerman.[142]

Cyclo-tris (2, 7-(1, 8-napthyridyl)-urea) (6)

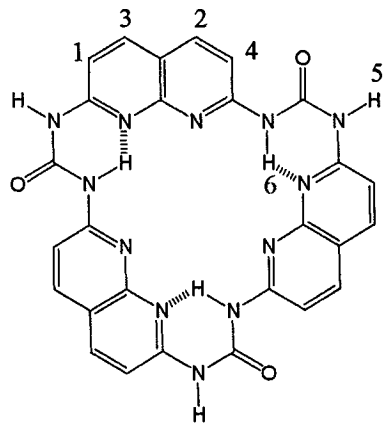

Diamine **5** (0.10 g, 0.63 mmol) was dispersed in 1 mL DMSO under nitrogen to form a yellow suspension at 120 °C. 1,1'-carbonyl-diimidazole (0.17 g, 0.94 mmol, 50 % molar excess) was dissolved in DMSO (0.2 mL) at room temperature under nitrogen and then added dropwise into the suspension. The solid was completely dissolved resulting in a clear yellow solution. The solution gradually became cloudy over a period of 30 minutes. The reaction was continued at 120 °C under nitrogen for 24 hours and then cooled to room temperature. The reaction mixture was filtered and washed with methanol to yield a

light yellow powder (0.075 g, 64%). ^{1}H NMR (300 MHz, DMSO-d_6): δ = 12.22 (s, 3H, H-6), 10.68 (s, 3H, H-5), 8.61 (d, J = 9.1 Hz, 3H. H-4), 8.37 (d, J = 9.1 Hz, 3H, H-3), 8.39 (d, J = 9.1 Hz, 3H, H-2), 7.26 (d, J = 9.1 Hz, 3H, H-1); IR (KBr, ν = cm^{-1}): 3140, 3120, 1720; MS (MALDI-TOF): m/z 558.7 $[M + H]^+$ (100%), 580.7 $[M + Na]^+$ (100%).

Cyclo-tris (2,7-(1,8-naphthryidyl)-formamidine) (7)

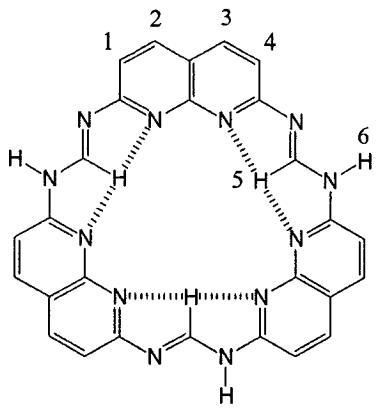

Diamine **5** (0.048 g, 0.3 mmol) was dissolved in DMSO (0.3 mL) at 120 °C to form a yellow suspension to which triethylorthoformate (0.089 g, 0.6 mmol) was added under nitrogen. The solution immediately turned bright yellow and turned red-brown in 2 hours. After cooling to room temperature, the product was precipitated with methanol. The solid was filtered and washed with methanol and vacuum dried at 60 °C for 24 hours to yield a bright yellow powder (0.038 g, 75%). ^{1}H NMR (300 MHz, DMSO-d_6): δ = 11.54 (s, 3H, H-6), 10.68 (s, 3H, H-5), 8.32 (d, J = 8.5, 6H, H-2, 3), δ 7.23 (d, J = 7.5 Hz, 6H, H-1, 4); ^{13}C (75 MHz, DMSO-d_6): δ = 154.53, 151.56, 139.03; IR (KBr, ν = cm^{-1}): 3375, 3202, 3315, 1654, 1594, 1121; MS (MALDI-TOF): m/z 510.9 $[M+H]^+$ (100 %), 532.9 $[M+Na]^+$ (100 %); 548. 9 $[M+K]^+$ (100 %).

(6-Chloro-pyridazin-3-yl)-phenylamine (8)

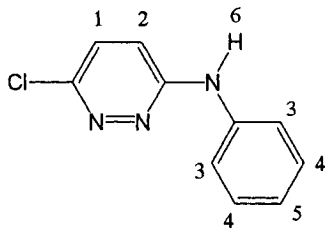

3,6-dichloropyridazine (4.0 g, 26.8 mmol) and aniline (2.5 g, 26.8 mmol) were dissolved in ethanol (20 mL) and reacted at 60 °C for 3.5 hours. When cooled to room temperature, isobutylamine (12 mL, 120mmol) was added and a precipitate formed at once. The solid was filtered and washed with ethanol twice to yield yellow flake like crystals (4.25 g, 77%). $R_f = 0.49$ (chloroform/acetone, 8/2); m.p. = 181-182 °C; ^{1}H NMR (300 MHz, $CDCl_3$): δ = 7.40 (m, 2H, H-4), 7.33 (m, 2H, H-3), 7.27 (d, J = 9.3 Hz, 1H, H-1), 7.18(m, 1H, H-5), 7.12 (d, J = 9.3 Hz, 1H, H-2); ^{13}C NMR (75 MHz, DMSO-d_6): δ = 157.48, 155.26, 138.68, 129.95, 129.85, 125.06, 121.93, 116.60; MALDI-TOF-MS: m/z: 205.6 $[M+H]^+$ (100%).

***N, N'*-Diphenyl-pyridazne-3, 6-diamine (9)**

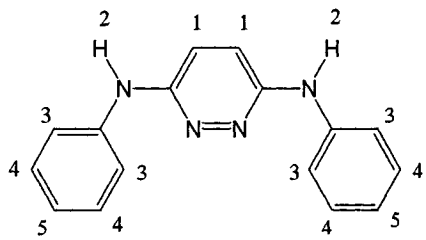

3,6-dichloropyridazine (2.0 g, 13.4 mmol) and aniline (3.75 g, 40.3 mmol) were reacted at 120 °C for 20 minutes. Ethanol (15 mL) was subsequently added and the product

mixture was refluxed for 2 hours. After cooling to room temperature, a yellow solid precipitated out that was isolated by filtration. The solid was redissolved in ethanol (20 mL) and then poured into saturated sodium bicarbonate solution (100 mL). The neutralized product was filtered and recrystallized in ethanol twice and the final product was isolated as golden flake-like crystals (1.78 g, 50.1%). R_f= 0.31(chloroform/acetone, 8/2); m.p. = 193.5-195.5 °C. ^{1}H NMR (300 MHz, DMSO-d_6): δ = 8.91(s, 2H, H-1), 7.73 (d, J = 8.1 Hz, 4H, H-2), 7.27(m, 4H, H-3), 7.10(s, 2H, H-1); 6.87(m, 2H, H-4); ^{13}C NMR (75 MHz, DMSO-d_6): δ = 152.24, 141.73, 128.64, 120.09, 120.05, 117.46; MALDI-TOF-MS: m/z: 262.7 $[M+H]^+$ (100%).

(6-Chloro-pyridazin-3-yl)-(4-decyl-phenyl)-amine (10)

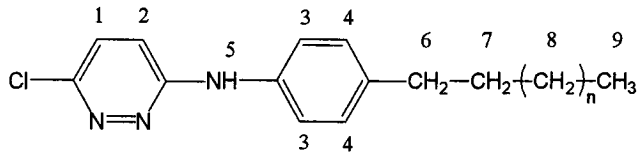

3,6-dichloropyridazine (0.17 g, 1.14 mmol) and 4-decylaniline (0.26 g, 1.14 mmol) were reacted at 70-80 °C for 1 hour. The crude product was dissolved in ethanol and precipitated in saturated sodium carbonate solution. After drying at 60 °C, the product was purified by silica gel column chromatography (chloroform/acetone, 9.5/0.5). The first fraction (0.17 g, 43%) was the mono-substituted product **10** and the second fraction (0.056 g) was identified as the bis-substituted pyridazine **11**. Product **10**: R_f = 0.77 (chloroform/acetone, 9.5/0.5); m.p = 106-107 °C. ^{1}H NMR (500 MHz, DMSO-d_6): δ = 9.37 (s, 1H, H-5), 7.57 (d, J = 8.5 Hz, 2H, H-3), 7.54 (d, J = 9.0 Hz, 1H, H-1), 7.16 (d, J = 9.0 Hz, 1H, H-2), 7.14(d, J = 8.5 Hz, 2H, H-4), 2.52 (t, J = 8.0 Hz, 2H, H-6), 1.54 (m,

2H, H-7), 1.23-1.27(m, 14 H, H-8), 0.84 (t, J = 6.5 Hz, 3H, H-9); ^{13}C NMR (75 MHz, $CDCl_3$): δ = 158.08, 148.03, 140.07, 136.30, 129.80, 129.48, 122.38, 115.99, 35.61, 32.12, 31.72, 29.84, 29.81, 29.72, 29.54, 29.50, 22.89, 14.33; MALDI-TOF-MS: m/z: 345.8 $[M+H]^+$ (100%).

***N, N'*-Bis-(4-decyl-phenyl)-pridazine-3,6-diamine (11)**

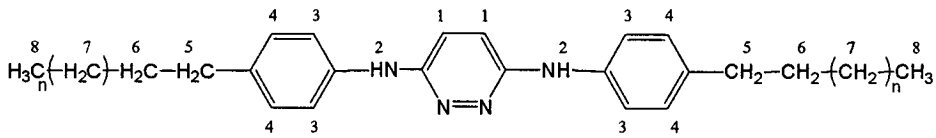

3,6-dichloropyridazine (0.50 g, 3.36 mmol) and 4-decylaniline (1.84 g, 7.87 mmol) were reacted at 120 °C for 15 minutes (the mixture became very viscous). The crude product was dissolved in ethanol (10 mL) and precipitated by increasing the pH with concentrated aqueous sodium hydroxide. The product was filtered and the solid was redissolved in chloroform and extracted with water to remove the salt. The organic layer was dried by anhydrous sodium sulfate and filtered. The solvent was removed from the filtrate under vacuum to afford golden flake-like crystals (1.5 g, 83%). R_f = 0.57 (chloroform/acetone, 8/2); m.p. = 193.5-195.5 °C; ^1H NMR (500 MHz, DMSO-d_6): δ = 8.76 (s, 2H, H-2), 7.61(d, J = 8.0 Hz, 4H, H-3), 7.08 (d, J = 8.5 Hz, 4H, H-4), 7.03 (s, 2H, H-1), 1.54 (t, 4H, H-6), 1.24-1.28 (m, 28H, H-7), 0.85 (t, J = 6.5 Hz, 6H, H-8); ^{13}C NMR (75 MHz, $CDCl_3$): δ = 153.64, 138.24, 138.04, 129.54, 120.41, 117.80, 35.54; 32.13, 31.83, 29.94, 29.84, 29.75, 29.56, 29.52, 22.91, 14.34; MALDI-TOF-MS: m/z: 543.5 $[M+H]^+$ (100%).

3-Chloro-6-dodecylpyridazine (12)

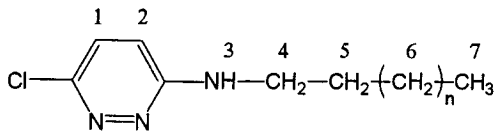

3,6-dichloropyridazine (4.0 g, 0.027 mol) and 1-dodecylamine (15 g, 0.081 mol) were reacted at 90-100 °C for 0.5 hours and then refluxed in ethanol (20 mL) for another hour. The crude product was precipitated in saturated sodium bicarbonate solution to yield a white powder (5.86 g, 73%). R_f= 0.67 (chloroform/acetone, 9.5/0.5); m.p = 85-86 °C; ^{1}H NMR (300 MHz, $CDCl_3$): δ = 7.15 (d, J = 9.3 Hz, 1H, H-1), 6.67 (d, J = 9.3, 1H, H-2), 5.02 (m, 1H, H-3), 3.36 (m, 2H, H-4), 1.64 (m, 2H, H-5), 1.25-1.37 (m, 18H, H-6), 0.88 (t, J = 6.9 Hz, 3H, H-7); ^{13}C NMR (75 MHz, $CDCl_3$): δ = 158.83, 146.58, 129.11, 116.06, 42.49, 32.14, 29.87, 29.847, 29.81, 29.57, 29.51, 27.20, 22.91, 14.34; MALDI-TOF-MS: m/z: 297.7 $[M+H]^+$ (100%).

_N, N'_-Didodecyl-pyridazine-3, 6-diamine (13)

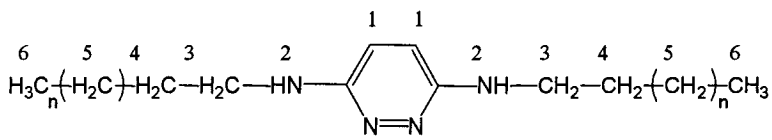

3-chloro-6-dodecylpyridazine **12** (1.0 g, 3.35 mmol) and 1-dodecylamine chloride **18** (1.49 g, 6.70 mmol) were mixed and purged with nitrogen for 15 minutes. The mixture was reacted at 170 °C for 3 hours. After cooling to room temperature, the black product mixture was dissolved in chloroform (20 mL) and extracted with water (3 x 15 mL). The organic layer was dried over anhydrous sodium sulfate and concentrated to about 10 mL by vacuum evaporation. Silica gel column chromatography (chloroform/methanol

/acetone, 8.5/1.5/0.5) was used to isolate the desired product (0.64 g, 42%). R_f = 0.50 (chloroform/methanol/acetone, 8.5/ 1.0/0.5); m.p. = 124-125 °C; ^{1}H NMR (300 MHz, $CDCl_3$): δ = 6.57 (s, 2H, H-1), 4.13 (m, 2H, H-2), 3.31 (m, 4H, H-3), 1.60 (m, 4H, H-4), 1.25-1.36 (m, 36H, H-5), 0.88 (t, J = 6.6 Hz, 6H, H-6); ^{13}C NMR (75 MHz, $CDCl_3$): δ = 154.57, 117.75, 42.91, 32.10, 29.92, 29.84, 29.80, 29.62, 29.53, 27.29, 22.87, 14.29; MALDI-TOF-MS: m/z: 447.1 $[M+H]^+$(100%).

(6-Chloro-pyridazin-3-yl)-isobutylamine (14)

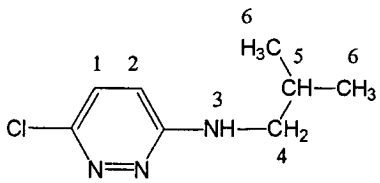

3,6-dichloropyridazine (4.0 g, 27 mmol) and isobutylamine (9.82 g, 135 mmol) were dissolved in ethanol (15 mL) and reacted under reflux for 3 hours. Excess isobutylamine was removed by vacuum evaporation and the product was recrystallized from ethanol to yield yellow needle like crystals (4.21 g, 78.5%). R_f = 0.39 (chloroform/acetone, 9/1); m.p. = 85-86 °C. ^{1}H NMR (300 MHz, $CDCl_3$): δ = 7.15 (d, J = 9.3 Hz, 1H, H-1), 6.67 (d, J = 9.3 Hz, 1H, H-2), 5.05 (s, 1H, H-3), 3.19 (m, 2H, H-4), 1.934 (m, 1H, H-5), 0.98 (d, J = 6.6 Hz, 6H, H-6). ^{13}C NMR (75 MHz, $CDCl_3$): δ = 158.95, 146.53, 129.10, 115.88, 49.93, 28.34, 20.42; MALDI-TOF-MS: m/z: 185.5 $[M+H]^+$(100%).

***N,N'*-Diisobutyl-pyridazine-3,6-diamine (15)**

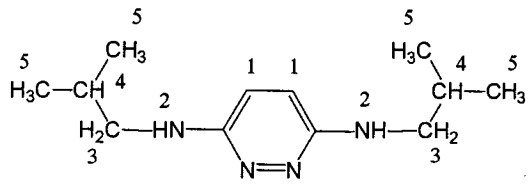

(6-Chloro-pyridazin-3-yl)-isobutylamine **14** (1.3 g, 7.0 mmol) and isobutylamine hydrochloride **19** (2.1 g, 19.5 mmol) were mixed and the flask was purged with nitrogen for 15 minutes. The mixture was reacted at 140 °C for 3 hours. After cooling to room temperature, the black product mixture was dissolved in chloroform (20 mL) and washed with water (3 x 5 mL). The organic layer was dried over anhydrous sodium sulfate and concentrated to about 10 mL by vacuum evaporation. Silica gel colum n chromatography (chloroform/methanol/acetone, 8.5/1.0/0.5) was used to isolate the desired product (0.66 g, 43%). R_f = 0.48 (chloroform/methanol/acetone, 8.5/1.0/0.5); m.p. = 141.5-142.5 °C; ^{1}H NMR (300 MHz, $CDCl_3$): δ = 6.62 (s, 2H, H-1), 4.40 (s, br, 2H, H-2), 3.13 (m, 4H, H-3), 1.90 (m, 2H, H-4), 0.94 (d, J = 6.6 Hz, 12H, H-5); ^{13}C NMR (75 MHz, $CDCl_3$) δ: 154.49, 118.03, 50.4, 28.32, 20.49; MALDI-TOF-MS: m/z: 222.7 $[M + H]^+$(100%).

_N_-Isobutyl-_N'_-phenyl-pridazine-3, 6-diamine (16)

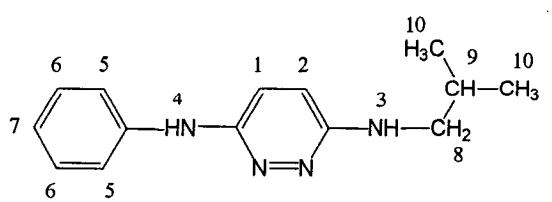

(6-Chloro-pyridazin-3-yl)-phenylamine **8** (0.416 g, 2.0 mmol) and isobutyl amine hydrochloride 19 (0.52 g, 4.75 mmol) were mixed and the flask was purged with nitrogen for 15 minutes. The mixture was reacted at 170 °C for 3 hours. After cooling to room temperature, the black product mixture was dissolved in chloroform (10 mL) and extracted with saturated sodium bicarbonate solution (2 x 2 mL) and water (3 x 2 mL). The organic layer was dried over anhydrous sodium sulfate and concentrated to about 10 mL by vacuum evaporation. Silica gel column chromatography (chloroform/ methanol/acetone, 8.5/1.0/0.5) was used to isolate the desired product (0.26 g, 53%). R_f = 0.46 (chloroform/methanol/acetone, 8.5/ 1.0/0.5); m.p. = 109-110.5 °C; ^{1}H NMR (300MHz, $CDCl_3$): δ = 7.28-7.30 (m, 4 H, H-5, 6), 7.04 (d, J = 9.0 Hz, 1H, H-1), 6.97(m, 1H, H-7), 6.85 (s, 1H, H-4), 6.65 (d, J = 9.0 Hz, 1H, H-2), 4.50 (m, 1H, H-4), 3.198 (m, 2H, H-8), 1.94 (m, 1H, H-9), 0.99 (d, J=6.6 Hz, 6H, H-10); ^{13}C NMR (75MHz, $CDCl_3$): δ = 155.87, 151.85, 141.56, 129.44, 121.93, 119.23, 118.79, 116.90, 50.31, 28.45, 20.52; MALDI-TOF-MS: m/z: 242.7 $[M+H]^+$(100%).

2-[6-(2-Hydroxy-ethylamino)-pyridazin-3-yl-amino]-ethanol (17)

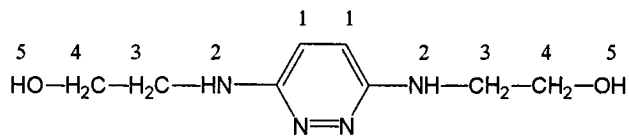

3,6-dichloropyridazine (2.0 g, 13.4 mmol) and ethanolamine (6.0 g, 98.2 mmol) were reacted at 150 - 160 °C for 6 hours. When cooled to room temperature, distilled water (5 mL) was added and the mixture was stirred overnight to allow the product to precipitate. The solid was filtered, washed with water and air-dried. After recrystalization from

ethanol, a yellow fluffy solid was obtained (1.9 g, 71%). R_f = 0.8 (chloroform/acetone, 8/2); m.p. = 167-168 °C; ^{1}H NMR (300 MHz, DMSO-d_6): δ = 6.69 (s, 2H, H-1), 5.93 (t, J = 5.4 Hz, 2H, H-2), 4.85 (s, 2H, H-5), 3.53 (m, 4H, H-4), 3.27 (m, 4H, H-3); ^{13}C NMR (75 MHz, DMSO-d_6): δ = 153.56, 118.70, 60.27, 44.14; MALDI-TOF-MS: m/z: 198.6 $[M+H]^+$(100%).

Dodecylamine hydrochloride (18)

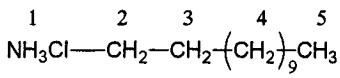

1-Dodecylamine (~10 g) dissolved in ethanol and excess concentrated hydrochloride acid (37%) was mixed at room temperature. The salt solution was placed in shallow dishes and air-dried in the fume hood. The product was isolated as a white powder in quantitative yield. m.p. = 175-176 °C; ^{1}H NMR (300 MHz, $CDCl_3$): δ = 8.29 (s, 3H, H-1), 2.99 (m, 2H, H-2), 1.77 (m, 2H, H-3), 1.26 (m, 18H, H-4), 0.89 (t, J = 6.6 Hz, 3H, H-5); ^{13}C NMR (75 MHz, $CDCl_3$): δ = 40.22, 32.13, 29.84, 29.83, 29.77, 29.61, 29.56, 29.20, 27.92, 26.72, 22.90, 14.32.

Isobutylamine hydrochloride (19)

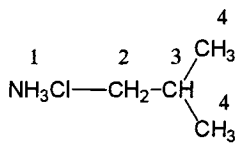

Isobutylamine (~10 g) diluted with ethanol (*ca.* 50 mL) and an excess of concentrated hydrochloric acid were mixed at room temperature. The salt solution was placed in

shallow dishes and air-dried in the fume hood. The product was obtained as a white powder in quantitative yield. m.p. = 157-158 °C; ^{1}H NMR (300 MHz, $CDCl_3$): δ = 8.34 (s, 3 H), 2.83 (m, 2H, H-2), 2.08 (m, 1H, H-3), 1.05 (d, J = 6.6 Hz, 6H, H-4); ^{13}C NMR (75 MHz, $CDCl_3$): δ = 47.06, 27.21, 20.16.

Macrocycle (20)

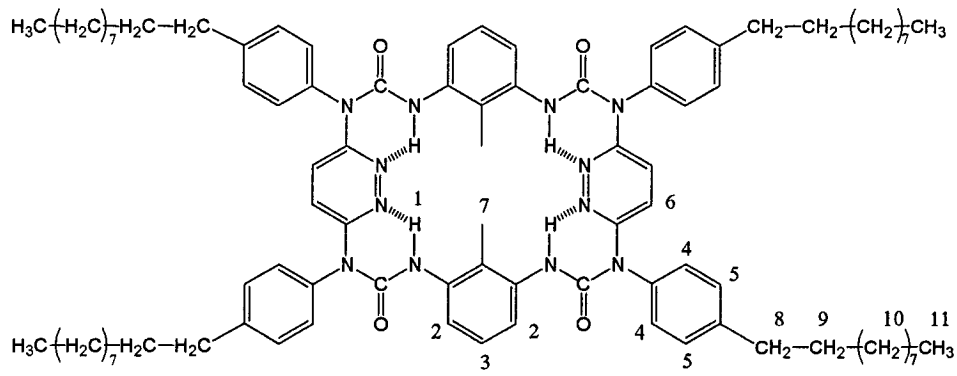

To a flask with dried *N, N'*-Bis-(4-decyl-phenyl)-pridazine-3,6-diamine **11** (0.90 g, 1.66 mmol) was added a solution of tolylene-2,6-diisocyanate (0.35 g, 2.0 mmol) in anhydrous chloroform (50 mL). The resulting light brown solution was allowed to react at 50 °C under nitrogen for 24 hours. The product mixture was concentrated to about 15 mL and purified by silica gel column chromatography (chloroform/acetone, 9.5/0.5) to yield 0.726 g (61%) of the target product. R_f= 0.67 (chloroform/acetone, 9.5/0.5); m.p. = 191-192 °C; ^{1}H NMR (300 MHz, $CDCl_3$): δ = 12.15 (s, 4H, H-1), 8.02 (d, J = 8.4 Hz, 4H, H-2), 7.31 (d, J = 8.4 Hz, 8H, H-4), 7.24 (d, J = 8.4 Hz, 8H, H-5), 7.10 (t, J = 8.4 Hz, 2H, H-3), 6.51 (s, 4H, H-6), 2.81 (s, 6H, H-7), 2.64 (m, 8H, H-8), 1.64 (m, 8H, H-9), 1.28-1.34 (m, 56H, H-10), 0.90 (t, J = 6.9 Hz, 12H, H-11); ^{13}C NMR (75 MHz, $CDCl_3$): δ =

154.99, 152.82, 143.98, 137.56, 136.96, 130.50, 129.69, 126.58, 122.13, 117.13, 116.55, 35.85, 32.10, 31.53, 29.83, 29.78, 29.71, 29.61, 29.53, 22.88, 14.69, 14.32; IR (KBr, ν in cm^{-1}): 2923, 2852, 1697, 1597, 1547, 1475, 1448, 1250; ESI (Q-TOF): m/z : 1433.949 $[M+H]^+$(90%).

Macrocycle (21)

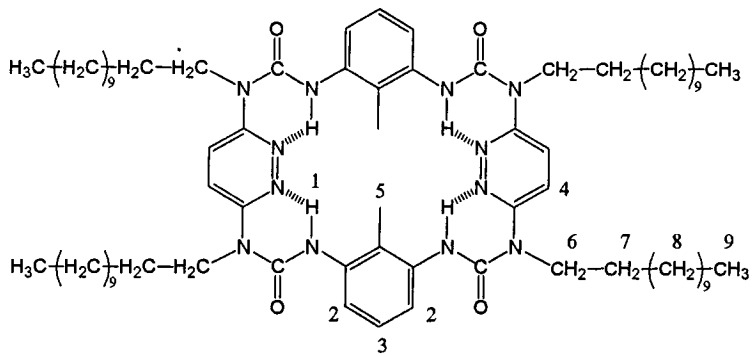

To a flask with *N, N'*-Didodecyl-pyridazine-3,6-diamine **13** (0.33 g, 0.74 mol) was added a solution of tolylene-2,6-diisocyanate (0.16 g, 0.89 mmol) in anhydrous chloroform (15 mL). The resulting yellow solution was allowed to react at 50 °C under nitrogen for 24 hours. The product mixture was concentrated to about 10 mL and purified by silica gel column chromatography (chloroform/acetone, 9.5/0.5) to yield the target product (0.31 g, 67.3%). R_f= 0.63 (chloroform/acetone, 9.5/0.5); m.p. = 194-95 °C; ^{1}H NMR (300 MHz, $CDCl_3$): δ = 11.69 (s, 4H, H-1), 7.80 (d, J = 8.1 Hz, 4H, H-2), 7.23 (s, 4H, H-4), 6.99 (t, J = 8.1 Hz, 2H, H-3), 3,88 (t, J = 6.3 Hz, 8H, H-6), 2.36 (s, 6H, H-5), 1.71 (m, 8H, H-7), 1.28-1.38 (m, 72H, H-8), 0.89 (t, J = 6.6 Hz, 12H, H-9); ^{13}C NMR (75 MHz, $CDCl_3$): δ = 153.86, 152.37, 137.61, 126.12, 120.82, 116.18, 116.01, 46.25, 32.14, 29.91, 29.89, 29.86, 29.83, 29.66, 29.57, 28.47, 27.19, 22.90, 14.77, 14.33; IR (KBr, ν in cm^{-1}): 2925,

2854, 1679, 1599, 1545, 1454, 1232; ESI: m/z : 1263.6 $[M+Na]^+$(100%), 1444.8 $[2M+Na]^+$ (100%).

Macrocycle (22)

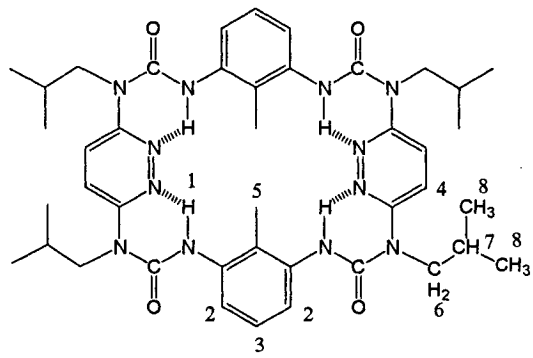

To a flask with of *N, N'*-Diisobutyl-pyridazine-3,6-diamine **15** (0.51 g, 2.28 mmol) was added a solution of tolylene-2,6-diisocyanate (0.40 g, 2.73 mmol) in anhydrous chloroform (20 mL). The resulting light brown solution was allowed to react at 50 °C under nitrogen for 24 hours. The product mixture was concentrated to about 10 mL and separated by silica gel column chromatography (chloroform/acetone, 9/1) to yield of the target product (0.35 g, 39%*). R_f = 0.55 (chloroform/acetone, 9/1); m.p. = 210-211 °C; ^{1}H NMR (300 MHz, $CDCl_3$): δ = 11.99 (s, 4H, H-1), 7.84 (d, J = 8.4 Hz, 4H, H-2), 7.43 (s, 4H, H-4), 7.22 (t, J = 8.4 Hz, 2H, H-3), 4.00 (d, J = 7.5 Hz, 8H, H-6), 2.56 (s, 6H, H-5), 1.96 (m, 4H, H-7), 1.00 (d, J = 6.6 Hz, 24H, H-8); ^{13}C NMR (75 MHz, $CDCl_3$): δ = 154.23, 153.28, 137.59, 126.54, 121.50, 118.10, 117.78, 51.35, 27.67, 20.15, 14.77; IR (KBr, ν in cm^{-1}): 2960, 2875, 1685, 1592, 1546, 1477, 1454, 1218; ESI: m/z : 793.3 $[M+H]^+$(100%), 815.1 $[M+Na]^+$(100%), 1586.2 $[2M+H]^+$(100%), 1607.2 $[2M+Na]^+$(80%).

* Some product was lost during transfer and the experiment was not repeated due to time limitations.

Macrocycle (23)

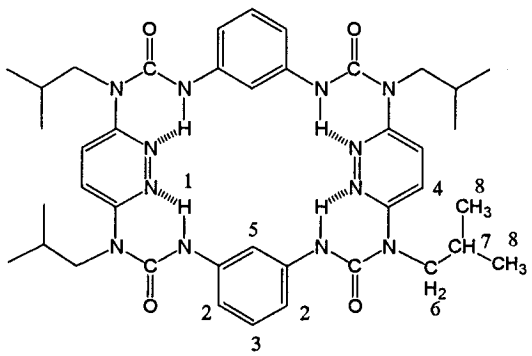

To a flask with 1,3-phenyl-diisocyanate (0.12 g, 0.75 mmol) in anhydrous chloroform (5 mL) was added a solution of *N, N'*-Diisobutyl-pyridazine-3,6-diamine **15** (0.15 g, 0.68 mmol) in anhydrous chloroform (5 mL). The resulting light brown solution was allowed to react at 50 °C under nitrogen for 24 hours. When the reaction was complete by TLC, methanol (5 mL) was added and the product mixture was stirred overnight at room temperature to neutralize unreacted isocyanate. Solvent was removed under vacuum and the product was redissolved in chloroform (10 mL) and filtered. The filtrate was concentrated to about half the volume and then separated by silica gel column chromatography (chloroform/acetone, 9/1) to yield 0.12 g (46.5%) of the target product. R_f = 0.55 (chloroform/acetone, 9/1); m.p. = 212-213 °C; ^{1}H NMR (300 MHz, $CDCl_3$): δ = 12.00 (s, 4H, H-1), 7.90 (d-d, ^3J = 8.4 Hz, ^4J = 2.1 Hz, 4H, H-2), 7.44 (s, 4H, H-4), 7.35 (t, J = 8.4 Hz, 2H, H-3), 6.76 (t, ^4J = 2.1 Hz, 2H, H-5), 3.96 (d, J = 7.5 Hz, 8H, H-6), 1.92 (m, J = 6.6 Hz, 4H, H-7), 0.97 (d, J = 6.6 Hz, 24H, H-8); ^{13}C NMR (75 MHz, $CDCl_3$): δ

= 154.23, 153.00, 139.17, 130.12, 121.85, 116.03, 111.26, 51.27, 27.60, 20.04; IR (KBr, v in cm^{-1}): 2962, 2877, 1680, 1610, 1570, 1549, 1495, 1454, 1338, 1232, 1209; MALDI-TOF-MS: m/z : 765.3 $[M+H]^+$(100%), 787.2 $[M+Na]^+$(100 %), 803.28 $[M+K]^+$(100%).

Trimer (24)

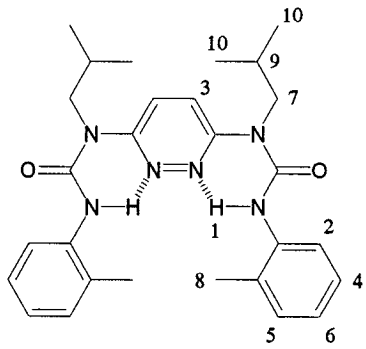

To a solution of *N,N'*-Diisobutyl-pyridazine-3,6-diamine **15** (0.22 g, 0.97 mmol) in anhydrous chloroform (4 mL), *o*-tolylene isocyanate (0.39 g, 2.9 mmol) was added through a syringe. The resulting light brown solution was allowed to react at 50 °C under nitrogen for 5 hours. When the reaction was complete by TLC, methanol (5 mL) was added and product mixture was stirred overnight at room temperature to react with the excess of *o*-tolylene isocyanate. Solvent was removed under vacuum and the product was redissolved in chlorofom (10 mL) and filtered. The filtrate was concentrated to about half the volume and then separated by silica gel column chromatography (chloroform/acetone, 9/1) to yield 0.36 g (74%) of the target product as a white wax. R_f = 0.63 (chloroform/ethyl acetate, 9/1); m.p. = 130-131 °C; ^1H NMR (300 MHz, $CDCl_3$): δ = 11.57 (s, 2H, H-1), 7.97 (m, 2H, H-2), 7.47 (s, 2H, H-3), 7.20-7.26 (m, 4H, H-4, 5), 7.04 (m, 2H, H-6), 3.98 (d, J = 6.9 Hz, 4H, H-7), 2.39 (s, 6H, H-8), 1.99 (m, 2H, H-9), 1.01 (d,

J = 6.6 Hz, 12H, H-10); ^{13}C NMR (300 MHz, $CDCl_3$): δ = 154.48, 153.46, 137.25, 130.40, 128.67, 126.72, 124.09, 122.31, 121.87, 51.48, 27.68, 20.10, 18.78; IR (KBr, ν in cm^{-1}): 2960, 2864, 1676, 1591, 1550, 1460, 1446, 1213; ESI: m/z: 489.2 $[M+H]^+$(100%), 511.1 $[M+Na]^+$(100%), 998.9 $[2M+Na]^+$ (100%).

Dimer (25)

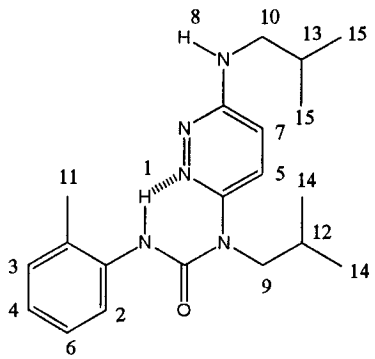

To a solution of *N,N'*-Diisobutyl-pyridazine-3,6-diamine **15** (0.38 g, 1.71 mmol) in anhydrous chloroform (20 mL) was added *o*-tolylene isocyanate (0.27 g, 2.05 mmol). The mixture was stirred at 50 °C under nitrogen for 5 hours. When the reaction was complete by TLC, methanol (5 mL) was added and the product mixture was stirred overnight at room temperature to react with the excess *o*-tolylene isocyanate. Solvent was then removed under vacuum and the product was redissolved in chloroform (20 mL) and filtered. The filtrate was concentrated to about 10 mL and purified by silica gel column chromatography (chloroform/ethyl acetate, 9/1) to yield 0.42 g (68%) of light yellow wax. R_f = 0.6 (chloroform/acetone, 9/1); m.p. = 89-90 °C; ^1H NMR (300 MHz, $CDCl_3$): δ = 10.60 (s, 1H, H-1), 7.82 (d, J = 7.5 Hz, 1H, H-2), 7.10-7.13 (m, 2H, H-3, 4), 7.07 (d, J=9.3 Hz, 1H, H-5), 6.95 (t, J = 7.5 Hz, 1H, H-6), 6.73 (d, J = 9.3 Hz, 1H, H-7), 5.23 (m,

1H, H-8), 3.79 (d, J = 6.9 Hz, 2H, H-9), 3.17 (m, 2H, H-10), 2.27 (s, 3H, H-11), 1.87 (m, 2H, H-11, 12), 0.95 (d, J = 6.6 Hz, 6H, H-14); 0.91 (d, J = 6.3 Hz, 6H, H-15); ^{13}C NMR (75 MHz, $CDCl_3$): δ = 156.81, 154.27, 151.70, 137.42, 130.19, 129.31, 126.35, 123.67, 122.53, 122.40, 117.44, 52.12, 49.58, 28.15, 27.68, 20.31, 19.93, 18.37; ESI: m/z : 356.3 $[M+H]^+$(100%), 378.2 $[M+Na]^+$(100%), 733.1 $[2M+Na]^+$(100%).

Pentamer (26)

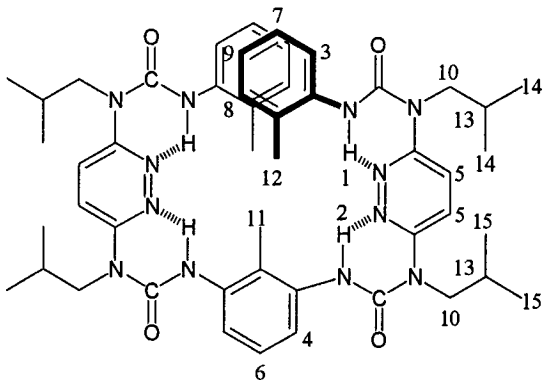

To a solution of monocapped dimer **25** (0.51 g, 1.45 mmol) in anhydrous chloroform (2 mL) at 40 °C, tolylene-2,6-diisocyanate (0.13 g, 0.72 mmol) was added dropwise through a syringe over a period of 4 hours under nitrogen. The reaction was allowed to proceed for another 20 hours. Then methanol (2 mL) was added and the product mixture was stirred at room temperature for 4 hours to remove DIT and its isocyanate derivatives formed during the reaction. The solvent was removed under vacuum and the solid residue was redissolved in chloroform (10 mL) and filtered. The filtrate was concentrated to about half the volume and purified by silica gel column chromatography (chloroform/acetone, 8/2) to yield 0.249 g of a light yellow product (39%). R_f = 0.7

(chloroform/acetone, 8/2); m.p. = 120-122 °C; ^{1}H NMR (300 MHz, $CDCl_3$): δ = 11.58 (s, 2H, H-1), 11.44 (s, 2H, H-2), 7.98 (d-d, ^{3}J = 7.8 Hz, 2H, H-3), 7.56 (d, J = 8.1 Hz, 2H, H-4), 7.47 (s, br, 4H, H-5), 7.23 (t, J = 8.1 Hz, 1H, H-6), 7.18 (t-d, ^{3}J = 7.8 Hz, 2H, H-7), 7.12 (m, 2H, H-8), 6.98 (t-d, ^{3}J = 7.5 Hz, 2H, H-9), 3.97 (m, 8H, H-10), 2.35 (s, 3H, H-11), 2.34 (s, 6H, H-12), 1.98 (m, 4H, H-13), 1.00 (d, J = 2.4 Hz, 12H, H-14), 0.99 (d, J = 6.6 Hz, 12H, H-15); ^{13}C NMR (75 MHz, $CDCl_3$): δ = 154.46, 153.86, 153.39, 137.41, 137.32, 130.34, 128.52, 126.68, 126.41, 124.05, 123.93, 122.00, 121.88, 120.81, 51.57, 51.48, 27.68, 20.10, 18.75, 13.64; ESI: m/z : 885.5 $[M+H]^+$ (100 %), 907.4 $[M+Na]^+$ (100%), 923.4 $[M+K]^+$(100%).

Mono-protected amine (27)

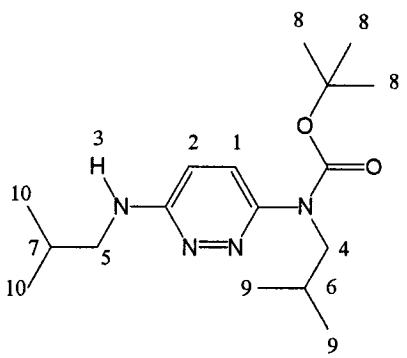

To a solution of *N,N'*-diisobutyl-pyridazine-3,6-diamine **15** (3.0 g, 13.5 mmol) in anhydrous chloroform (20 mL) was added triethylamine (2.9 g, 28.8 mmol) dropwise over a period of 10 minutes. After the mixture was stirred for an additional 10 minutes, a solution of di-*tert*-butyl-dicarbonate (3.0 g, 13.8 mmol) in anhydrous chloroform (5 mL) was added dropwise over 15 minutes and the reaction was allowed to proceed at room temperature for 24 hours. Solvent was removed under vacuum and the product residue

was redissolved in chloroform (30 mL) and filtered. The filtrate was concentrated to about 15 mL and purified by silica gel column chromatography (chloroform/acetone, 8.5/1.5) to yield a yellow fluffy powder (2.87 g, 66%). R_f = 0.45 (chloroform/actone, 9/1); m.p. = 122-123 °C; ^{1}H NMR (300 MHz, $CDCl_3$): δ = 7.42 (d, J = 9.6 Hz, 1H, H-1), 6.63 (d, J = 9.6 Hz, 1H, H-2), 4.83 (s, 1H, H-3), 3.82 (d, J = 7.2 Hz, 2H, H-4), 3.22 (m, 2H, H-5), 1.95 (m, 2H, H-6, 7), 1.48 (s, 9H, H-8), 0.99 (d, J = 6.6 Hz, 6H, H-9), 0.86 (d, J = 6.6 Hz, 6H, H-10); ^{13}C NMR (75 MHz, $CDCl_3$): δ = 157.33, 154.71, 151.45, 127.73, 114.54, 81.16, 54.54, 50.00, 28.51, 28.42, 27.97, 20.48, 20.24; MALDI-TOF-MS: m/z: 322.8 $[M+H]^+$(100%).

Bis-protected trimer (28)

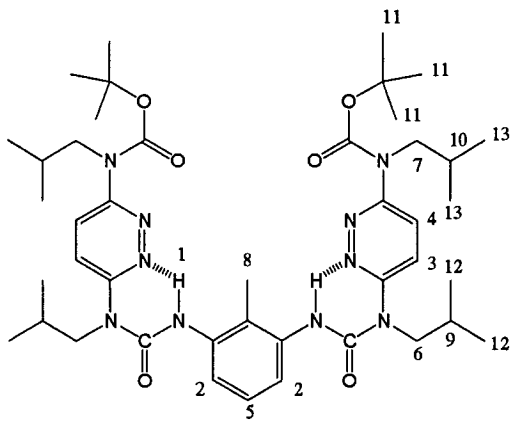

To a solution of mono-protected monomer **27** (0.135 g, 0.42 mmol) in anhydrous chloroform (0.4 mL), tolylene-2,6-diisocyanate (0.036 g, 0.21 mmol) was added through a syringe. The yellow solution was allowed to react at 60 °C under nitrogen for 24 hours. When the reaction was complete by TLC, methanol (2 mL) was added and the solution was stirred overnight at room temperature. The solvent was removed under vacuum and

the product was rediisolved in chloroform (10 mL) and filtered. The filtrate was concentrated to about 5 mL and then purified by silica gel column chromatography (chloroform/acetone, 9/1) to yield a white waxy product (0.126 g, 73.4%). R_f = 0.55 (chloroform/acetone, 9/1); m.p. = 116-117 °C; ^{1}H NMR (300 MHz, $CDCl_3$): δ = 11.86 (s, 2H, H-1), 7.91 (d, J = 9.9 Hz, 2H, H-2), 7.62 (d, J = 8.1 Hz, 2H, H-3), 7.29 (d, J = 9.9 Hz, 2H, H-4), 7.20 (t, J = 8.1 Hz, 1H, H-5), 3.94 (d, J = 6.9 Hz, 8H, H-6, 7), 2.35 (s, 3H, H-8), 2.01 (m, 4H, H-9, 10), 1.53(s, 18H, H-11), 0.97 (d, J = 6.6 Hz, 12H, H-12), 0.90 (d, J = 6.6 Hz, 12H, H-13); ^{13}C NMR (75 MHz, $CDCl_3$): δ = 155.79, 154.39, 154.09, 137.71, 127.24, 126.31, 123.71, 120.32, 119.22, 82.14, 54.11, 51.49, 28.42, 28.12, 27.60, 20.31, 20.13, 13.43; MALDI-TOF-MS: m/z : 819.4 $[M+H]^+$(100%), 841.4 $[M+Na]^+$(100%), 857.4 $[M+K]^+$(100%).

Notes and references

[1] B. Dietrich, P. Viout, J. M. Lehn, *Macrocyclic Chemistry: Aspects of Organic and Inorganic Supra Molecular Chemistry*, VCH, Weinheim, **1993**, p384.

[2] A. Ostrowicki, E. Koepp, F. Vogtle, in *Topics in Current Chemistry, Vol. 161*, Springer-Verlag, New York, **1992**, p37-67.

[3] P. Knops, N. Sendhoff, H. B. Mekelburger, F. Vogtle, in *Topics in Current Chemistry, Vol. 161*, Springer-Verlag, New York, **1992**, p1-36.

[4] M. Malesevic, U. Strijowski, D. Bachle, N. Sewald, *Journal of Biotechnology* **2004**, *112*, 73-77.

[5] P. Ruggli, *Justus Liebigs Annalen der Chemie* **1912**, *392*, 92-100.

[6] E. P. Kyba, R. E. Davis, C. W. Hudson, A. M. John, S. B. Brown, M. J. McPhaul, L.-K. Liu, A. C. Glover, *Journal of the American Chemical Society* **1981**, *103*, 3868-3875.

[7] E. P. Kyba, S.-S. P. Chou, *Journal of Organic Chemistry* **1981**, *46*, 860-863.

[8] S. J. Rodgers, C. Y. Ng, K. N. Raymond, *Journal of the American Chemical Society* **1985**, *107*, 4094-4095.

[9] J. Fastrez, *Journal of Physical Chemistry* **1989**, *93*, 2635-2642.

[10] G. Ercolani, L. Mandolini, P. Mencarelli, *Gazzetta Chimica Italiana* **1989**, *119*, 209-214.

[11] L. C. Tan, R. M. Pagni, G. W. Kabalka, M. Hillmyer, J. Woosley, *Tetrahedron Letters* **1992**, *33*, 7709-7712.

[12] D. H. Busch, *Journal of Inclusion Phenomena and Molecular Recognition in Chemistry* **1992**, *12*, 389-395.

[13] D. H. Busch, A. L. Vance, A. G. Kolchinski, in *Comprehensive Supramolecular Chemistry, Vol. 9*, Pergomon, New York, **1996**, p1-42.

[14] C. J. Pedersen, *Journal of the American Chemical Society* **1967**, *89*, 7017-7036.

[15] C. J. Pedersen, *Angewandte Chemie* **1988**, *100*, 1053-1059.

[16] B. Odell, M. V. Reddington, A. M. Z. Slawin, N. Spencer, J. F. Stoddart, D. J. Williams, *Angewandte Chemie* **1988**, *100*, 1605-1608.

[17] J.-M. Lehn, *Polymer International* **2002**, *51*, 825-839.

[18] G. Cooke, V. M. Rotello, *Chemical Society Reviews* **2002**, *31*, 275-286.

[19] H. S. Chan, K. A. Dill, *Physics Today* **1993**, *46*, 24-32.

[20] K. A. Dill, S. Bromberg, K. Yue, K. M. Fiebig, D. P. Yee, P. D. Thomas, H. S. Chan, *Protein Science* **1995**, *4*, 561-602.

[21] S. H. Gellman, *Accounts of Chemical Research* **1998**, *31*, 173-180.

[22] A. R. Sanford, B. Gong, *Current Organic Chemistry* **2003**, *7*, 1649-1659.

[23] A. R. Sanford, K. Yamato, X. Yang, L. Yuan, Y. Han, B. Gong, *European journal of biochemistry* **2004**, *271*, 1416-1425.

[24] I. Huc, *European Journal of Organic Chemistry* **2004**, 17-29.

[25] D. Seebach, T. Kimmerlin, R. Sebesta, M. A. Campo, A. K. Beck, *Tetrahedron* **2004**, *60*, 7455-7506.

[26] L. J. Prins, D. N. Reinhoudt, P. Timmerman, *Angewandte Chemie, International Edition* **2001**, *40*, 2382-2426.
[27] O. Ikkala, G. ten Brinke, *Chemical Communications* **2004**, 2131-2137.
[28] M.-E. Perron, F. Monchamp, H. Duval, D. Boils-Boissier, J. D. Wuest, *Pure and Applied Chemistry* **2004**, *76*, 1345-1351.
[29] F. J. Carver, C. A. Hunter, R. J. Shannon, *Journal of the Chemical Society, Chemical Communications* **1994**, 1277-1280.
[30] H. Jiang, J.-M. Leger, P. Guionneau, I. Huc, *Organic Letters* **2004**, *6*, 2985-2988.
[31] L. Yuan, W. Feng, K. Yamato, A. R. Sanford, D. Xu, H. Guo, B. Gong, *Journal of the American Chemical Society* **2004**, *126*, 11120-11121.
[32] L. Pauling, R. B. Corey, *Journal of the American Chemical Society* **1950**, *72*, 5349.
[33] L. Pauling, R. B. Corey, *Proceedings of the National Academy of Sciences of the United States of America* **1951**, *37*, 282-285.
[34] J. D. Watson, F. H. Crick, *Nature* **1953**, *171*, 737-738.
[35] J. C. Nelson, J. G. Saven, J. S. Moore, P. G. Wolynes, *Science* **1997**, *277*, 1793-1796.
[36] D. J. Hill, M. J. Mio, R. B. Prince, T. S. Hughes, J. S. Moore, *Chemical reviews* **2001**, *101*, 3893-4012.
[37] C. Schmuck, *Angewandte Chemie, International Edition* **2003**, *42*, 2448-2452.
[38] R. P. Cheng, *Current Opinion in Structural Biology* **2004**, *14*, 512-520.
[39] D. M. Bassani, J.-M. Lehn, G. Baum, D. Fenske, *Angewandte Chemie, International Edition in English* **1997**, *36*, 1845-1847.
[40] L. A. Cuccia, J.-M. Lehn, J.-C. Homo, M. Schmutz, *Angewandte Chemie, International Edition* **2000**, *39*, 233-237.
[41] A. Petitjean, L. A. Cuccia, J.-M. Lehn, H. Nierengarten, M. Schmutz, *Angewandte Chemie, International Edition* **2002**, *41*, 1195-1198.
[42] S. T. Howard, *Journal of the American Chemical Society* **1996**, *118*, 10269-10274.
[43] M. Ohkita, J.-M. Lehn, G. Baum, D. Fenske, *Chemistry--A European Journal* **1999**, *5*, 3471-3481.
[44] M. T. Stone, J. S. Moore, *Organic Letters* **2004**, *6*, 469-472.
[45] D. J. Hill, J. S. Moore, *Proceedings of the National Academy of Sciences of the United States of America* **2002**, *99*, 5053-5057.
[46] A. Tanatani, M. J. Mio, J. S. Moore, *Journal of the American Chemical Society* **2001**, *123*, 1792-1793.
[47] K. Oh, K. S. Jeong, J. S. Moore, *Nature* **2001**, *414*, 889-893.
[48] V. Berl, I. Huc, R. G. Khoury, J.-M. Lehn, *Chemistry--A European Journal* **2001**, *7*, 2810-2820.
[49] V. Berl, I. Huc, R. G. Khoury, M. J. Krische, J.-M. Lehn, *Nature* **2000**, *407*, 720-723.
[50] V. Berl, I. Huc, R. G. Khoury, J.-M. Lehn, *Chemistry--A European Journal* **2001**, *7*, 2798-2809.
[51] C. Dolain, V. Maurizot, I. Huc, *Angewandte Chemie, International Edition* **2003**, *42*, 2738-2740.

[52] X. Yang, A. L. Brown, M. Furukawa, S. Li, W. E. Gardinier, J. Bukowski Eric, F. V. Bright, C. Zheng, X. c. Zeng, B. Gong, *Chemical communications* **2003**, 56-57.
[53] X. Yang, L. Yuan, K. Yamato, A. L. Brown, W. Feng, M. Furukawa, X. C. Zeng, B. Gong, *Journal of the American Chemical Society* **2004**, *126*, 3148-3162.
[54] K. Okuyama, T. Hasegawa, M. Ito, N. Mikami, *Journal of Physical Chemistry* **1984**, *88*, 1711-1716.
[55] P. S. Corbin, S. C. Zimmerman, P. A. Thiessen, N. A. Hawryluk, T. J. Murray, *Journal of the American Chemical Society* **2001**, *123*, 10475-10488.
[56] J. J. van Gorp, J. A. J. M. Vekemans, E. W. Meijer, *Chemical Communications* **2004**, 60-61.
[57] A. R. Sanford, K. Yamato, X. Yang, L. Yuan, Y. Han, B. Gong, *European Journal of Biochemistry* **2004**, *271*, 1416-1425.
[58] S. Yagi, I. Yonekura, M. Awakura, M. Ezoe, T. Takagishi, *Chemical Communications* **2001**, 557-558.
[59] W. Zhang, J. S. Moore, *Journal of the American Chemical Society* **2004**, *126*, 12796.
[60] M. C. Etter, *Accounts of Chemical Research* **1990**, *23*, 120-126.
[61] M. C. Etter, Z. Urbanczyk-Lipkowska, M. Zia-Ebrahimi, T. W. Panunto, *Journal of the American Chemical Society* **1990**, *112*, 8415-8426.
[62] M. C. Etter, S. M. Reutzel, *Journal of the American Chemical Society* **1991**, *113*, 2586-2598.
[63] V. Semetey, C. Hemmerlin, C. Didierjean, A. P. Schaffner, A. G. Giner, A. Aubry, J. P. Briand, M. Marraud, G. Guichard, *Organic letters* **2001**, *3*, 3843-3846.
[64] D. Ranganathan, C. Lakshmi, I. L. Karle, *Journal of the American Chemical Society* **1999**, *121*, 6103-6107.
[65] D. Ranganathan, *Accounts of Chemical Research* **2001**, *34*, 919-930.
[66] D. Ranganathan, C. Lakshmi, *Chemical Communications* **2001**, 1250-1251.
[67] L. S. Shimizu, M. D. Smith, A. D. Hughes, *Chemical Communications* **2001**, 1592-1593.
[68] L. S. Shimizu, A. D. Hughes, M. D. Smith, M. J. Davis, B. P. Zhang, H.-C. Zur Loye, K. D. Shimizu, *Journal of the American Chemical Society* **2003**, *125*, 14972-14973.
[69] F. Bohme, C. Kunert, H. Komber, D. Voigt, P. Friedel, M. Khodja, H. Wilde, *Macromolecules* **2002**, *35*, 4233-4237.
[70] X.-Q. Li, X.-K. Jiang, X.-Z. Wang, Z.-T. Li, *Tetrahedron* **2004**, *60*, 2063-2069.
[71] U. Luning, C. Kuhl, A. Uphoff, *European Journal of Organic Chemistry* **2002**, 4063-4070.
[72] G. R. Newkome, S. J. Garbis, V. K. Majestic, F. R. Fronczek, G. Chiari, *Journal of Organic Chemistry* **1981**, *46*, 833-839.
[73] J. P. Collin, M. T. Youinou, *Inorganica Chimica Acta* **1992**, *201*, 29-34.
[74] When the reaction was carried out in deuterated DMSO, it was observed (by NMR) that the reaction was ca. 80% complete after only 1 hour.
[75] M. C. Etter, *Journal of Physical Chemistry* **1991**, *95*, 4601-4610.

[76] C.-H. Chien, M.-k. Leung, J.-K. Su, G.-H. Li, Y.-H. Liu, Y. Wang, *Journal of Organic Chemistry* **2004**, *69*, 1866-1871.
[77] F. H. Beijer, R. P. Sijbesma, H. Kooijman, A. L. Spek, E. W. Meijer, *Journal of the American Chemical Society* **1998**, *120*, 6761-6769.
[78] X.-Z. Wang, X.-Q. Li, X.-B. Shao, X. Zhao, P. Deng, X.-K. Jiang, Z.-T. Li, Y.-Q. Chen, *Chemistry--A European Journal* **2003**, *9*, 2904-2913.
[79] G. R. Desiraju, *Angewandte Chemie, International Edition in English* **1995**, *34*, 2311-2327.
[80] G. R. Desiraju, *Accounts of Chemical Research* **1996**, *29*, 441-449.
[81] S. P. Newton, J. F. Stoddart, W. Hayes, *Supramolecular Science* **1996**, *3*, 221-236.
[82] T. Steiner, G. Koellner, *Chemical Communications* **1997**, 1207-1208.
[83] K. N. Houk, S. Menzer, S. P. Newton, F. M. Raymo, J. F. Stoddart, D. J. Williams, *Journal of the American Chemical Society* **1999**, *121*, 1479-1487.
[84] J. G. Hansen, N. Feeder, D. G. Hamilton, M. J. Gunter, J. Becher, J. K. M. Sanders, *Organic Letters* **2000**, *2*, 449-452.
[85] Y. Ge, L. Miller, T. Ouimet, D. K. Smith, *Journal of Organic Chemistry* **2000**, *65*, 8831-8838.
[86] L. V. Sudha, D. N. Sathyanarayana, S. N. Bharati, *Magnetic Resonance in Chemistry* **1987**, *25*, 474-479.
[87] When the substituent and carbonyl bond are situated at the same side of urea C-N bond, conformation is E, when they are on the opposite sides, the comformation is Z.
[88] S. Anderson, H. L. Anderson, J. K. M. Sanders, *Accounts of Chemical Research* **1993**, *26*, 469-475.
[89] S. Patai, *The Chemistry of Amidines and Imidates*, John Wiley & Sons, London, **1975**, p677.
[90] R. Anulewicz, I. Wawer, T. M. Krygowski, F. Maennle, H.-H. Limbach, *Journal of the American Chemical Society* **1997**, *119*, 12223-12230.
[91] I. D. Cunningham, J. S. Blanden, J. Llor, L. Munoz, A. P. Sharratt, *Journal of the Chemical Society, Perkin Transactions 2: Physical Organic Chemistry* **1991**, 1747-1750.
[92] I. D. Cunningham, J. Llor, L. Munoz, *Journal of the Chemical Society, Perkin Transactions 2: Physical Organic Chemistry* **1991**, 1751-1753.
[93] I. D. Cunningham, J. Llor, L. Munoz, *Journal of the Chemical Society, Perkin Transactions 2: Physical Organic Chemistry* **1992**, 2253-2256.
[94] I. D. Cunningham, J. Llor, L. Munoz, *Journal of the Chemical Society, Perkin Transactions 2: Physical Organic Chemistry* **1992**, 331-332.
[95] N. Khazanovich, J. R. Granja, D. E. McRee, R. A. Milligan, M. R. Ghadiri, *Journal of the American Chemical Society* **1994**, *116*, 6011-6012.
[96] M. R. Ghadiri, J. R. Granja, L. K. Buehler, *Nature* **1994**, *369*, 301-304.
[97] J. Sanchez-Quesada, M. R. Ghadiri, H. Bayley, O. Braha, *Journal of the American Chemical Society* **2000**, *122*, 11757-11766.
[98] W. S. Horne, C. D. Stout, M. R. Ghadiri, *Journal of the American Chemical Society* **2003**, *125*, 9372-9376.

[99] D. T. Bong, T. D. Clark, J. R. Granja, M. R. Ghadiri, *Angewandte Chemie, International Edition* **2001**, *40*, 988-1011.
[100] D. Ranganathan, M. G. Kumar, R. S. K. Kishore, I. L. Karle, *Chemical Communications* **2001**, 273-274.
[101] D. Ranganathan, M. G. Kumar, I. L. Karle, *Chemical Communications* **2001**, 271-272.
[102] D. Ranganathan, M. P. Samant, I. L. Karle, *Journal of the American Chemical Society* **2001**, *123*, 5619-5624.
[103] F. Schwanke, O. Safarowsky, C. Heim, G. Silva, F. Vogtle, *Helvetica Chimica Acta* **2000**, *83*, 3279-3290.
[104] P. R. Dave, G. Doyle, T. Axenrod, H. Yazdekhasti, H. L. Ammon, *Journal of Organic Chemistry* **1995**, *60*, 6946-6952.
[105] J. Van Esch, F. Schoonbeek, M. De Loos, H. Kooijman, A. L. Spek, R. M. Kellogg, B. L. Feringa, *Chemistry--A European Journal* **1999**, *5*, 937-950.
[106] S. Hoger, A.-D. Meckenstock, S. Muller, *Chemistry--A European Journal* **1998**, *4*, 2423-2434.
[107] S. Hoger, A.-D. Meckenstock, *Chemistry--A European Journal* **1999**, *5*, 1686-1691.
[108] S. Hoger, *Macromolecular Symposia* **1999**, *142*, 185-191.
[109] S. Hoger, K. Bonrad, S. Rosselli, A.-D. Ramminger, T. Wagner, B. Silier, S. Wiegand, W. Haussler, G. Lieser, V. Scheumann, *Macromolecular Symposia* **2002**, *177*, 185-191.
[110] F. Bohme, M. Rillich, H. Komer, *Macromolecular Chemistry and Physics* **1995**, *196*, 3209-3216.
[111] H. Komber, H.-H. Limbach, F. Bohme, C. Kunert, *Journal of the American Chemical Society* **2002**, *124*, 11955-11963.
[112] P. Friedel, J. Tobisch, D. Jehnichen, J. Bergmann, T. Taut, M. Rillich, C. Kunert, F. Bohme, *Journal of Applied Crystallography* **1998**, *31*, 874-880.
[113] C. Kunert, D. Voigt, P. Friedel, H. Komber, F. Bohme, *Journal of Polymer Science, Part A: Polymer Chemistry* **2001**, *39*, 1280-1287.
[114] D. Lowik, C. R. Lowe, WO 2001042228, **2001**.
[115] D. W. P. M. Lowik, C. R. Lowe, *European Journal of Organic Chemistry* **2001**, 2825-2839.
[116] M. R. Johnson, WO 2001046193, **2001**.
[117] S. J. Swamy, B. Veerapratap, D. Nagaraju, K. Suresh, P. Someshwar, *Tetrahedron* **2003**, *59*, 10093-10096.
[118] B. Dutta, P. Bag, B. Adhikary, U. Floerke, K. Nag, *Journal of Organic Chemistry* **2004**, *69*, 5419-5427.
[119] R. H. DeWolfe, R. M. Roberts, *Journal of the American Chemical Society* **1954**, *76*, 4379-4381.
[120] R. M. Roberts, R. H. DeWolfe, *Journal of the American Chemical Society* **1954**, *76*, 2411-2414.
[121] F. Bohme, C. Klinger, H. Komber, L. Haubler, D. Jehnichen, *Journal of Polymer Science, Part A: Polymer Chemistry* **1998**, *36*, 929-938.
[122] F. Maennle, H.-H. Limbach, *Angewandte Chemie, International Edition in English* **1996**, *35*, 441-442.

[123] np represents napthyridine and f represents formal.
[124] C. A. Hunter, *Chemical Society Reviews* **1994**, *23*, 101-109.
[125] M. Kumagai, *Nippon Kagaku Zasshi* **1961**, *82*, 227-229.
[126] H. Vorbrueggen, K. Krolikiewicz, *Chemische Berichte* **1984**, *117*, 1523-1541.
[127] I. Parrot, C.-G. Wermuth, M. Hibert, *Tetrahedron Letters* **1999**, *40*, 7975-7978.
[128] J. Clayden, N. Greeves, S. Warren, P. Wothers, *Organic chemistry*, Oxford University Press Inc. New York, New York, **2001**,
[129] M. Watanabe, S. Kajigaeshi, S. Kanemasa, *Synthesis* **1977**, 761-763.
[130] G. Maghioros, G. Schlewer, C. G. Wermuth, J. Lagrange, P. Lagrange, *Nouveau Journal de Chimie* **1983**, *7*, 667-672.
[131] T. J. Curphey, K. S. Prasad, *Journal of Organic Chemistry* **1972**, *37*, 2259-2266.
[132] The correlations of other protons are similiar to macrocycle 22.
[133] The STM measurements presented in this section of the thesis were carried out by Dr. Louis Cuccia and Dr. Ulrich Ziener.
[134] M. M. S. Abdel-Mottaleb, PhD thesis, Katholieke Universiteit leuven (Leuven), **2003**.
[135] A. Ohira, M. Sakata, C. Hirayama, M. Kunitake, *Organic & Biomolecular Chemistry* **2003**, *1*, 251-253.
[136] S. De Feyter, F. C. De Schryver, *Chemical Society Reviews* **2003**, *32*, 393-150.
[137] A. S. Shetty, J. Zhang, J. S. Moore, *Journal of the American Chemical Society* **1996**, *118*, 1019-1027.
[138] J.-L. Hou, M.-X. Jia, X.-K. Jiang, Z.-T. Li, G.-J. Chen, *Journal of Organic Chemistry* **2004**, *69*, 6228-6237.
[139] G. S. Hanan, U. S. Schubert, D. Volkmer, E. Riviere, J.-M. Lehn, N. Kyritsakas, J. Fischer, *Canadian Journal of Chemistry* **1997**, *75*, 169-182.
[140] R. H. Martin, N. Defay, H. P. Figeys, M. Flammang-Barbieux, J. P. Cosyn, M. Gelbcke, J. J. Schurter, *Tetrahedron* **1969**, *25*, 4985-4998.
[141] H. Wynberg, *Accounts of Chemical Research* **1971**, *4*, 65-73.
[142] Personal communication.

Appedix A

Table A.1. Crystal data and struture refinement for macrocycle **7**.

Empirical formula	C31 H31 N12 O2.50 S1.50
Formula weight	659.77
Wavelength	1.54178 °A
Temperature	100 (2) K
Crystal system, space group	Orthorhombic, Pbcn
Unit cell dimensions	a = 31.1325 (6) Å α = 90
	b = 8.5333 (2) Å β = 90
	c = 22.9610 (4) Å γ = 90
Volume	6099.9 (2) $Å^3$
Z, calculated density	8,1.437 Mg/m^3
Absorption coefficient	1.718 mm^{-1}
F(000)	7455
Crystal description	need-like, yellow
Crystal size	0.35 × 0.08 × 0.05 mm
Measured reflections	57006
Independent reflections	3816[*R*(int) = 0.044]
Reflections with $I > 2\sigma(I)$	2282
Theta range for data collection	2.84 to 71.51°
Index ranges	-32 <= h <= 32
	-8 <= k <=8
	-24 <=l <=24
Refinement on F^2	$R[F^2 > 2(F^2)] = 0.0394$
	$wR(F^2) = 0.0687$
	$w = 1/[\sigma^2(F_o^2) + (0.0181P)^2]$
	where $P = (F_o2 + 2F_c^2)/3$
Goodness-of-fit on F^2	1.004
Largest diff. Peak and hole	0.196 and -0.277e/$Å^3$

All non-H atoms were refined by full-matrix least-squares with anisotropic displacement parameters. The H atoms were generated geometrically (C—H 0.95 to 0.98, N—H 0.88 and O—H 0.84 Å) and were included in the refinement in the riding model approximation. Data collection: SMART (Bruker, 1999). Cell refinement: SMART (Bruker, 1999). Data reduction: SAINT (Bruker, 1999). Program(s) used to solve structure: SHELXS97 Sheldrick, 1997). Program(s) used to refine structure: SHELXL97 (Sheldrick, 1997). Molecular graphics: SHELXTL (Bruker, 1997).

Table A.2. Bond length (Å) for macrocycle **7**.

Bond	Length	Bond	Length
C1—N39	1.289 (3)	C22—N23	1.315 (4)
C1—N2	1.347 (3)	C22—N26	1.386 (4)
N2—C3	1.402 (3)	N23—C24	1.351 (3)
C3—N12	1.319 (3)	C24—N25	1.357 (3)
C3—C4	1.417 (4)	N26—C27	1.353 (4)
C4—C5	1.354 (4)	C27—N28	1.285 (3)
C5—C6	1.416 (4)	N28—C29	1.412 (4)
C6—C7	1.411 (4)	C29—N38	1.319 (4)
C6—C11	1.412 (4)	C29—C30	1.418 (4)
C7—C8	1.364 (4)	C30—C31	1.363 (4)
C8—C9	1.419 (4)	C31—C32	1.403 (4)
C9—N10	1.324 (3)	C32—C37	1.404 (4)
C9—N13	1.411 (3)	C32—C33	1.409 (4)
N10—C11	1.362 (3)	C33—C34	1.363 (4)
C11—N12	1.366 (3)	C34—C35	1.407 (4)
N13—C14	1.288 (3)	C35—N36	1.333 (4)
C14—N15	1.357 (3)	C35—N39	1.401 (4)
N15—C16	1.386 (3)	N36—C37	1.359 (3)
C16—N25	1.315 (3)	C37—N38	1.373 (4)
C16—C17	1.427 (4)	C41—O41	1.411 (3)
C17—C18	1.349 (4)	S50—O51	1.5282 (18)
C18—C19	1.402 (4)	S50—C52	1.779 (3)
C19—C20	1.402 (4)	S50—C53	1.786 (3)
C19—C24	1.426 (4)	S60—O61	1.518 (5)
C20—C21	1.352 (4)	S60—C62	1.798 (16)
C21—C22	1.418 (4)	S60—C63	1.808 (16)

Table A.3. Bond angles (°) for macrocycle **7**.

Atoms	Angle	Atoms	Angle
N39—C1—N2	120.9 (3)	N26—C22—C21	116.9 (3)
C1—N2—C3	124.9 (3)	C22—N23—C24	117.4 (3)
N12—C3—N2	117.2 (3)	N23—C24—N25	115.5 (3)
N12—C3—C4	125.0 (3)	N23—C24—C19	122.3 (3)
N2—C3—C4	117.7 (3)	N25—C24—C19	122.2 (3)
C5—C4—C3	118.1 (3)	C16—N25—C24	117.1 (3)
C4—C5—C6	119.6 (3)	C27—N26—C22	124.4 (3)
C7—C6—C11	118.0 (3)	N28—C27—N26	121.0 (3)
C7—C6—C5	124.1 (3)	C27—N28—C29	115.5 (3)
C11—C6—C5	117.8 (3)	N38—C29—N28	120.9 (3)
C8—C7—C6	119.3 (3)	N38—C29—C30	123.5 (3)
C7—C8—C9	118.7 (3)	N28—C29—C30	115.6 (3)
N10—C9—N13	120.8 (3)	C31—C30—C29	118.8 (3)
N10—C9—C8	123.6 (3)	C30—C31—C32	119.3 (3)
N13—C9—C8	115.6 (3)	C31—C32—C37	118.7 (3)
C9—N10—C11	117.7 (3)	C31—C32—C33	124.3 (3)
N10—C11—N12	114.7 (3)	C37—C32—C33	117.0 (3)
N10—C11—C6	122.5 (3)	C34—C33—C32	120.0 (3)
N12—C11—C6	122.8 (3)	C33—C34—C35	119.1 (3)
C3—N12—C11	116.6 (3)	N36—C35—N39	120.8 (3)
C14—N13—C9	116.3 (3)	N36—C35—C34	122.8 (3)
N13—C14—N15	121.2 (3)	N39—C35—C34	116.4 (3)
C14—N15—C16	124.4 (3)	C35—N36—C37	117.9 (3)
N25—C16—N15	118.6 (3)	N36—C37—N38	114.9 (3)
N25—C16—C17	124.9 (3)	N36—C37—C32	123.2 (3)
N15—C16—C17	116.5 (3)	N38—C37—C32	121.9 (3)
C18—C17—C16	117.6 (3)	C29—N38—C37	117.9 (3)
C17—C18—C19	120.2 (3)	C1—N39—C35	117.4 (3)
C18—C19—C20	124.8 (3)	O51—S50—C52	106.19 (12)
C18—C19—C24	117.9 (3)	O51—S50—C53	104.73 (13)
C20—C19—C24	117.3 (3)	C52—S50—C53	98.61 (14)
C21—C20—C19	120.9 (3)	O61—S60—C62	106.6 (1)
C20—C21—C22	117.0 (3)	O61—S60—C63	104.5 (9)
N23—C22—N26	117.9 (3)	C62—S60—C63	98.3 (8)
N23—C22—C21	125.1 (3)		

Table A.4. Hydrogen-bonding distance (Å) and angles (°) for macrocycle **7**.

D—H· · ·A	D—H	H· · ·A	D· · ·A	D—H· · ·A
N2—H2· · ·O41i	0.88	1.99	2.832 (3)	160.5
N15—H15· · ·O51ii	0.88	1.96	2.832 (3)	170.3
N26—H26· · ·O61iii	0.88	2.28	2.773 (9)	115.1
N26—H26· · ·O61iv	0.88	2.34	3.017 (8)	133.4
O41—H41· · ·O51	0.84	1.86	2.692 (3)	168.5
N10—H14· · ·N25	2.277	2.502	4.702 (4)	159.42
N23—H27· · ·N38	2.501	2.309	4.709 (4)	156.4
N36—H1· · ·N12	2.307	2.502	4.740 (4)	160.61

Table A.5. Fractional atomic coordinates and equivalent isotropic displacement parameters ($Å^2$) for macrocycle **7**.

$$U_{eq} = (1/3)\Sigma^i\Sigma^j U^{ij} a^i a^j \, a_i a_j$$

Atom	Occupancy	x	y	z	U_{eq}
H1	1	0.38410 (11)	0.0603 (4)	0.54081 (13)	0.0253 (9)
C1	1	0.3793	0.1254	0.5079	0.030
N2	1	0.35104 (8)	−0.0204 (3)	0.56395 (10)	0.0244 (7)
H2	1	0.3570	−0.0902	0.5910	0.037
C3	1	0.30784 (11)	−0.0013 (4)	0.54820 (14)	0.0231 (9)
C4	1	0.27661 (11)	−0.0860 (4)	0.58021 (13)	0.0258 (9)
H4	1	0.2847	−0.1526	0.6115	0.031
C5	1	0.23485 (11)	−0.0694 (4)	0.56496 (13)	0.0277 (9)
H5	1	0.2131	−0.1249	0.5854	0.033
C6	1	0.22374 (11)	0.0312 (4)	0.51827 (13)	0.0226 (8)
C7	1	0.18139 (10)	0.0539 (4)	0.49801 (14)	0.0296 (9)
H7	1	0.1583	−0.0035	0.5145	0.036
C8	1	0.17403 (10)	0.1593 (4)	0.45444 (14)	0.0281 (9)
H8	1	0.1457	0.1773	0.4405	0.034
C9	1	0.20948 (11)	0.2415 (4)	0.43042 (13)	0.0226 (9)
N10	1	0.24978 (8)	0.2183 (3)	0.44664 (10)	0.0225 (7)
C11	1	0.25720 (11)	0.1131 (4)	0.49010 (13)	0.0202 (8)
N12	1	0.29939 (9)	0.0965 (3)	0.50522 (10)	0.0234 (7)
N13	1	0.19923 (8)	0.3542 (3)	0.38766 (11)	0.0251 (7)
C14	1	0.23122 (11)	0.4185 (4)	0.36134 (13)	0.0239 (9)
H14	1	0.2597	0.3898	0.3719	0.029
N15	1	0.22502 (8)	0.5265 (3)	0.31882 (10)	0.0236 (7)
H15	1	0.1984	0.5546	0.3110	0.035
C16	1	0.25772 (12)	0.5957 (4)	0.28693 (13)	0.0219 (8)
C17	1	0.24493 (11)	0.6987 (4)	0.24112 (12)	0.0265 (9)
H17	1	0.2155	0.7185	0.2334	0.032
C18	1	0.27616 (11)	0.7667 (4)	0.20924 (13)	0.0258 (9)
H18	1	0.2688	0.8349	0.1781	0.031
C19	1	0.31946 (11)	0.7371 (4)	0.22190 (13)	0.0231 (8)
C20	1	0.35431 (12)	0.7990 (4)	0.19077 (13)	0.0320 (9)
H20	1	0.3491	0.8668	0.1587	0.038
C21	1	0.39514 (11)	0.7634 (4)	0.20577 (13)	0.0361 (10)
H21	1	0.4189	0.8030	0.1844	0.043
C22	1	0.40088 (12)	0.6643 (4)	0.25476 (14)	0.0359 (10)
N23	1	0.36967 (9)	0.6008 (3)	0.28528 (10)	0.0284 (8)
C24	1	0.32897 (12)	0.6352 (4)	0.26940 (13)	0.0234 (9)
N25	1	0.29773 (9)	0.5634 (3)	0.30084 (10)	0.0226 (7)
N26	1	0.44279 (9)	0.6297 (4)	0.27052 (12)	0.0644 (11)
H26	1	0.4634	0.6566	0.2464	0.097

(Continued)

Atom	Occupancy	x	y	z	U_{eq}
C27	1	0.45415 (11)	0.5575 (4)	0.32066 (15)	0.0378 (10)
H27	1	0.4325	0.5235	0.3469	0.045
N28	1	0.49384 (9)	0.5342 (4)	0.33338 (12)	0.0501 (9)
C29	1	0.50142 (11)	0.4542 (4)	0.38621 (15)	0.0335 (9)
C30	1	0.54346 (10)	0.4694 (4)	0.40934 (14)	0.0346 (10)
H30	1	0.5643	0.5320	0.3901	0.042
C31	1	0.55336 (10)	0.3924 (4)	0.45962 (15)	0.0353 (10)
H31	1	0.5814	0.4001	0.4758	0.042
C32	1	0.52173 (11)	0.3018 (4)	0.48717 (14)	0.0276 (9)
C33	1	0.52785 (11)	0.2211 (4)	0.54007 (15)	0.0387 (10)
H33	1	0.5550	0.2246	0.5590	0.046
C34	1	0.49490 (11)	0.1380 (4)	0.56406 (14)	0.0388 (10)
H34	1	0.4989	0.0822	0.5994	0.047
C35	1	0.45486 (11)	0.1361 (4)	0.53568 (15)	0.0265 (9)
N36	1	0.44766 (8)	0.2115 (3)	0.48577 (11)	0.0266 (7)
C37	1	0.48071 (11)	0.2934 (4)	0.46191 (14)	0.0256 (8)
N38	1	0.47104 (8)	0.3691 (3)	0.41080 (11)	0.0322 (8)
N39	1	0.42211 (9)	0.0503 (3)	0.56279 (10)	0.0277 (7)
C41	1	0.64472 (11)	0.3618 (4)	0.33921 (13)	0.0464 (11)
H41A	1	0.6445	0.3878	0.3808	0.070
H41B	1	0.6203	0.4126	0.3200	0.070
H41C	1	0.6716	0.3988	0.3217	0.070
O41	1	0.64152 (7)	0.1979 (3)	0.33230 (8)	0.0347 (6)
H41	1	0.6385	0.1763	0.2968	0.052
S50	1	0.61095 (3)	0.19301 (10)	0.17181 (3)	0.0272 (2)
O51	1	0.64359 (6)	0.1384 (2)	0.21718 (8)	0.0302 (6)
C52	1	0.64098 (9)	0.2889 (4)	0.11634 (12)	0.0307 (9)
H52A	1	0.6544	0.3833	0.1324	0.046
H52B	1	0.6218	0.3182	0.0843	0.046
H52C	1	0.6633	0.2180	0.1017	0.046
C53	1	0.59683 (9)	0.0197 (3)	0.13265 (12)	0.0347 (9)
H53A	1	0.6230	−0.0351	0.1205	0.052
H53B	1	0.5800	0.0481	0.0982	0.052
H53C	1	0.5797	−0.0491	0.1578	0.052
S60	0.50	0.51331 (6)	0.0344 (3)	0.23756 (10)	0.0490 (6)
O61	0.50	0.4971 (4)	−0.1127 (5)	0.2675 (3)	0.050 (2)
C62	0.50	0.4670 (8)	0.131 (3)	0.2077 (12)	0.065 (9)
H62A	0.50	0.4577	0.0765	0.1724	0.097
H62B	0.50	0.4744	0.2399	0.1980	0.097
H62C	0.50	0.4437	0.1306	0.2364	0.097
C63	0.50	0.5243 (8)	0.169 (3)	0.2964 (11)	0.051 (6)
H63A	0.50	0.4985	0.1815	0.3204	0.077
H63B	0.50	0.5326	0.2713	0.2803	0.077
H63C	0.50	0.5478	0.1282	0.3204	0.077

Table A.6. Anisotropic displacement parameters ($Å^2$) for macrocycle **7**.

Atom	U_{11}	U_{22}	U_{33}	U_{12}	U_{13}	U_{23}
C1	0.035 (3)	0.030 (2)	0.010 (2)	−0.001 (2)	0.005 (2)	−0.0005 (17)
N2	0.0305 (19)	0.0274 (19)	0.0153 (16)	0.0016 (15)	−0.0017 (15)	0.0060 (13)
C3	0.031 (3)	0.022 (2)	0.016 (2)	0.0032 (19)	0.0039 (19)	−0.0091 (18)
C4	0.037 (3)	0.028 (2)	0.013 (2)	−0.0010 (19)	0.0005 (19)	−0.0011 (16)
C5	0.040 (3)	0.027 (2)	0.017 (2)	−0.0062 (19)	0.0068 (19)	−0.0030 (18)
C6	0.029 (2)	0.024 (2)	0.015 (2)	−0.0007 (19)	0.0037 (18)	−0.0045 (18)
C7	0.030 (3)	0.032 (3)	0.027 (2)	−0.0042 (19)	0.0040 (19)	−0.0031 (19)
C8	0.024 (2)	0.035 (3)	0.026 (2)	0.0008 (19)	−0.0010 (18)	−0.0033 (19)
C9	0.033 (2)	0.021 (2)	0.013 (2)	0.0015 (19)	0.002 (2)	−0.0059 (17)
N10	0.0273 (18)	0.0252 (19)	0.0151 (16)	0.0050 (14)	−0.0003 (14)	0.0019 (14)
C11	0.028 (2)	0.020 (2)	0.013 (2)	0.0012 (18)	−0.0004 (19)	−0.0053 (17)
N12	0.031 (2)	0.0262 (19)	0.0130 (17)	0.0046 (14)	−0.0029 (14)	0.0017 (13)
N13	0.0298 (19)	0.028 (2)	0.0173 (17)	−0.0023 (15)	0.0011 (15)	−0.0001 (15)
C14	0.030 (3)	0.026 (2)	0.016 (2)	0.0080 (19)	−0.0068 (18)	−0.0055 (18)
N15	0.0237 (18)	0.0282 (19)	0.0188 (17)	0.0069 (14)	−0.0030 (14)	0.0003 (15)
C16	0.033 (3)	0.020 (2)	0.012 (2)	−0.0008 (19)	0.0041 (19)	−0.0048 (17)
C17	0.032 (2)	0.027 (2)	0.020 (2)	0.0088 (19)	−0.0058 (19)	−0.0013 (19)
C18	0.036 (3)	0.026 (2)	0.014 (2)	0.0034 (19)	−0.0016 (19)	−0.0001 (17)
C19	0.030 (2)	0.024 (2)	0.016 (2)	−0.0031 (18)	0.0000 (19)	0.0002 (17)
C20	0.045 (3)	0.031 (2)	0.019 (2)	−0.007 (2)	−0.006 (2)	0.0023 (17)
C21	0.037 (3)	0.052 (3)	0.019 (2)	−0.011 (2)	0.0011 (19)	0.0106 (19)
C22	0.028 (3)	0.057 (3)	0.022 (2)	−0.006 (2)	−0.007 (2)	0.005 (2)
N23	0.024 (2)	0.044 (2)	0.0170 (18)	−0.0026 (15)	−0.0010 (15)	0.0038 (14)
C24	0.032 (3)	0.026 (2)	0.012 (2)	−0.004 (2)	0.0036 (19)	−0.0068 (17)
N25	0.0226 (18)	0.030 (2)	0.0148 (17)	0.0036 (15)	0.0006 (15)	−0.0017 (13)
N26	0.029 (2)	0.132 (3)	0.032 (2)	−0.014 (2)	−0.0019 (17)	0.047 (2)
C27	0.037 (3)	0.054 (3)	0.022 (2)	−0.010 (2)	0.003 (2)	0.009 (2)
N28	0.027 (2)	0.097 (3)	0.0267 (19)	−0.0043 (18)	−0.0055 (16)	0.0283 (19)
C29	0.026 (3)	0.050 (3)	0.025 (2)	0.002 (2)	0.001 (2)	0.000 (2)
C30	0.022 (2)	0.050 (3)	0.032 (2)	0.0014 (19)	0.0043 (19)	0.005 (2)
C31	0.025 (2)	0.040 (3)	0.040 (3)	0.003 (2)	−0.008 (2)	0.001 (2)
C32	0.025 (2)	0.032 (2)	0.026 (2)	0.000 (2)	−0.0044 (19)	0.0026 (19)
C33	0.032 (3)	0.042 (3)	0.042 (3)	0.001 (2)	−0.014 (2)	0.008 (2)
C34	0.035 (3)	0.047 (3)	0.035 (2)	−0.002 (2)	−0.014 (2)	0.0130 (19)
C35	0.030 (3)	0.025 (2)	0.024 (2)	0.0029 (19)	0.000 (2)	−0.0041 (18)
N36	0.0312 (19)	0.0323 (19)	0.0163 (17)	−0.0021 (15)	0.0001 (15)	−0.0005 (15)
C37	0.026 (2)	0.029 (2)	0.022 (2)	0.002 (2)	0.0023 (19)	−0.0046 (19)
N38	0.030 (2)	0.049 (2)	0.0181 (18)	−0.0045 (16)	0.0011 (15)	0.0087 (16)
N39	0.0289 (19)	0.035 (2)	0.0189 (17)	−0.0016 (16)	−0.0040 (16)	−0.0005 (14)
C41	0.068 (3)	0.040 (3)	0.030 (2)	0.013 (2)	0.008 (2)	−0.004 (2)
O41	0.0554 (16)	0.0339 (17)	0.0148 (13)	0.0019 (13)	−0.0059 (13)	0.0005 (12)
S50	0.0272 (5)	0.0364 (6)	0.0181 (5)	0.0023 (5)	−0.0002 (5)	−0.0007 (4)
O51	0.0292 (14)	0.0449 (16)	0.0163 (13)	0.0110 (11)	−0.0079 (11)	−0.0027 (11)
C52	0.033 (2)	0.039 (2)	0.021 (2)	−0.0067 (18)	0.0013 (17)	0.0031 (17)
C53	0.040 (2)	0.033 (2)	0.031 (2)	−0.0016 (18)	−0.0082 (17)	−0.0009 (18)
S60	0.0450 (19)	0.0515 (15)	0.0504 (18)	−0.0021 (11)	0.0162 (12)	−0.0032 (13)
O61	0.056 (4)	0.023 (3)	0.070 (7)	0.017 (4)	0.009 (6)	−0.002 (3)
C62	0.078 (13)	0.069 (17)	0.048 (9)	0.027 (13)	0.019 (8)	0.037 (10)
C63	0.079 (12)	0.040 (9)	0.035 (10)	−0.008 (9)	0.005 (8)	0.003 (8)

Appendix B

Table B.1. Crystal data and structure refinement for macrocycle **22**.

Empirical formula	C21.33 H28.33 Cl N6 O2
Formula weight	436.28
Temperature	100(2) K
Wavelength	0.71073 Å
Crystal system, space group	trogonal, p-3
Unit cell dimensions	a = 20.888(4) Å α = 90 °
	b = 20.888(4) Å β = 90 °
	c = 8.774(4) Å γ = 120 °
Volume	3315.2(17) $Å^3$
Z, Calculated density	6, 1.311 Mg/mm^3
Absorption coefficient	0.203 mm^{-1}
F(000)	1388
Crystal color	Colorless
Crystal size	0.3 x 0.2 x 0.1 mm
Theta range for data collection	2.98 to 26.97 °
Limiting indices	-21<=h<=26
	-23<=k<=26
	-10<=l<=10
Reflections collected / unique	16251 / 4348 [R(int) = 0.0744]
Refinement method	Full-matrix least-squares on F^2
Data / restraints / parameters	4348 / 0 / 277
Goodness-of-fit on F^2	1.014
Final R indices [$I>2\sigma(I)$]	R1 = 0.0496, wR2 = 0.1179
R indices (all data	R1 = 0.0956, wR2 = 0.1438
Extinction coefficient	0.0000(7)
Largest diff. peak and hole	0.604 and -0.531 $e.Å^{-3}$

All non-H atoms were refined by full-matrix least-squares with anisotropic displacement parameters. The H atoms were generated geometrically (C—H 0.95 to 0.98, N—H 0.88 and O—H 0.84 Å) and were included in the refinement in the riding model approximation. Data collection: Brucker D8 X-ray diffractometer. Computing structure solution: SHELXS-97 (Sheldrick, 1990). Computing structure refinement: SHELXL-97 (Sheldrick, 1997).

Table B.2. Atomic coordinates (x 10^4) and equivalent isotropic displacement parameters ($Å^2$ x 10^3) for macrocycle **22**. U(eq) is defined as one third of the trace of the orthogonalized Uij tensor.

Atom	x	y	z	U(eq)
Cl(1)	7254(1)	4240(1)	8029(1)	48(1)
O(1)	5823(1)	3917(1)	4519(2)	30(1)
O(2)	7692(1)	8076(1)	11265(2)	22(1)
N(1)	5482(1)	4492(1)	6263(2)	20(1)
N(2)	6708(1)	5059(1)	5311(2)	19(1)
N(3)	6573(1)	5711(1)	7351(2)	18(1)
N(4)	6825(1)	6312(1)	8264(2)	19(1)
N(5)	7740(1)	7486(1)	9108(2)	17(1)
N(6)	6772(1)	6893(1)	10870(2)	20(1)
C(1)	8752(2)	9274(2)	6812(3)	31(1)
C(2)	8117(1)	8507(2)	7209(3)	22(1)
C(3)	7415(2)	8537(2)	7543(3)	28(1)
C(4)	8342(1)	8203(1)	8552(3)	18(1)
C(5)	7404(1)	7514(1)	10487(3)	17(1)
C(6)	6405(1)	6754(1)	12289(3)	17(1)
C(7)	6787(1)	7065(1)	13636(3)	19(1)
C(8)	6406(2)	6867(1)	15002(3)	21(1)
C(9)	7511(1)	6865(1)	8159(3)	17(1)
C(10)	8008(1)	6831(2)	7107(3)	22(1)
C(11)	7749(1)	6241(2)	6161(3)	22(1)
C(12)	7003(1)	5673(1)	6282(3)	18(1)
C(13)	7200(1)	5007(1)	4162(3)	19(1)
C(14)	7262(1)	5416(1)	2685(3)	21(1)
C(15)	7845(2)	5390(2)	1683(3)	30(1)
C(16)	6524(2)	5092(2)	1847(3)	29(1)
C(17)	5977(1)	4446(1)	5325(3)	20(1)
C(18)	4340(2)	3639(1)	4946(3)	21(1)
C(19)	4723(1)	3944(1)	6296(3)	17(1)
C(20)	4359(1)	3742(1)	7703(3)	17(1)
C(21)	4768(2)	4051(2)	9179(3)	23(1)
C(22)	6667	3333	7401(6)	35(1)

Table B.3. Bond length (Å) for macrocycle **22**.

Atoms	Bond length	Atoms	Bond length
Cl(1)-C(22)	1.753(2)	C(7)-H(7)	0.95
O(1)-C(17)	1.212(3)	C(8)-C(18)#1	1.379(4)
O(2)-C(5)	1.226(3)	C(8)-H(8)	0.95
N(1)-C(17)	1.362(3)	C(9)-C(10)	1.418(4)
N(1)-C(19)	1.418(3)	C(10)-C(11)	1.354(4)
N(1)-H(1)	0.88	C(10)-H(10)	0.95
N(2)-C(12)	1.400(3)	C(11)-C(12)	1.413(4)
N(2)-C(17)	1.420(3)	C(11)-H(11)	0.95
N(2)-C(13)	1.482(3)	C(13)-C(14)	1.522(4)
N(3)-C(12)	1.329(3)	C(13)-H(13A)	0.99
N(3)-N(4)	1.354(3)	C(13)-H(13B)	0.99
N(4)-C(9)	1.320(3)	C(14)-C(15)	1.526(4)
N(5)-C(9)	1.409(3)	C(14)-C(16)	1.526(4)
N(5)-C(5)	1.413(3)	C(14)-H(14A)	1
N(5)-C(4)	1.476(3)	C(15)-H(15A)	0.98
N(6)-C(5)	1.351(3)	C(15)-H(15B)	0.98
N(6)-C(6)	1.413(3)	C(15)-H(15C)	0.98
N(6)-H(6)	0.88	C(16)-H(16A)	0.98
C(1)-C(2)	1.523(4)	C(16)-H(16B)	0.98
C(1)-H(1A)	0.98	C(16)-H(16C)	0.98
C(1)-H(1B)	0.98	C(18)-C(8)#1	1.378(4)
C(1)-H(1C)	0.98	C(18)-C(19)	1.392(4)
C(2)-C(4)	1.521(4)	C(18)-H(18)	0.95
C(2)-C(3)	1.525(4)	C(19)-C(20)	1.400(3)
C(2)-H(2A)	1	C(20)-C(6)#1	1.404(4)
C(3)-H(3A)	0.98	C(20)-C(21)	1.507(4)
C(3)-H(3B)	0.98	C(21)-H(21A)	0.98
C(3)-H(3C)	0.98	C(21)-H(21B)	0.98
C(4)-H(4A)	0.99	C(21)-H(21C)	0.98
C(4)-H(4B)	0.99	C(22)-Cl(1)#2	1.7531(19)
C(6)-C(7)	1.392(4)	C(22)-Cl(1)#3	1.7531(19)
C(6)-C(20)#1	1.404(4)	C(22)-H	0.96(5)
C(7)-C(8)	1.383(4)		

Table B.4. Bond angles (°) for macrocycle **22**.

Atoms	Bond angle	Atoms	Bond angle
C(17)-N(1)-C(19)	122.5(2)	C(9)-C(10)-H(10)	120.8
C(17)-N(1)-H(1)	118.8	C(10)-C(11)-C(12)	119.4(2)
C(19)-N(1)-H(1)	118.8	C(10)-C(11)-H(11)	120.3
C(12)-N(2)-C(17)	127.1(2)	C(12)-C(11)-H(11)	120.3
C(12)-N(2)-C(13)	118.5(2)	N(3)-C(12)-N(2)	118.9(2)
C(17)-N(2)-C(13)	114.3(2)	N(3)-C(12)-C(11)	119.8(2)
C(12)-N(3)-N(4)	120.8(2)	N(2)-C(12)-C(11)	121.3(2)
C(9)-N(4)-N(3)	121.2(2)	N(2)-C(13)-C(14)	113.9(2)
C(9)-N(5)-C(5)	126.6(2)	N(2)-C(13)-H(13A)	108.8
C(9)-N(5)-C(4)	117.6(2)	C(14)-C(13)-H(13A)	108.8
C(5)-N(5)-C(4)	115.5(2)	N(2)-C(13)-H(13B)	108.8
C(5)-N(6)-C(6)	125.8(2)	C(14)-C(13)-H(13B)	108.8
C(5)-N(6)-H(6)	117.1	H(13A)-C(13)-H(13B)	107.7
C(6)-N(6)-H(6)	117.1	C(13)-C(14)-C(15)	108.4(2)
C(2)-C(1)-H(1A)	109.5	C(13)-C(14)-C(16)	112.2(2)
C(2)-C(1)-H(1B)	109.5	C(15)-C(14)-C(16)	110.7(2)
H(1A)-C(1)-H(1B)	109.5	C(13)-C(14)-H(14A)	108.5
C(2)-C(1)-H(1C)	109.5	C(15)-C(14)-H(14A)	108.5
H(1A)-C(1)-H(1C)	109.5	C(16)-C(14)-H(14A)	108.5
H(1B)-C(1)-H(1C)	109.5	C(14)-C(15)-H(15A)	109.5
C(4)-C(2)-C(1)	109.1(2)	C(14)-C(15)-H(15B)	109.5
C(4)-C(2)-C(3)	111.8(2)	H(15A)-C(15)-H(15B)	109.5
C(1)-C(2)-C(3)	110.5(2)	C(14)-C(15)-H(15C)	109.5
C(4)-C(2)-H(2A)	108.4	H(15A)-C(15)-H(15C)	109.5
C(1)-C(2)-H(2A)	108.4	H(15B)-C(15)-H(15C)	109.5
C(3)-C(2)-H(2A)	108.4	C(14)-C(16)-H(16A)	109.5
C(2)-C(3)-H(3A)	109.5	C(14)-C(16)-H(16B)	109.5
C(2)-C(3)-H(3B)	109.5	H(16A)-C(16)-H(16B)	109.5

(Continued)

Atoms	Bond angle	Atoms	Bond angle
H(3A)-C(3)-H(3B)	109.5	C(14)-C(16)-H(16C)	109.5
C(2)-C(3)-H(3C)	109.5	H(16A)-C(16)-H(16C)	109.5
H(3A)-C(3)-H(3C)	109.5	H(16B)-C(16)-H(16C)	109.5
H(3B)-C(3)-H(3C)	109.5	O(1)-C(17)-N(1)	123.5(2)
N(5)-C(4)-C(2)	113.3(2)	O(1)-C(17)-N(2)	119.5(2)
N(5)-C(4)-H(4A)	108.9	N(1)-C(17)-N(2)	116.9(2)
C(2)-C(4)-H(4A)	108.9	C(8)#1-C(18)-C(19)	119.5(2)
N(5)-C(4)-H(4B)	108.9	C(8)#1-C(18)-H(18)	120.2
C(2)-C(4)-H(4B)	108.9	C(19)-C(18)-H(18)	120.2
H(4A)-C(4)-H(4B)	107.7	C(18)-C(19)-C(20)	120.8(2)
O(2)-C(5)-N(6)	123.9(2)	C(18)-C(19)-N(1)	120.4(2)
O(2)-C(5)-N(5)	120.0(2)	C(20)-C(19)-N(1)	118.7(2)
N(6)-C(5)-N(5)	116.2(2)	C(19)-C(20)-C(6)#1	118.2(2)
C(7)-C(6)-C(20)#1	121.1(2)	C(19)-C(20)-C(21)	121.6(2)
C(7)-C(6)-N(6)	121.8(2)	C(6)#1-C(20)-C(21)	120.3(2)
C(20)#1-C(6)-N(6)	117.1(2)	C(20)-C(21)-H(21A)	109.5
C(8)-C(7)-C(6)	119.1(2)	C(20)-C(21)-H(21B)	109.5
C(8)-C(7)-H(7)	120.5	H(21A)-C(21)-H(21B)	109.5
C(6)-C(7)-H(7)	120.5	C(20)-C(21)-H(21C)	109.5
C(18)#1-C(8)-C(7)	121.3(2)	H(21A)-C(21)-H(21C)	109.5
C(18)#1-C(8)-H(8)	119.3	H(21B)-C(21)-H(21C)	109.5
C(7)-C(8)-H(8)	119.3	Cl(1)-C(22)-Cl(1)#2	110.61(16)
N(4)-C(9)-N(5)	119.0(2)	Cl(1)-C(22)-Cl(1)#3	110.61(16)
N(4)-C(9)-C(10)	120.3(2)	Cl(1)#2-C(22)-Cl(1)#3	110.61(16)
N(5)-C(9)-C(10)	120.8(2)	Cl(1)-C(22)-H	108.31(18)
C(11)-C(10)-C(9)	118.3(2)	Cl(1)#2-C(22)-H	108.31(17)
C(11)-C(10)-H(10)	120.8	Cl(1)#3-C(22)-H	108.31(16)

Table B.5. Anisotropic displacement parameters ($Å^2 \times 10^3$) for macrocycle **22**. The anisotropic displacement factor exponent takes the form:

$$-2\,pi^2\,[\,h^2\,a^{*2}\,U11 + \ldots + 2\,h\,k\,a^*\,b^*\,U12\,]$$

Atom	U11	U22	U33	U23	U13	U12
Cl(1)	50(1)	37(1)	49(1)	-1(1)	-11(1)	15(1)
O(1)	27(1)	17(1)	38(1)	-8(1)	10(1)	4(1)
O(2)	22(1)	16(1)	25(1)	-4(1)	2(1)	7(1)
N(1)	17(1)	16(1)	23(1)	-3(1)	3(1)	5(1)
N(2)	17(1)	16(1)	21(1)	-3(1)	2(1)	7(1)
N(3)	18(1)	16(1)	18(1)	-2(1)	1(1)	7(1)
N(4)	17(1)	17(1)	19(1)	-1(1)	0(1)	7(1)
N(5)	16(1)	13(1)	20(1)	-2(1)	0(1)	5(1)
N(6)	18(1)	18(1)	20(1)	-1(1)	2(1)	6(1)
C(1)	29(2)	26(2)	36(2)	5(1)	6(1)	12(1)
C(2)	21(1)	20(1)	23(1)	0(1)	2(1)	10(1)
C(3)	26(2)	24(2)	35(2)	0(1)	-2(1)	14(1)
C(4)	12(1)	16(1)	22(1)	-1(1)	1(1)	4(1)
C(5)	15(1)	16(1)	21(1)	1(1)	0(1)	9(1)
C(6)	18(1)	13(1)	20(1)	1(1)	1(1)	8(1)
C(7)	20(1)	17(1)	22(1)	-4(1)	-2(1)	10(1)
C(8)	23(2)	20(1)	22(1)	-1(1)	-3(1)	12(1)
C(9)	17(1)	15(1)	18(1)	1(1)	-1(1)	8(1)
C(10)	16(1)	21(1)	26(1)	-2(1)	1(1)	8(1)
C(11)	18(1)	24(2)	25(1)	-2(1)	3(1)	11(1)
C(12)	18(1)	17(1)	20(1)	1(1)	0(1)	10(1)
C(13)	17(1)	18(1)	23(1)	-3(1)	2(1)	9(1)
C(14)	21(1)	15(1)	24(1)	-1(1)	2(1)	7(1)
C(15)	30(2)	30(2)	25(2)	0(1)	5(1)	11(1)
C(16)	30(2)	27(2)	29(2)	5(1)	-1(1)	14(1)
C(17)	20(1)	15(1)	23(1)	2(1)	3(1)	7(1)
C(18)	25(2)	18(1)	19(1)	2(1)	2(1)	10(1)
C(19)	17(1)	12(1)	22(1)	-1(1)	2(1)	7(1)
C(20)	19(1)	14(1)	19(1)	-3(1)	-1(1)	7(1)
C(21)	21(1)	22(1)	20(1)	-4(1)	-1(1)	6(1)
C(22)	41(2)	41(2)	23(3)	0	0	21(1)

Table B.6. Hydrogen coordinates (x 10^4) and isotropic displacement parameters (A^2 x 10^3) for macrocycle **22**.

Atom	x	y	z	U(eq)
H(1)	5639	4877	6870	80
H(6)	6570	6544	10174	80
H(1A)	9197	9245	6597	46
H(1B)	8846	9609	7672	46
H(1C)	8620	9461	5911	46
H(2A)	8021	8176	6312	26
H(3A)	7013	8040	7793	42
H(3B)	7280	8721	6644	42
H(3C)	7503	8868	8407	42
H(4A)	8765	8143	8245	21
H(4B)	8509	8566	9396	21
H(7)	7303	7409	13618	80
H(8)	6663	7085	15922	80
H(10)	8511	7213	7066	80
H(11)	8064	6209	5423	80
H(13A)	7013	4479	3926	22
H(13B)	7700	5209	4608	22
H(14A)	7431	5944	2934	25
H(15A)	8314	5600	2241	45
H(15B)	7915	5678	754	45
H(15C)	7682	4876	1412	45
H(16A)	6158	5116	2505	43
H(16B)	6353	4575	1583	43
H(16C)	6587	5376	914	43
H(18)	4591	3780	3996	80
H(21A)	4421	3845	10034	34
H(21B)	4993	4590	9175	34
H(21C)	5155	3919	9289	34

Appendix C

Table C.1. Crystal data and structure refinement for macrocycle **23**.

Empirical formula	C41 H53 Cl3 N12 O4
Formula weight	884.30
Temperature	100(2) K
Wavelength	0.71073 Å
Crystal system, space group	monoclinic, p2(1)/c
Unit cell dimensions	a = 14.760(2) Å α = 90 °
	b = 20.888(3) Å β = 94.946°
	c = 8.774(2) Å γ = 90 °
Volume	4352.9 $Å^3$
Z, Calculated density	4, 1.349 Mg/mm^3
Absorption coefficient	0.267 mm^{-1}
F(000)	1864
Crystal color	Colorless
Crystal size	0.5 x 0.02 x 0.01 mm
Theta range for data collection	2.85 to 25.00 °
Limiting indices	-17<=h<=17
	-12<=k<=22
	-18<=l<=18
Reflections collected / unique	19061 / 7608 [R(int) = 0.0744]
Refinement method	Full-matrix least-squares on F^2
Data / restraints / parameters	7608 / 54 / 579
Goodness-of-fit on F^2	1.032
Final R indices [$I>2\sigma(I)$]	R1 = 0.0719, wR2 = 0.1893
R indices (all data	R1 = 0.1078, wR2 = 0.2231
Extinction coefficient	0.0015(8)
Largest diff. peak and hole	2.142 and -0.764 $e.Å^{-3}$

All non-H atoms were refined by full-matrix least-squares with anisotropic displacement parameters. The H atoms were generated geometrically (C—H 0.95 to 0.98, N—H 0.88 and O—H 0.84 Å) and were included in the refinement in the riding model approximation. Data collection: Brucker D8 X-ray diffractometer. Computing structure solution: SHELXS-97 (Sheldrick, 1990). Computing structure refinement: SHELXL-97 (Sheldrick, 1997).

Table C.2. Atomic coordinates (x 10^4) and equivalent isotropic displacement parameters ($Å^2$ x 10^3) for macrocycle **23**. U(eq) is defined as one third of the trace of the orthogonalized Uij tensor.

Atom	x	y	z	U(eq)
O(1)	3213(3)	2054(3)	4385(4)	117(3)
O(2)	9045(2)	2130(2)	2083(2)	26(1)
O(3)	10192(2)	-1371(2)	4262(2)	32(1)
O(4)	5677(2)	34(2)	7993(2)	24(1)
N(1)	4291(3)	2536(3)	3592(3)	63(2)
N(2)	5746(2)	2073(2)	3449(2)	23(1)
N(3)	6568(2)	2083(2)	3126(2)	19(1)
N(4)	7640(2)	2583(2)	2270(2)	19(1)
N(5)	8083(2)	1459(2)	2793(2)	19(1)
N(6)	9153(2)	-526(2)	4444(2)	20(1)
N(7)	9493(2)	-1386(2)	5517(2)	21(1)
N(8)	8343(2)	-625(2)	5890(2)	21(1)
N(9)	7749(2)	-387(2)	6440(2)	22(1)
N(10)	7048(2)	-436(2)	7742(2)	24(1)
N(11)	6061(2)	3(2)	6600(2)	19(1)
N(12)	4609(2)	1565(2)	4504(2)	21(1)
C(5)	3986(3)	2027(3)	4187(4)	54(2)
C(6)	4484(2)	1071(2)	5163(2)	19(1)
C(7)	3637(3)	864(2)	5413(3)	23(1)
C(8)	3609(3)	362(2)	6057(2)	23(1)
C(9)	4389(3)	67(2)	6469(2)	21(1)
C(10)	5225(2)	280(2)	6221(2)	18(1)
C(11)	5270(2)	775(2)	5568(2)	16(1)
C(12)	6220(3)	-120(2)	7465(2)	20(1)
C(13)	7261(3)	-497(3)	8688(3)	39(1)
C(14)	8062(4)	-49(5)	9025(4)	74(2)
C(15)	7900(5)	707(5)	8773(5)	81(2)
C(16)	8227(7)	-109(5)	9994(4)	137(5)
C(17)	7714(3)	-675(2)	7206(3)	23(1)
C(18)	8333(3)	-1197(3)	7502(3)	36(1)
C(19)	8940(3)	-1429(2)	6956(3)	32(1)
C(20)	8910(2)	-1137(2)	6114(2)	19(1)
C(21)	9964(3)	-2052(2)	5726(3)	23(1)
C(22)	9330(3)	-2679(2)	5635(3)	27(1)
C(23)	8930(5)	-2763(3)	4692(3)	55(2)

(Continued)

Atom	x	y	z	U(eq)
C(24)	9863(4)	-3328(3)	5953(4)	52(1)
C(25)	9642(2)	-1099(2)	4692(3)	20(1)
C(26)	9182(2)	-159(2)	3660(2)	19(1)
C(27)	9678(3)	-369(2)	2972(3)	25(1)
C(28)	9618(3)	33(2)	2223(3)	28(1)
C(29)	9118(3)	636(2)	2142(3)	27(1)
C(30)	8638(2)	852(2)	2837(2)	19(1)
C(31)	8674(2)	450(2)	3580(2)	17(1)
C(32)	8305(2)	2045(2)	2373(2)	19(1)
C(33)	7841(3)	3129(2)	1641(2)	20(1)
C(34)	7331(3)	3017(2)	742(2)	21(1)
C(35)	7577(3)	2325(2)	336(3)	28(1)
C(36)	7550(3)	3630(2)	169(3)	24(1)
C(37)	6791(2)	2595(2)	2610(2)	19(1)
C(38)	6184(3)	3160(2)	2424(3)	27(1)
C(39)	5368(3)	3149(2)	2757(3)	34(1)
C(40)	5142(3)	2576(3)	3268(3)	33(1)
Cl(3)	5539(1)	805(1)	9731(1)	36(1)
Cl(2)	6460(1)	729(1)	11454(1)	47(1)
Cl(1)	5080(1)	1769(1)	11059(1)	61(1)
C(41)	5425(3)	914(3)	10848(3)	34(1)
C(50)	3668(5)	3161(4)	3498(5)	18(2)
C(51)	2690(70)	3420(150)	3550(110)	2000(70)
C(52)	1890(80)	3420(90)	4110(90)	550(60)
C(53)	2416(11)	3800(10)	2699(11)	61(5)
C(50')	3391(9)	2820(5)	2908(8)	61(3)
C(51')	3214(8)	3546(6)	3240(6)	121(4)
C(52')	3169(8)	3518(6)	4219(6)	85(3)
C(53')	2322(9)	3575(10)	2650(11)	66(5)

Table C.3. Bond lengths (Å) for macrocycle **23**.

Atoms	Bond length	Atoms	Bond length
O(1)-C(5)	1.207(6)	C(8)-C(9)	1.387(6)
O(2)-C(32)	1.227(4)	C(9)-C(10)	1.384(5)
O(3)-C(25)	1.212(5)	C(10)-C(11)	1.390(5)
O(4)-C(12)	1.229(5)	C(13)-C(14)	1.515(9)
N(1)-C(40)	1.394(5)	C(14)-C(16)	1.501(9)
N(1)-C(5)	1.439(6)	C(14)-C(15)	1.512(11)
N(1)-C(50)	1.508(9)	C(17)-C(18)	1.404(6)
N(1)-C(50')	1.714(14)	C(18)-C(19)	1.356(6)
N(2)-C(40)	1.326(5)	C(19)-C(20)	1.415(6)
N(2)-N(3)	1.351(4)	C(21)-C(22)	1.522(6)
N(3)-C(37)	1.323(5)	C(22)-C(24)	1.528(6)
N(4)-C(37)	1.400(5)	C(22)-C(23)	1.534(7)
N(4)-C(32)	1.424(5)	C(26)-C(31)	1.385(5)
N(4)-C(33)	1.476(5)	C(26)-C(27)	1.401(5)
N(5)-C(32)	1.349(5)	C(27)-C(28)	1.387(6)
N(5)-C(30)	1.420(5)	C(28)-C(29)	1.371(6)
N(6)-C(25)	1.350(5)	C(29)-C(30)	1.398(5)
N(6)-C(26)	1.406(5)	C(30)-C(31)	1.381(5)
N(7)-C(20)	1.397(5)	C(33)-C(34)	1.538(5)
N(7)-C(25)	1.424(5)	C(34)-C(36)	1.521(5)
N(7)-C(21)	1.475(5)	C(34)-C(35)	1.523(6)
N(8)-C(20)	1.316(5)	C(37)-C(38)	1.418(6)
N(8)-N(9)	1.351(4)	C(38)-C(39)	1.351(6)
N(9)-C(17)	1.311(5)	C(39)-C(40)	1.408(6)
N(10)-C(12)	1.397(5)	Cl(3)-C(41)	1.761(4)
N(10)-C(17)	1.416(5)	Cl(2)-C(41)	1.758(5)
N(10)-C(13)	1.474(5)	Cl(1)-C(41)	1.754(5)
N(11)-C(12)	1.358(5)	C(50)-C(51)	1.53(3)
N(11)-C(10)	1.421(5)	C(51)-C(53)	1.53(3)
N(12)-C(5)	1.338(6)	C(51)-C(52)	1.53(3)
N(12)-C(6)	1.413(5)	C(50')-C(51')	1.513(5)
C(6)-C(11)	1.391(5)	C(51')-C(52')	1.521(5)
C(6)-C(7)	1.399(5)	C(51')-C(53')	1.537(5)
C(7)-C(8)	1.387(6)		

Table C.4. Bond angles (°) for macrocycle **23**.

Atoms	Angle	Atoms	Angle
C(40)-N(1)-C(5)	127.5(4)	C(18)-C(19)-C(20)	118.3(4)
C(40)-N(1)-C(50)	118.8(4)	N(8)-C(20)-N(7)	119.7(3)
C(5)-N(1)-C(50)	112.2(4)	N(8)-C(20)-C(19)	120.3(4)
C(40)-N(1)-C(50')	115.7(5)	N(7)-C(20)-C(19)	120.1(3)
C(5)-N(1)-C(50')	109.9(5)	N(7)-C(21)-C(22)	112.7(3)
C(50)-N(1)-C(50')	41.9(5)	C(21)-C(22)-C(24)	108.4(4)
C(40)-N(2)-N(3)	121.3(3)	C(21)-C(22)-C(23)	110.8(4)
C(37)-N(3)-N(2)	120.8(3)	C(24)-C(22)-C(23)	111.5(4)
C(37)-N(4)-C(32)	126.9(3)	O(3)-C(25)-N(6)	124.1(4)
C(37)-N(4)-C(33)	118.3(3)	O(3)-C(25)-N(7)	119.3(4)
C(32)-N(4)-C(33)	114.2(3)	N(6)-C(25)-N(7)	116.6(3)
C(32)-N(5)-C(30)	122.7(3)	C(31)-C(26)-C(27)	119.2(4)
C(25)-N(6)-C(26)	126.6(3)	C(31)-C(26)-N(6)	116.1(3)
C(20)-N(7)-C(25)	127.7(3)	C(27)-C(26)-N(6)	124.6(4)
C(20)-N(7)-C(21)	117.1(3)	C(28)-C(27)-C(26)	118.3(4)
C(25)-N(7)-C(21)	115.1(3)	C(29)-C(28)-C(27)	122.6(4)
C(20)-N(8)-N(9)	121.2(3)	C(28)-C(29)-C(30)	118.9(4)
C(17)-N(9)-N(8)	120.3(3)	C(31)-C(30)-C(29)	119.2(4)
C(12)-N(10)-C(17)	126.3(3)	C(31)-C(30)-N(5)	118.5(3)
C(12)-N(10)-C(13)	116.4(3)	C(29)-C(30)-N(5)	122.2(4)
C(17)-N(10)-C(13)	117.2(3)	C(30)-C(31)-C(26)	121.7(3)
C(12)-N(11)-C(10)	122.8(3)	O(2)-C(32)-N(5)	123.2(4)
C(5)-N(12)-C(6)	125.3(3)	O(2)-C(32)-N(4)	119.3(3)
O(1)-C(5)-N(12)	124.8(4)	N(5)-C(32)-N(4)	117.5(3)
O(1)-C(5)-N(1)	119.2(4)	N(4)-C(33)-C(34)	112.8(3)
N(12)-C(5)-N(1)	116.0(4)	C(36)-C(34)-C(35)	111.2(3)
C(11)-C(6)-C(7)	119.3(4)	C(36)-C(34)-C(33)	107.9(3)
C(11)-C(6)-N(12)	116.2(3)	C(35)-C(34)-C(33)	112.2(3)
C(7)-C(6)-N(12)	124.4(3)	N(3)-C(37)-N(4)	119.5(3)
C(8)-C(7)-C(6)	118.6(4)	N(3)-C(37)-C(38)	120.1(3)
C(7)-C(8)-C(9)	122.5(4)	N(4)-C(37)-C(38)	120.4(3)
C(10)-C(9)-C(8)	118.5(4)	C(39)-C(38)-C(37)	118.7(4)
C(9)-C(10)-C(11)	120.1(3)	C(38)-C(39)-C(40)	119.2(4)
C(9)-C(10)-N(11)	122.6(3)	N(2)-C(40)-N(1)	119.6(4)
C(11)-C(10)-N(11)	117.3(3)	N(2)-C(40)-C(39)	119.8(4)
C(10)-C(11)-C(6)	121.0(3)	N(1)-C(40)-C(39)	120.6(4)
O(4)-C(12)-N(11)	123.0(4)	Cl(1)-C(41)-Cl(2)	109.9(2)
O(4)-C(12)-N(10)	120.2(3)	Cl(1)-C(41)-Cl(3)	110.3(3)
N(11)-C(12)-N(10)	116.8(3)	Cl(2)-C(41)-Cl(3)	110.4(2)
N(10)-C(13)-C(14)	113.0(5)	N(1)-C(50)-C(51)	145(10)
C(16)-C(14)-C(15)	109.8(6)	C(50)-C(51)-C(53)	107(3)
C(16)-C(14)-C(13)	110.8(8)	C(50)-C(51)-C(52)	144(6)
C(15)-C(14)-C(13)	110.6(5)	C(53)-C(51)-C(52)	109(6)
N(9)-C(17)-C(18)	121.2(4)	C(51')-C(50')-N(1)	103.2(8)
N(9)-C(17)-N(10)	118.5(4)	C(50')-C(51')-C(52')	109.2(9)
C(18)-C(17)-N(10)	120.3(4)	C(50')-C(51')-C(53')	89.7(10)
C(19)-C(18)-C(17)	118.4(4)	C(52')-C(51')-C(53')	118.9(11)

Appendix D

Table D.1. Crystal data and structure refinement for trimer **24**.

Empirical formula	C28 H36 Cl3 N6 O2
Formula weight	488.63
Temperature	100(2) K
Wavelength	0.71073 Å
Crystal system, space group	monoclinic, p2(1)/c
Unit cell dimensions	a = 26.127(5) Å α = 90 ° b = 11.364(2) Å β = 104.207 (3)° c = 18.603(3) Å γ = 90 °
Volume	5354.5 (17) $Å^3$
Z, Calculated density	8, 1.212 mg/mm^3
Absorption coefficient	0.079 mm^{-1}
F(000)	2096
Crystal color	Colorless
Crystal size	0.5 x 0.3 x 0.05 mm
Theta range for data collection	2.87 to 25.00 °
Limiting indices	-22<=h<=31 -13<=k<=13 -22<=l<=20
Reflections collected / unique	24278 / 9272 [R(int) = 0.0700]
Refinement method	Full-matrix least-squares on F^2
Data / restraints / parameters	9373 / 0 / 650
Goodness-of-fit on F^2	0.996
Final R indices [$I>2\sigma(I)$]	R1 = 0.0950, wR2 = 0.1942
R indices (all data	R1 = 0.1995, wR2 = 0.2757
Extinction coefficient	0.0024(4)
Largest diff. peak and hole	0.858 and -0.809 $e.Å^{-3}$

All non-H atoms were refined by full-matrix least-squares with anisotropic displacement parameters. The H atoms were generated geometrically (C—H 0.95 to 0.98, N—H 0.88 and O—H 0.84 Å) and were included in the refinement in the riding model approximation. Data collection: Brucker D8 X-ray diffractometer. Computing structure solution: SHELXS-97 (Sheldrick, 1990). Computing structure refinement: SHELXL-97 (Sheldrick, 1997).

Table D.2. Atomic coordinates (x 10^4) and equivalent isotropic displacement parameters ($Å^2$ x 10^3) for trimer **24**. U(eq) is defined as one third of the trace of the orthogonalized Uij tensor.

Atom	x	y	z	U(eq)
N(1)	191(3)	10423(5)	3737(4)	67(2)
N(1A)	2524(2)	4570(4)	2683(2)	38(1)
N(2)	290(3)	9181(6)	2774(3)	68(2)
N(2A)	2807(2)	6274(4)	2186(2)	35(1)
N(3)	1085(2)	9289(4)	3695(3)	48(1)
N(3A)	3522(2)	5135(4)	2805(2)	36(1)
N(4)	1552(2)	8846(4)	4093(3)	44(1)
N(4A)	4019(2)	4706(4)	2892(2)	36(1)
N(5)	2213(3)	7403(4)	4357(3)	57(2)
N(5A)	4827(2)	4577(4)	2558(2)	36(1)
N(6)	2512(2)	9277(4)	4834(2)	47(1)
N(6A)	4893(2)	3840(4)	3765(2)	39(1)
O(1)	-462(3)	10215(5)	2667(4)	99(2)
O(1A)	1941(2)	6008(4)	2179(2)	49(1)
O(2)	3034(2)	7652(4)	5122(2)	62(1)
O(2A)	5552(2)	3553(4)	3173(2)	55(1)
C(1)	-87(4)	11038(7)	4173(6)	76(2)
C(1A)	2178(2)	3686(5)	2820(3)	40(1)
C(2)	226(4)	11514(7)	4831(5)	75(3)
C(2A)	2417(2)	2706(5)	3227(3)	44(2)
C(3)	822(3)	11405(7)	5027(4)	75(2)
C(3A)	3006(3)	2595(6)	3478(4)	66(2)
C(4)	-25(4)	12093(8)	5305(5)	95(3)
C(4A)	2092(3)	1821(6)	3383(4)	55(2)
C(5)	-570(5)	12233(9)	5119(7)	108(4)
C(5A)	1547(3)	1890(6)	3153(4)	53(2)
C(6)	-863(5)	11795(9)	4478(10)	129(5)
C(6A)	1322(3)	2847(6)	2750(4)	56(2)
C(7)	-635(4)	11193(7)	3993(7)	95(3)
C(7A)	1631(3)	3748(5)	2582(4)	51(2)
C(8)	-29(5)	9979(7)	3056(7)	86(3)
C(8A)	2390(2)	5617(5)	2347(3)	35(1)
C(9)	81(4)	8868(7)	1982(4)	90(3)
C(9A)	2660(2)	7457(4)	1872(3)	37(1)
C(10)	240(6)	9815(13)	1466(5)	195(8)
C(10A)	2811(6)	8414(7)	2400(4)	188(8)
C(11)	-194(6)	9669(10)	695(6)	183(7)

(Continued)

Atom	x	y	z	U(eq)
C(11A)	2659(7)	9615(8)	1983(5)	228(10)
C(12)	742(8)	9900(17)	1499(5)	344(17)
C(12A)	2871(5)	8484(7)	3082(4)	114(4)
C(13)	774(3)	8668(6)	3167(3)	55(2)
C(13A)	3330(2)	5891(4)	2271(3)	33(1)
C(14)	917(4)	7547(8)	2999(4)	87(3)
C(14A)	3630(2)	6299(5)	1797(3)	38(1)
C(15)	1378(4)	7086(7)	3388(4)	88(3)
C(15A)	4127(3)	5882(5)	1887(3)	39(1)
C(16)	1715(3)	7789(6)	3939(3)	55(2)
C(16A)	4318(2)	5059(4)	2457(3)	35(1)
C(17)	2364(4)	6153(5)	4328(4)	74(2)
C(17A)	5082(3)	4671(5)	1934(3)	42(2)
C(18)	2245(5)	5443(6)	4948(5)	87(3)
C(18A)	5389(3)	5795(5)	1896(4)	48(2)
C(19)	1667(5)	5225(8)	4868(5)	110(4)
C(19A)	5836(3)	5998(7)	2578(4)	78(3)
C(20)	2528(5)	4261(7)	5009(6)	129(5)
C(20A)	5599(3)	5758(6)	1209(4)	59(2)
C(21)	2616(3)	8102(5)	4805(3)	52(2)
C(21A)	5117(3)	3942(5)	3184(3)	39(1)
C(22)	2902(3)	10090(5)	5205(3)	47(2)
C(22A)	5137(2)	3450(4)	4486(3)	38(1)
C(23)	2760(3)	10915(5)	5665(3)	47(2)
C(23A)	4834(2)	3495(4)	5009(3)	35(1)
C(24)	2209(3)	10976(5)	5761(3)	50(2)
C(24A)	4266(2)	3895(5)	4795(3)	42(2)
C(25)	3145(3)	11717(5)	6020(3)	50(2)
C(25A)	5067(3)	3179(5)	5738(3)	41(2)
C(26)	3645(3)	11719(6)	5904(3)	55(2)
C(26A)	5593(3)	2813(5)	5954(3)	46(2)
C(27)	3777(3)	10919(6)	5418(3)	55(2)
C(27A)	5881(3)	2765(5)	5430(3)	44(2)
C(28)	3410(3)	10102(6)	5071(3)	53(2)
C(28A	5662(3)	3074(5)	4704(3)	44(2)

Table D.3. Bond lengths (Å) for trimer **24**.

Atoms	Bond length	Atoms	Bond length
N(1)-C(8)	1.354(12)	C(11)-H(11A)	0.98
N(1)-C(1)	1.401(10)	C(11)-H(11B)	0.98
N(1)-H(1A)	0.88	C(11)-H(11C)	0.98
N(1A)-C(8A)	1.351(7)	C(11A)-H(11D)	0.98
N(1A)-C(1A)	1.415(7)	C(11A)-H(11E)	0.98
N(1A)-H(1AA)	0.88	C(11A)-H(11F)	0.98
N(2)-C(8)	1.416(11)	C(12)-H(12A)	0.98
N(2)-C(13)	1.421(9)	C(12)-H(12B)	0.98
N(2)-C(9)	1.484(8)	C(12)-H(12C)	0.98
N(2A)-C(13A)	1.406(7)	C(12A)-H(12D)	0.98
N(2A)-C(8A)	1.412(7)	C(12A)-H(12E)	0.98
N(2A)-C(9A)	1.479(7)	C(12A)-H(12F)	0.98
N(3)-C(13)	1.316(8)	C(13)-C(14)	1.384(11)
N(3)-N(4)	1.359(7)	C(13A)-C(14A)	1.395(7)
N(3A)-C(13A)	1.316(7)	C(14)-C(15)	1.349(12)
N(3A)-N(4A)	1.360(6)	C(14)-H(14A)	0.95
N(4)-C(16)	1.328(8)	C(14A)-C(15A)	1.352(8)
N(4A)-C(16A)	1.317(7)	C(14A)-H(14B)	0.95
N(5)-C(16)	1.413(9)	C(15)-C(16)	1.421(10)
N(5)-C(21)	1.415(9)	C(15)-H(15A)	0.95
N(5)-C(17)	1.479(7)	C(15A)-C(16A)	1.410(8)
N(5A)-C(16A)	1.407(7)	C(15A)-H(15B)	0.95
N(5A)-C(21A)	1.422(7)	C(17)-C(18)	1.501(10)
N(5A)-C(17A)	1.477(6)	C(17)-H(17A)	0.99
N(6)-C(21)	1.366(7)	C(17)-H(17B)	0.99
N(6)-C(22)	1.423(8)	C(17A)-C(18A)	1.519(8)
N(6)-H(6A)	0.88	C(17A)-H(17C)	0.99
N(6A)-C(21A)	1.353(7)	C(17A)-H(17D)	0.99
N(6A)-C(22A)	1.408(7)	C(18)-C(19)	1.501(13)
N(6A)-H(6AA)	0.88	C(18)-C(20)	1.524(10)
O(1)-C(8)	1.213(11)	C(18)-H(18A)	1
O(1A)-C(8A)	1.222(7)	C(18A)-C(20A)	1.511(8)
O(2)-C(21)	1.219(8)	C(18A)-C(19A)	1.517(10)
O(2A)-C(21A)	1.224(7)	C(18A)-H(18B)	1
C(1)-C(7)	1.398(11)	C(19)-H(19A)	0.98
C(1)-C(2)	1.404(12)	C(19)-H(19B)	0.98
C(1A)-C(7A)	1.391(8)	C(19)-H(19C)	0.98
C(1A)-C(2A)	1.404(8)	C(19A)-H(19D)	0.98

(Continued)

Atoms	Bond length	Atoms	Bond length
C(2)-C(4)	1.387(11)	C(19A)-H(19E)	0.98
C(2)-C(3)	1.515(11)	C(19A)-H(19F)	0.98
C(2A)-C(4A)	1.393(8)	C(20)-H(20A)	0.98
C(2A)-C(3A)	1.501(9)	C(20)-H(20B)	0.98
C(3)-H(3B)	0.98	C(20)-H(20C)	0.98
C(3)-H(3C)	0.98	C(20A)-H(20D)	0.98
C(3)-H(3D)	0.98	C(20A)-H(20E)	0.98
C(3A)-H(3AB)	0.98	C(20A)-H(20F)	0.98
C(3A)-H(3AC)	0.98	C(22)-C(23)	1.380(8)
C(3A)-H(3AD)	0.98	C(22)-C(28)	1.410(9)
C(4)-C(5)	1.390(14)	C(22A)-C(28A)	1.398(8)
C(4)-H(4B)	0.95	C(22A)-C(23A)	1.398(8)
C(4A)-C(5A)	1.385(9)	C(23)-C(25)	1.397(9)
C(4A)-H(4AB)	0.95	C(23)-C(24)	1.495(9)
C(5)-C(6)	1.343(16)	C(23A)-C(25A)	1.390(8)
C(5)-H(5A)	0.95	C(23A)-C(24A)	1.510(8)
C(5A)-C(6A)	1.369(9)	C(24)-H(24A)	0.98
C(5A)-H(5AA)	0.95	C(24)-H(24B)	0.98
C(6)-C(7)	1.379(14)	C(24)-H(24C)	0.98
C(6)-H(6B)	0.95	C(24A)-H(24D)	0.98
C(6A)-C(7A)	1.387(8)	C(24A)-H(24E)	0.98
C(6A)-H(6AB)	0.95	C(24A)-H(24F)	0.98
C(7)-H(7A)	0.95	C(25)-C(26)	1.375(9)
C(7A)-H(7AA)	0.95	C(25)-H(25A)	0.95
C(9)-C(10)	1.564(12)	C(25A)-C(26A)	1.396(8)
C(9)-H(9A)	0.99	C(25A)-H(25B)	0.95
C(9)-H(9B)	0.99	C(26)-C(27)	1.384(9)
C(9A)-C(10A)	1.454(9)	C(26)-H(26A)	0.95
C(9A)-H(9AA)	0.99	C(26A)-C(27A)	1.371(8)
C(9A)-H(9AB)	0.99	C(26A)-H(26B)	0.95
C(10)-C(12)	1.30(2)	C(27)-C(28)	1.377(9)
C(10)-C(11)	1.605(13)	C(27)-H(27A)	0.95
C(10)-H(10A)	1	C(27A)-C(28A)	1.377(8)
C(10A)-C(12A)	1.242(10)	C(27A)-H(27B)	0.95
C(10A)-C(11A)	1.573(11)	C(28)-H(28A)	0.95
C(10A)-H(10B)	1	C(28A)-H(28B)	0.95

Table D.4. Bond angles (°) for trimer **24**.

Atoms	Bond angle	Atoms	Bond angle
C(8)-N(1)-C(1)	124.5(9)	C(5)-C(6)-C(7)	121.4(13)
C(8)-N(1)-H(1A)	117.8	C(5)-C(6)-H(6B)	119.3
C(1)-N(1)-H(1A)	117.8	C(7)-C(6)-H(6B)	119.3
C(8A)-N(1A)-C(1A)	127.2(5)	C(5A)-C(6A)-C(7A)	120.9(6)
C(8A)-N(1A)-H(1AA)	116.4	C(5A)-C(6A)-H(6AB)	119.5
C(1A)-N(1A)-H(1AA)	116.4	C(7A)-C(6A)-H(6AB)	119.5
C(8)-N(2)-C(13)	127.1(7)	C(6)-C(7)-C(1)	119.2(12)
C(8)-N(2)-C(9)	114.5(8)	C(6)-C(7)-H(7A)	120.4
C(13)-N(2)-C(9)	118.5(7)	C(1)-C(7)-H(7A)	120.4
C(13A)-N(2A)-C(8A)	126.4(5)	C(6A)-C(7A)-C(1A)	120.1(6)
C(13A)-N(2A)-C(9A)	118.5(4)	C(6A)-C(7A)-H(7AA)	120
C(8A)-N(2A)-C(9A)	115.1(5)	C(1A)-C(7A)-H(7AA)	120
C(13)-N(3)-N(4)	121.1(6)	O(1)-C(8)-N(1)	126.5(10)
C(13A)-N(3A)-N(4A)	120.0(4)	O(1)-C(8)-N(2)	117.9(11)
C(16)-N(4)-N(3)	120.5(6)	N(1)-C(8)-N(2)	115.6(9)
C(16A)-N(4A)-N(3A)	120.7(5)	O(1A)-C(8A)-N(1A)	124.3(5)
C(16)-N(5)-C(21)	127.0(5)	O(1A)-C(8A)-N(2A)	119.8(5)
C(16)-N(5)-C(17)	119.7(6)	N(1A)-C(8A)-N(2A)	116.0(5)
C(21)-N(5)-C(17)	113.2(6)	N(2)-C(9)-C(10)	110.9(6)
C(16A)-N(5A)-C(21A)	127.1(4)	N(2)-C(9)-H(9A)	109.5
C(16A)-N(5A)-C(17A)	117.4(5)	C(10)-C(9)-H(9A)	109.5
C(21A)-N(5A)-C(17A)	115.3(5)	N(2)-C(9)-H(9B)	109.5
C(21)-N(6)-C(22)	121.9(6)	C(10)-C(9)-H(9B)	109.5
C(21)-N(6)-H(6A)	119.1	H(9A)-C(9)-H(9B)	108.1
C(22)-N(6)-H(6A)	119.1	C(10A)-C(9A)-N(2A)	114.3(5)
C(21A)-N(6A)-C(22A)	127.1(5)	C(10A)-C(9A)-H(9AA)	108.7
C(21A)-N(6A)-H(6AA)	116.5	N(2A)-C(9A)-H(9AA)	108.7
C(22A)-N(6A)-H(6AA)	116.5	C(10A)-C(9A)-H(9AB)	108.7
C(7)-C(1)-N(1)	124.8(10)	N(2A)-C(9A)-H(9AB)	108.7
C(7)-C(1)-C(2)	120.2(9)	H(9AA)-C(9A)-H(9AB)	107.6
N(1)-C(1)-C(2)	115.1(8)	C(12)-C(10)-C(9)	116.0(14)
C(7A)-C(1A)-C(2A)	119.9(5)	C(12)-C(10)-C(11)	122.2(12)
C(7A)-C(1A)-N(1A)	124.0(5)	C(9)-C(10)-C(11)	104.0(8)
C(2A)-C(1A)-N(1A)	116.2(5)	C(12)-C(10)-H(10A)	104.2
C(4)-C(2)-C(1)	118.1(9)	C(9)-C(10)-H(10A)	104.2
C(4)-C(2)-C(3)	120.4(10)	C(11)-C(10)-H(10A)	104.2
C(1)-C(2)-C(3)	121.5(8)	C(12A)-C(10A)-C(9A)	133.1(10)
C(4A)-C(2A)-C(1A)	118.2(6)	C(12A)-C(10A)-C(11A)	113.7(7)
C(4A)-C(2A)-C(3A)	120.4(6)	C(9A)-C(10A)-C(11A)	108.8(6)
C(1A)-C(2A)-C(3A)	121.4(5)	C(12A)-C(10A)-H(10B)	96.9
C(2)-C(3)-H(3B)	109.5	C(9A)-C(10A)-H(10B)	96.9
C(2)-C(3)-H(3C)	109.5	C(11A)-C(10A)-H(10B)	96.9
H(3B)-C(3)-H(3C)	109.5	C(10)-C(11)-H(11A)	109.5
C(2)-C(3)-H(3D)	109.5	C(10)-C(11)-H(11B)	109.5

(Continued)

Atoms	Bond angle	Atoms	Bond angle
H(3B)-C(3)-H(3D)	109.5	H(11A)-C(11)-H(11B)	109.5
H(3C)-C(3)-H(3D)	109.5	C(10)-C(11)-H(11C)	109.5
C(2A)-C(3A)-H(3AB)	109.5	H(11A)-C(11)-H(11C)	109.5
C(2A)-C(3A)-H(3AC)	109.5	H(11B)-C(11)-H(11C)	109.5
H(3AB)-C(3A)-H(3AC)	109.5	C(10A)-C(11A)-H(11D)	109.5
C(2A)-C(3A)-H(3AD)	109.5	C(10A)-C(11A)-H(11E)	109.5
H(3AB)-C(3A)-H(3AD)	109.5	H(11D)-C(11A)-H(11E)	109.5
H(3AC)-C(3A)-H(3AD)	109.5	C(10A)-C(11A)-H(11F)	109.5
C(2)-C(4)-C(5)	120.8(11)	H(11D)-C(11A)-H(11F)	109.5
C(2)-C(4)-H(4B)	119.6	H(11E)-C(11A)-H(11F)	109.5
C(5)-C(4)-H(4B)	119.6	C(10)-C(12)-H(12A)	109.5
C(5A)-C(4A)-C(2A)	121.9(6)	C(10)-C(12)-H(12B)	109.5
C(5A)-C(4A)-H(4AB)	119	H(12A)-C(12)-H(12B)	109.5
C(2A)-C(4A)-H(4AB)	119	C(10)-C(12)-H(12C)	109.5
C(6)-C(5)-C(4)	120.2(12)	H(12A)-C(12)-H(12C)	109.5
C(6)-C(5)-H(5A)	119.9	H(12B)-C(12)-H(12C)	109.5
C(4)-C(5)-H(5A)	119.9	C(10A)-C(12A)-H(12D)	109.5
C(6A)-C(5A)-C(4A)	119.0(6)	C(10A)-C(12A)-H(12E)	109.5
C(6A)-C(5A)-H(5AA)	120.5	H(12D)-C(12A)-H(12E)	109.5
C(4A)-C(5A)-H(5AA)	120.5	C(10A)-C(12A)-H(12F)	109.5
H(12D)-C(12A)-H(12F)	109.5	H(20A)-C(20)-H(20B)	109.5
H(12E)-C(12A)-H(12F)	109.5	C(18)-C(20)-H(20C)	109.5
N(3)-C(13)-C(14)	120.6(8)	H(20A)-C(20)-H(20C)	109.5
N(3)-C(13)-N(2)	118.2(6)	H(20B)-C(20)-H(20C)	109.5
C(14)-C(13)-N(2)	121.2(7)	C(18A)-C(20A)-H(20D)	109.5
N(3A)-C(13A)-C(14A)	121.6(5)	C(18A)-C(20A)-H(20E)	109.5
N(3A)-C(13A)-N(2A)	117.8(5)	H(20D)-C(20A)-H(20E)	109.5
C(14A)-C(13A)-N(2A)	120.6(5)	C(18A)-C(20A)-H(20F)	109.5
C(15)-C(14)-C(13)	119.5(8)	H(20D)-C(20A)-H(20F)	109.5
C(15)-C(14)-H(14A)	120.3	H(20E)-C(20A)-H(20F)	109.5
C(13)-C(14)-H(14A)	120.3	O(2)-C(21)-N(6)	123.7(7)
C(15A)-C(14A)-C(13A)	118.5(5)	O(2)-C(21)-N(5)	119.9(6)
C(15A)-C(14A)-H(14B)	120.8	N(6)-C(21)-N(5)	116.4(6)
C(13A)-C(14A)-H(14B)	120.8	O(2A)-C(21A)-N(6A)	124.6(6)
C(14)-C(15)-C(16)	118.7(7)	O(2A)-C(21A)-N(5A)	118.7(5)
C(14)-C(15)-H(15A)	120.6	N(6A)-C(21A)-N(5A)	116.7(5)
C(16)-C(15)-H(15A)	120.6	C(23)-C(22)-C(28)	120.7(6)
C(14A)-C(15A)-C(16A)	118.5(5)	C(23)-C(22)-N(6)	118.3(6)
C(14A)-C(15A)-H(15B)	120.8	C(28)-C(22)-N(6)	120.9(5)
C(16A)-C(15A)-H(15B)	120.8	C(28A)-C(22A)-C(23A)	119.5(5)
N(4)-C(16)-N(5)	117.5(6)	C(28A)-C(22A)-N(6A)	123.7(5)
N(4)-C(16)-C(15)	119.4(8)	C(23A)-C(22A)-N(6A)	116.7(5)
N(5)-C(16)-C(15)	123.0(7)	C(22)-C(23)-C(25)	117.7(7)

(Continued)

Atoms	Bond angle	Atoms	Bond angle
N(4A)-C(16A)-N(5A)	118.8(5)	C(22)-C(23)-C(24)	121.2(6)
N(4A)-C(16A)-C(15A)	120.7(5)	C(25)-C(23)-C(24)	121.1(6)
N(5A)-C(16A)-C(15A)	120.5(5)	C(25A)-C(23A)-C(22A)	118.8(5)
N(5)-C(17)-C(18)	112.4(5)	C(25A)-C(23A)-C(24A)	120.1(5)
N(5)-C(17)-H(17A)	109.1	C(22A)-C(23A)-C(24A)	121.0(5)
C(18)-C(17)-H(17A)	109.1	C(23)-C(24)-H(24A)	109.5
N(5)-C(17)-H(17B)	109.1	C(23)-C(24)-H(24B)	109.5
C(18)-C(17)-H(17B)	109.1	H(24A)-C(24)-H(24B)	109.5
H(17A)-C(17)-H(17B)	107.9	C(23)-C(24)-H(24C)	109.5
N(5A)-C(17A)-C(18A)	116.2(5)	H(24A)-C(24)-H(24C)	109.5
N(5A)-C(17A)-H(17C)	108.2	H(24B)-C(24)-H(24C)	109.5
C(18A)-C(17A)-H(17C)	108.2	C(23A)-C(24A)-H(24D)	109.5
N(5A)-C(17A)-H(17D)	108.2	C(23A)-C(24A)-H(24E)	109.5
C(18A)-C(17A)-H(17D)	108.2	H(24D)-C(24A)-H(24E)	109.5
H(17C)-C(17A)-H(17D)	107.4	C(23A)-C(24A)-H(24F)	109.5
C(17)-C(18)-C(19)	113.9(9)	H(24D)-C(24A)-H(24F)	109.5
C(17)-C(18)-C(20)	110.0(7)	H(24E)-C(24A)-H(24F)	109.5
C(19)-C(18)-C(20)	108.6(8)	C(26)-C(25)-C(23)	121.9(6)
C(17)-C(18)-H(18A)	108	C(26)-C(25)-H(25A)	119
C(19)-C(18)-H(18A)	108	C(23)-C(25)-H(25A)	119
C(20)-C(18)-H(18A)	108	C(23A)-C(25A)-C(26A)	121.5(6)
C(20A)-C(18A)-C(19A)	110.2(6)	C(23A)-C(25A)-H(25B)	119.3
C(20A)-C(18A)-C(17A)	108.8(5)	C(26A)-C(25A)-H(25B)	119.3
C(19A)-C(18A)-C(17A)	113.4(6)	C(25)-C(26)-C(27)	120.0(7)
C(20A)-C(18A)-H(18B)	108.1	C(25)-C(26)-H(26A)	120
C(19A)-C(18A)-H(18B)	108.1	C(27)-C(26)-H(26A)	120
C(17A)-C(18A)-H(18B)	108.1	C(27A)-C(26A)-C(25A)	118.7(6)
C(18)-C(19)-H(19A)	109.5	C(27A)-C(26A)-H(26B)	120.6
C(18)-C(19)-H(19B)	109.5	C(25A)-C(26A)-H(26B)	120.6
H(19A)-C(19)-H(19B)	109.5	C(28)-C(27)-C(26)	119.5(7)
C(18)-C(19)-H(19C)	109.5	C(28)-C(27)-H(27A)	120.3
H(19A)-C(19)-H(19C)	109.5	C(26)-C(27)-H(27A)	120.3
H(19B)-C(19)-H(19C)	109.5	C(26A)-C(27A)-C(28A)	121.2(6)
C(18A)-C(19A)-H(19D)	109.5	C(26A)-C(27A)-H(27B)	119.4
C(18A)-C(19A)-H(19E)	109.5	C(28A)-C(27A)-H(27B)	119.4
H(19D)-C(19A)-H(19E)	109.5	C(27)-C(28)-C(22)	120.1(6)
C(18A)-C(19A)-H(19F)	109.5	C(27)-C(28)-H(28A)	119.9
H(19D)-C(19A)-H(19F)	109.5	C(22)-C(28)-H(28A)	119.9
H(19E)-C(19A)-H(19F)	109.5	C(27A)-C(28A)-C(22A)	120.3(6)
C(18)-C(20)-H(20A)	109.5	C(27A)-C(28A)-H(28B)	119.8
C(18)-C(20)-H(20B)	109.5	C(22A)-C(28A)-H(28B)	119.8

Table D.5. Anisotropic displacement parameters ($Å^2$ x 10^3) for trimer **24**.
The anisotropic displacement factor exponent takes the form:
$-2\ pi^2\ [\ h^2\ a^{*2}\ U11 + ... + 2\ h\ k\ a^*\ b^*\ U12\ ]$

Atom	U11	U22	U33	U23	U13	U12
N(1)	81(5)	38(3)	86(5)	11(3)	31(4)	-13(3)
N(1A)	39(3)	37(3)	38(3)	4(2)	7(2)	-9(2)
N(2)	87(5)	69(4)	40(3)	24(3)	3(3)	-33(4)
N(2A)	41(3)	31(2)	34(2)	0(2)	11(2)	-6(2)
N(3)	68(4)	35(3)	47(3)	0(2)	26(3)	-13(3)
N(3A)	46(3)	32(3)	32(2)	1(2)	15(2)	-3(2)
N(4)	69(4)	29(3)	44(3)	-2(2)	33(3)	-1(3)
N(4A)	43(3)	30(2)	39(3)	0(2)	21(2)	-4(2)
N(5)	96(5)	33(3)	47(3)	-7(3)	27(3)	12(3)
N(5A)	53(3)	26(2)	38(3)	-1(2)	26(2)	2(2)
N(6)	75(4)	30(3)	33(3)	-3(2)	9(3)	6(3)
N(6A)	52(3)	28(2)	42(3)	3(2)	20(2)	6(2)
O(1)	79(5)	65(4)	146(6)	34(4)	12(4)	-21(3)
O(1A)	43(3)	44(2)	55(3)	1(2)	3(2)	-10(2)
O(2)	97(4)	42(3)	50(3)	7(2)	23(3)	23(3)
O(2A)	67(3)	45(3)	65(3)	9(2)	38(3)	22(2)
C(1)	93(7)	44(4)	109(7)	25(5)	57(6)	0(4)
C(1A)	49(4)	40(3)	31(3)	-1(3)	12(3)	-15(3)
C(2)	95(7)	63(5)	89(6)	42(5)	62(6)	17(5)
C(2A)	42(4)	49(4)	40(3)	7(3)	6(3)	-11(3)
C(3)	102(7)	84(6)	48(4)	13(4)	35(4)	17(5)
C(3A)	51(5)	60(5)	78(5)	33(4)	-3(4)	-11(4)
C(4)	122(9)	88(6)	100(7)	50(5)	77(7)	29(6)
C(4A)	64(5)	48(4)	54(4)	10(3)	16(4)	-15(4)
C(5)	144(12)	68(7)	151(11)	58(7)	115(10)	25(7)
C(5A)	55(5)	45(4)	63(4)	-4(3)	21(4)	-21(3)
C(6)	125(11)	53(6)	253(17)	31(8)	133(13)	-2(6)
C(6A)	47(4)	43(4)	77(5)	-5(4)	15(4)	-12(3)
C(7)	70(6)	43(5)	183(10)	24(6)	51(7)	-8(4)
C(7A)	50(4)	36(3)	64(4)	-2(3)	11(3)	-12(3)
C(8)	93(8)	41(5)	133(9)	24(5)	49(7)	-14(5)
C(8A)	37(4)	40(3)	28(3)	-5(3)	6(3)	-7(3)
C(9)	115(7)	88(6)	51(4)	17(4)	-10(4)	-66(6)
C(9A)	48(4)	31(3)	31(3)	1(2)	7(3)	-3(3)
C(10)	297(18)	216(14)	31(5)	21(6)	-41(7)	-190(14)

(Continued)

Atom	U11	U22	U33	U23	U13	U12
C(10A)	410(20)	50(5)	37(4)	-29(4)	-74(8)	99(9)
C(11)	264(17)	83(8)	131(10)	25(7)	-88(10)	-18(9)
C(11A)	480(30)	53(6)	64(6)	-26(5)	-97(10)	107(10)
C(12)	500(30)	510(30)	60(6)	-133(12)	146(12)	-490(30)
C(12A)	248(13)	44(4)	40(4)	1(4)	16(6)	-6(6)
C(13)	97(6)	45(4)	29(3)	0(3)	24(4)	-17(4)
C(13A)	44(4)	26(3)	29(3)	-4(2)	9(3)	-10(3)
C(14)	121(8)	95(7)	37(4)	-24(4)	3(5)	-2(6)
C(14A)	53(4)	32(3)	30(3)	4(2)	15(3)	-5(3)
C(15)	161(10)	53(5)	53(5)	-33(4)	30(6)	-4(6)
C(15A)	58(4)	29(3)	37(3)	0(3)	23(3)	-8(3)
C(16)	91(6)	43(4)	39(4)	-11(3)	34(4)	-5(4)
C(16A)	52(4)	19(3)	38(3)	-7(2)	19(3)	-6(3)
C(17)	136(8)	32(4)	66(5)	-7(3)	46(5)	19(4)
C(17A)	62(4)	28(3)	48(3)	-4(3)	35(3)	-1(3)
C(18)	158(10)	32(4)	90(6)	-7(4)	66(7)	14(5)
C(18A)	59(4)	27(3)	70(4)	-2(3)	41(4)	-5(3)
C(19)	192(12)	59(6)	97(7)	-4(5)	73(8)	-5(7)
C(19A)	107(7)	68(5)	72(5)	-19(4)	44(5)	-37(5)
C(20)	245(14)	38(5)	122(8)	7(5)	79(9)	42(7)
C(20A)	65(5)	55(4)	66(4)	2(4)	35(4)	-9(4)
C(21)	92(6)	34(3)	35(3)	0(3)	27(4)	9(4)
C(21A)	55(4)	21(3)	46(3)	-4(3)	26(3)	0(3)
C(22)	78(5)	32(3)	28(3)	1(3)	5(3)	7(3)
C(22A)	57(4)	20(3)	41(3)	-2(2)	17(3)	1(3)
C(23)	70(5)	38(3)	32(3)	8(3)	11(3)	15(3)
C(23A)	46(4)	19(3)	41(3)	-1(2)	14(3)	-2(2)
C(24)	70(5)	42(4)	33(3)	-6(3)	5(3)	20(3)
C(24A)	52(4)	34(3)	44(3)	3(3)	19(3)	1(3)
C(25)	71(5)	35(3)	39(3)	-1(3)	2(3)	8(3)
C(25A)	61(4)	25(3)	41(3)	0(3)	16(3)	-7(3)
C(26)	73(5)	50(4)	36(3)	3(3)	0(3)	-1(4)
C(26A)	65(5)	27(3)	44(4)	2(3)	11(3)	-2(3)
C(27)	76(5)	50(4)	39(4)	13(3)	13(3)	4(4)
C(27A)	50(4)	27(3)	54(4)	0(3)	11(3)	2(3)
C(28)	81(5)	46(4)	34(3)	7(3)	20(3)	11(4)
C(28A)	54(4)	30(3)	52(4)	0(3)	20(3)	4(3)

Table D.6. Hydrogen coordinates (x 10^4) and isotropic displacement parameters (A^2 x 10^3) for trimer **24**.

Atom	x	y	z	U(eq)
H(1A)	532	10317	3918	80
H(1AA)	2864	4420	2834	46
H(6A)	2194	9537	4617	56
H(6AA)	4558	4040	3682	47
H(3B)	932	10973	4634	113
H(3C)	940	10979	5497	113
H(3D)	981	12191	5077	113
H(3AB)	3097	1857	3752	100
H(3AC)	3149	3259	3801	100
H(3AD)	3157	2596	3045	100
H(4B)	178	12398	5762	113
H(4AB)	2248	1150	3655	66
H(5A)	-737	12640	5446	129
H(5AA)	1332	1282	3273	64
H(6B)	-1235	11902	4357	154
H(6AB)	948	2894	2583	67
H(7A)	-847	10886	3543	114
H(7AA)	1469	4409	2304	61
H(9A)	-309	8809	1870	108
H(9B)	221	8092	1884	108
H(9AA)	2827	7584	1456	45
H(9AB)	2272	7482	1668	45
H(10A)	149	10582	1668	234
H(10B)	3194	8427	2403	226
H(11A)	-137	10269	344	275
H(11B)	-548	9764	779	275
H(11C)	-163	8885	490	275
H(11D)	2776	10269	2328	342
H(11E)	2275	9655	1789	342
H(11F)	2831	9671	1571	342
H(12A)	937	10026	2014	515
H(12B)	802	10566	1195	515
H(12C)	864	9173	1312	515
H(12D)	2971	7712	3308	170
H(12E)	2539	8738	3191	170
H(12F)	3149	9057	3286	170

(Continued)

Atom	x	y	z	U(eq)
H(14A)	693	7106	2614	105
H(14B)	3489	6856	1420	45
H(15A)	1476	6306	3295	106
H(15B)	4342	6138	1573	47
H(17A)	2746	6103	4355	89
H(17B)	2171	5812	3848	89
H(17C)	4805	4593	1466	51
H(17D)	5326	3996	1962	51
H(18A)	2384	5882	5421	105
H(18B)	5138	6472	1848	58
H(19A)	1481	5979	4836	164
H(19B)	1618	4784	5299	164
H(19C)	1524	4768	4416	164
H(19D)	6014	6740	2524	118
H(19E)	6089	5348	2632	118
H(19F)	5694	6038	3018	118
H(20A)	2907	4391	5069	193
H(20B)	2388	3801	4558	193
H(20C)	2471	3830	5439	193
H(20D)	5306	5644	772	88
H(20E)	5850	5105	1249	88
H(20F)	5779	6501	1162	88
H(24A)	1996	10351	5469	75
H(24B)	2055	11743	5590	75
H(24C)	2215	10873	6286	75
H(24D)	4118	3864	5230	63
H(24E)	4063	3376	4408	63
H(24F)	4248	4703	4607	63
H(25A)	3059	12276	6351	60
H(25B)	4864	3212	6096	50
H(26A)	3899	12271	6157	66
H(26B)	5748	2601	6454	55
H(27A)	4119	10932	5326	66
H(27B)	6239	2514	5571	53
H(28A)	3499	9545	4740	63
H(28B)	5868	3032	4349	52

Table D.7. Anisotropic displacement parameters ($Å^2$ x 10^3) for macrocycle **22**. The anisotropic displacement factor exponent takes the form:

$$-2\,pi^2\,[\,h^2\,a^{*2}\,U11 + \ldots + 2\,h\,k\,a^*\,b^*\,U12\,]$$

Atom	U11	U22	U33	U23	U13	U12
O(1)	39(2)	135(5)	188(6)	138(5)	71(3)	56(3)
O(2)	18(1)	32(2)	29(2)	9(1)	6(1)	1(1)
O(3)	28(2)	33(2)	37(2)	7(1)	14(1)	14(1)
O(4)	25(2)	33(2)	15(1)	0(1)	4(1)	1(1)
N(1)	28(2)	72(3)	93(4)	65(3)	31(2)	27(2)
N(2)	18(2)	28(2)	24(2)	9(2)	5(1)	4(2)
N(3)	16(2)	22(2)	18(2)	3(1)	4(1)	0(1)
N(4)	18(2)	21(2)	20(2)	5(1)	6(1)	2(1)
N(5)	17(2)	22(2)	19(2)	4(1)	5(1)	3(1)
N(6)	19(2)	19(2)	22(2)	0(1)	5(1)	4(1)
N(7)	15(2)	18(2)	27(2)	2(1)	-1(1)	3(1)
N(8)	16(2)	25(2)	22(2)	0(1)	2(1)	2(1)
N(9)	18(2)	28(2)	19(2)	1(1)	2(1)	2(1)
N(10)	26(2)	32(2)	14(2)	2(1)	0(1)	7(2)
N(11)	20(2)	24(2)	14(2)	2(1)	1(1)	2(1)
N(12)	18(2)	23(2)	24(2)	7(1)	3(1)	5(1)
C(5)	33(3)	59(4)	74(4)	49(3)	25(3)	20(3)
C(6)	20(2)	19(2)	17(2)	-3(2)	3(2)	-3(2)
C(7)	14(2)	32(2)	21(2)	-1(2)	2(2)	0(2)
C(8)	17(2)	30(2)	22(2)	0(2)	4(2)	-7(2)
C(9)	23(2)	24(2)	17(2)	2(2)	5(2)	-3(2)
C(10)	18(2)	22(2)	12(2)	-5(2)	-1(1)	0(2)
C(11)	14(2)	19(2)	16(2)	-4(2)	4(1)	-4(2)
C(12)	23(2)	18(2)	18(2)	1(2)	3(2)	-3(2)
C(13)	48(3)	55(3)	13(2)	4(2)	1(2)	26(2)
C(14)	35(3)	145(7)	39(3)	-44(4)	-17(2)	35(4)
C(15)	55(4)	119(7)	67(5)	-17(4)	-5(3)	-49(4)
C(16)	193(10)	155(9)	50(4)	-56(5)	-68(5)	133(8)
C(17)	25(2)	27(2)	17(2)	-3(2)	-1(2)	5(2)
C(18)	49(3)	41(3)	17(2)	3(2)	-1(2)	22(2)
C(19)	39(3)	36(3)	21(2)	0(2)	-5(2)	19(2)
C(20)	16(2)	20(2)	21(2)	-3(2)	-4(2)	0(2)
C(21)	17(2)	21(2)	30(2)	3(2)	3(2)	5(2)
C(22)	29(2)	20(2)	31(2)	1(2)	1(2)	1(2)

(Continued)

Atom	U11	U22	U33	U23	U13	U12
C(23)	86(4)	33(3)	43(3)	-3(2)	-9(3)	-24(3)
C(24)	61(4)	22(3)	72(4)	12(3)	2(3)	3(2)
C(25)	13(2)	18(2)	28(2)	-2(2)	1(2)	-2(2)
C(26)	16(2)	20(2)	21(2)	-3(2)	2(2)	-3(2)
C(27)	25(2)	23(2)	26(2)	-6(2)	7(2)	3(2)
C(28)	33(2)	31(2)	23(2)	-5(2)	10(2)	6(2)
C(29)	34(2)	30(2)	17(2)	-1(2)	4(2)	4(2)
C(30)	16(2)	20(2)	20(2)	-4(2)	1(2)	-1(2)
C(31)	14(2)	18(2)	19(2)	-5(2)	3(1)	-1(2)
C(32)	18(2)	26(2)	14(2)	1(2)	-2(1)	0(2)
C(33)	22(2)	20(2)	21(2)	6(2)	5(2)	1(2)
C(34)	20(2)	25(2)	20(2)	5(2)	5(2)	-2(2)
C(35)	35(2)	24(2)	24(2)	2(2)	3(2)	1(2)
C(36)	21(2)	29(2)	22(2)	10(2)	5(2)	3(2)
C(37)	18(2)	22(2)	16(2)	1(2)	2(1)	-1(2)
C(38)	31(2)	21(2)	30(2)	11(2)	11(2)	8(2)
C(39)	29(2)	35(3)	39(3)	19(2)	14(2)	16(2)
C(40)	24(2)	42(3)	36(3)	18(2)	13(2)	9(2)
Cl(3)	41(1)	45(1)	21(1)	-3(1)	7(1)	-5(1)
Cl(2)	38(1)	73(1)	30(1)	8(1)	0(1)	-17(1)
Cl(1)	80(1)	51(1)	52(1)	-18(1)	14(1)	8(1)
C(41)	35(3)	44(3)	23(2)	-6(2)	7(2)	-12(2)
C(50)	19(2)	17(2)	19(2)	3(2)	1(2)	4(2)
C(51)	2000(70)	2000(70)	2000(70)	0(2)	173(7)	0(2)
C(52)	550(60)	550(60)	550(60)	0(2)	48(6)	0(2)
C(53)	59(5)	60(5)	64(5)	3(2)	3(2)	5(2)
C(50')	64(4)	59(4)	59(4)	-1(2)	8(2)	-4(2)
C(51')	120(4)	122(4)	121(4)	1(2)	12(2)	0(2)
C(52')	85(4)	86(4)	84(4)	1(2)	8(2)	-1(2)
C(53')	65(6)	65(6)	69(6)	3(2)	3(2)	5(2)

Table D.8. Hydrogen coordinates (x 10^4) and isotropic displacement parameters (A^2 x 10^3) for macrocycle **23**.

Atom	x	y	z	U(eq)
H(5A)	7574	1454	3050	23
H(6A)	8778	-366	4810	24
H(7A)	3092	1062	5147	27
H(8B)	3034	214	6222	28
H(9B)	4351	-274	6911	25
H(11B)	5846	912	5395	19
H(13A)	7397	-991	8835	47
H(13B)	6720	-358	8984	47
H(14A)	8616	-217	8759	89
H(15A)	7825	746	8139	122
H(15B)	8421	989	9000	122
H(15C)	7349	875	9017	122
H(16A)	8748	182	10198	206
H(16B)	8354	-597	10152	206
H(16C)	7686	49	10264	206
H(18A)	8328	-1383	8070	43
H(19A)	9374	-1778	7136	39
H(21A)	10248	-2031	6330	27
H(21B)	10456	-2113	5336	27
H(22A)	8820	-2604	6011	32
H(23A)	8518	-3165	4648	82
H(23B)	9423	-2837	4316	82
H(23C)	8593	-2339	4508	82
H(24A)	10106	-3259	6557	78
H(24B)	10365	-3406	5590	78
H(24C)	9458	-3735	5917	78
H(27A)	10045	-777	3017	29
H(28A)	9938	-115	1748	34
H(29A)	9096	903	1623	32
H(31A)	8342	594	4049	20
H(33A)	8503	3134	1580	24
H(33B)	7672	3590	1868	24
H(34A)	6663	3020	808	26
H(35A)	7236	2275	-233	41
H(35B)	7422	1940	714	41

(Continued)

Atom	x	y	z	U(eq)
H(35C)	8230	2316	266	41
H(36A)	7235	3570	-410	35
H(36B)	8208	3650	123	35
H(36C)	7349	4066	426	35
H(38A)	6348	3538	2072	32
H(39A)	4951	3523	2647	40
H(41A)	4952	582	11025	40
H(50A)	3782	3321	2908	22
H(50B)	4008	3497	3890	22
H(51A)	2923	3867	3826	2400
H(52A)	2091	3251	4696	832
H(52B)	1415	3102	3851	832
H(52C)	1641	3889	4145	832
H(53A)	2917	3783	2324	92
H(53B)	2272	4288	2821	92
H(53C)	1879	3572	2407	92
H(51B)	3670	3894	3067	145
H(52D)	3788	3507	4506	127
H(52E)	2841	3097	4371	127
H(52F)	2851	3932	4409	127
H(53D)	2459	3589	2042	100
H(53E)	1981	3995	2784	100
H(53F)	1956	3160	2749	100

Appendix E

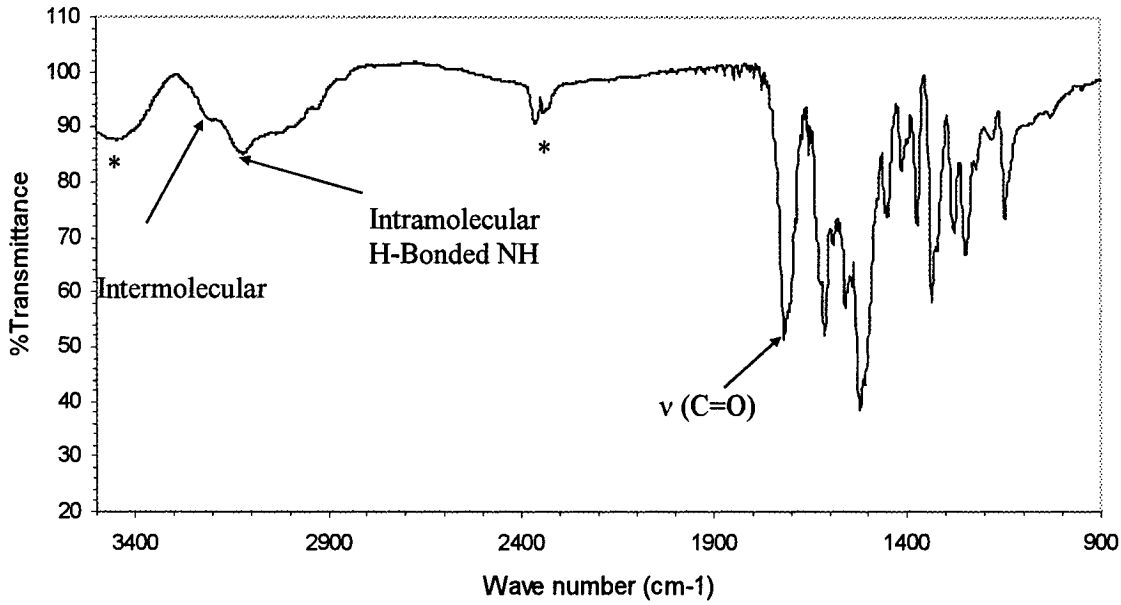

Figure E.1. FTIR spectrum of macrocycle **6** in KBr. The signals denoted with asterisks at 3460 cm^{-1} and 2306-2395 cm^{-1} are due to water and carbon dioxide, respectively.

In the FTIR spectrum (Figure E.1), there are two N-H stretching bands from macrocycle **6** at 3140 and 3210 cm^{-1} that can be assigned to the intra- and inter-molecular hydrogen bonded N-H's, respectively.[1] The absorptions on the shoulder of the intramolecular hydrogen bonded N-H signal may be caused by other minor macrocycles.

[1] (a) M. C. Etter, *Accounts of Chemical Research* **1990**, *23*, 120-126; (b) E. P. Kyba, S.-S. P. Chou, *Journal of Organic Chemistry* **1981**, *46*, 860-863; (c) D. L. Pavia, G. M. Lampman, G. S. Kriz, *Introduction to spectroscopy*, 3rd ed., John Vondeling, Fort Worth, **2001**, p579.

The signal appearing at 1720 cm^{-1} belongs to the stretching vibration of carbonyl groups involved in hydrogen bonding interactions.[2]

[2] (a) M. C. Etter, Z. Urbanczyk-Lipkowska, M. Zia-Ebrahimi, T. W. Panunto, *Journal of the American Chemical Society* **1990**, *112*, 8415-8426; (b) F. H. Beijer, R. P. Sijbesma, H. Kooijman, A. L. Spek, E. W. Meijer, *Journal of the American Chemical Society* **1998**, *120*, 6761-6769; (c) Y. Ge, L. Miller, T. Ouimet, D. K. Smith, *Journal of Organic Chemistry* **2000**, *65*, 8831-8838; (d) X.-Z. Wang, X.-Q. Li, X.-B. Shao, X. Zhao, P. Deng, X.-K. Jiang, Z.-T. Li, Y.-Q. Chen, *Chemistry--A European Journal* **2003**, *9*, 2904-2913; (e) C.-H. Chien, M.-k. Leung, J.-K. Su, G.-H. Li, Y.-H. Liu, Y. Wang, *Journal of Organic Chemistry* **2004**, *69*, 1866-1871; (f) X.-Q. Li, X.-K. Jiang, X.-Z. Wang, Z.-T. Li, *Tetrahedron* **2004**, *60*, 2063-2069.

Appendix E

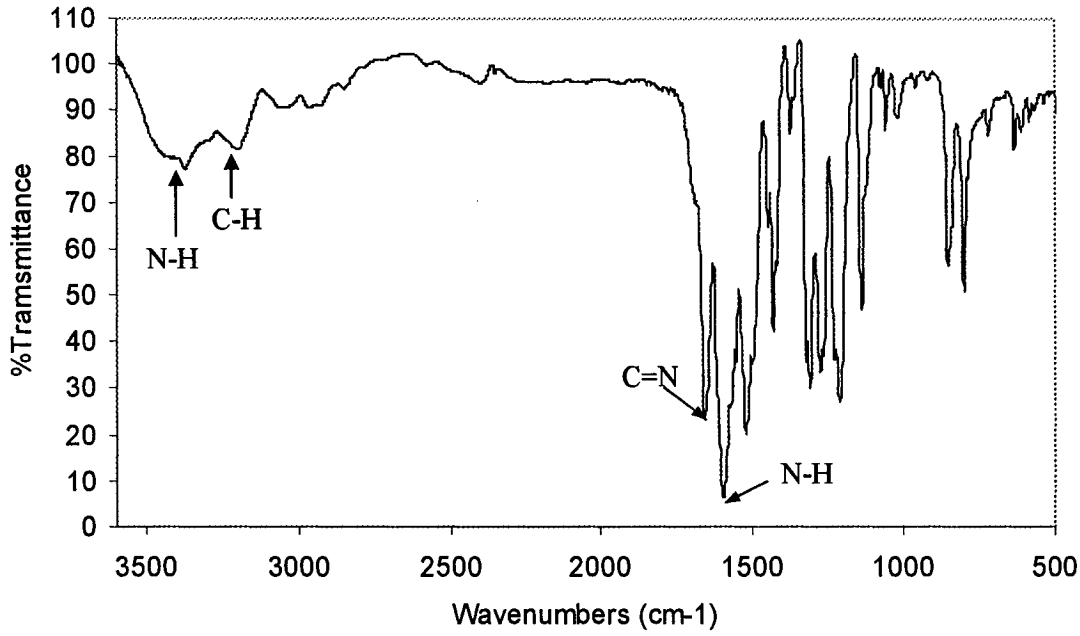

Figure E.2. IR spectrum of macrocycle 7 in KBr.

In the infrared spectrum of macrocycle 7 (Figure E.2), the C=N double bond stretching occurs at 1654 cm^{-1}, which fall in the normal range for these types of vibrations (*ca.* 1580-1660 cm^{-1}).[3] The N-H bending vibration appeared as a strong sharp absorption at 1594 cm^{-1}, and the stretching appeared at 3375 cm^{-1} overlapping with the broad O-H stretching vibration (3412 cm^{-1}) caused by water trapped in the sample. Absorption at 3202 cm^{-1} was assigned to the formal C-H stretching vibration.

[3] S. Patai, *The Chemistry of Amidines and Imidates*, John Wiley & Sons, London, **1975**, p677.

Appendix E

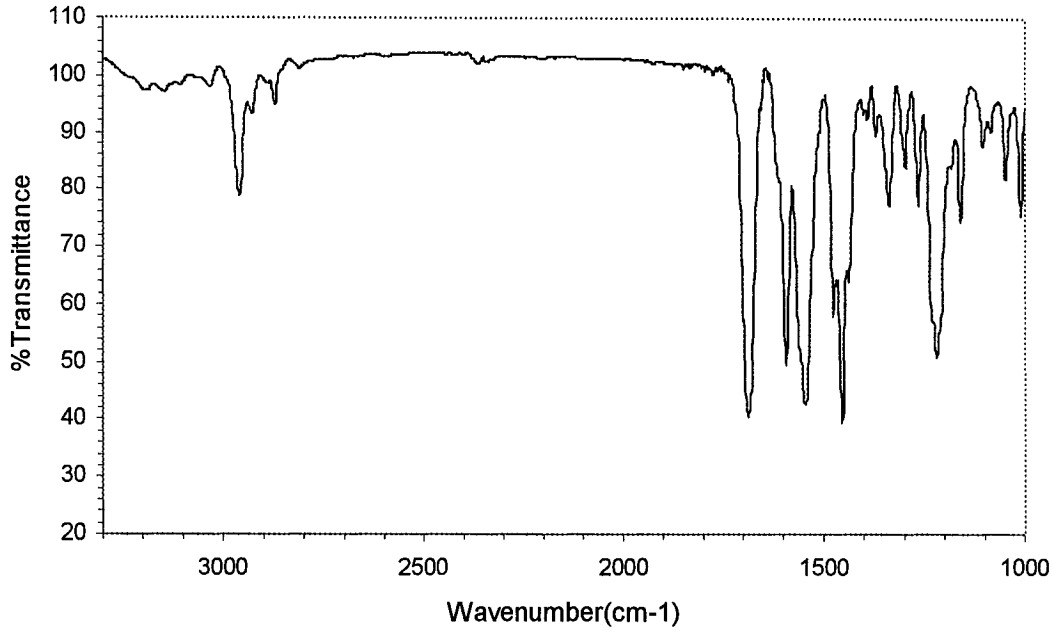

Figure E.3. IR spectrum of macrocycle **22** in KBr.

Normally, the amide N-H stretching vibration appears at around 3300 cm^{-1}.[3] However, in macrocycles **20-23** the N-H vibration appears below 3000 cm^{-1}. This lower frequency is consistent with the formation of hydrogen bonds with heterocyclic nitrogen lone pairs.[3-5] Compared to **20** (2923 cm^{-1}) (Figure E.4) and **21** (2925 cm^{-1}) (Figure E.5), **22** (2960 cm^{-1}) (Figure E.3) and **23** (2962 cm^{-1}) (Figure E.6) have absorption signals at higher frequencies. The difference could be due to intermolecular interactions. A common feature of macrocycles **21**, **22**and **23** is that the urea nitrogens are connected directly to the methylene groups. In the solid state structure of macrocycle **22** intermolecular hydrogen bonds form between this methylene group and the carbonyl oxygen (Section 3.3.2.2). This may explain the lower frequencies for the C=O stretch in **21**, **22**, and **23** as compared to **20**, where the urea nitrogen is connected to a phenyl group and this type of hydrogen bonding is not present.

Appendix E

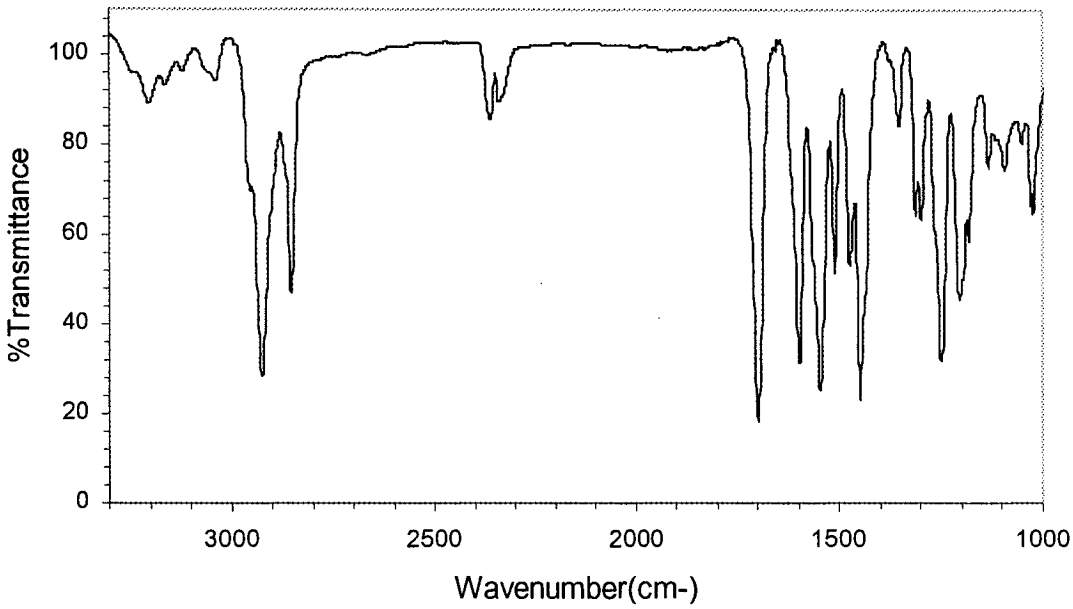

Figure E.4. IR spectra of macrocycle **20** in KBr.

Appendix E

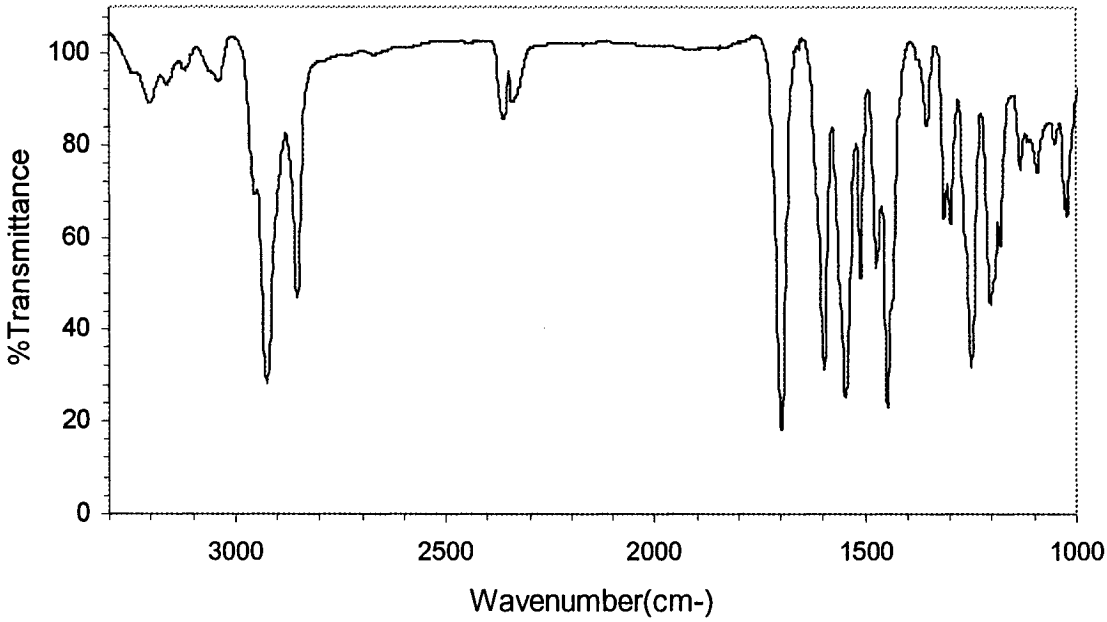

Figure E.5. IR spectrum of macrocycle **21** in KBr.

Appendix E

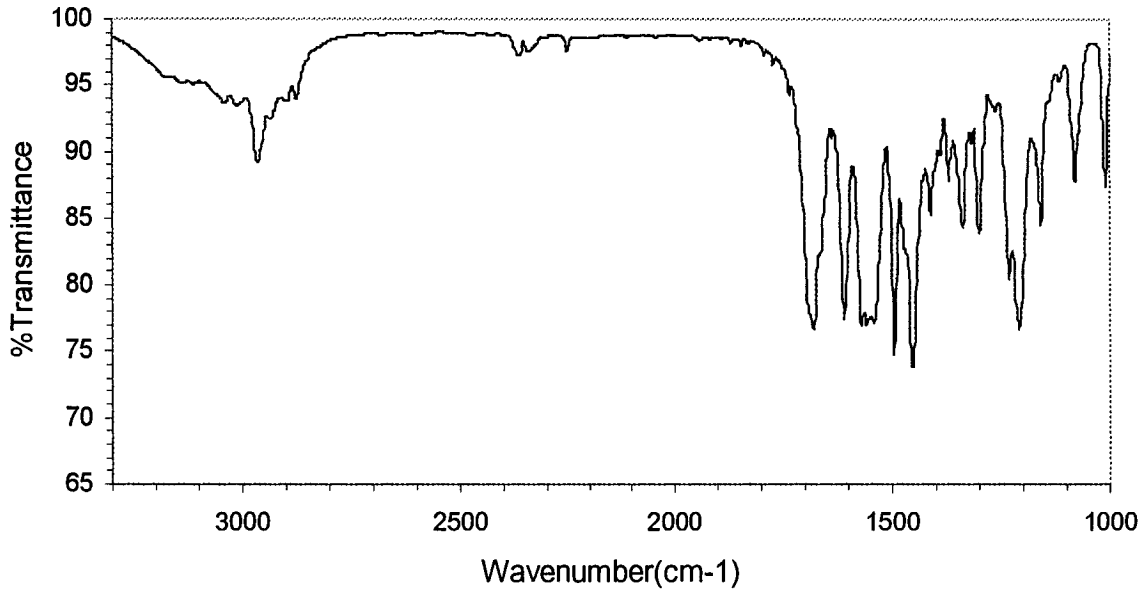

Figure E.6. IR spectrum of macrocycle **23** in KBr.

Appendix E

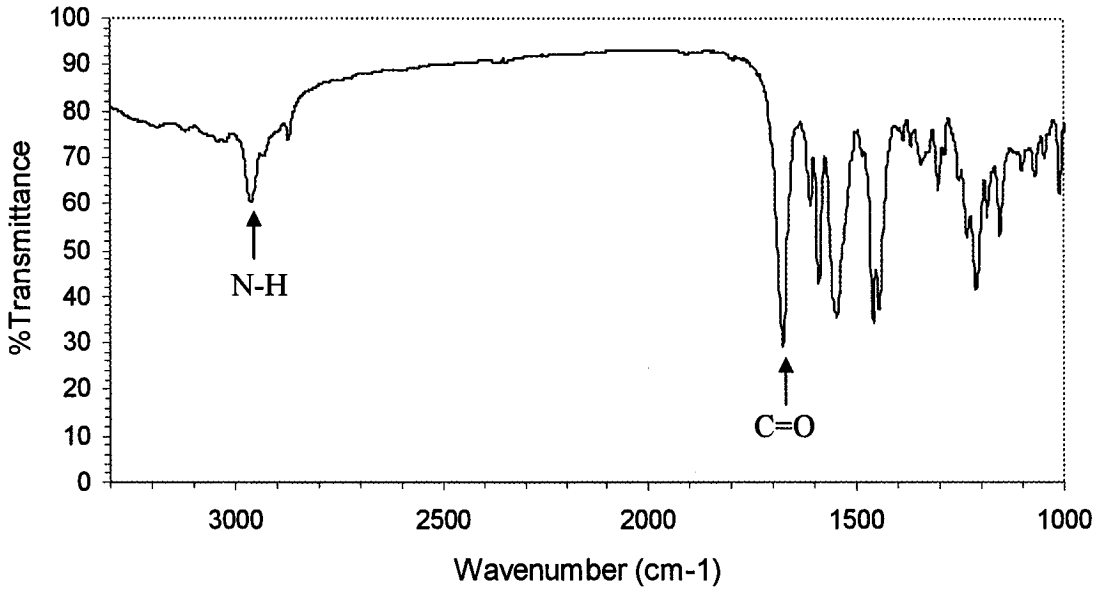

Figure E.7. IR spectrum of trimer **24** in KBr.

The decreased frequency for the N-H stretching vibration at 2960 cm^{-1} in the IR spectrum (Figure E.7) is characteristic of hydrogen-bonded N-H absorptions that were also observed in the corresponding macrocycles. The absorption at 1676 cm^{-1} belongs to the C=O stretching vibration.